NASA TECHNICAL MEMORANDUM

NASA TM X-2721

SYMPOSIUM ON REUSABLE SURFACE INSULATION FOR SPACE SHUTTLE

Volume III - Thermal Protection System Design and Optimization

Held at
Ames Research Center
Moffett Field, Calif.
November 1-3, 1972

NATIONAL AERONAUTICS AND SPACE ADMINISTRATION • WASHINGTON, D. C. • SEPTEMBER 1973

1. Report No. NASA TM X-2721	2. Government Accession No.	3. Recipient's Catalog No.
4. Title and Subtitle Symposium on Reusable Surface Insulation for Space Shuttle, Volume III - Thermal Protection System Design and Optimization		5. Report Date September 1973
		6. Performing Organization Code
7. Author(s)		8. Performing Organization Report No. A-4725
9. Performing Organization Name and Address NASA Ames Research Center Moffett Field, Calif. 94035		10. Work Unit No. 502-37-02
		11. Contract or Grant No.
12. Sponsoring Agency Name and Address National Aeronautics and Space Administration Washington, D. C. 20546		13. Type of Report and Period Covered Technical Memorandum
		14. Sponsoring Agency Code

15. Supplementary Notes Held at NASA Ames Research Center, November 1–3, 1972.

16. Abstract

The conference encompasses three technology efforts, each published as a separate volume.

Volume   I - RSI Fabrication, Improvement, Morphology and Properties (NASA TM X-2719)
Volume II - Environmental Testing (NASA TM X-2720)
Volume III - Thermal Protection System Design and Optimization (NASA TM X-2721)

17. Key Words (Suggested by Author(s)) Thermal Protection System Reusable Surface Insulation Space Shuttle	18. Distribution Statement Unclassified – Unlimited	
19. Security Classif. (of this report) Unclassified	20. Security Classif. (of this page) Unclassified	21. No. of Pages 386	22. Price* $6.00

Page Intentionally Left Blank

FOREWORD

Howard K. Larson

One of the critical technology needs of the Space Shuttle is develop-
ment of a reusable thermal protection system (TPS). The baseline
material for a large part of the shuttle TPS is now reusable surface
insulation (RSI). Because of the rapid progress which has occurred
in this development effort during FY'72-'73, it was deemed appropriate
to review the state of RSI technology at this time. Therefore, Ames
Research Center, under the auspices of the Shuttle Thermal Protection
Systems and Materials Technology Working Group, hosted a three-day
symposium on Reusable Surface Insulation for Thermal Protection of
the Space Shuttle on November 1-3, 1972.

The objective of this symposium was to define the state-of-the-art
for RSI materials. The meeting was divided into five sequential half-
day sessions; each session addressing a specific technology area.

The first session "RSI Fabrication and Improvement" was chaired by
Howard E. Goldstein of NASA-Ames, and included papers discussing the
development of silica, mullite and alumino-silicate RSI materials.
Rigid and flexible RSI materials were described. The results reported
showed that mullite, silica and alumino-silicate rigid fibrous RSI
materials could be fabricated reproducibly. One paper described a
somewhat different RSI concept, a rigid closed pore alumino-silicate
insulation having good physical stability. Also described was a
silica non-rigid insulation which offers the possibility of minimizing
strain compatibility problems with the structure. While substantial
improvements have been made in the past two years, it was pointed out
by many of the papers that much effort is still required to optimize
the RSI materials. Substantial improvement in physical properties and
thermal stability should be expected with continued research.

The second session "RSI Morphology and Properties" was chaired by
Salvatore J. Grisaffe, NASA-Lewis, and included papers describing the
detailed mechanical and thermophysical properties of the rigid fibrous
RSI materials and their coatings. The mechanical properties as a
function of temperature for REI mullite and LI-1500 were presented.
One paper described a comparison of the mechanical and thermophysical
properties of HCF, REI mullite, and LI-1500. Radiant energy transmis-
sion through mullite RSI was discussed in one paper and the high
temperature surface optical properties of all the RSIs were discussed
in another paper. The final paper described the microstructure of
mullite fibers. This session demonstrated that the mechanical proper-
ties of the RSI materials are reasonably well understood, though the
precision of the reported values is still in doubt. Thermal conduc-
tivity, particularly radiant heat transfer effects, are not well
defined for the fibrous mullite materials. Emittances of the surface
coatings of all the RSI materials are still questionable and require
further study.

The third session "Environmental Testing I" was chaired by David H. Greenshields, NASA-MSC, and described the results of arc-plasma testing of the RSI materials. Most of these papers were concerned with both techniques for proper convective heating environment simulation and the response of the materials to the environment. Two papers described thermal response in gaps due to laminar and turbulent heating, respectively. In both studies, large panels simulating shuttle heat shield configurations were used. Other papers described the internal thermal response, catalytic wall effects and material response to cyclic heating. These studies were carried out on small models in uniform stagnation region heating regimes. Significantly higher thermal efficiency was reported for silica RSI compared with mullite RSI. Silica RSI coatings were also shown to be more chemically stable and less subject to cracking due to thermal shock.

The fourth session "Environmental Testing II" was chaired by John D. Buckley, NASA-Langley, and included papers that discussed the results of several diverse environmental testing programs. There were papers on the response of the RSI coatings in both convective and radiative heating environments. In these papers, emphasis was placed on the chemical and morphological changes that occur due to each heating environment. Significant differences were shown between the effects of radiant and convective heating. Convective heating was shown to have more severe effects. Other papers in the session described the effects of combined salt spray and cyclic radiant heating. It was shown that salt spray is more deleterious for silica than for mullite. Cold soak, acoustical rain erosion, and meteoroid impact tests were also described. The results of large panel tests in radiant heating and acoustic environments showed the silica RSI to be more stable. Mullite materials experienced thermostructural failures in these tests.

The fifth session "Thermal Protection System Design and Optimization" was chaired by George Strouhal, NASA-MSC, and included papers describing a number of specific design problems. Among these problems were the adhesive cold soak, the effect of optical properties on thermal design and techniques for mechanical attachment of RSI to the structure. The design concept of a non-rigid silica heat shield was described. Papers on mullite and silica RSI, respectively, contrasted the design philosophies and development maturities of the respective systems. Finally, a paper on thermostructural analysis of RSI application showed that mullite was much more subject to thermal stress failure than silica.

In conclusion, it is felt that the Symposium fulfilled its intended purpose in providing an "open forum" for Industry and Government to present, receive, and discuss the most recent results of a young, intensive technology program. NASA needed the results of this RSI technology program in order to make important decisions as to which of the RSI materials to choose for the shuttle heat shield. Early in 1973, NASA made the announcement that silica was chosen for the base material and that a coating with a ratio of solar absorptance to room temperature emittance of 1.0 would be baselined.

CONTENTS

SYMPOSIUM CO-CHAIRMEN: Howard K. Larson,
Ames Research Center
David H. Greenshields,
Manned Spacecraft Center

VOLUME I. - RSI FABRICATION, IMPROVEMENT, MORPHOLOGY, AND PROPERTIES

Session I - RSI Fabrication and Improvement
Chairman: Howard E. Goldstein
Ames Research Center

Session II - RSI Morphology and Properties
Chairman: Salvatore J. Grisaffe
Lewis Research Center

VOLUME II. - ENVIRONMENTAL TESTING

Session III - Environmental Testing I
                Chairman: David H. Greenshields
                            Manned Spacecraft Center

Session IV - Environmental Testing II
Chairman: John D. Buckley
Langley Research Center

CHARACTERIZATION OF ADHESIVES FOR ATTACHING REUSABLE SURFACE INSULATION ON SPACE SHUTTLE VEHICLES

H. P. Owen and M. T. Carroll
General Dynamics
Convair Aerospace Division
Fort Worth, Texas

FOREWORD

INTRODUCTION

National Aeronautics and Space Administration, Manned Spacecraft Center is currently developing reusable surface insulation (RSI) for the space shuttle vehicles using silica and mullite fibers. These fibers are felted and compacted to provide ceramic tiles. Porosity of the tiles necessitates the application of a thin, impervious, protective coating on the exposed surfaces. To date, the most promising coatings are glass-type glazes that have a very low strain-to-failure threshold; therefore, the attachment mechanism for the tiles must be of a flexible nature.[1,2,3] Because of this requirement and a bond line use temperature range of 117 to 590°K (-250 to 600°F), the elastomeric room temperature vulcanizing (RTV) silicone adhesive systems appear to be the most promising attachment system.

The literature contains some data for these systems, but these data are incomplete, particularly in design data such as shear, tensile, and compression moduli over the required temperature range. Also there is a need for suitable adhesive systems with even lower modulus and density than those currently available.

The Fort Worth operation of General Dynamics' Convair Aerospace Division contracted with NASA, MSC to conduct extensive testing to provide design data on the following RTV silicone materials: General Electric's RTV-560, Dow Corning's 93-046, and Martin Marietta's SLA-561. In addition, Convair Aerospace developed a fourth system, with lower modulus and lower density, which comprises Raybestos Manhattan's closed cell silicone rubber sponge, RL-1973, bonded to substrates with GE's RTV-560. This system was incorporated in the overall test program.

This paper describes the research program that resulted in development and selection of the low density, low modulus RL-1973/RTV-560 adhesive system. Test methods developed and used to obtain tensile, shear, and compression moduli data over the temperature range of 105 to 590° K (-270 to 600° F) are discussed and data obtained are presented. Density, thermal expansion, and thermal conductivity test methods and data are shown. Tests to determine stress relaxation of GE RTV-560 under constant strain at temperatures down to 105° K (-270° F) are discussed and data presented.

LIST OF SYMBOLS

RTV - room temperature vulcanizing

$^\circ$K - degrees Kelvin

$^\circ$F - degrees Fahrenheit

m - meter

in - inch

Hg - mercury

N/m^2 - newton per square meter

psi - pounds per square inch

Tg - glass transition temperature

PROGRAM OVERVIEW

(Figure 1)

An overview of the total program conducted to date is shown in Figure 1. Since
time does not permit discussion of the complete program, only those portions of
the program dealing with adhesive development, modulus, density and thermal prop-
erties were selected for this presentation.

The objective of this program was to develop design allowables type data for the
three commercially available silicone adhesives shown here and to develop a lower
modulus, lower density adhesive system through modification of existing silicone
elastomeric materials. Data developed are intended for use in stress analysis work
to optimize the space shuttle vehicle's thermal protection system consisting of
RSI, adhesive attachment, and substrate structure

Although not presented in this paper, considerable test work was conducted to
determine the effects of bond line thickness and strain rates. Except for the
RL-1973 sponge, effects of bond line thickness varying from .00076 m (.030 in.)
to .00635 m (.25 in.) was not too apparent. Neither were the effects of strain
rates of .00033 to .0066 m/m per second (.02 to 0.4/in./in./min). These low
strain rates were selected to simulate those which the adhesives will experience
due to loads in the vehicle structures. Rubbery materials are normally tested at
much higher strain rates.

Poisson's ratio was determined for all four adhesives over the temperature range
shown. Generally, values obtained average about 0.5. Analysis of data obtained
has not been completed.

Development of the low density, low modulus RM/RL-1973/GE RTV-560 adhesive system
will be discussed first. Formulation work and tests leading up to the selection
of this system as the fourth adhesive to be included in the program will be
presented.

PROGRAM OVERVIEW

DEVELOPMENT
OF
REDUCED
MODULUS
AND
LOWER DENSITY
ADHESIVE

ADHESIVE SYSTEMS

- GE RTV-560
- DC 93-046
- MMC SLA-561
- GE RTV-560/RL 1973

TESTS

- Tensile Stress-Strain
- Shear Stress-Strain
- Poisson's Ratio (3 Load Rates)
    - Shear Modulus
    - Tensile Modulus
- Compression
- Density (RT)
- Thermal Expansion
- Specific Heat
- Thermal Conductivity
- Thermal Cycling
- Constant Strain/Stress Relaxation

ENVIRONMENTAL TEST
CONDITIONS

- 105^0K (-270^0F)
- 144^0K (-200^0F)
- 158^0K (-175^0F)
- 172^0K (-150^0F)
- 219^0K (-65^0F)
- 297^0K (75^{0}F)
- 422^0K (300^{0}F)
- 450^0K (350^{0}F)
- 561^0K (550^{0}F)
- 589^0K (600^{0}F)

939

Figure 1

ADHESION IN TENSION OF REDUCED
DENSITY ADHESIVE FORMULATIONS TESTED AT 297° K (75° F)
(Figure 2)

Decreasing the modulus and density of the adhesive would effect a substantial weight savings in the space shuttle thermal protection system. The approach taken in this program was to modify existing silicone adhesives with low density fillers to reduce both modulus and density yet retain sufficient strength properties to provide reliable attachment of the RSI to the space shuttle vehicle surfaces. Effects of glass microballoons, 50 and 100 percent by volume, in GE RTV-560 are shown in Figure 2 along with the RL-1973/GE RTV-560 adhesive system. Tensile stress-strain curves are based on tests of 2024T851 aluminum-to-aluminum butt joints with .0016 m (.064 in.) bond line thicknesses. Slope of the curves show that the glass microballoons increase the modulus of GE RTV-560 rather than decrease it. The RL-1973/GE RTV-560 system has low modulus and considerably greater elongation than the base adhesive, RTV-560.

ADHESION IN TENSION OF REDUCED DENSITY ADHESIVE FORMULATIONS TESTED AT $297^{\circ}K$ ($75^{\circ}F$)

Figure 2

Shear stress-strain curves in Figure 3 show the same trend as the tensile stress-strain curves in Figure 2. As will be shown later, the adhesive system comprising RL-1973 silicone sponge sandwiched between thin bond lines of GE RTV-560 has a density less than half that of the solid adhesives tested. Even though it has a very low modulus, it possesses adequate strength to compete with the solid adhesives.

Shear stress-strain data shown here were derived from tests of single lap shear specimens using 2024T81 aluminum as the adherends and bond line thicknesses of approximately .00016 m (.064 in.). The aluminum was acid cleaned and primed with GE's SE 4155 primer. Strain rate was .0066 m/m/sec (0.4 in./in./min).

In this formulation work, other low density fillers were evaluated such as Emerson Cumming's IG-101 and Union Carbide's BJ0-0930 microballoons. These materials were unsatisfactory. They caused the GE RTV-560 to gell without the addition of catalyst.

A very low modulus RTV silicone, Dow Corning's 77-137 was also included in the program. As originally supplied it exhibited substandard strength but later versions show adequate strength. Characterization of the later version designated as X3-6004 is continuing.

ADHESION IN SHEAR OF REDUCED DENSITY ADHESIVE FORMULATIONS TESTED AT 297°K (75°F)
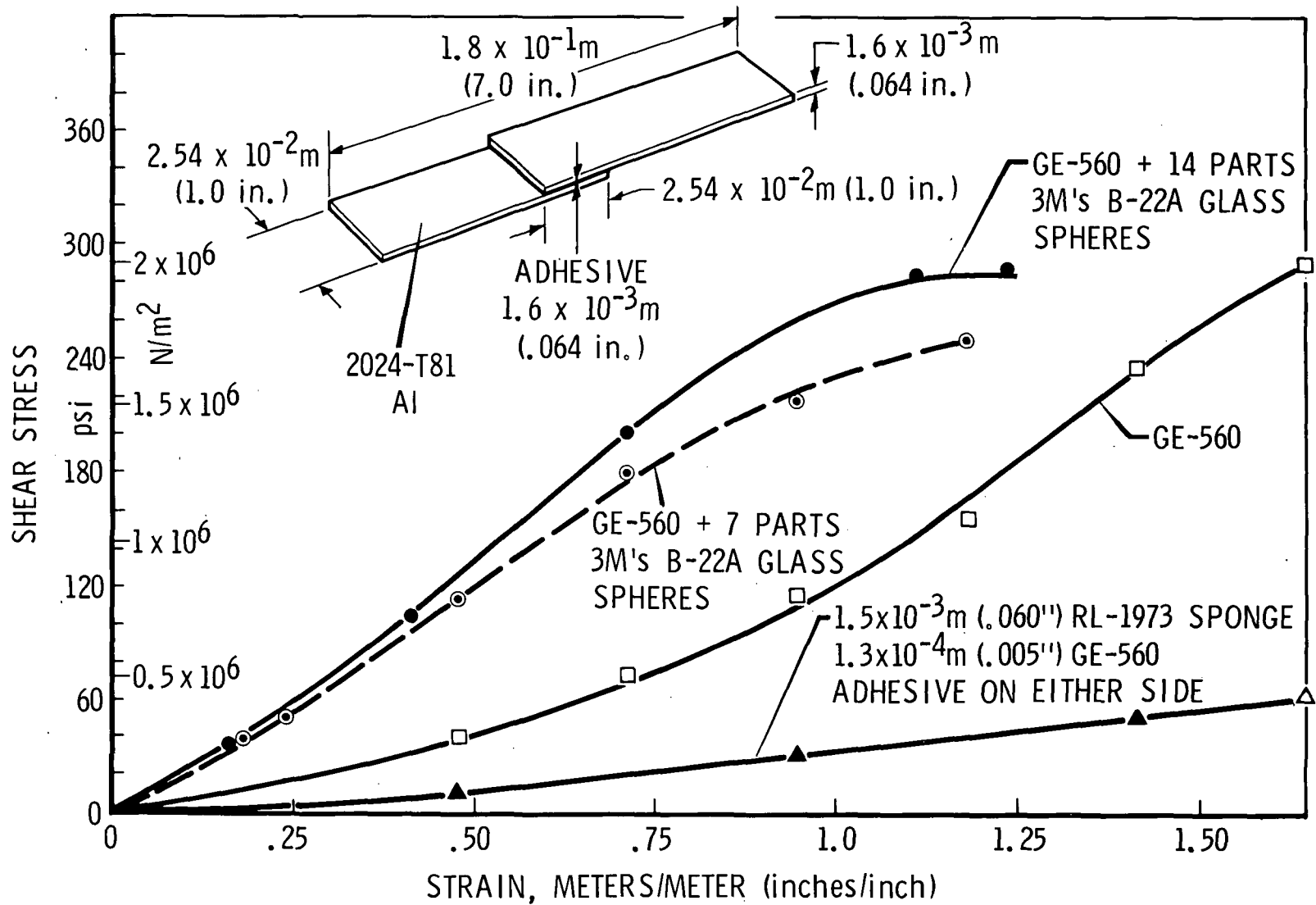
Figure 3

EFFECT OF PRESSURE VS. TIME ON VOLUME OF RM/RL-1973
CLOSED CELL SILICONE SPONGE
(Figure 4)

The RL-1973 sponge exhibits volumetric changes when exposed to variations in pressure. The magnitude of change has been estimated by placing specimens of known dimensions upon standard grids in a variable pressure chamber and noting dimensional changes vs. time at pressure. Figure 4 shows that the sponge expands immediately when the pressure is reduced from atmospheric to 1.688×10^3 N/m^2 (29.5" Hg vacuum) but begins returning to its original dimensions as air diffuses from the closed cells. On release of the vacuum, the sponge immediately contracts and again begins returning to its original dimensions as pressure in the cells returns to atmospheric. This characteristic may or may not be a drawback. Comparable data on the solid RTV adhesives was not determined.

EFFECT OF PRESSURE VS. TIME ON VOLUME OF RM/RL-1973 CLOSED CELL SILICONE SPONGE
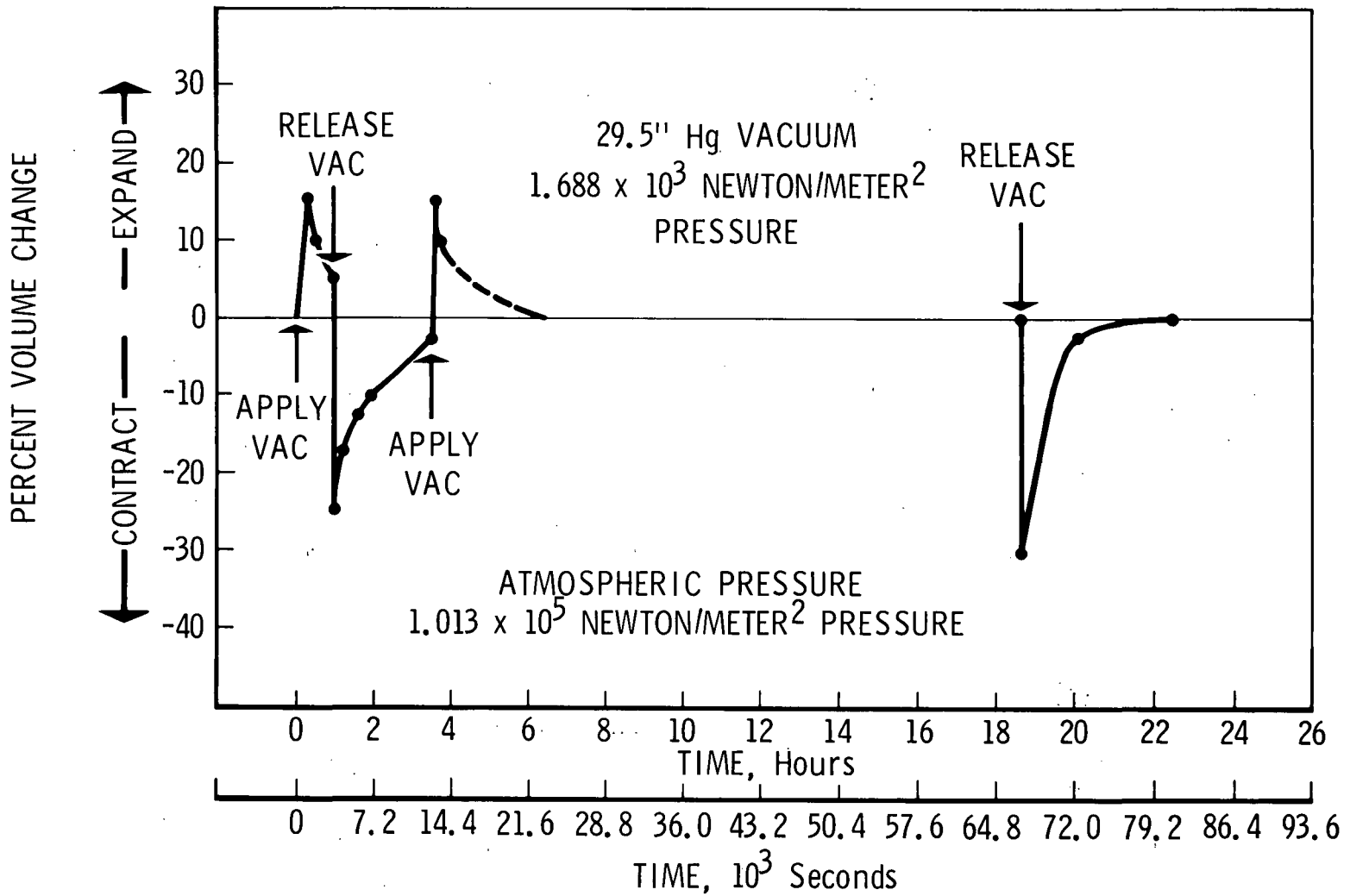
Figure 4

DENSITY OF ADHESIVE SYSTEMS
(Figure 5)

Density of the adhesive systems are tabulated in Figure 5. These data were determined at room conditions using the hydrostatic method described in ASTM-D-297, Section 17(C). GE RTV-560 has the highest and RM/RL-1973 the lowest density. Since the RM/RL-1973 must be bonded to substrates with one of the solid RTV adhesives, this adds to its density, e.g., in a 1.8×10^{-3} m (.070 in.) bond line, the GE RTV-560 increases the density of the RL-1973/GE RTV-560 system by 50 percent. Of course, in thicker bond lines the same weight of GE RTV-560 would be used, thus the added density would not be as great in terms of percent increase.

DENSITY OF ADHESIVE SYSTEMS

ADHESIVE	DENSITY	
	kg/m^3	(gm/cc)
GE RTV 560	1400	(1.40)
DC 93-046	1080	(1.08)
MMC SLA-561	1050	(1.05)
RM/RL-1973	300	(.30)
RL-1973/GE RTV 560 (1.8 x 10^{-3}m (.070") Bond Line	460	(.46)

Figure 5

947

TENSILE MODULUS CAMERA TEST SETUP
(Figure 6)

As noted in Figure 6, tensile modulus was determined from flat strips of material .00254 m (0.1 in.) thick, 0.33 m (12 in.) long, and 0.064 m (2.5 in.) wide with 0.025 m (1 in.) wide aluminum doublers bonded on each end. The test section was .05 m (2 in.) by 0.13 m (5 in.) in the center of the specimen face bench marked with 0.0005 m (0.02 in.) diameter dots. The dots were applied using a template and white colored GE RTV-102 adhesive.

During testing, photographs at incremental loadings were made using a 35 mm Beattie-Colman Veritron camera tied in electrically with the device on the Scott tester, Figure 6, that makes specific load indicating "blips" on the chart paper. Using this method a sequence of photographs were obtained that could be related directly to the sequence of "blips" (stress values) on the chart paper.

These photographs were later measured for calculation of tensile modulus values. Axial measurements and corresponding stress values were fed directly into a Hewlett-Packard 2116A computer programmed to give a print out of moduli along with a "least squares" value (the slope of the least-squares linear line through the stress-strain points). Transverse measurements were also made at the same time for determination of Poisson's ratio.

TENSILE MODULUS CAMERA TEST SETUP
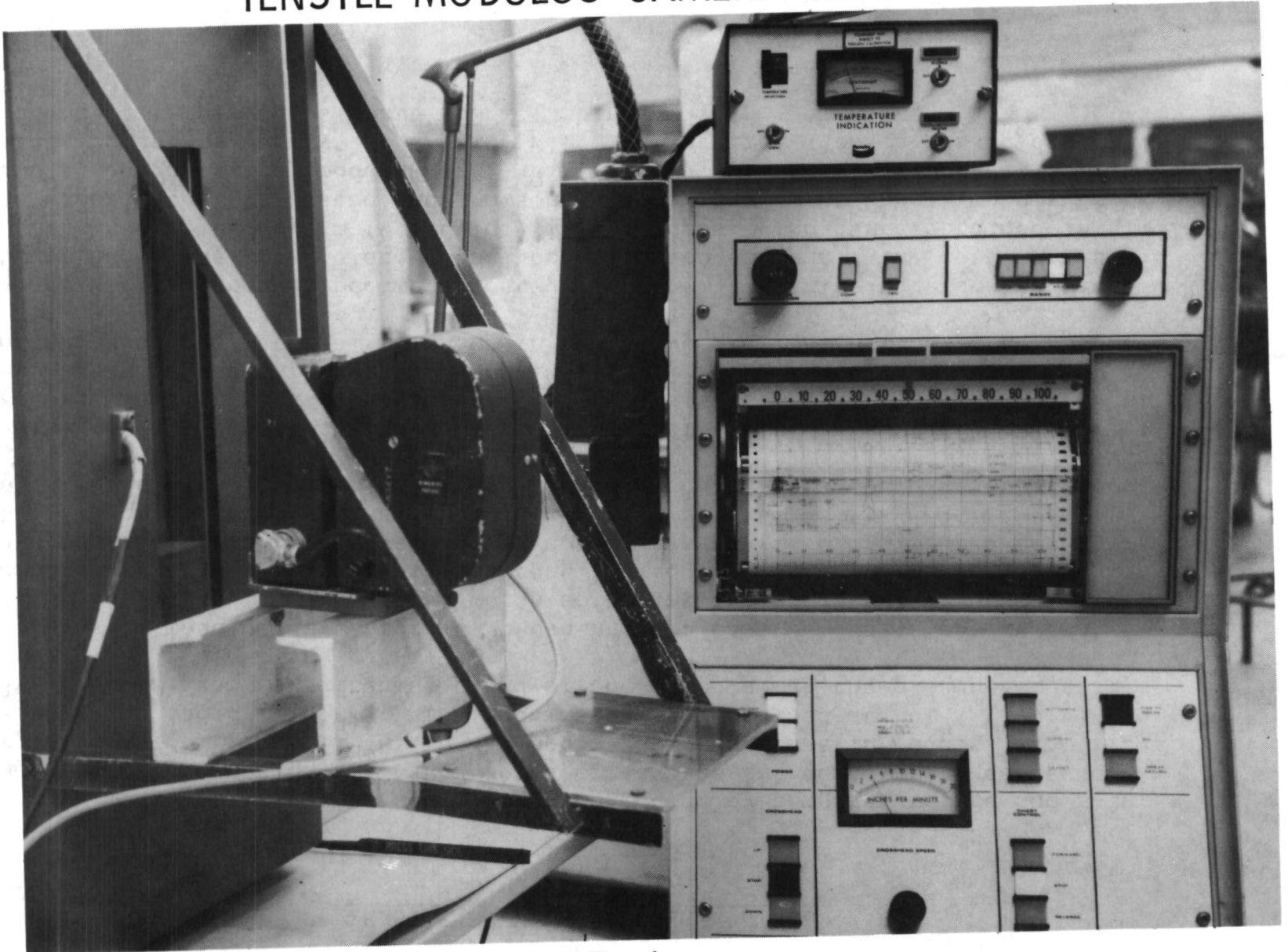
Figure 6

TENSILE MODULUS VS. TEMPERATURE
(Figure 7)

Tensile moduli of the four adhesives as affected by temperature are shown in Figure 7. The modulus of GE RTV-560 decreases as the temperature decreases from 450^OK (350^OF) to 219^OK (-65^OF) and a rapid increase in modulus from 172^OK (-150^OF) to 158^OK (-175^OF). The modulus values obtained at 561^OK (550^OF) and 589^OK (600^OF) show a softening trend of the material at these temperatures.

The tensile modulus curve for DC 93-046 has the same general shape as that for GE RTV-560. The temperature at which softening begins is 422^OK (300^OF) and the temperature at which the rapid increase in modulus begins is 219^OK (-65^OF). This material deteriorated and could not be tested at 561^OK (550^OF) and 589^OK (600^OF). Also, the strains developed in the material as it cooled to 105^OK (-270^OF) caused the specimens to crack and no data could be obtained.

The curve for MMC SLA-561 is similar to those of the other two materials and shows a decrease in modulus as the temperature decreases from 450^OK (350^OF) to 219^OK (-65^OF) and a rapid increase in modulus from 172^OK (-150^OF) to 144^OK (-200^OF). Softening of the material is shown in the curve from 561^OK (550^OF) to 589^OK (600^OF).

The RM/RL-1973 sponge specimens tested for tensile modulus were coated with GE RTV-560 on each face to simulate actual bond line conditions. The coating was 0.00013 m (0.005 in.) to 0.00025 m (0.010 in.) in thickness. The curve obtained is similar to the other materials tested and shows a minimum modulus at approximately 366^OK (200^OF) and a maximum modulus at 144^OK (-200^OF). The rapid increase in modulus beings at approximately 172^OK (-150^OF). The material shows a marked drop in modulus at temperatures above 450^OK (350^OF).

TENSILE MODULUS VS. TEMPERATURE
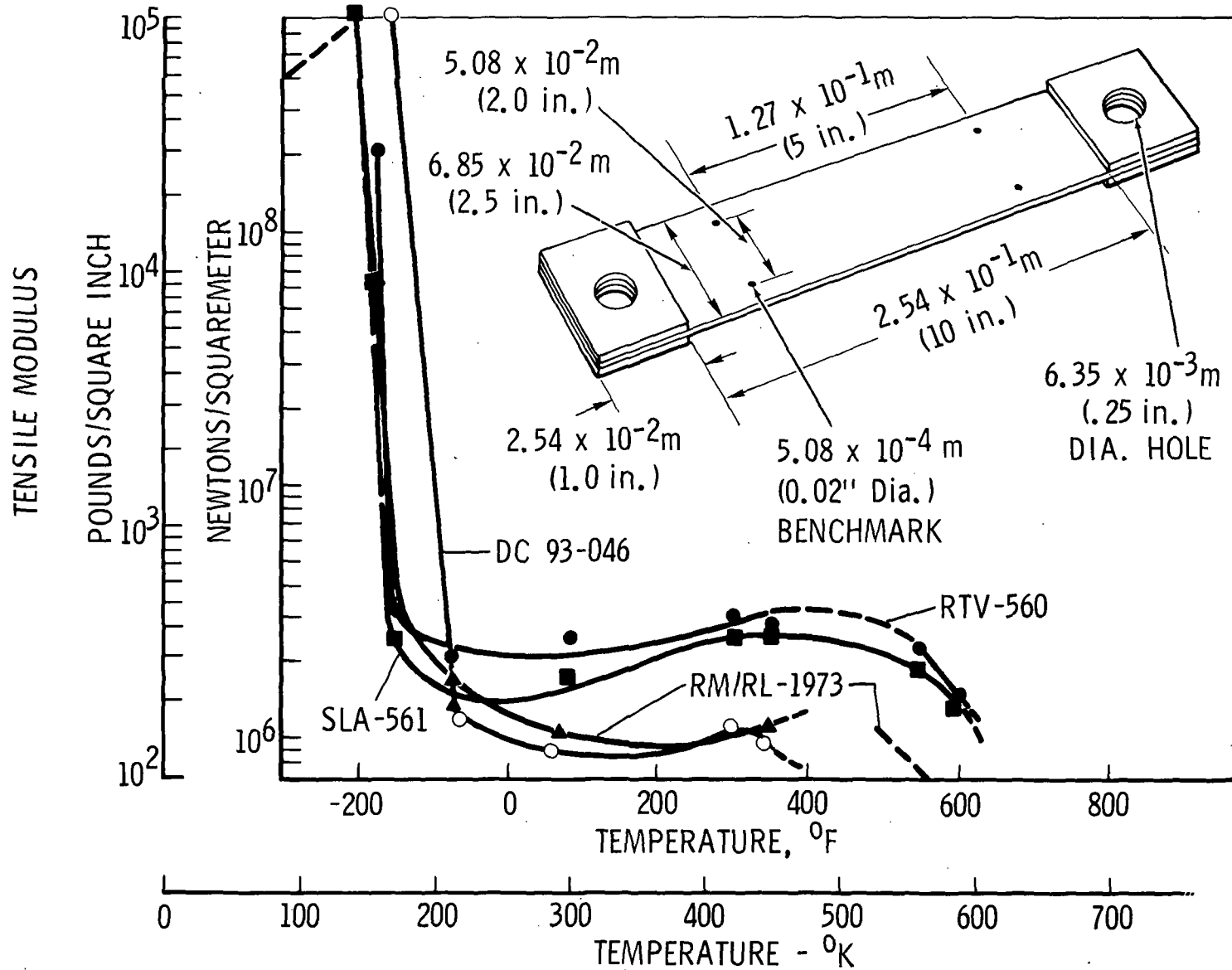
Figure 7

TORSIONAL SHEAR MODULUS VS. TEMPERATURE
(Figure 8)

Shear modulus tests were conducted on double overlap shear specimens as shown in Figure 8. The bond line thickness was 0.006 m (0.25 in.). The specimens were pinned through the holes at each end and load was applied through the center hole. A load deflection curve was obtained during testing, the slope of which was used for calculating shear modulus.

The shear modulus curves are of the same general form as the tensile modulus curves. GE RTV-560 shows a decrease in shear modulus as the temperature decreases to room temperature, and a rapid increase in modulus from 172°K (-150°F) to 158°K (-175°F) followed by a decrease in modulus to 105°K (-270°F). Softening of the material is shown by the break in the curve above 450°K (350°F).

DC 93-046 shows a drop in modulus above 422°K (300°F) and a rapid increase in modulus from 228°K to 144°K (-200°F). This material has the highest glass transition temperature of the four materials tested.

MMC SLA-561 shows a decrease from 422°K (300°F) to 255°K (0°F) and a rapid increase in modulus from 172°K (-150°F) to 144°K (-200°F) followed by a decrease in modulus below 144°K (-200°F). Softening of the material begins at approximately 450°K (350°F).

The RM/RL-1973 sponge shows a relatively constant modulus from 422°K (300°F) to 219°K (-65°F) followed by a sharp increase from 172°K (-150°F) to 144°K (-200°F). The modulus then decreases between 144°K (-200°F) and 105°K (-270°F). A distinct drop in modulus is shown by the curve above 422°K (300°F). RM/RL-1973 exhibits the lowest modulus of the four materials tested.

TORSIONAL SHEAR MODULUS VS. TEMPERATURE

Figure 8

<u>COMPRESSION MODULUS VS. TEMPERATURE</u>
(Figure 9)

Elevated temperatures were extremely detrimental to the thick bodied compression specimens, particularly since 1800 seconds (30 minutes) to 3600 seconds (one hour) were required to bring the specimens to ambient temperature. At 450^OK (350^OF) and above the DC 93-046 sponged internally. At 561^OK (550^OF) and $58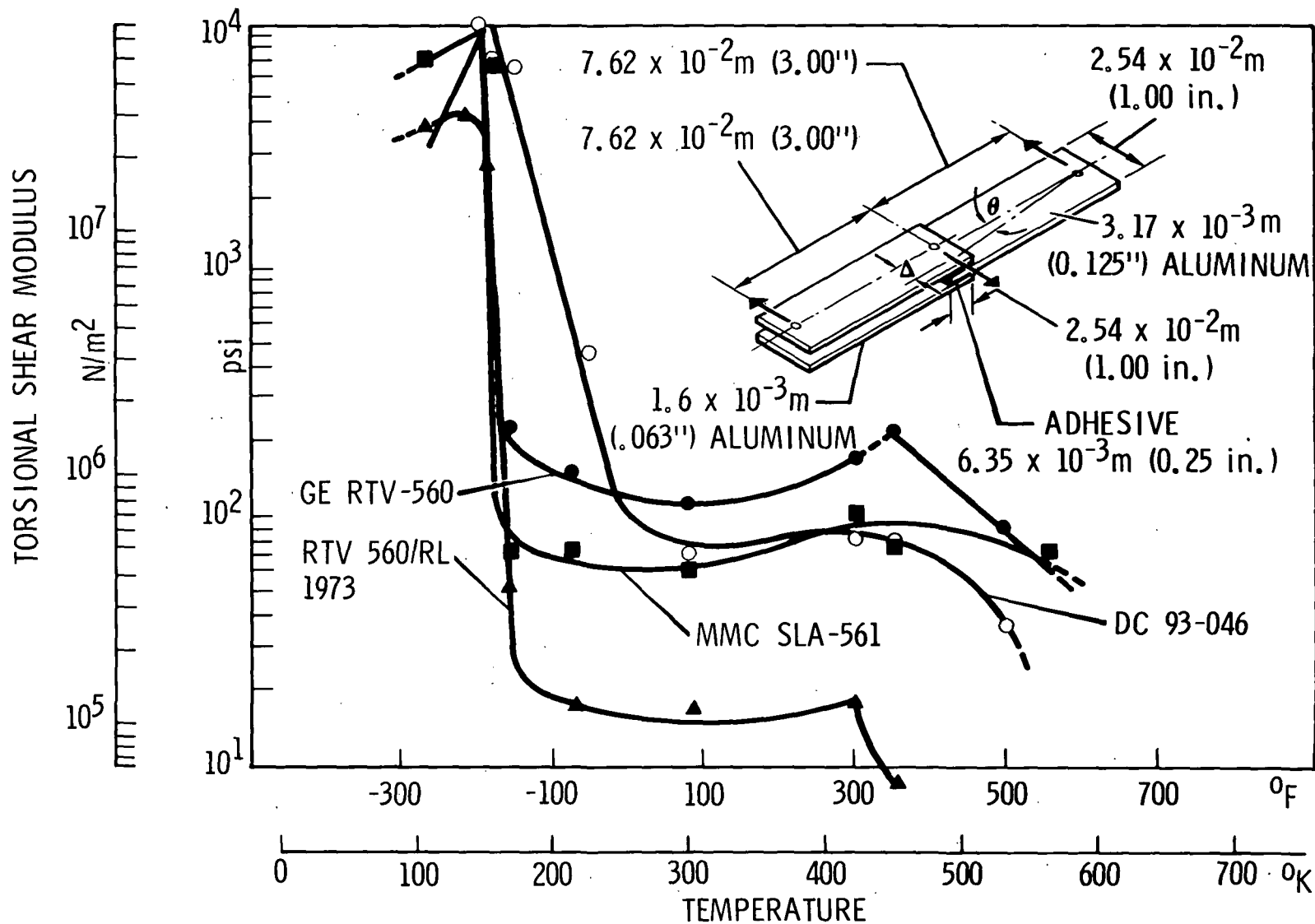9^O$K ($600^O$F) the GE RTV-560 also sponged internally while the SLA-561 cracked. At temperatures above 450^OK (350^OF) the RL-1973 sponge expanded and buckled under load. Because of these effects, data at temperatures above 450^OK (350^OF) were unobtainable. Deformation of specimens under incremental compression loads was taken from photographs the same as the tensile modulus specimens.

The curves shown in **Figure 9** for compression moduli are similar to those obtained for tensile moduli. GE RTV-560 shows a decrease in modulus from room temperature to 219^OK (-65^OF) then a rapid increase in modulus from 172^OK (-150^OF) to 144^OK (-200^OF) followed by a decrease in modulus below 144^OK (-200^OF).

DC 93-046 shows an increase in modulus with decrease in temperature. Compression tests on this material could not be conducted at temperatures below 158^OK (-175^OF). At 144^OK (-200^OF) the stresses developed in this material were so high that when the door of the environmental chamber was opened to insert additional specimens the slight thermal shock caused the cold specimens to fracture.

The curve for MMC SLA-561 is similar to that of GE RTV-560. It shows a decrease in modulus from room temperature to 219^OK (-65^OF), a rapid increase from 172^OK (-150^OF) to 144^OK (-200^OF), and another decrease below 144^OK (-200^OF). Softening of the material occurs above 450^OK (350^OF).

RM/RL-1973 shows a decrease in modulus as the temperature decreases from 450^OK (350^OF) to 219^OK (-65^OF) followed by a rapid increase in modulus from 172^OK (-150^OF) to 105^OK (-270^OF). Softening begins at 450^OK (350^OF).
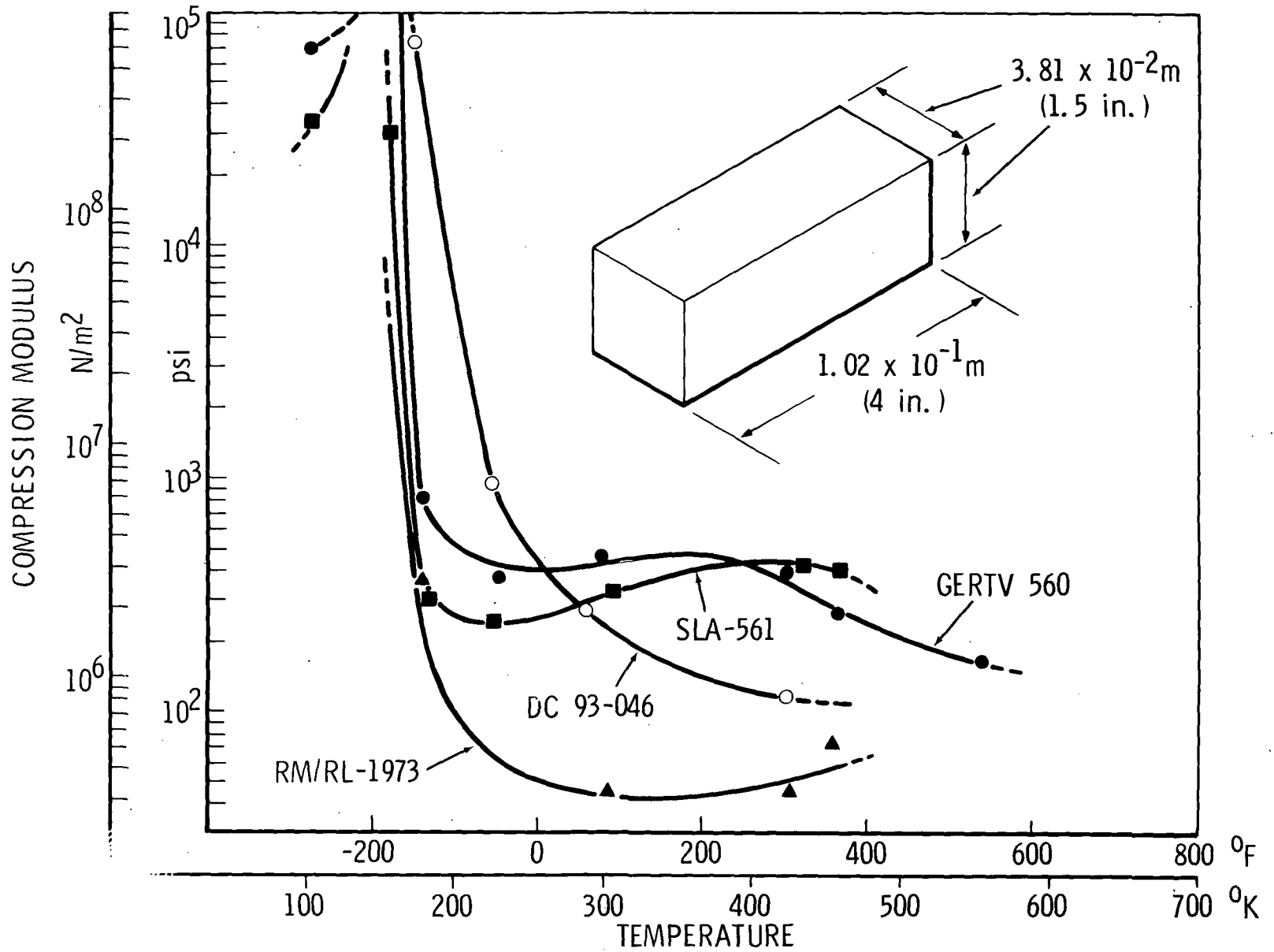
Figure 9

STRESS RELAXATION AT CONSTANT STRAIN
(Figure 10)

Stress relaxation of GE RTV-560 under constant strain at 297, 158, 144, and 105°K is shown in **Figure 10**. Band shaped specimens used in this test were .1016 m (4.0 in.) in diameter with a rectangular cross section, .00635 m (.25 in.) wide and .003717 m (.125 in.) thick. At 297 and 158°K (75 and -175°F) the specimens were subjected to a constant strain of 10 percent elongation. At 144 and 105°K (-200 and -270°F) the GE RTV-560 was too stiff and brittle to withstand 10 percent elongation; therefore, a constant strain of 0.4 percent elongation was used.

An interesting point observed in these plots of stress vs. time at constant strain is that the greatest stress relaxation, 87 percent, occurs at the glass transition temperature, 158°K (-175°F). Above and below this temperature, percent stress relaxation at constant strain is less. Moreover, it will be noted that the majority of the stress relaxation at 158°K (-175°F) occurs in the first 300 seconds (5 min.) whereas at the other test temperature the majority of the stress relaxation occurs over the first 3600 seconds (1 hr.).

STRESS RELAXATION AT CONSTANT STRAIN OF GE RTV-560

105^0K (-270^{0}F) 0.4%E

144^0K (-200^{0}F) 0.4%E

297^0K (RT) 10%E

158^0K (-175^{0}F) 10%E

STRESS psi

N/m^2

14×10^6

12×10^6

8×10^6

4×10^6

2400

2000

1600

1200

800

400

0

MINUTES

20   40   60   80   100   120   140   160   180

SECONDS

0   1200   2400   3600   4800   6000   7200   8400   9600   10,800
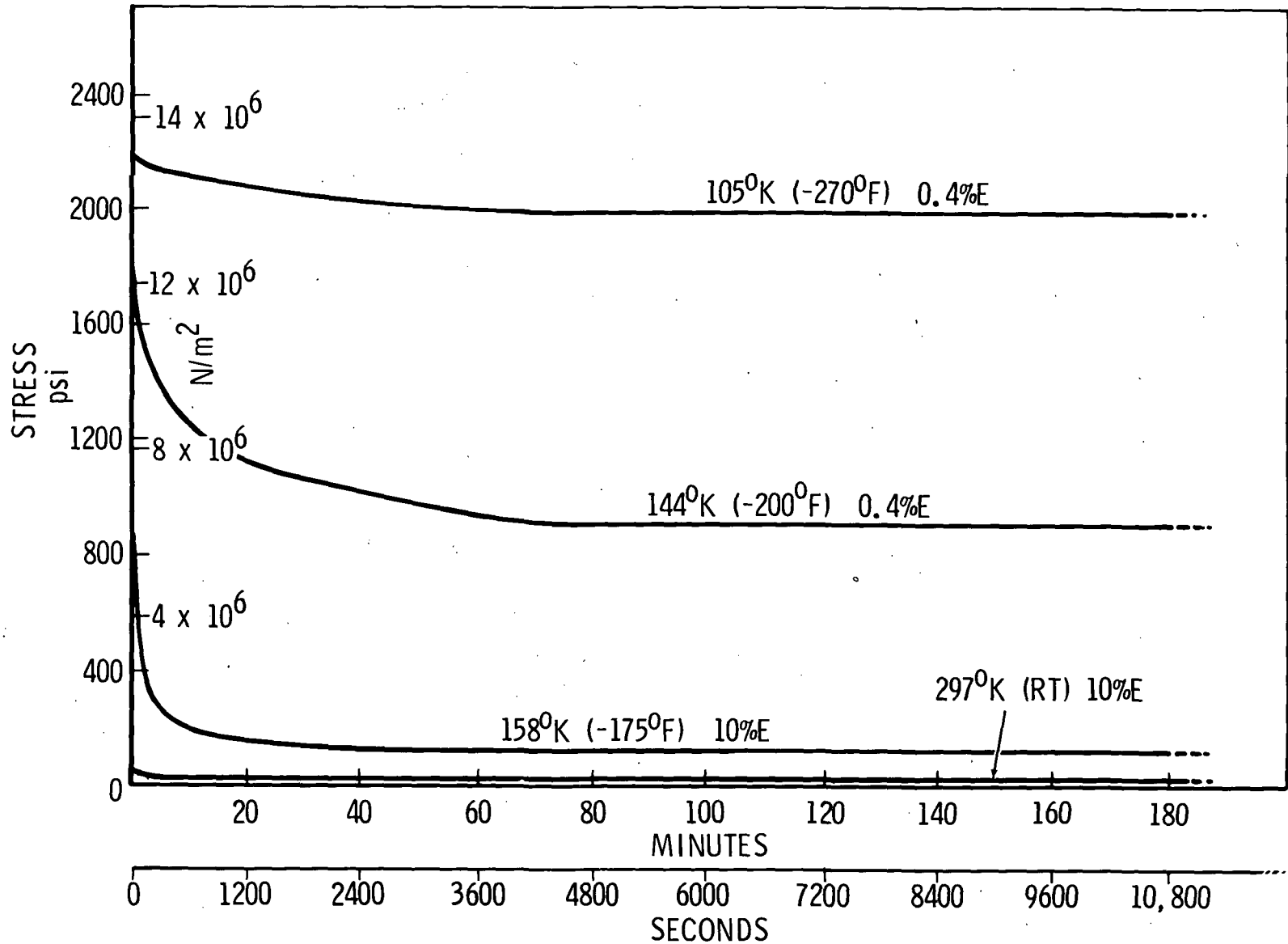
Figure 10

LINEAR THERMAL EXPANSION VS. TEMPERATURE
(Figure 11)

Linear thermal expansion of the four adhesives is shown in Figure 11 over a temperature range of 106 to 535°K (-270 to 500°F). The three solid adhesives GE RTV-560, DC 93-046 and MMC SLA-561 show approximately the same thermal expansion over the test temperature range. RM/RL-1973 sponge follows the same trend as the solid adhesives down to 297°K (75°F), then it shows an increased rate of contraction.

These data were determined with a Perkin-Elmer Differential Scanning Calorimeter, model DSC-1B with its accessory Thermomechanical Analyzer, model TMS-1. The TMS-1 uses a sample .0127 m (.5 in.) long x .0032 (.125 in.) to .0064 m (.25 in.) in diameter. This instrument with a floating extensometer probe eliminates sample indentation by the probe.

Glass transition temperature (Tg), 158.3°K (-175°F) is easily seen for the GE RTV-560 by the sharp break in the curve, whereas Tg for the other three adhesive systems are not so sharp and readily apparent.

LINEAR THERMAL EXPANSION VS. TEMPERATURE
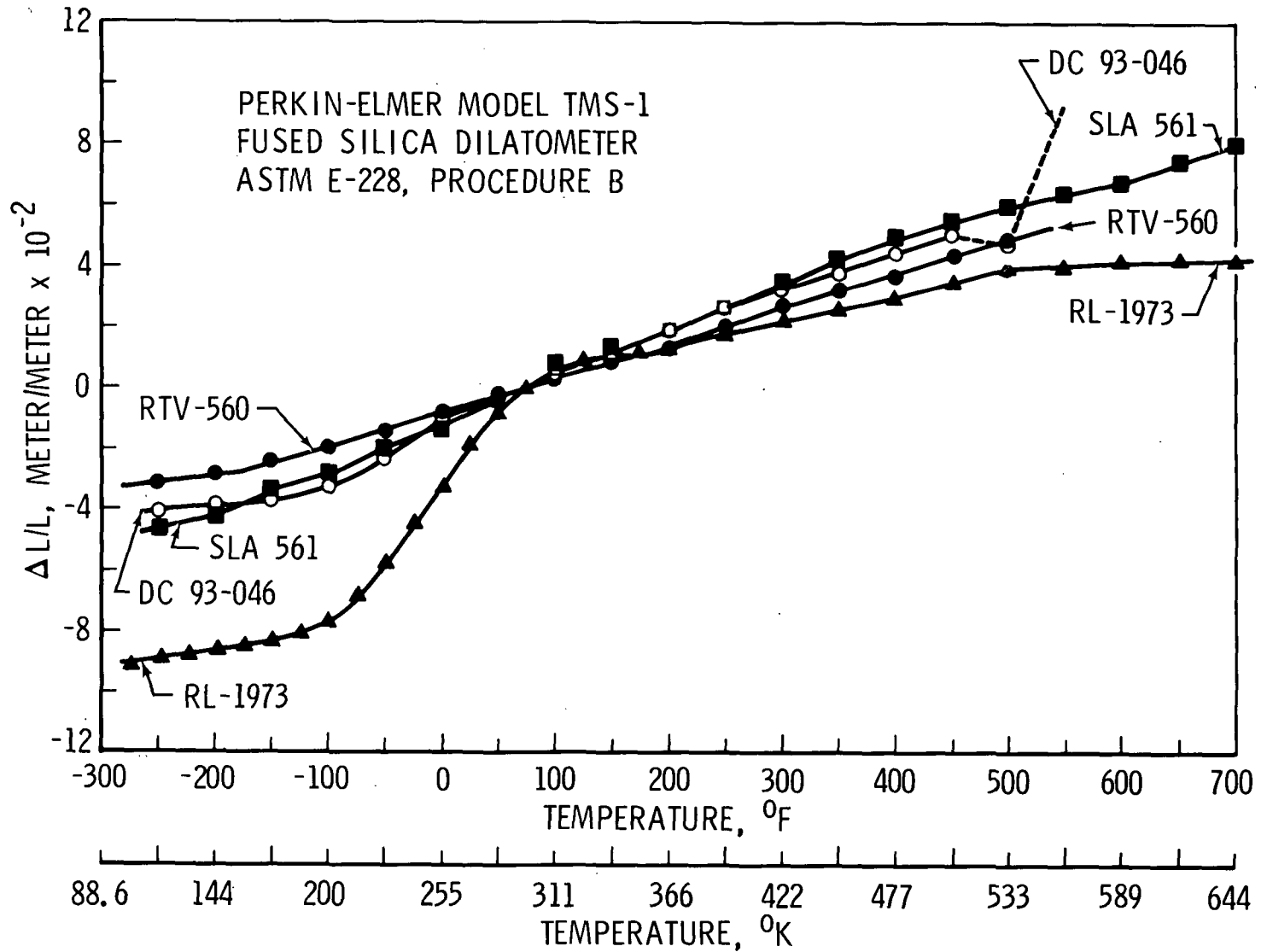
Figure 11

THERMAL CONDUCTIVITY VS. MEAN TEMPERATURE
(Figure 12)

Thermal conductivity of the four adhesives is shown in Figure 12 over a mean temperature range of 88.8 to $535^{O}K$ (-300 to $500^{O}F$). GE RTV-560 has the highest and RM/RL-1973 has the lowest thermal conductivity. This is to be expected based on density; i.e., the more dense the material the greater the thermal conductivity.

These data were obtained using the guarded hot plate method specified in ASTM C-177. One matched pair of specimens was used for each material. The specimens were .3048 m (12 inches) square by .00635 m (1/4 inch) thick. The center .2 x .2 m (8 x 8 inch) area represented the test section, with and the guard section comprised the remainder of the specimen, a .051 m (2 in.) wide band around outer edge. The test and guard heaters of the hot plate were of identical dimension, and a differential thermopile was used to maintain the guard section at the same temperature as the test section.

Glass transition points of the four adhesives are more discernible in this family of curves than those showing thermal expansion. Tg for GE RTV-560, MMC SLA-561, and RM-RL-1973 are all approximately $158^{O}K$ (-$175^{O}F$). Tg for DC-93-046 is about $228^{O}K$ (-$50^{O}F$).

THERMAL CONDUCTIVITY VS. MEAN TEMPERATURE
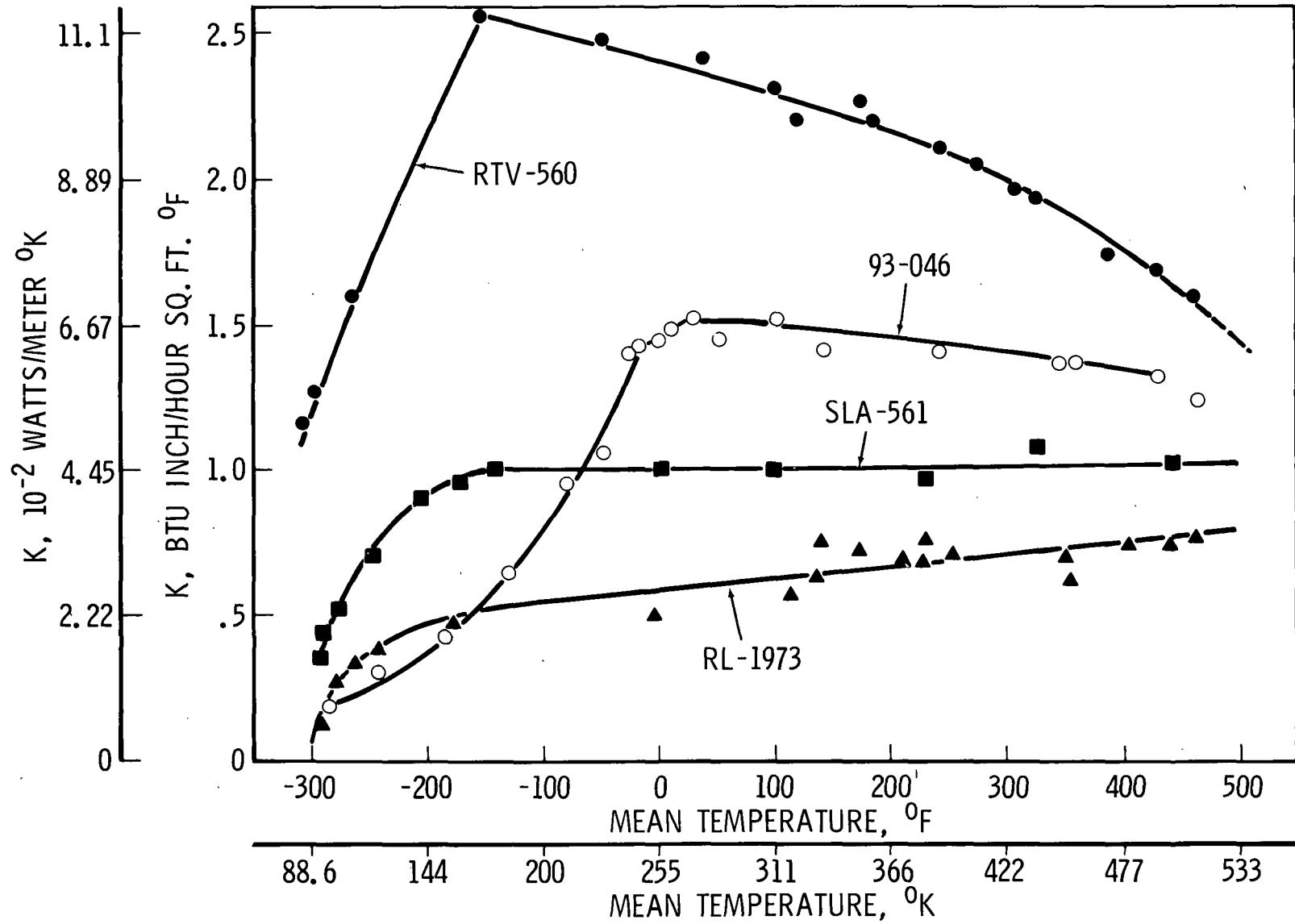
Figure 12

CONCLUSIONS
(Figure 13)

Advantages and disadvantages of the four adhesive systems characterized in this program are shown in Figure 13. In addition to these desirable and undesirable characteristics of the adhesives the following conclusions can be drawn from this extensive development and testing program:

1. An adhesive system comprising a closed cell silicone rubber sponge, RM/RL-1973, bonded to substrates with thin bond lines of GE RTV 560 exhibits density and modulus values approximately one third that of the solid RTV silicone adhesives.

2. Utilization of glass or phenolic microballoons as fillers in RTV silicone adhesives reduce density but increase modulus of the vulcanized materials.

3. The silicone elastomer based adhesives appear to be complex systems rather than homogeneous, isotropic materials. Tensile, shear, and compression properties plotted versus temperature verify this conjecture. It is also substantiated by the erratic stress relaxation behavior of the adhesives under constant strain.

4. Constant strain-stress relaxation tests on GE RTV-560 produce interesting data in that stress relaxation is most pronounced near the glass transition temperature. The same trend is apparent with the other three adhesive systems. At temperatures above and below Tg, percent stress relaxation at constant strain is less.

CONCLUSIONS

ADHESIVE	ADVANTAGES	DISADVANTAGES
GE RTV 560	• EASY PROCESSING • BEST LOW TEMPERATURE PROPERTIES • HIGHEST STRENGTH AT INTERMEDIATE TEMP	• HIGHEST DENSITY • HIGHEST MODULUS • THICK SECTIONS BLISTER INTERNALLY AT 561^0K (550^0F)
DC 93-046	• SECOND LOWEST MODULUS	• VISCOUS, DIFFICULT TO PROCESS • HIGHEST GLASS TRANSITION TEMPERATURE • CRACKS ON THERMAL SHOCK AT 144^0K (-200^0F) • THICK SECTIONS REVERT AND BLISTER INTERNALLY AT 561^0K (550^0F)
SLA-561	• BEST HIGH TEMP. STRENGTH • EASY PROCESSING, EASIEST TO DEGAS	• WEAK IN SHEAR STRENGTH • THICK SECTIONS CRACK AT 561^0K (550^0F) • FRESH SLA-561 HAS LOW ADHESION TO CURED SLA-561
RL-1973/ GE RTV 560	• LOWEST DENSITY • LOWEST MODULUS	• VOLUME SENSITIVE TO PRESSURE CHANGE • LOWEST STRENGTH • MUST BE SLICED TO DESIRED THICKNESS • COMPATIBILITY WITH BASE ADHESIVE MUST BE DETERMINED

963

Figure 13

REFERENCES

1. Hiltz, A. A., Thibault, H. G., and Curtis, F. P., "Bonding of Reusable Surface Insulation," Paper presented at National SAMPE Technical Conference, Huntsville, Ala., 5-7 October 1971.

2. Hess, T. E., and Michalak, R. J., "Reusable Surface Insulation Thermal Protection System Development Program," Final Report NAS9-12084 (NASA, MSC) General Electric, Philadelphia, Pa.,   May 1972.

3. Michalak, R. J., Hess, T. E., and Gluck, R. L., "Structural Design Aspects of Reusable Surface Insulation Thermal Protection Systems," AIAA Paper No. 72-372, April, 1972.

964

EFFECT OF OPTICAL PROPERTIES

ON THERMAL DESIGN

by

C.L. Statham and R.T. Tsutsui

North American Rockwell

Downey, California

SUBSYSTEM TEMPERATURE LIMITS
(Figure 1)

When considering the effect of external surface optical properties, subsystems contained within the vehicle must be considered in addition to the thermal protection system. Representative subsystem temperature limits for orbital flight (long term) and entry transients (short term) are presented.

SUBSYSTEM TEMPERATURE LIMITS
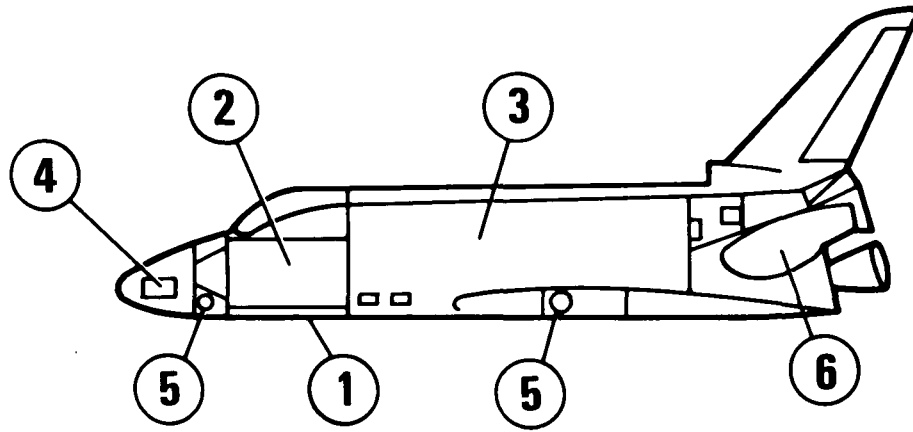
SUBSYSTEM	TEMPERATURE LIMITS ~ °K (°F)		
	MIN	MAX	
	ON-ORBIT	ON-ORBIT	ENTRY
① TPS (BONDLINE)	116 (-250)	—	450 (350)
② CABIN (WALLS)	289 (60)	318 (113)	322 (120)
③ CARGO BAY WALLS	200 (-100)	339 (150)	366 (200)
④ FWD RCS PROP. TANKS	277 (40)	325 (125)	339 (150)
⑤ LANDING GEAR TIRES	219 (-65)	394 (250)	422 (300)
⑥ OMS PROP. TANKS	277 (40)	325 (125)	339 (150)

Figure 1

ALUMINUM BONDLINE TEMPERATURE EXTREMES VS β ANGLE
(Figure 2)

The orbital mission phase requires that the vehicle be unrestricted in attitude relative to thermal requirements. In addition, the vehicle must be capable of flying in high inclination orbits. The effect of a long duration cold or hot soak (steady state) on the TPS bondline temperature is presented as a function of β angle. As it can be seen, the high β angle flights (at high inclination orbits) represent the hottest and coldest conditions for design. It should also be noted that the value of the solar absorptance to emittance ratio (α_s/ϵ) is the prime factor in limiting the hot soak temperatures, whereas the emittance alone is the prime factor for limiting the cold soak temperature extremes.

ALUMINUM BONDLINE TEMPERATURE
EXTREMES VS β ANGLE
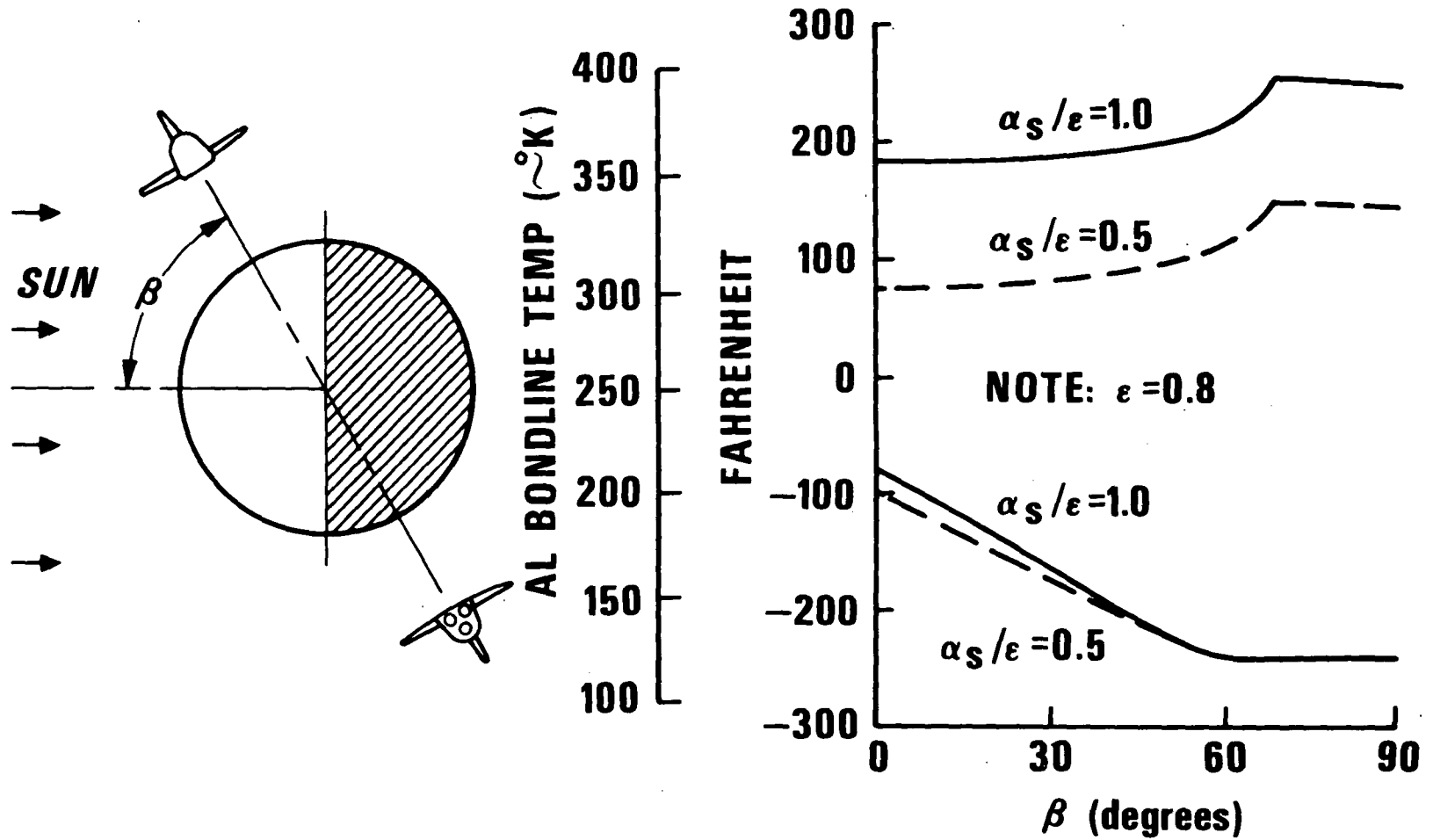
Figure 2

TRANSIENT ORBITAL HOT SOAK

(Figure 3)

Transient response of the bondline to hot soak at high orbit β angles (e.g., β = 90°) are presented for representative thin and thick locations for two values of surface coatings. The thickness at location A is 1.27 cm (.5 inch) and the thickness at location B is 4.83 cm (1.9 inch). As expected, the thickness of RSI has a significant influence on the response. In addition, the design of the interior subsystem thermal control system (TCS) can have a significant influence on the TPS transient response rate. For the values shown, the interior subsystems are thermally isolated from the TPS.

TRANSIENT ORBITAL HOT SOAK
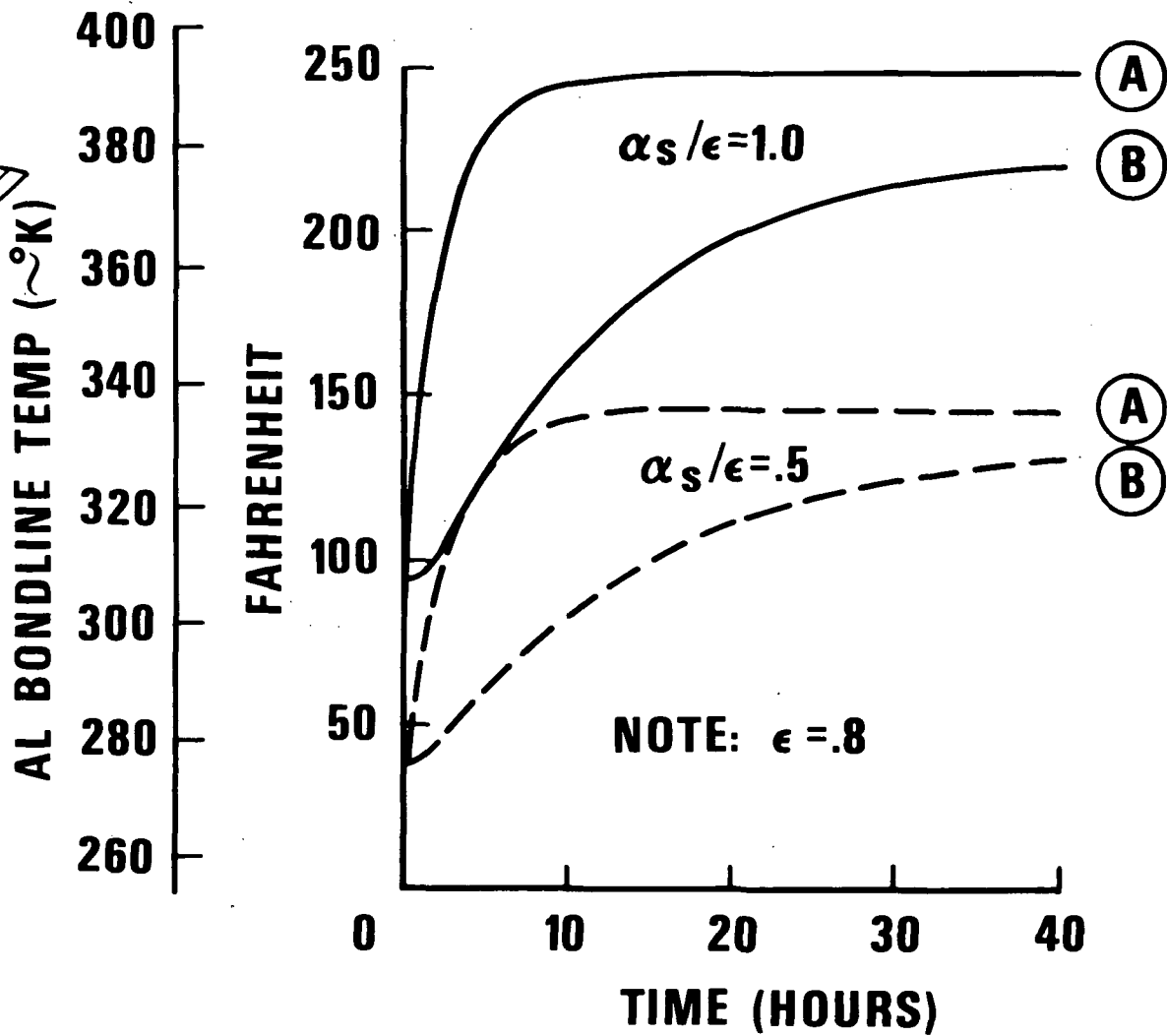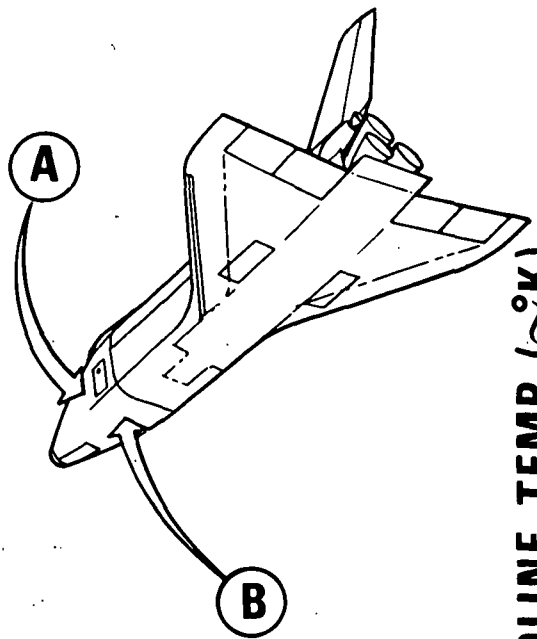
Figure 3

TPS WEIGHT SENSITIVITY TO α_s/ε

(Figure 4)

The sensitivity of the TPS weight to the external coating α_s/ε property has been computed for the orbiter vehicle. The orbital attitude, entry heating history, and surface emittance were assumed constant. As it can be seen, the value of α_s/ε does have a significant influence on the TPS weight requirement. This effect of α_s/ε is primarily due to increased orbital pre-entry temperatures as α_s/ε increases. For the values shown, the coating properties are assumed constant over the total vehicle surface area.

TPS WEIGHT SENSITIVITY TO α_s/ϵ

$$W_{REF} \simeq 11350 \text{ KG} \quad (25000 \text{ LB})$$

α_s/ϵ
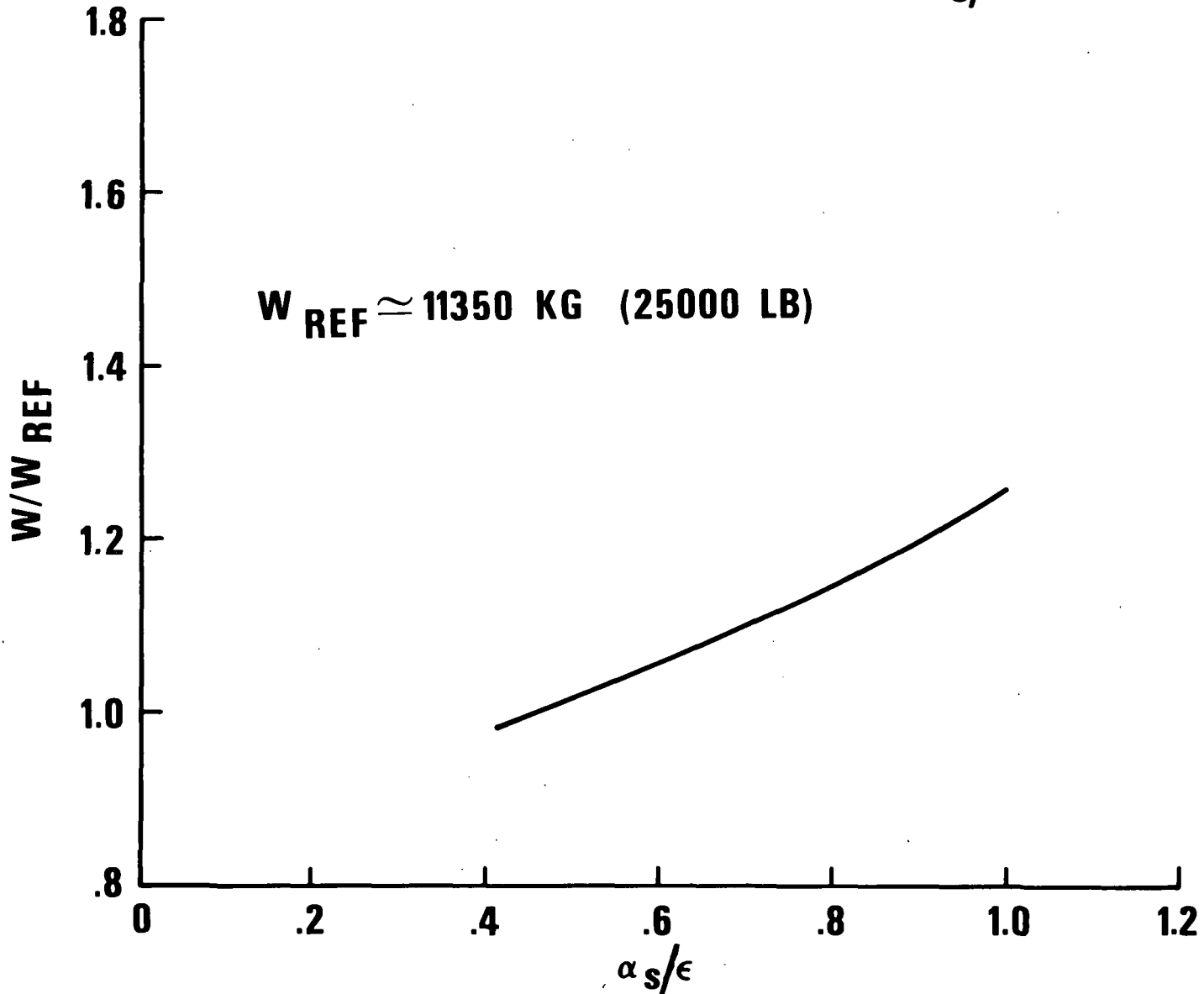
Figure 4

TCS WEIGHT SENSITIVITY TO α_s/ε

(Figure 5)

Corresponding to the TPS sensitivity, the subsystem thermal control system (TCS) has a similar sensitivity to the coating α_s/ε ratio. As in the case of the TPS, the TCS weight increase shown with increasing α_s/ε ratio reflects the higher orbital temperatures that may be attained prior to entry heating. It should be noted that above an α_s/ε ratio of approximately 0.8, active cooling of additional large subsystems may be required.

TCS WEIGHT SENSITIVITY TO α_s/ϵ

MAY REQUIRE ACTIVE
COOLING FOR $\alpha_s/\epsilon > 0.8$

$W_{REF} \simeq 2000$ KG (4400 LB)
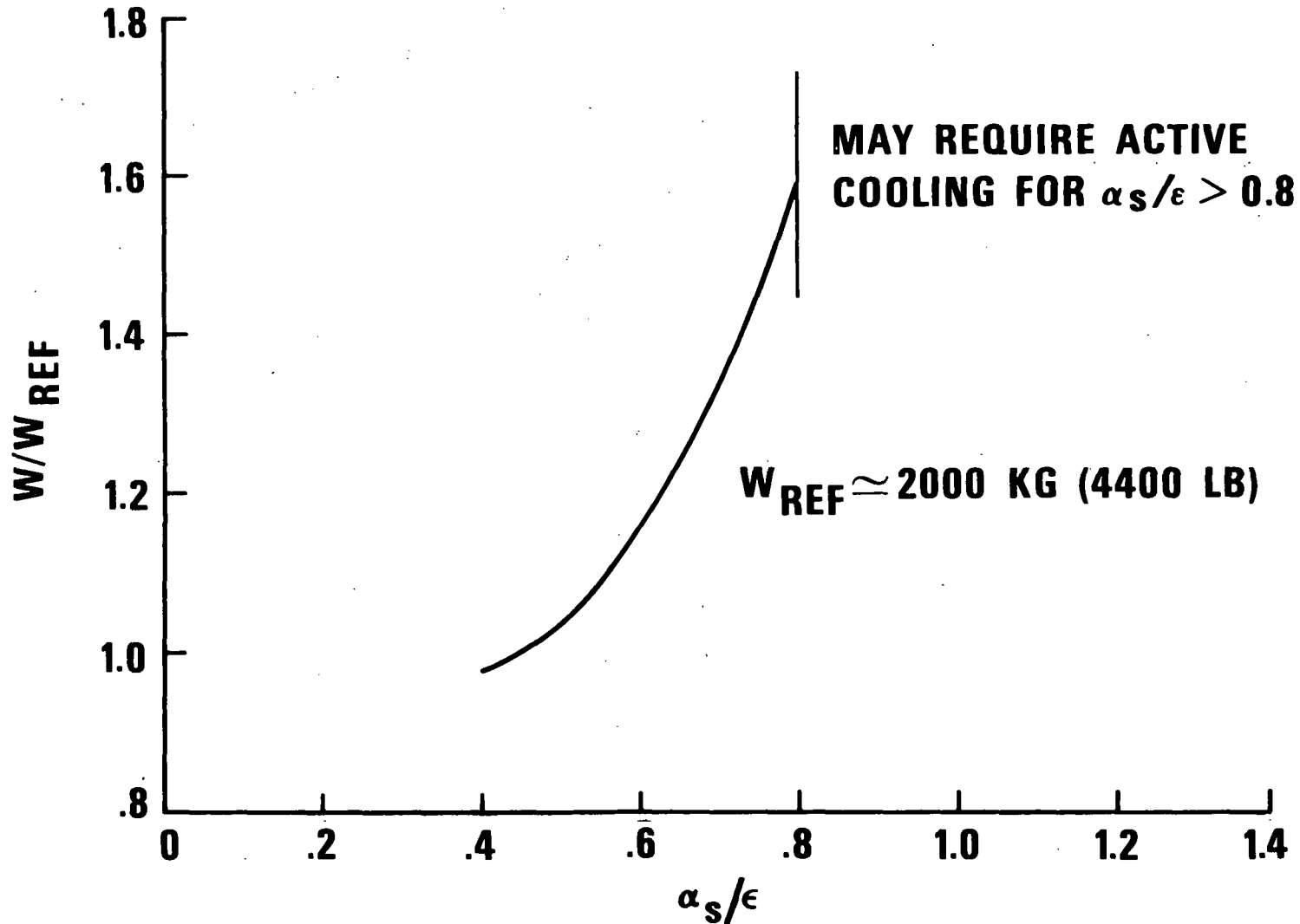
Figure 5

975

MAXIMUM TPS SURFACE TEMPERATURES

(LAUNCH AND ENTRY)

(Figure 6)

Since the degree of difficulty in providing reusable surface optical coatings is
significantly influenced by the maximum expected temperature exposure, a study has been
performed to evaluate a partially coated vehicle surface. The maximum local temperatures
used in this evaluation are presented as being representative of the maximum value
attained during either boost or entry heating conditions. As it can be seen, there is a
significant area of the vehicle that remains below 811°K (1000°F) (50% of the total).
Conversely, only 25% of the total surface reaches temperatures in excess of 1310°K
(1900°F).

MAXIMUM TPS SURFACE TEMPERATURES
(LAUNCH AND ENTRY)

1227°K(1750°F)

1310°K(1900°F)   616°K(650°F)

727°K(850°F)

727°K(850°F)

1532°K(2300°F)

1644°K(2500°F)

727°K(850°F)

616°K(650°F)

1532°K(2300°F)

1644°K(2500°F)

1310°K(1900°F)

1227°K(1750°F)

1227°K(1750°F)

727°K(850°F)

1310°K(1900°F)

1310°K(1900°F)

1532°K(2300°F)

1644°K(2500°F)

1310°K(1900°F)

1227°K(1750°F)

616°K(650°F)

727°K(850°F)

727°K(850°F)

616°K(650°F)

977

Figure 6

TPS/TCS WEIGHT SENSITIVITY TO SURFACE

AREA COVERED WITH COATING

(Figure 7)

To evaluate the effectiveness of a partially coated surface, it has been assumed that a coating with $\alpha_s/\varepsilon = 0.5$, $\varepsilon = .8$ properties could be maintained only up to a given temperature. The range of temperatures considered for the coating maintainability was taken from 477°K (400°F) to 1644°K (2500°F). The surface area below a given maximum temperature was obtained from figure 6 and is shown on the double abscissia of figure 7. The effect on the combined TPS and TCS weight is then presented as a function of the percent of surface area coated and the maximum entry (or launch) temperature allowable for a coated surface. All surfaces that are not coated are assumed to have an $\alpha_s/\varepsilon = 1.0$.

TPS/TCS WEIGHT SENSITIVITY TO
SURFACE AREA COVERED WITH COATING

$$W_{Reference} \simeq 13350 \text{ KG } (29400 \text{ LB}) \text{ TPS+TCS}$$

y-axis: $\dfrac{\Delta \text{WEIGHT}_{TPS+TCS}}{W_{Reference}}$

x-axis: % OF SURFACE AREA COATED

$\leq$

T_{MAX} 477   616   811   1089   1644°K
(400)   (650)   (1000)   (1500)   (2500)°F
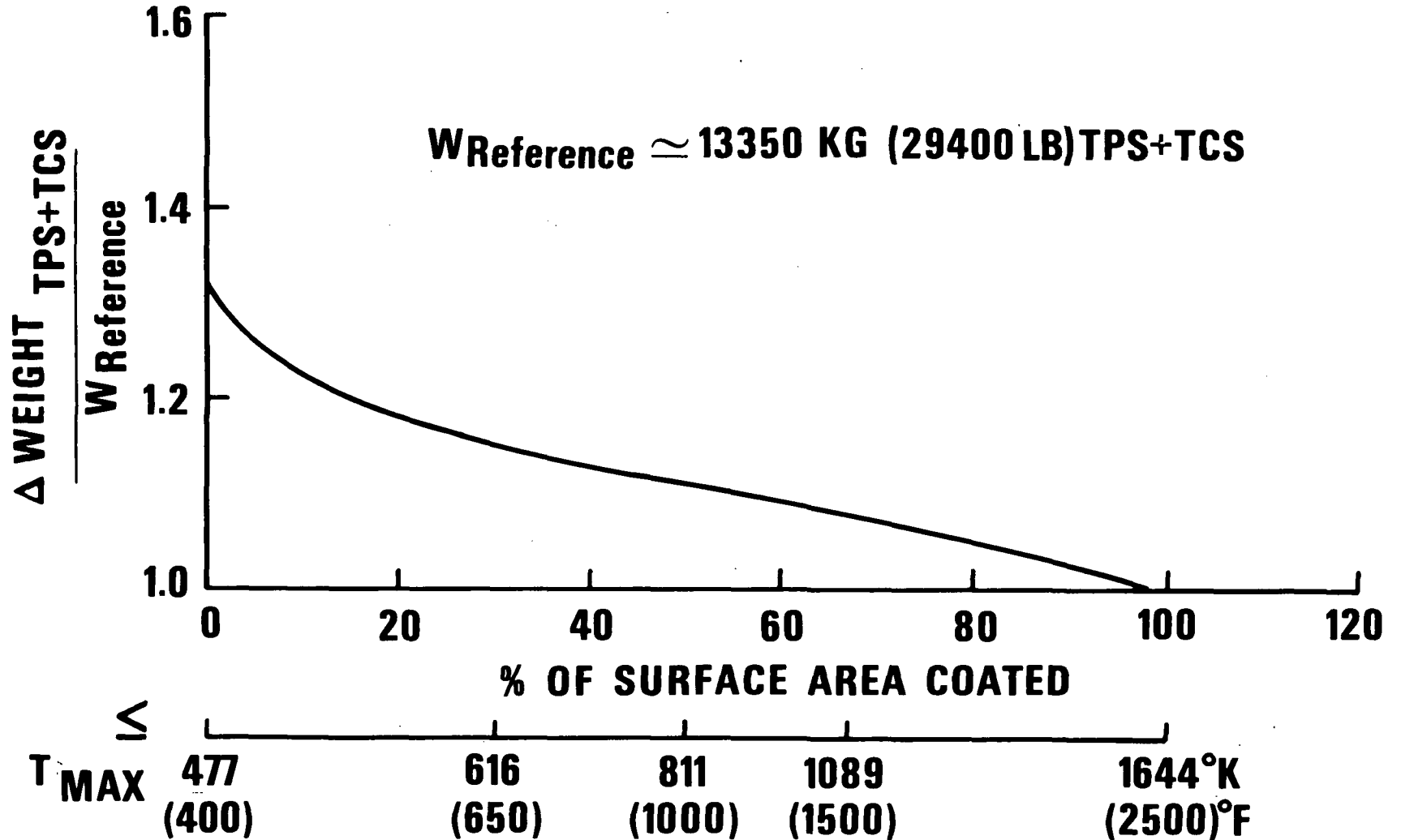
Figure 7

EFFECT OF OPTICAL PROPERTIES
ON THERMAL DESIGN

CONCLUSIONS

- LOW α_s/ϵ EXTERNAL COATINGS FOR ORBITAL CONDITIONS AND HIGH ϵ FOR ENTRY CONDITIONS PRODUCE THE MINIMUM TPS & TCS WEIGHTS.

- COATINGS WITH LOW α_s/ϵ PROPERTIES SHOULD BE APPLIED OVER THE MAXIMUM PRACTICAL AREA .

CLOSED-PORE INSULATION THERMAL PROTECTION SYSTEM
DESIGN CONCEPT DEVELOPMENT

A. Varisco and H.G. Harris

Grumman Aerospace Corporation

Bethpage, New York

INTRODUCTION

NASA, and MSC is particular, have demonstrated a desire to fully evaluate the nonmetallic reusable surface insulations for the thermal protection system of the Space Shuttle. Efforts to date have concentrated on fibrous materials requiring complex, brittle coatings to provide a water repellent surface and to produce the required emissivities. Additionally, the fibrous material's low strength complicates its attachment to the primary structure, wherein strain isolators and bonding are employed with all the associated inspection problems.

A project was initiated at Grumman to develop an insulating material that would not require any coating and would have sufficient strength to be mechanically fastened. This work led to the development of a unique closed-pore ceramic foam insulation (CPI) produced from low cost fly ash cenospheres.

A NASA funded program was initiated with the following objectives:

- Characterization of the CPI material and definition of possible failure modes of the material system

- Development of promising CPI TPS concepts including integration to the vehicle and in-depth structural and thermal analysis

- Fabrication and test program to evaluate thermal and mechanical performance, thermal shock and reuse characteristics, and design details such as joints and seals.

Two basic design approaches were developed, bonded and mechanically fastened. A description of the concepts is presented in addition to fabrication and test results.

CPI MATERIAL DESIGN CHARACTERISTICS
(Figure 1)

A closed-pore ceramic foam insulation material (CPI) has been developed that offers potential for use as a reusable external heat shield for the Space Shuttle. The outstanding characteristics of the material are listed in figure 1.

Of primary significance is the material's overall <u>design flexibility</u>. CPI's good machinability, chemical stability, and superior mechanical properties offer a much greater potential for exploring unique attachment concepts or system tailoring than fibrous insulations. Various unique design concepts are possible with the material, some of which combine CPI with the fibrous insulations currently under development. Mechanical attachments in lieu of bonding are feasible with CPI. This would eliminate the difficult task of NDT inspection and provide a fail-safe surface in the event of surface tile failure.

CPI MATERIAL DESIGN CHARACTERISTICS

o RIGIDITY
      - EASILY HANDLED
      - HARD SURFACE

o MACHINEABLE
      - COMPLEX SHAPES
      - STEPS & GROOVES FOR SEALS
      - DESIGN FLEXIBILITY

o WATER REPELLANT

o MECHANICAL ATTACHMENTS FEASIBLE
      - ELIMINATE BONDING
      - SIMPLIFY VEHICLE INTEGRATION
      - POSITIVE RETENTION

o USE AS A COATING MATERIAL
      - HIGH EMISSIVITY (.82 - .88)
      - HIGH EROSION RESISTANCE

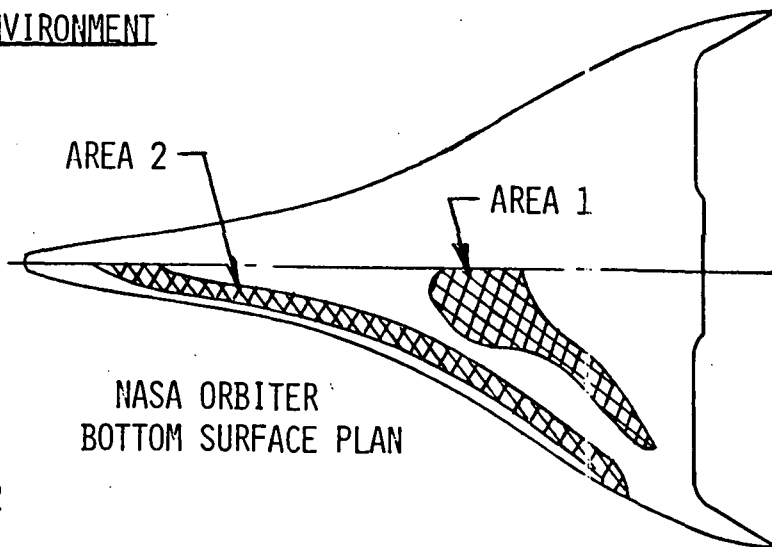FIGURE 1

DESIGN ENVIRONMENT

(Figure 2)

Figure 2 illustrates the design environment in which the Closed-Pore Insulation (CPI) TPS is required to operate. The environment was established by NASA and identifies two areas of the Shuttle Orbiter lower surface.

Area 1 receives moderate heating as illustrated in the time-temperature history. A peak temperature of 1085°K (1500°F) is reached. The design differential pressure during ascent and entry is shown in the table.

Area 2, as illustrated on the orbiter lower surface plan, is closer to the leading edge and receives increased heating. A peak temperature of 1390°K (2050°F) is reached. For increased margin, the Area 2 heating is perturbed. This increased heating, 1530°K (2300°F) peak, is illustrated by the Area 2P time-temperature history. The Area 2 ascent and entry pressure loads are shown in the table. The Area 2P pressure loads are the same as those of Area 2.

DESIGN ENVIRONMENT

NASA ORBITER
BOTTOM SURFACE PLAN
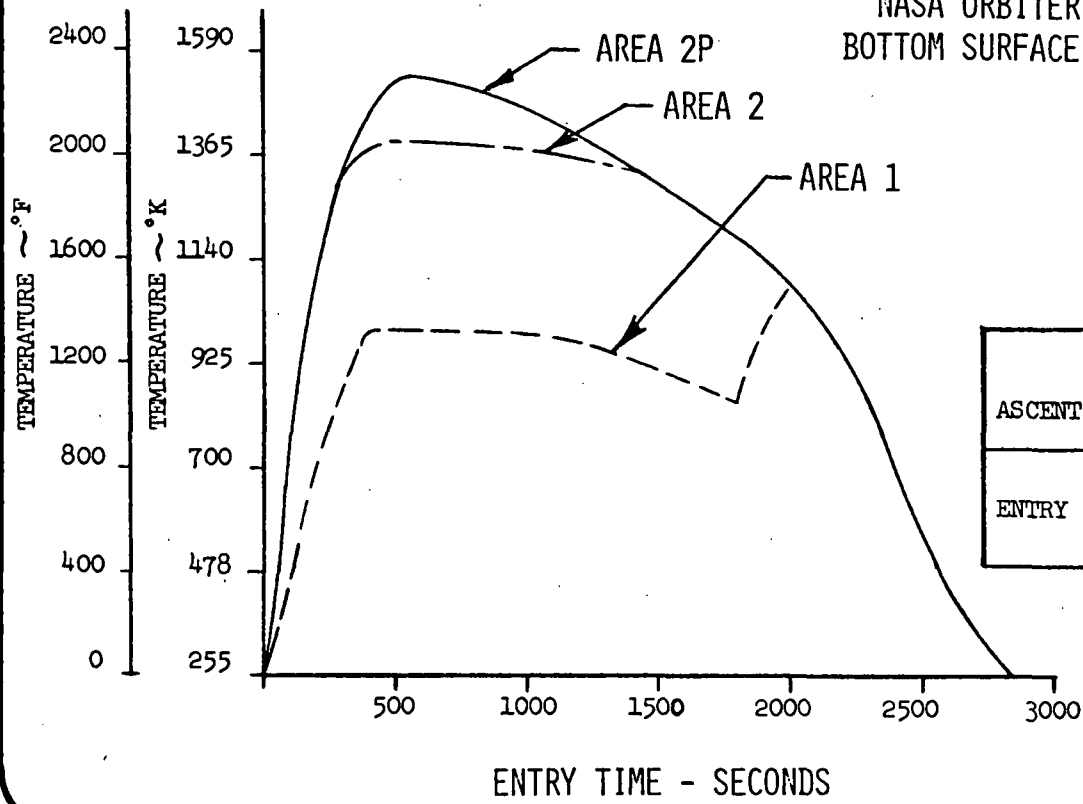
FIGURE 2

DESIGN CONCEPT DEVELOPMENT

(Figure 3)

As illustrated in the figure, two basic approaches emerged with the material: directly bonded concepts and mechanically fastened concepts. The concepts were selected on the basis of low weight, low cost, and maximum reliability. Strain isolation techniques and minimizing heat shorts to the primary structure were accorded primary attention.

The bonded concepts received initial study because of their inherent lightness and simplicity. Two designs were developed, both very similar, but tailored to each of the Area 1 and Area 2P requirements. The Area 1 design uses rigidized Kaowool fibers. The Area 2P design adds a small thickness of rigidized mullite fibers to keep the Kaowool fibers to temperatures below 1210°K (1700°F).

In contrast to the bonded concepts, the mechanically fastened concepts take maximum advantage of the CPI material and its ability to carry pressure loads without the use of a substrate. A surface tile is employed to beam the pressure loads to the standoffs, which transmit them to the primary structure. The advantages of these approaches are that no bonding is required and efficient low density insulations can be used. Of significant importance is the fail-safe nature of these concepts wherein a separate, packaged insulation system is employed that is independent of the CPI surface tile and can resist the re-entry environment in the event of surface tile failure. The standoffs serve as strain isolators with these concepts and greatly simplify integration with the vehicle.

Five mechanically fastened concepts are presented. Each offers a different approach to the total TPS. Each of the concepts contain certain desirable features in addition to problem areas. The concepts are described in detail in subsequent figures.

DESIGN CONCEPT DEVELOPMENT

O TWO BASIC APPROACHES

O CPI/BONDED CONCEPTS

  —CPI/KAOWOOL - AREA 1
  —CPI/MULLITE/KAOWOOL - AREA 2P

O CPI/MECHANICALLY FASTENED CONCEPTS

  — CPI/WEB STANDOFF
  — CPI/SQUARE PLUG
  — CPI/POST - SNAP WASHER
  — CPI/POST - SLIDING BUSHING HEX TILE
  — CPI/POST - SLIDING BUSHING SQUARE TILE

FIGURE 3

CPI/KAOWOOL BONDED CONCEPT - AREA 1

(Figure 4)

The Area 1 bonded concept is illustrated in this figure. The concept employs a thin .305 cm (.120 inch) CPI tile, which basically acts as a coating. The CPI is bonded to a block of rigidized Kaowool using refractory Kaowool cement. Kaowool is a commercially available alumino-silicate fiber which is thermally stable to 1313°K (1900°F) easily meeting the Area 1 environment. The cost of a rigidized Kaowool block is approximately $32/m^2 ($3/ft^2) in the 3.33 cm (1.31 inch) thickness illustrated. Additionally, the Kaowool fibers offer good thermal expansion match with the CPI.

Strain isolation for the system is provided by a molded silicone rubber mat that is bonded to the Kaowool. Holes are incorporated in the mat-Kaowool joint and the configuration of the mat permits good venting. Although the strain isolation system was not optimized, it was included for thermal representation. The isolator design, however, does simplify panel removal and permits larger panels to be used.

As illustrated, the four sides of the Kaowool fibers are sealed from moisture absorption by use of an Inconel foil enclosure. This concept eliminates the need for coated sides and all the associated inspection problems.

An interpanel seal is incorporated as illustrated in Detail A. The Kaowool block is chamfered and the silica rope seal is bonded into the cavity as shown.

The concept weight breakdown is as follows:

kg/m^2	lb/ft^2	
2.15	.44	CPI
8.00	1.64	Kaowool
.29	.06	Foil
3.22	.66	Strain isolator
.49	.10	Bond
14.15	2.90	

As indicated, the strain isolator represents approximately 23% of the total weight and is an area where weight savings can be made.

CPI/KAOWOOL BONDED CONCEPT - AREA 1

686
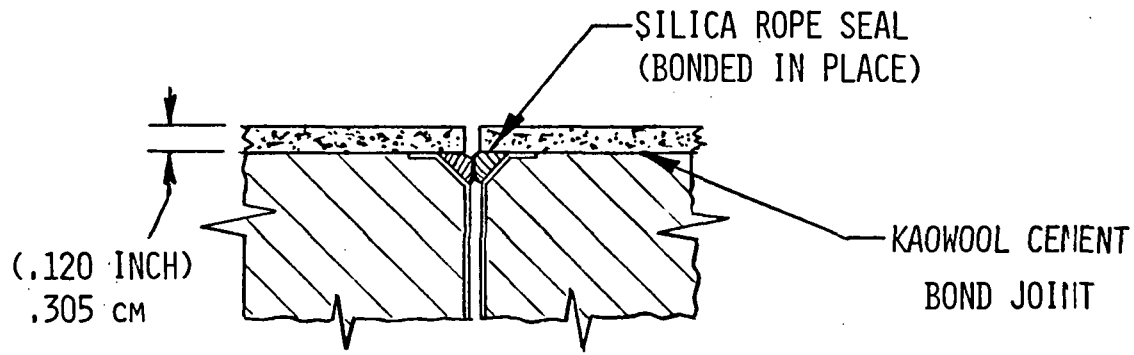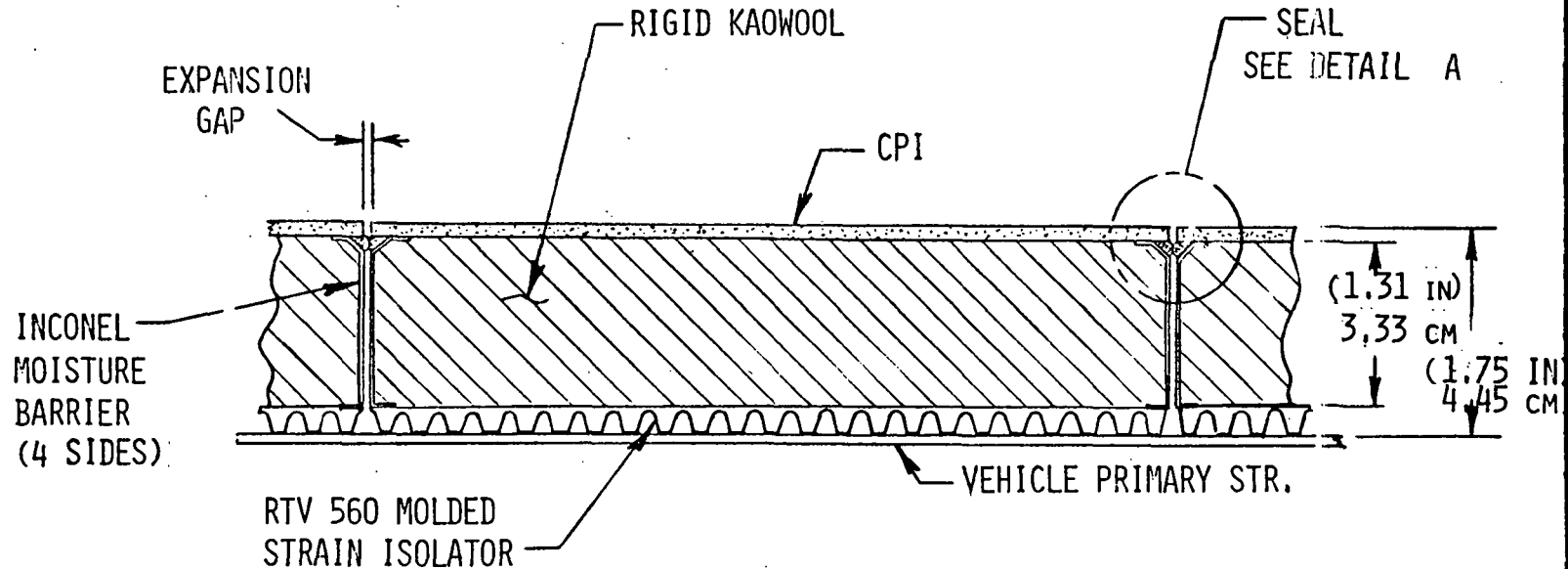
DETAIL A

FIGURE 4

CPI/BONDED AREA 1 TEST COMPONENT PRIOR TO ASSEMBLY

(Figure 5)

This figure illustrates the panel elements prior to assembly. The photo illustrates the
technique for enclosing the Kaowool rigid fiber block sides with Inconel foil formed around the
sides and the overlapped corners spotwelded for maximum retention. Subsequent bonding of the
CPI and the strain isolator also contribute to foil retention. The additional strain isolator
mat without any bonding agent is shown upside down for clarity.

066

FIGURE 5

991

CPI/BONDED - AREA 1 TEST COMPONENT

(Figure 6)

The photo illustrates the Area 1 Bonded Test Component after assembly. Although a 16.5 x 16.5 cm (6.5 x 6.5 inch) component was fabricated, a larger panel size is possible because of the higher strain to failure of both the fibers and the CPI surface tile. Contract limitations did not permit larger scale-up of the concept.

Note the silica rope seal bonded to the panel around the CPI periphery. The seal was incorporated in the component for evaluation during thermal cycling. Note also the oversize aluminum plate, which represents the heat sink mass required to perform the thermal test under atmospheric conditions while still keeping the same thicknesses of CPI and Kaowool obtained from flight condition thermal properties.

GRUMMAN

993
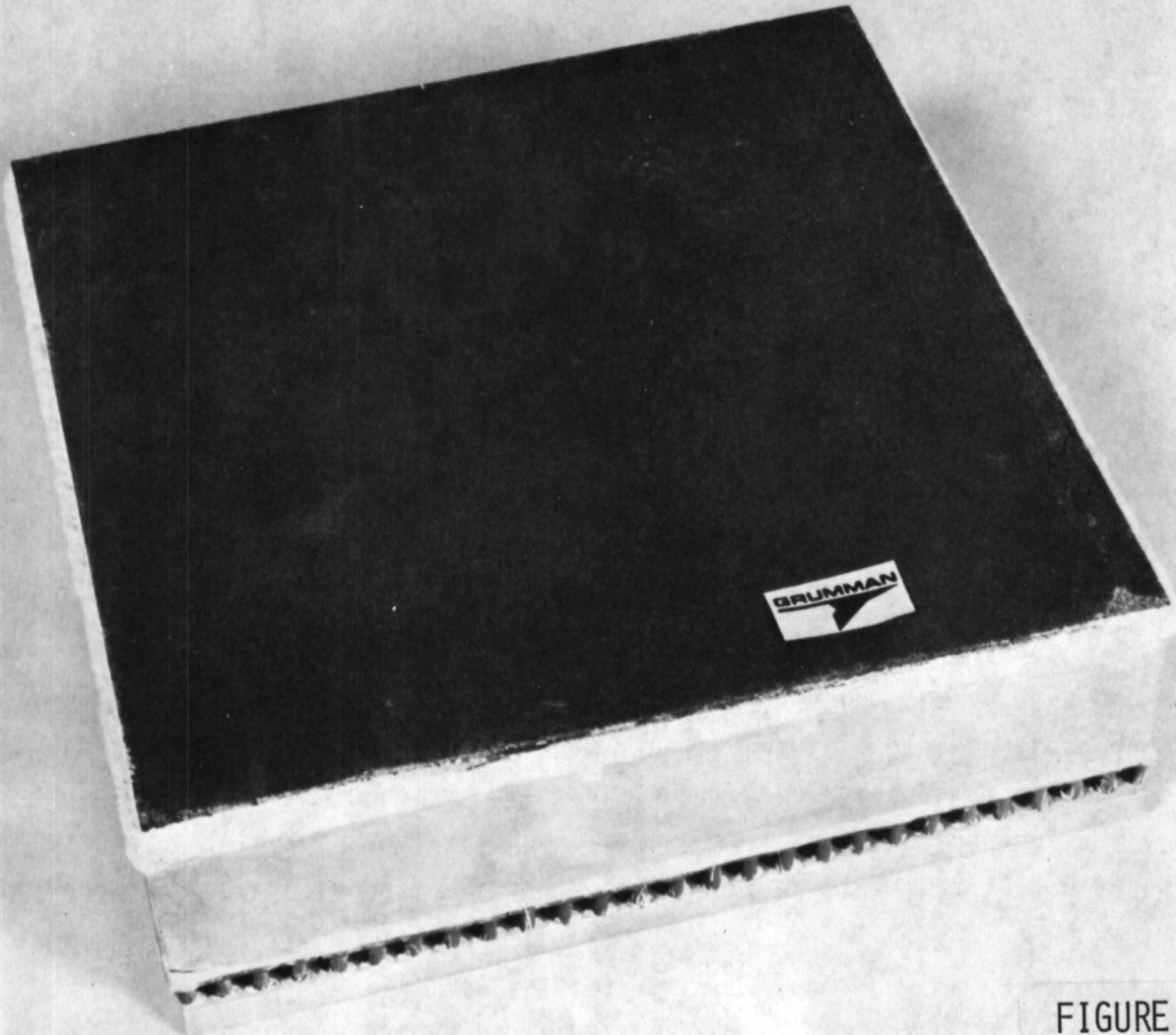
FIGURE 6

CRITICAL TEMPERATURE DISTRIBUTIONS - AREA 1 HEATING

(Figure 7)

Critical temperature distributions for the bonded concept of Area 1 are shown in this figure. Temperature-time histories throughout the structure thickness were determined analytically for vehicle flight conditions using the Grumman one-dimensional transient thermal analysis program. A total of ten thermal nodes were used for modeling. The temperature distributions shown are for three critical times: when the maximum thermal gradient occurs in the CPI on heat-up, at peak surface temperature, and at maximum reverse thermal gradient in CPI on cool-down.

Note that at the time of peak ΔT in the CPI during heat-up, the upper area of the Kaowool insulation experiences severe thermal gradients. All in-house panel testing using the Area 1 environment however, has indicated the Kaowool material can easily accommodate these gradients.

CRITICAL TEMPERATURE DISTRIBUTIONS
AREA 1 HEATING
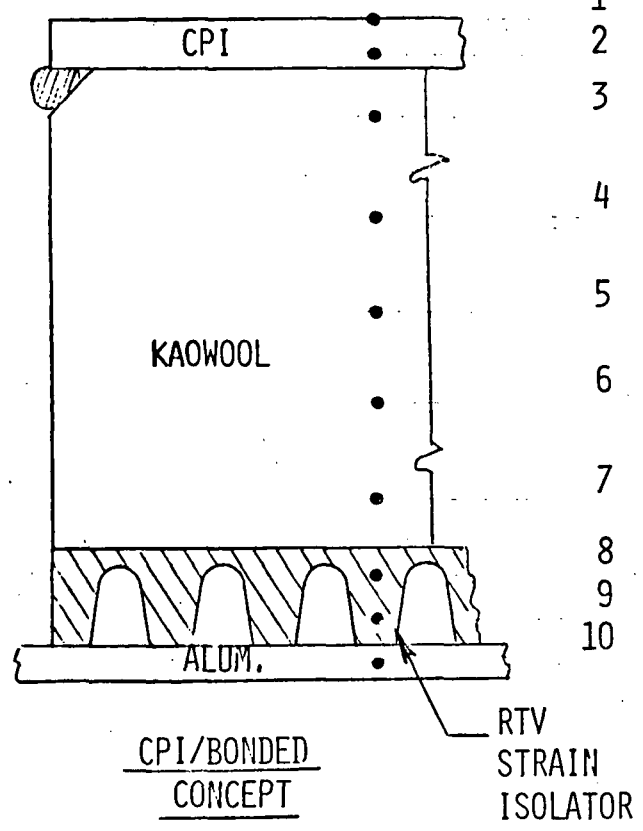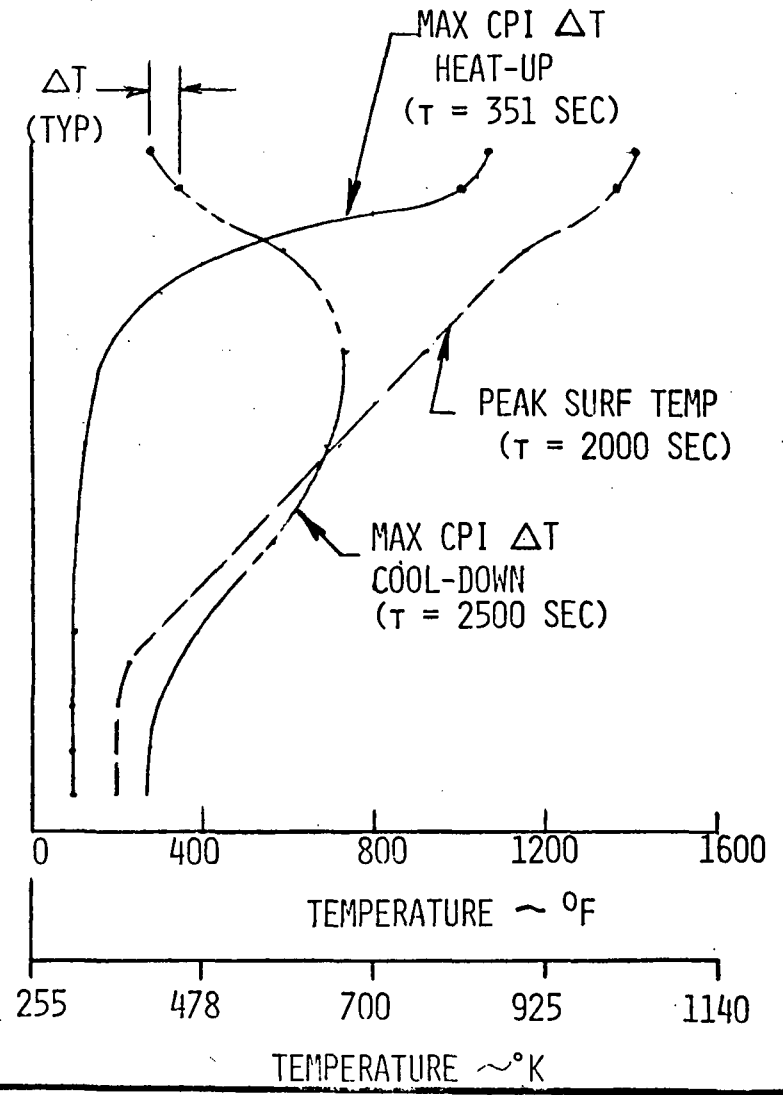
FIGURE 7

CPI/KAOWOOL - MULLITE BONDED CONCEPT - AREA 2P
(Figure 8)

The Area 2P Bonded Concept is illustrated in this figure. The design is generally similar to the Area 1 concept except that mullite is employed to protect the Kaowool fibers from the higher temperature environment. A .76 cm (.30 inch) thickness of mullite is adequate to lower the temperature to 1200°K (1700°F) at the Kaowool-mullite interface.

A diffusion bond joint provided the best joining technique for the CPI to mullite interface and was employed in the concept. The diffusion bond was achieved at 1590°K (2400°F) and 1380 N/m^2 (.20 psi) pressure for one hour. This results from good chemical and thermal compatibility between CPI and mullite. Kaowool cement was used at the mullite-Kaowool joint.

Both the RTV rubber strain isolator and the interpanel seal joint are identical to the one employed for the Area 1 concept. These are fully described in figure 4.

A TD-Ni20Cr foil moisture barrier is employed, because of the higher Area 2P operating temperature. The concept weight breakdown is as follows:

kg/m^2	lb/ft^2	
2.25	.44	CPI
1.85	.38	Mullite
14.05	2.88	Kaowool
.78	.16	Foil
3.22	.66	Strain isolator
.49	.10	Bond
22.64	4.62	

CPI/KAOWOOL - MULLITE BONDED CONCEPT AREA 2P
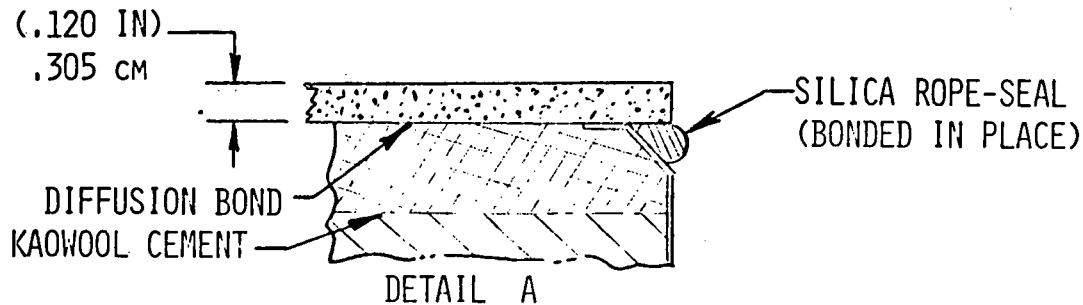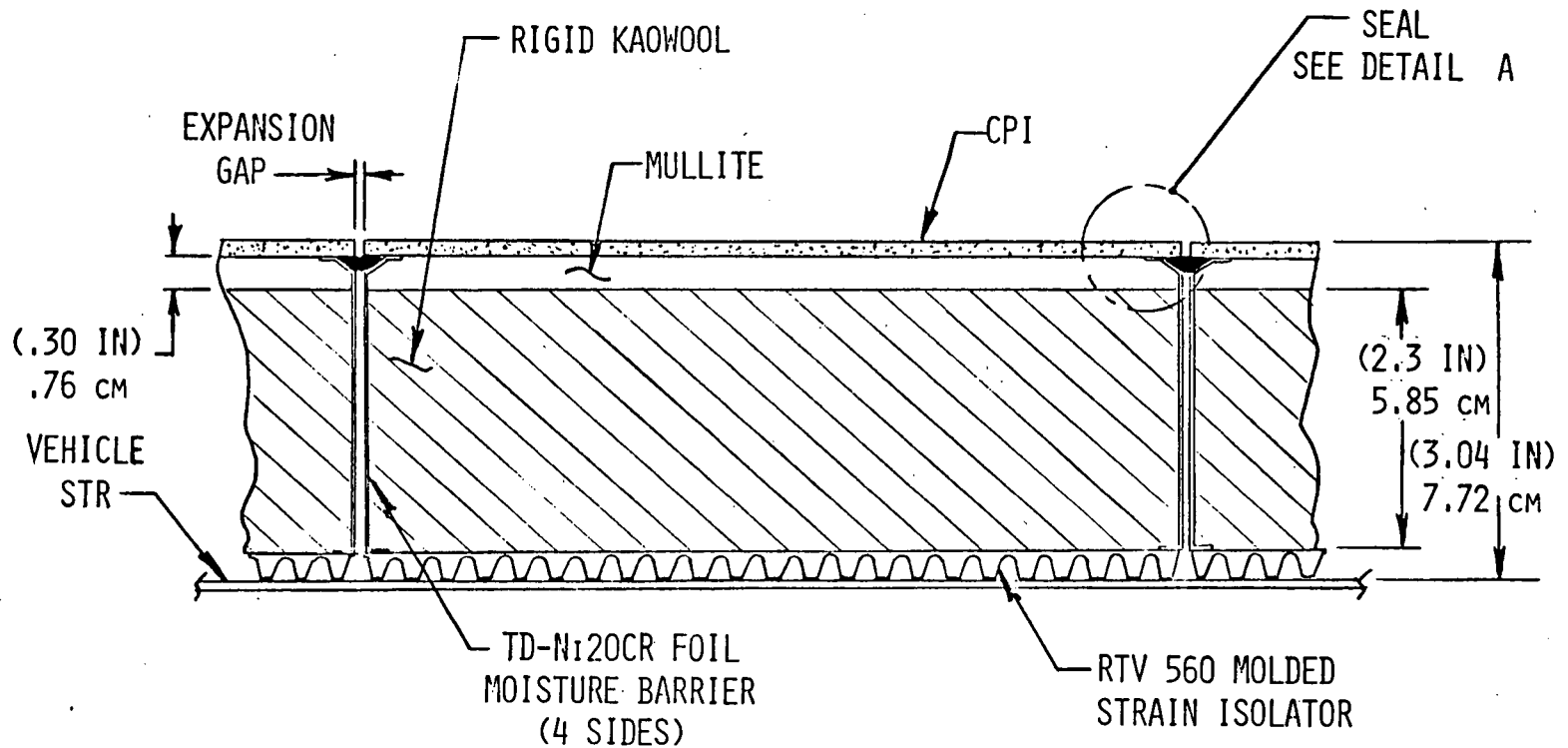
FIGURE 8

CPI/BONDED AREA 2P TEST COMPONENT

(Figure 9)

The photo illustrates the Area 2P bonded test component after assembly. Although a 16.5 x 16.5 cm (6.5 x 6.5 inch) component was fabricated, larger panel sizes are possible with these materials. The TD-Ni20Cr foil moisture barrier and the silica rope seal were not added to the component so that the edges of the panel could be inspected during thermal cycling. This was deemed necessary because thermal analysis indicated high thermal gradients will occur during Area 2P thermal cycling.

CPI/BONDED AREA 2P TEST COMPONENT

GRUMMAN

666
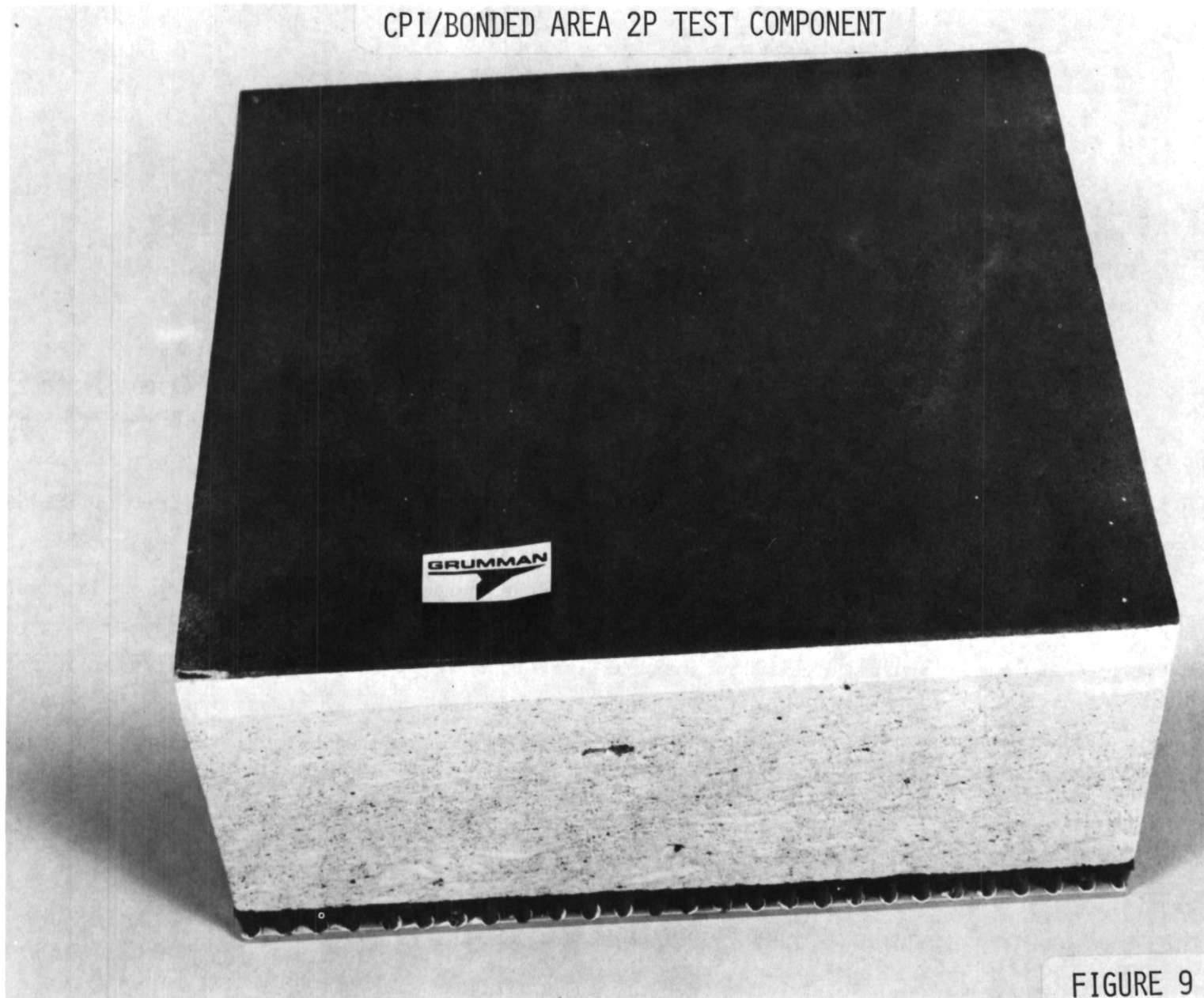
FIGURE 9

CRITICAL TEMPERATURE DISTRIBUTIONS - AREA 2P HEATING
(Figure 10)

Critical temperature distributions for the bonded concept of Area 2P are shown in this figure. Temperature-time histories throughout the structure thickness were determined analytically for vehicle flight conditions using the Grumman one-dimensional transient thermal analysis program. A total of 17 thermal nodes were used for modeling. The temperature distributions shown are for four critical times: when the maximum thermal gradient occurs in the CPI on heat-up, at peak surface temperature, at maximum reverse thermal gradient in CPI on cool-down, and when the peak temperature is reached in the aluminum substructure.

Note that at time (t = 300 sec) the thermal gradient through the mullite layer is approximately 865°K (1100°F) which could cause thermal stress problems. At peak surface temperature (t = 600 sec) the upper 1/4 of the Kaowool fibers experience a large thermal gradient of approximately 1090°K (1500°F). The Kaowool peak temperature at the mullite interface (point A), however, does not exceed 1200°K (1700°F), as shown. These high thermal gradients in the rigidized mullite and Kaowool fibers could cause failure and need further evaluation.

CRITICAL TEMPERATURE DISTRIBUTIONS

AREA 2P HEATING
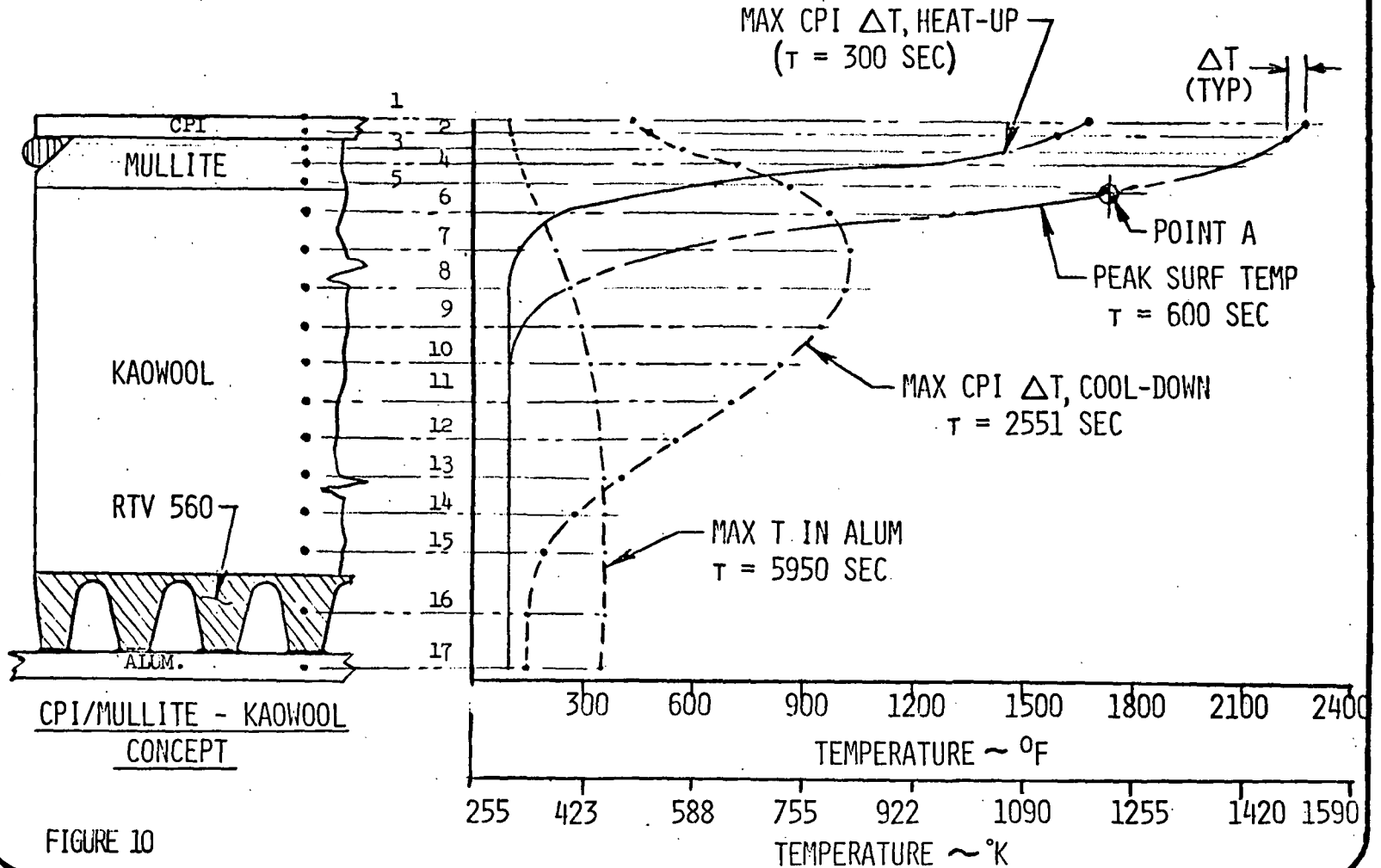
FIGURE 10

CPI/WEB STANDOFF TEST COMPONENT
(Figure 11)

An early mechanically supported concept is shown in this figure. A 15.2 x 25.4 cm (6.0 x 10.0 inch) CPI surface tile is used, supported on metallic web type standoffs, which are insulated from and mechanically attached to the primary structure. The CPI support clips are designed to permit the tile to expand and contract as required, while still resisting vertical loads. This is achieved by orienting the clips and the supporting port along radial lines emanating from the panel's geometric center. Three additional clips are used along the longitudinal edges to keep the CPI bending stresses within acceptable limits. As illustrated, the webs are located to pick up the vehicle stringers. TD-Ni20Cr screws are used, through holes in order to retain the tile. The screws are covered with CPI plugs as shown.

Some advantages of the concept include:

• Positive tile retention. Screws are positive and easy to inspect. Additionally, the web standoff transfers normal and in-plane loads directly to the primary structure.

• Support clips permit tile expansion and contraction.

• Independent, foil enclosed insulation package which is fail-safe in the event of tile failure.

Some disadvantages of the concept include:

• Holes are required in the CPI tile, which causes stress concentrations. Additionally, bonded plugs are required on installation.

• Excessive heat shorting occurs through the web-standoffs.

• Four very complex, packaged insulation elements are required for each panel.

• Screws are close to the hot surface and are prone to oxidation.

• Concept is not weight competitive with later systems.

The insight gained in the evaluation of this concept led to the development of improved design concepts described in the following figures.

CPI/WEB STANDOFF TEST COMPONENT
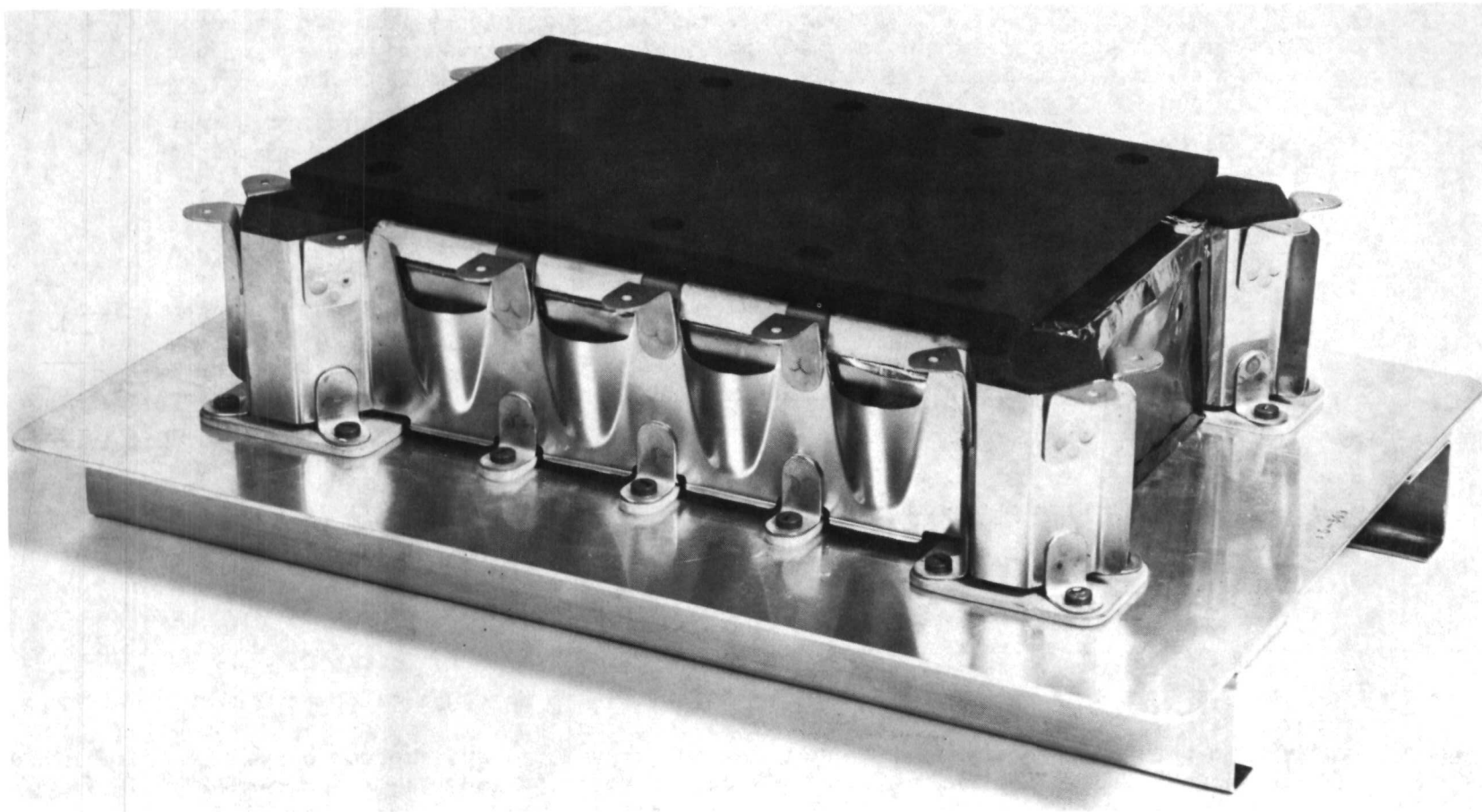
1003

FIGURE 11

CPI/POST - SQUARE-PLUG CONCEPT

(Figure 12)

This concept employs a metallic post standoff, which offers minimum weight and heat shorting, since each post supports four surface tiles. Special, dish-shaped metallic retainers are employed that are designed to support the tiles as illustrated and are positively retained by a special screw which threads into the post. The entire support assembly is protected by a CPI plug which is retained by a pin fixed to the plug with a bonded CPI torus shaped boss. A seal is incorporated in each tile to prevent leakage.

Some advantages of the concept include:

• Easily inspectable and positive primary retention system - with plug removed.

• Relative ease of assembly and removal. Only one plug required with a simple push - in installation.

• Simple, large size independent insulation package possible, with minimal post penetrations.

• Minimal weight and heat shorting of support posts, which are easily integrated to the vehicle and provide very good strain isolation.

Some disadvantages of the concept include:

• No positive lateral restraint of the CPI tile is possible because the retainers must be designed to permit the tile to expand and contract. (Restraint occurs when the tile "bottoms.")

• Redundant up-load path. It is possible to overload the CPI plug retainer for negative pressure conditions.

• Close tolerances are required between metallic retainers to ensure in-plane expansion without excessive looseness. The various elements accumulate too many tolerances in addition to tolerances developed with the three adjacent tiles.

The redundant up-load aspect and the difficulty of meeting the tolerance requirements were considered such difficult problems that the concept was not developed further.

CPI/POST SQUARE PLUG CONCEPT

20.3 x 20.3 CM A1
17.8 x 17.8 CM A2P

8 x 8 IN AREA 1
7 x 7 IN AREA 2P

9.15 x 9.15 CM
CPI PLUG

3.6 x 3.6 IN CPI PLUG
(PUSH IN PLACE)

PLAN VIEW

A

A

TINNERMAN NUT
(PLUG RETAINER)

SCREW

CPI PLUG

SEAL

CPI TILE

RETAINERS
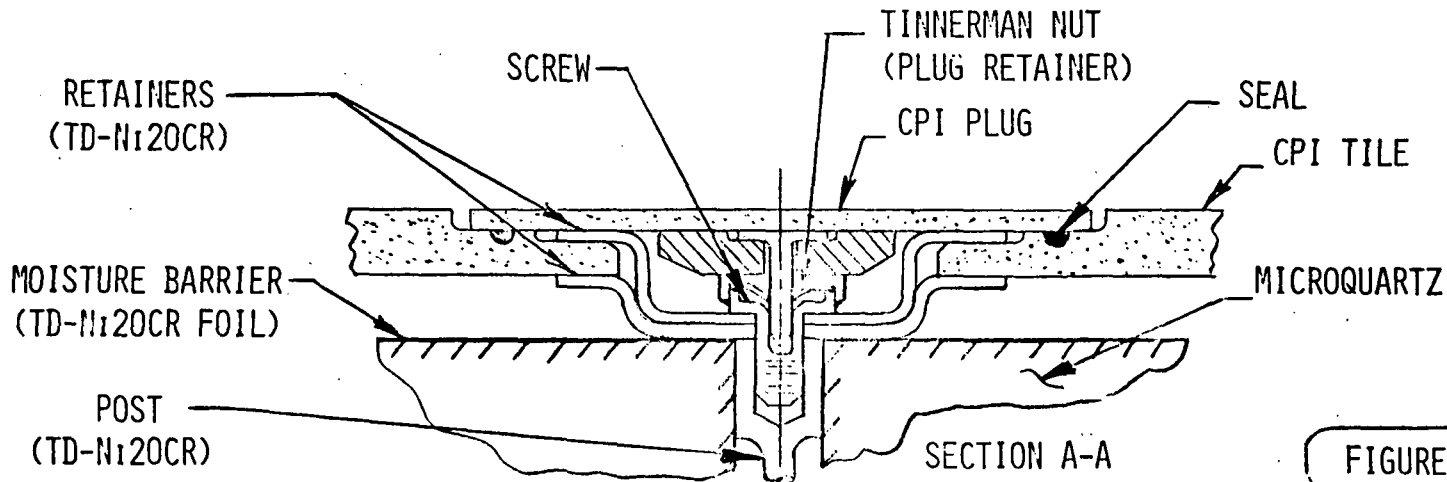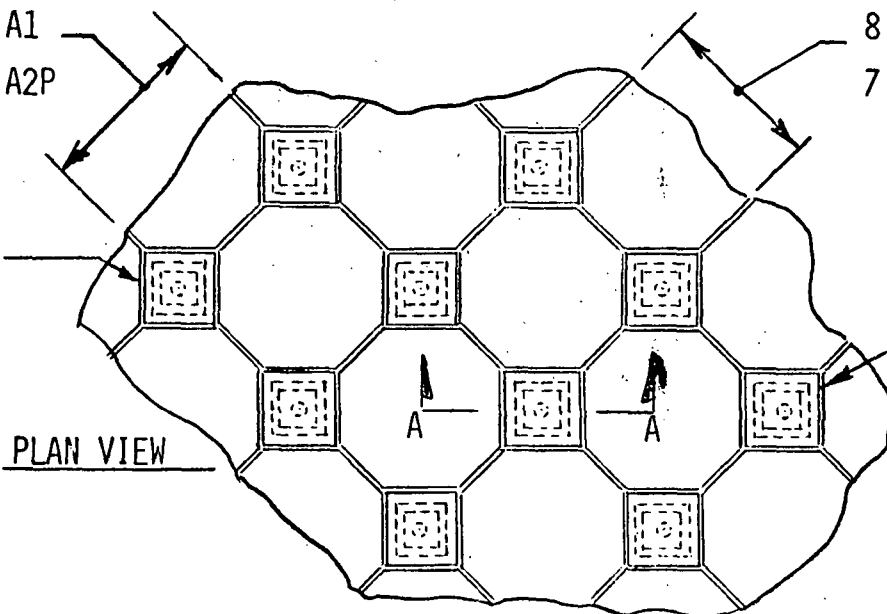(TD-Ni20CR)

MOISTURE BARRIER
(TD-Ni20CR FOIL)

MICROQUARTZ

POST
(TD-Ni20CR)

SECTION A-A

FIGURE 12

CPI/POST - SNAP WASHER CONCEPT

(Figure 13)

A promising concept is illustrated in this figure. The concept employs a metallic post standoff, which offers minimum weight and heat shorting, since each post supports four surface tiles. A flat star-shaped metallic support plate is used which is screwed into and supported by the post. Four specially notched pins are welded to the plate as illustrated in the enlarged detail. The pins are designed to fit into oversized holes in the CPI tile, and the tile is retained by a special snap-washer type nut, which is designed to permit tile expansion and contraction. The pin and washer is protected by a CPI plug bonded in place after installation. The concept permits use of a lap interpanel seal as illustrated and an independent insulation package, which can use more efficient low density insulations.

A 20.3 x 20.3 cm (8 x 8 inch) tile size is used in Area 1 and a 17.8 x 17.8 cm (7 x 7 inch) size is used in Area 2P. Tile size was determined by holding tile thickness to .76 cm (.375 inch) and keeping within material allowable strengths as measured in a material evaluation program.

Some advantages of the concept include:

• No bonding is required with the primary fastening system.

• Simple snap-in tile retention with simple inspection of the fasteners prior to plug installation.

• Minimal weight and heat shorting of the support posts, which are easily integrated with the vehicle and provide good strain isolation.

• An independent low density insulation package can be used, which provides fail-safe capability.

• Adaptability to curved surfaces.

Some disadvantages of the concept include:

• Holes are required in the CPI tile which cause stress concentrations. Additionally, plugs are required on installation and must be broken for panel removal.

• Snap washers are located close to the hot surface with possible degradation of spring action.

• Movement of tiles occurs during lateral loading as a result of oversize holes required for in-plane tile expansion.

The CPI/Post - Snap Washer concept offers the lightest system of all the post-supported schemes and was extensively tested in the program.

CPI/POST SNAP WASHER CONCEPT

SEE DETAIL

CPI TILE

FOIL

ANCHOR NUT

VEHICLE STRUCTURE

MICROQUARTZ INSUL
(6 LBS/FT^3)
96 KG/M^3

SILICON LAM
INSULATOR

TD-Ni20CR SUPPORT
PLATE & PIN

SEAL

SNAP WASHER
CPI PLUG

POST

SUPPORT DETAIL
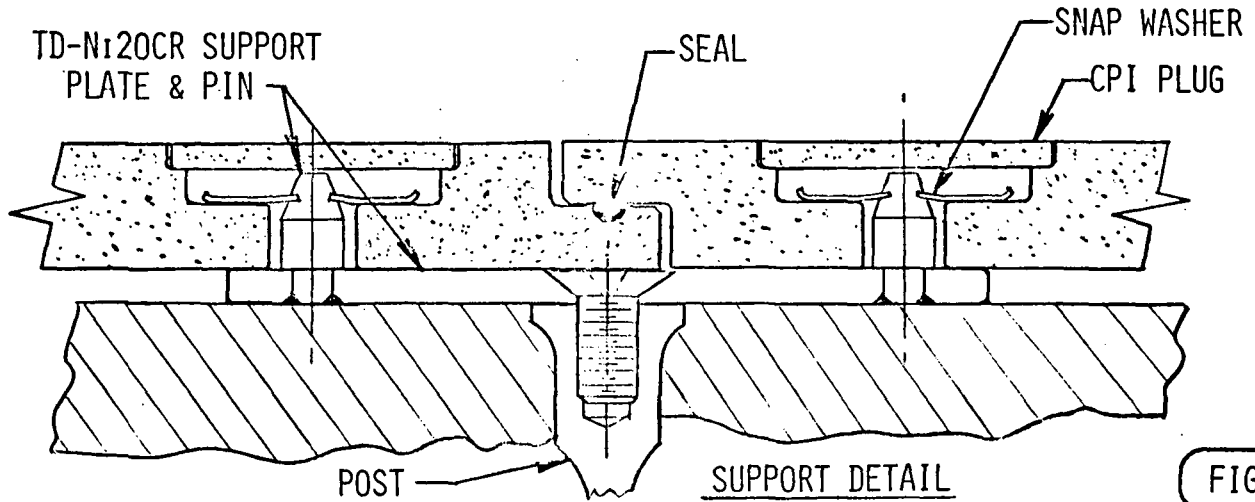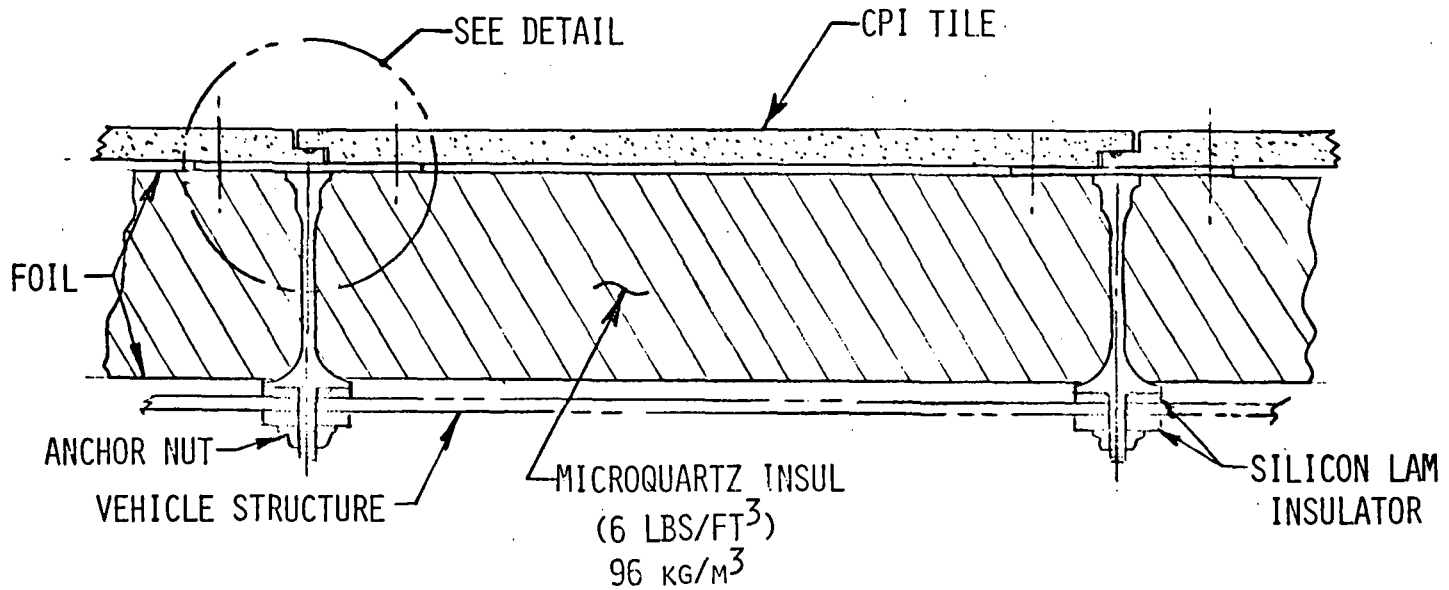
FIGURE 13

1007

CPI/POST - SNAP WASHER TEST COMPONENT
(Figure 14)

This figure shows the CPI/Post - Snap Washer test component. Two 10.2 x 10.2 cm (4.0 x 4.0 inch) CPI tiles are used because the test component was designed when the lower strength, 8% cobalt oxide material was being baselined in the program. Shown in the figure are the snap washers in place and the surface plugs prior to bonding. Also shown are the star-shaped support plates.

A TD-Ni20Cr foil moisture barrier is used to protect the 96 kg/m^3 (6 lb/ft^3) microquarts insulation.

Note the oversize aluminum plate, which represents the heat sink mass required to perform the thermal test under atmospheric conditions while keeping the insulation at the thickness obtained from flight condition thermal properties.

1008

CPI/POST - SNAP WASHER TEST COMPONENT

FIGURE 14

1009
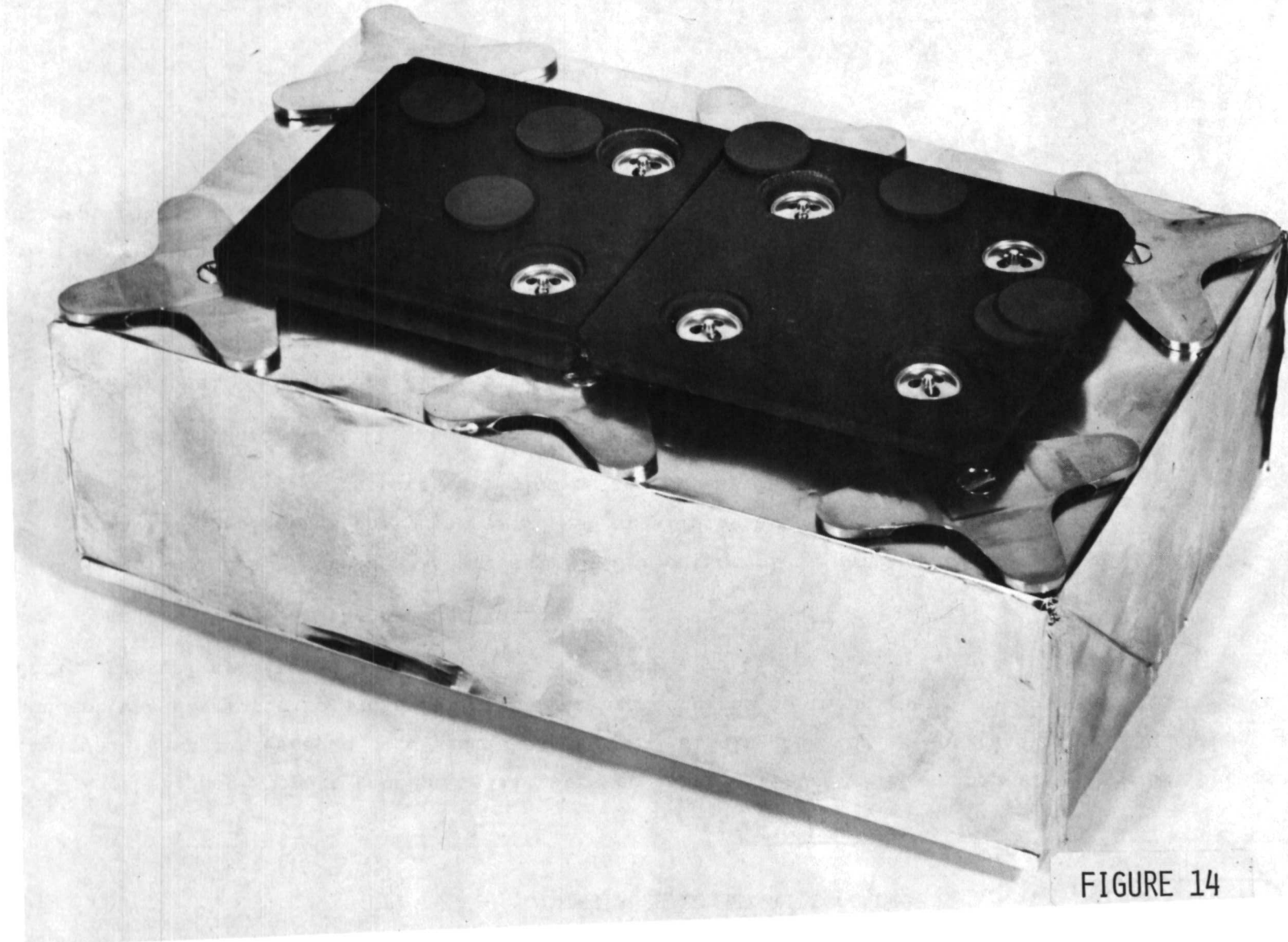
CPI/POST - SLIDING BUSHING HEX TILE CONCEPT
(Figure 15)

Another post-support concept is illustrated in this figure. The concept is different because it employs a hexagonal-shaped tile and makes use of a sliding bushing retention system. The hexagonal concept was developed to avoid failures that had occurred in the corners of square-shaped specimens during thermal cycling as a result of tile warping.

Some advantages of the concept include:

- Minimum corner stresses as a result of CPI out-of-plane warping due to thermal gradients.
- Radial in-plane expansion accommodated by sliding bushing design.
- More uniform tile support which lowers the stress level in the CPI.

Some disadvantages of the concept include:

- Hexagonal tile is more difficult to manufacture with increased tolerance buildup.
- Unconventional tile shape. Edge treatment is difficult and special tiles would be required.
- Concept is slightly heavier than an identical system using a square tile.

Development of the 4% cobalt oxide material eliminated most tile warping. Additionally, this concept led to development of a lighter and more promising concept, which is described in the next figure.

CPI/POST - SLIDING BUSH HEXAGONAL TILE CONCEPT

HEX SHAPED TILE
25.4 CM
(10 IN.)

PLAN VIEW

EXPANSION GAP

PLAN VIEW

SUPPORT PLATE

ALLEN WRENCH
ACCESS

SEAL

POST

MICROQUARTZ INSUL
(6 LBS/FT³)
96 KG/M³

FOIL
MOISTURE BARR.

VEHICLE PRIM
STRUCTURE

ANCHOR NUT
ON VEHICLE

SILICONE LAM
INSULATOR
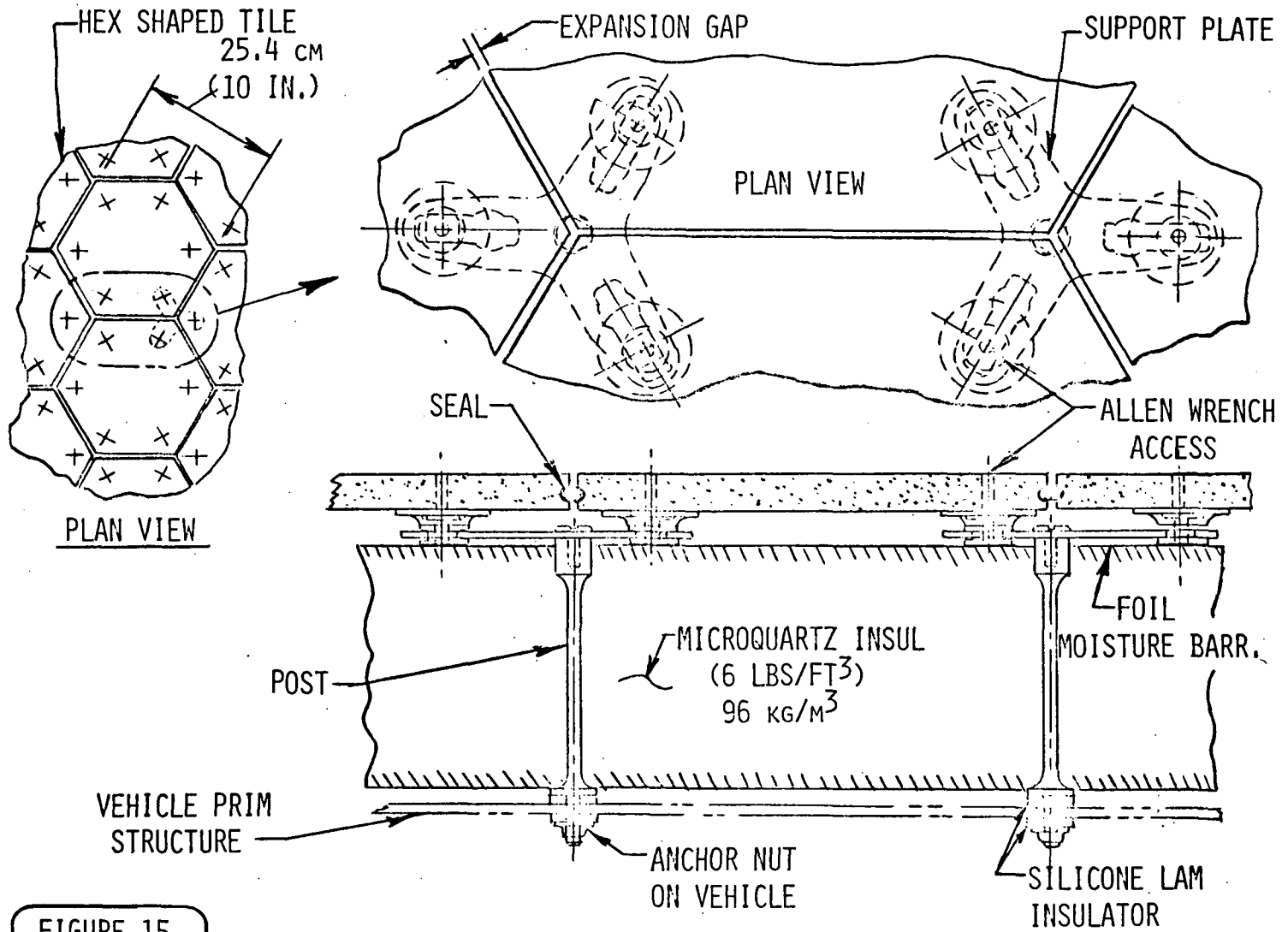
FIGURE 15

1011

CPI/POST – SLIDING BUSHING CONCEPT SQUARE TILE

(Figure 16)

The concept finally baselined in the program is illustrated in this figure. The concept employs the post-type standoff previously described. A star-shaped support plate is used, which is stamped with slotted holes. A special bushing is used, which is designed to fit the slotted opening without the use of any tools. The bushing supports a blind, Tinnerman type nut as illustrated. A simple flat .95 cm (.375 inch) CPI tile supports a CPI stud retainer, which retains a straight shanked TD-Ni20Cr shoulder pin. The CPI stud retainer is bonded to the surface tile (figure 17).

Engagement of the four pins into the bushing-nut assembly ensures a secure simple push-in installation of the tile assembly. The bushings slide within the slots and permit tile thermal expansion. The various seal concepts possible with this concept are described in figure 17. A 20.3 x 20.3 cm (8 x 8 inch) tile size is used in Area 1 and a 17.8 x 17.8 cm (7 x 7 inch) size is used in Area 2P.

Some advantages of this concept include:

- An independent, low density insulation package can be used providing fail-safe capability in the event of tile failure.

- Concept permits simple push-in installation.

- With the concept illustrated (blind nut) no holes are required in the CPI surface tile.

- Post standoffs provide minimum weight and heat shorting. Additionally, they are easily integrated with the vehicle and provide good strain isolation from the primary structure.

- The concept offers alternate retention concepts as illustrated in figure 17.

- The surface tile has positive restraint in all directions.

Some disadvantages of the concept include:

- More detail parts are required.

- A CPI to CPI joint is required for pin retention with the blind design.

- A small increase in total TPS depth is required to clear the pin retainer.

The concept offers the most advantages of all the approaches studied and is very close to the lowest weight system. This concept was therefore baselined, and will receive extensive testing in the program.

CPI/POST - SLIDING BUSHING CONCEPT SQUARE TILE

PLAN VIEW

METALLIC SUPPORT PLATE

EXPANSION GAP

SILICA ROPE SEAL (BONDED TO TILE)

CPI TILE

CPI STUD RETAINER

BLIND NUT

FOIL MOISTURE BARRIER

SLIDING BUSHING

ANCHOR NUT

POST

MICROQUARTZ INSUL (6 LBS/FT^3) 96 KG/M^3

SILICON LAM INSULATOR
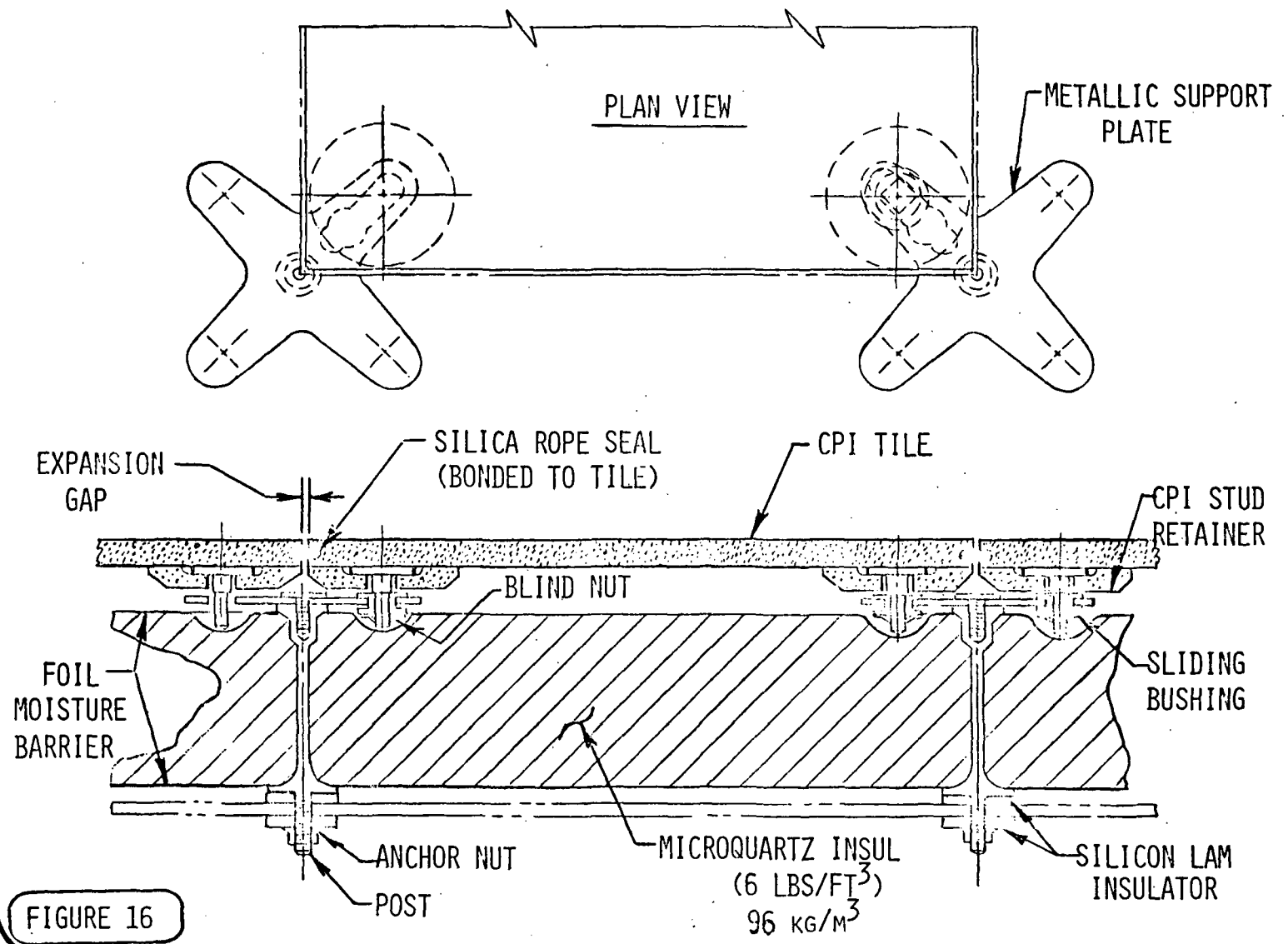
FIGURE 16

1013

CPI/POST - SLIDING BUSHING, RETENTION CONCEPTS
(Figure 17)

The versatility of the sliding bushing concept is illustrated in the three alternate designs of this figure.

The screw-down concept illustrated in the upper portion of the figure offers a design with maximum positive retention. A bonded surface plug is required to protect the screw after installation. Panel removal is achieved by breaking the plug and removing the screw. This design could be employed where frequent access behind the TPS is required.

The screw-down concept with a surface hole eliminates the need for a surface plug, but still provides positive retention. A surface hole is provided to permit allen wrenching of the shoulder screw. The hole could be filled with a room temperature setting Kaowool cement. A bonded CPI screw retainer is required with this design.

The blind design is shown in the lower illustration. This design could be used in areas where access is not required. No surface holes are necessary, and a simple push-down installation is possible. A bonded CPI screw retainer is required with this design. Removal of the tile, however, requires panel destruction.

CPI/POST SLIDING BUSHING - RETENTION CONCEPTS

SCREW — CPI PLUG
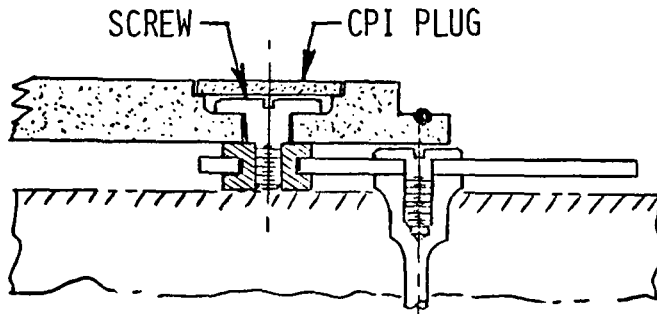
SCREW-DOWN CONCEPT

o SURFACE PLUG REQ'D

o MAX POSITIVE RETENTION

o SIMPLE INSPECTION
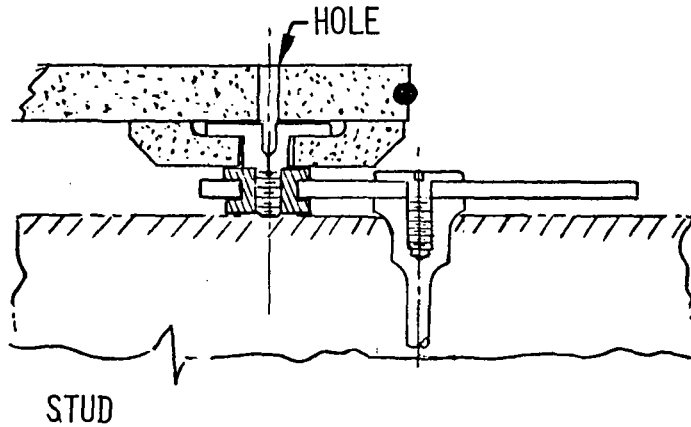
— HOLE

SCREW-DOWN CONCEPT
(SURFACE HOLE)

o MAX POSITIVE RETENTION

o BONDED CPI SCREW RETAINER REQ'D

STUD
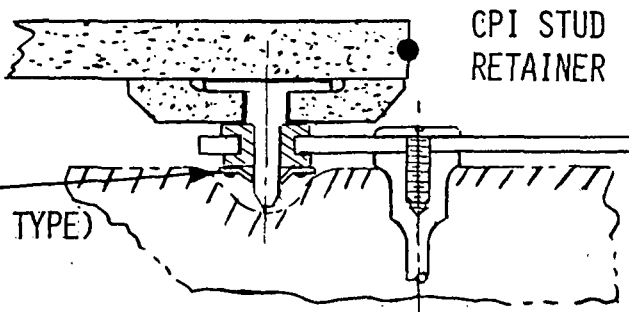
CPI STUD RETAINER

BLIND CONCEPT

o NO SURFACE HOLES

o SIMPLE PUSH-DOWN INSTALLATION

o BONDED CPI STUD RETAINER REQ'D

NUT
(TINNERMAN TYPE)

FIGURE 17

1015

CRITICAL TEMP DISTRIBUTIONS

AREA 1 HEATING

(Figure 18)

The results of a thermal analysis of the CPI/Post Sliding Bushing mechanically fastened concept are shown in this figure. The analysis was made on a model having 11 thermal nodes using Grumman's one-dimensional transient thermal analysis programs, which did not take into account tile edge effects. However, the effects of the metallic standoff supports on the thermal analysis were considered by computing an effective conductivity for the panel. For Area 1 heating the results show the thermal distributions at three critical times: when the maximum temperature gradient occurs across the CPI on heat-up, at the peak surface temperature, and when a maximum negative gradient occurs across the CPI tile on cool-down. The thermal gradients are easily accommodated in this design concept.

One important advantage of this concept is that no thermal stresses can be developed in the low density nonrigid fiberous insulation package.

CRITICAL TEMP DISTRIBUTIONS
AREA 1 HEATING

1017
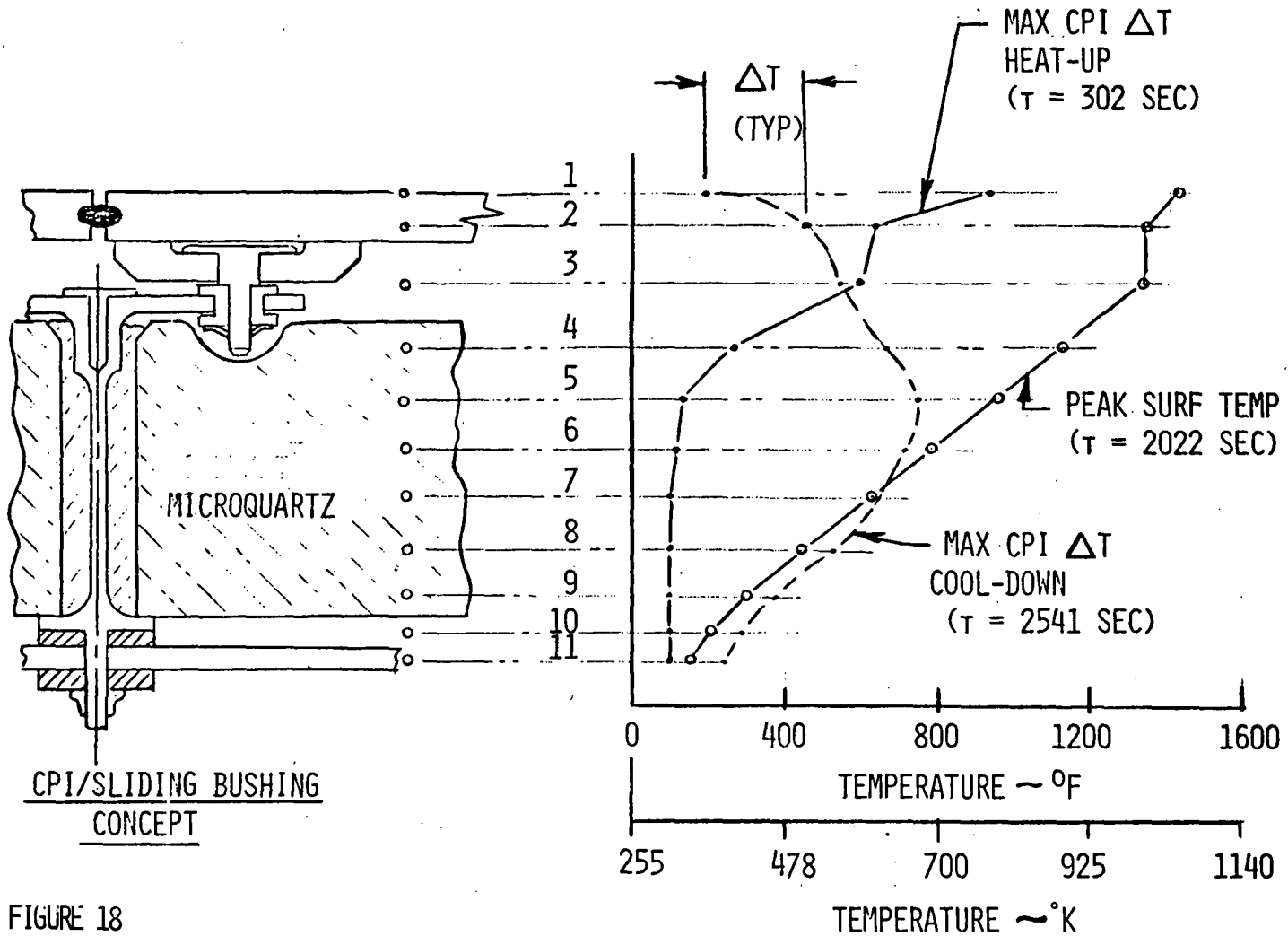
FIGURE 18

CPI/POST SLIDING BUSHING TEST COMPONENT

(Figure 19)

The CPI/Post Sliding Bushing test component is shown in this figure. The component was designed for Area 1 testing. Although the concept permits a 20.3 x 20.3 cm (8 x 8 inch) tile size, the tile fabricated is 18.8 x 18.8 cm (7.4 x 7.4 inch), which is the limit of the existing CPI molding fixtures. The simplicity and fail-safe characteristics of the insulation package are clearly shown in the figure. The insulation material used in the component is 96 kg/m^3 (6 lb/ft^3) microquartz, which is protected from moisture by a TD-Ni20Cr foil package. TD-Ni20Cr foil was used so that Area 2P thermal cycling tests could be performed with the same component. Additional aluminum will be added to the heat sink plate to compensate for the higher heating levels during Area 2P testing.

Because of contract limitations, no interpanel seal was incorporated in the component.

Area 1 and Area 2P testing of the component is planned.
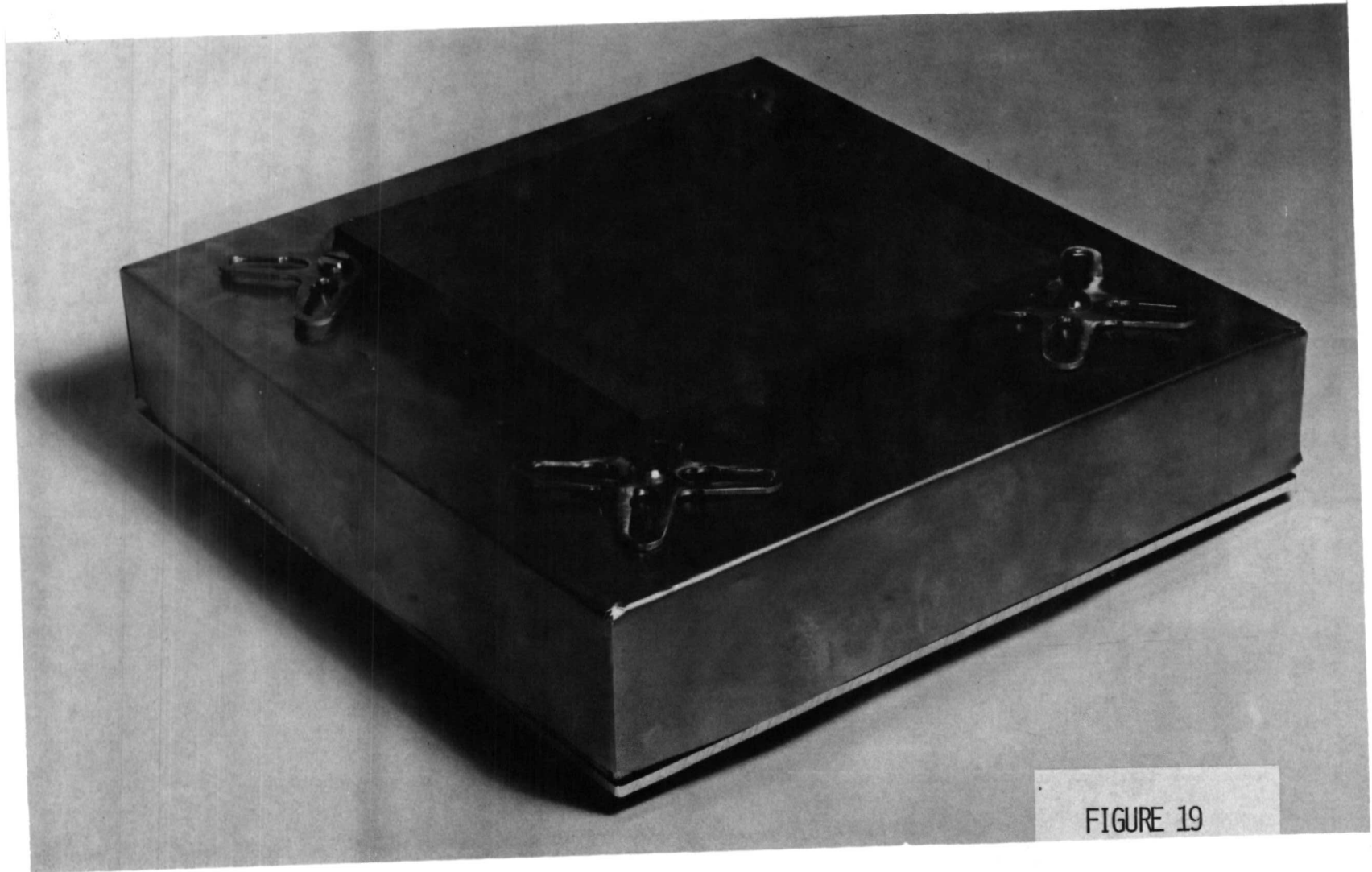
1019

FIGURE 19

CPI/CPI BOND JOINT TEST SPECIMENS

(Figure 20)

The most critical element of the CPI/Post Sliding Bushing Concept is the CPI stud retainer bonded to the surface tile (figure 17) blind concept. This figure shows elemental test specimens fabricated to evaluate two CPI to CPI bonding systems developed in the program. The specimen configuration is fully representative of the actual elements except that a simple torus was machined without the counterbored stud pocket.

The CPI cement is made by mixing 4% CPI powder and a colloidal silica binder. The mixture is placed between the parts and the assembly cured at 1365°K (2000°F) for one hour.

The second specimen was bonded using Kaowool refractory cement. This is a much simpler system to use. The Kaowool cement air dries in a short time and final curing occurs at a relatively low temperature.

The specimens were extensively tested. The test conditions and results are listed in figure 23.

CPI/CPI BOND JOINT TEST SPECIMENS

CPI CEMENT

KAOWOOL CEMENT
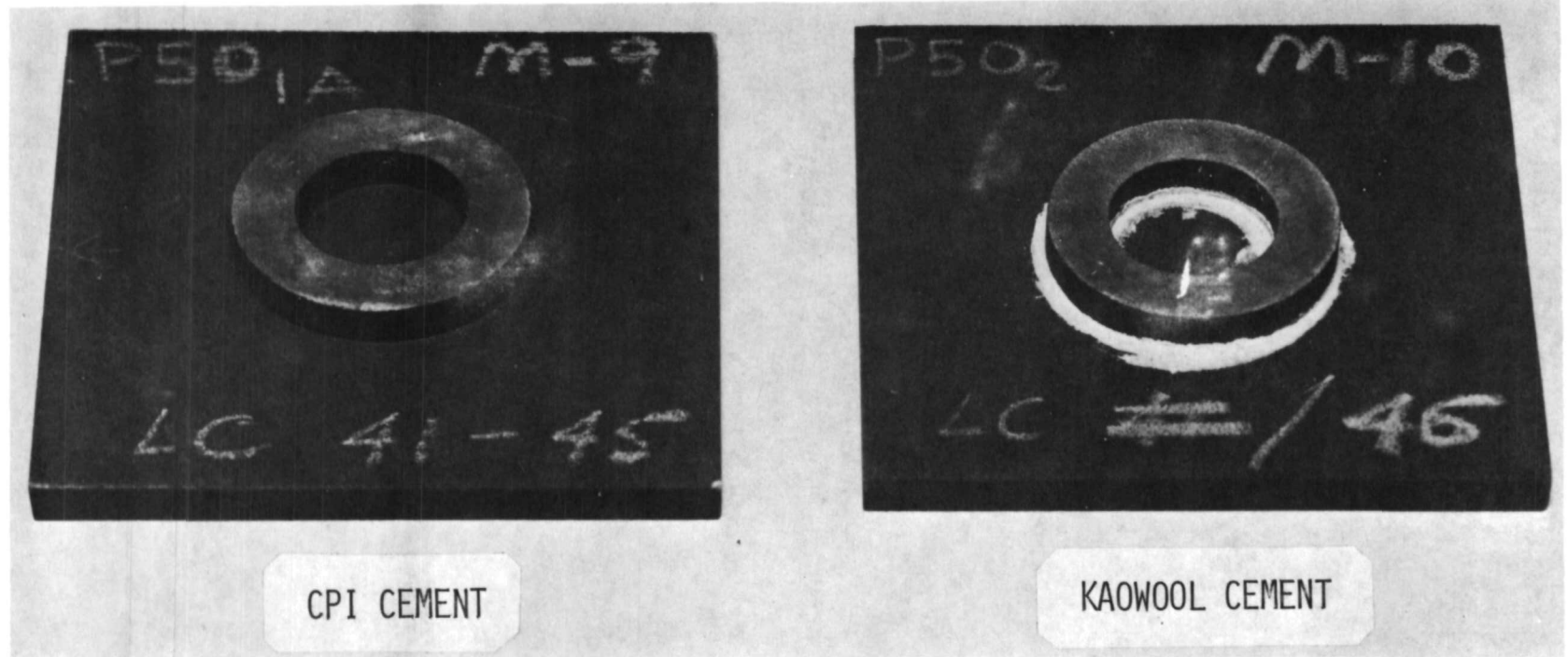
FIGURE 20

WEIGHTS - MECHANICALLY FASTENED CONCEPTS

(Figure 21)

A summary of weights for all of the mechanically fastened concepts is shown in this figure. Both Area 1 and Area 2P designs are shown for comparison. It can be seen that the lightest designs are the CPI/post using snap washers and the CPI/post with sliding bushings on square tiles. These two concepts were chosen for fabrication and thermal evaluation.

WEIGHTS - MECHANICALLY FASTENED CONCEPTS

CONCEPT	*WEIGHTS KG/M^2 $(LB./FT.^2)$	
	AREA 1	AREA 2P
CPI/WEB STANDOFF	22.3 (4.57)	27.3 (5.58)
CPI/SQUARE PLUG	18.7 (3.82)	27.5 (5.63)
CPI/POST - SNAP WASHER	15.1 (3.09)	22.6 (4.63)
CPI/POST - SLIDING BUSHING, HEX TILE	17.9 (3.67)	27.0 (5.52)
CPI/POST - SLIDING BUSHING, SQUARE TILE	16.6 (3.40)	24.5 (5.09)

*ALL WEIGHTS INCLUDE +5% FACTOR

FIGURE 21

CPI SEAL CONCEPTS
(Figure 22)

Development of a boundary layer gas seal has received considerable attention in nonmetallic TPS development programs. Existing systems, with their fiberous nature and thin coatings, are limited to simple butt-type joints, which may prove inadequate to protect the primary supporting bond joint.

This figure illustrates the versatility of the CPI material and its ability to be used to fabricate simple but positive interpanel seals. Concepts are shown that can be utilized with both bonded and mechanically fastened concepts.

It should be noted that the special properties of CPI, such as its hard wear-resistant surface, machinability, and ability to be mechanically fastened to the substructure make it attractive in conjunction with other systems. For example, there are areas where present RSI systems are not suitable. Doors will require hard edge members for sealing and handling. The interface with carbon/carbon leading edges if used, will require a transition area to the basic RSI panels. Areas thermally isolated from the basic structure, such as the cabin and cargo doors where extreme cold soak temperature could preclude the use of bonded joints, are natural areas for CPI. However, evaluation of these "special use" areas for CPI was beyond the scope of the existing program.

CPI SEAL CONCEPTS

• <u>BONDED</u>
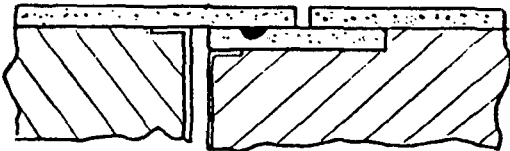
<u>LAP</u>
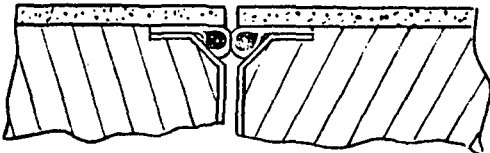
<u>TADPOLE BUTT</u>
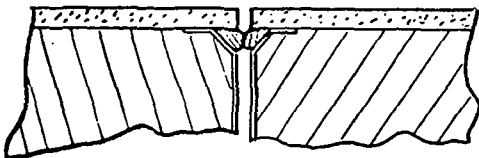
<u>CORNER BUTT</u>

• <u>MECHANICALLY FASTENED</u>

<u>LAP BUTT</u>

<u>LAP</u>

<u>STRAIGHT BUTT</u>

1025

FIGURE 22

TPS PANEL STATUS AND TEST RESULTS
(Figure 23)

The panels fabricated and tested in the program are listed in this figure. As indicated, panels were fabricated for all the promising weight competitive bonded, and mechanically fastened concepts.

The status of Area 1 and Area 2P bonded components testing is indicated.

Two mechanically fastened concepts, the CPI/Post Snap Washer and the CPI/Post Sliding Bushing, have been tested as indicated. Further testing will emphasize the preferred Sliding Bushing component. Note the many successful test cycles, at various heating levels and including cold soak, that the CPI/CPI bond joint specimens have undergone.

TPS PANEL STATUS & TEST RESULTS

- CPI/KAOWOOL BONDED COMPONENT
    - 25 CYCLES AREA 1 HEATING (COMPLETED)
    - 7 THERMAL CYCLES 50-120°F WHILE HOLDING 90% HUMIDITY

- CPI/MULLITE BOND TEST PANEL
    - 20 CYCLES AREA 2 HEATING

- CPI/MULLITE-KAOWOOL BONDED COMPONENT
    - AREA 2 TESTING TO START 10/24/72

- CPI/POST - SNAP WASHER COMPONENT (AD 517)
    - 25 CYCLES AREA 1 HEATING (COMPLETED)
    - 24 CYCLES AREA 2 HEATING (COMPLETED)
    - AREA 2P HEATING TO START 10/26/72

- CPI/POST - SLIDING BUSHING COMPONENT
    - 5 CYCLES AREA 1 HEATING (COMPLETED)
    - AREA 2P HEATING TO START 10/26/72

- CPI/CPI BOND JOINT TORUS SPECIMEN (SEE FIGURE 20)
    - 25 CYCLES AREA 1 HEATING (COMPLETED)
    - 25 CYCLES AREA 2 HEATING (COMPLETED)
    - 3 CYCLES AREA 2P HEATING
    - 3 HOURS AT -200°F

FIGURE 23

SUMMARY

- MATERIAL SUCCESSFULLY DEVELOPED

  - REQUIRES NO COATING

  - MECHANICAL ATTACHMENTS FEASIBLE

  - WATER REPELLANT

- FEASIBILITY OF CPI COMPOSITE DESIGN DEMONSTRATED

  - BONDED CONCEPTS

  - MECHANICALLY FASTENED CONCEPTS

- MORE OPTIMIZATION WORK REQUIRED

- DEVELOPMENT OF CPI FOR "SPECIAL USE" AREAS WARRANTED

MECHANICAL ATTACHMENT OF REUSABLE SURFACE

INSULATION TO SPACE SHUTTLE PRIMARY STRUCTURE

by

R.W. Fleck and J.K. Lehman

McDonnell Douglas Astronautics Company - East

St. Louis, Missouri

ATTACHMENT COMPARISON

(Figure 1)

Three methods of attaching RSI tiles to Shuttle primary structure have been proposed; direct bond, mechanical attachment, and subpanels with standoffs. All three attachment methods may have application on Shuttle. Direct bond and subpanel approaches have been evaluated by several contractors on previous CRAD studies. Mechanical attachment approaches are currently being evaluated by McDonnell Douglas Astronautics Company - East under Contract NAS-9-12854 to NASA-MSC.

The direct bond approach is lightweight but is difficult to refurbish and inspect. The subpanel approach is heavier but allows for easy refurbishment since TPS subpanels are easily removed and replaced. The mechanical attachment approach allows easy refurbishment and inspection and is lightweight when an efficient insulator is used between RSI tiles and primary structure.

ATTACHMENT COMPARISON
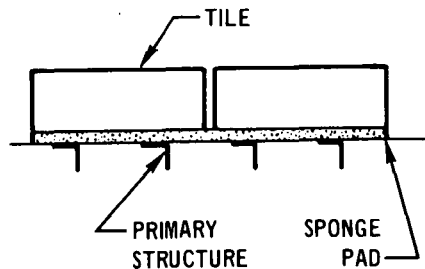
DIRECT BOND	SUBPANELS	✓ MECHANICAL ATTACHMENTS
• LIGHTWEIGHT • SILICONE SPONGE PAD STRAIN ISOLATES TILES, ACCOMMODATES WAVY SKINS, BUCKLES & PROTRUDING RIVETS • PROVIDES CONTINUOUS SUPPORT OF RSI TILE	• EASY REFURBISHMENT • FAIR INSPECTABILITY	• LIGHTWEIGHT (EFFICIENT INSULATOR BETWEEN TILE & STRUCTURE) • EASY REFURBISHMENT AND INSPECTION • ATTACHMENTS STRAIN ISOLATE TILES, ACCOMMODATE WAVY SKINS, BUCKLES AND PROTRUDING RIVETS • EASY HEIGHT AND GAP ADJUSTMENT
• DIFFICULT TO REFURBISH AND INSPECT	• WEIGHT PENALTY (SUBPANEL AND STANDOFF WEIGHT)	• REQUIRES FURTHER EVALUATION
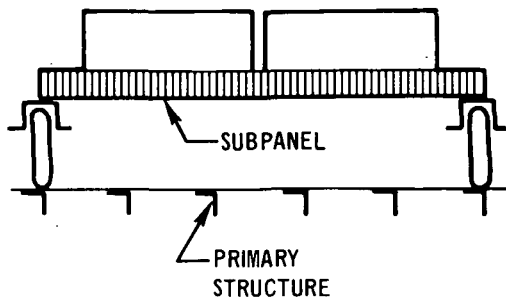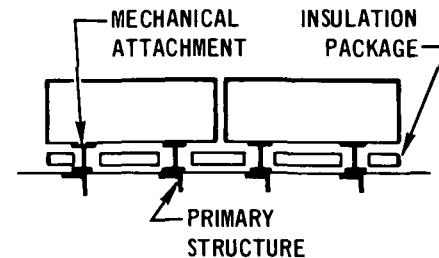
Figure 1

1031

REQUIREMENTS AND ENVIRONMENTS

(Figure 2)

Requirements for mechanical attachment concepts were established early in the study to aid in evaluating candidate approaches. The most important requirements are to provide for easy installation, removal, inspection, and adjustment of tiles. Another requirement, which is unique to mechanical attachments, is to provide a menas of restricting the flow of hot gases behind tiles.

Significant environments, used for the design of mechanical attachment concepts, are also shown on this chart. Differential pressures of -31.0×10^3 N/m^2 (-4.5 psi) and 41.4×10^3 N/m^2 (+6.0 psi) were used to determine attachment tensile and compressive loads. Venting studies have shown that it is unlikely that these high differential pressures will occur because of the large gaps between tiles. However, these pressures result in reasonable attachment loads and resulting designs should survive ground handling. A 30 g lateral acceleration due to acoustic and vibration environments was assumed in order to determine attachment shear loads.

REQUIREMENTS AND ENVIRONMENTS

REQUIREMENTS

- STRAIN ISOLATE TILES

- PERMIT BUCKLING SKINS AND PROTRUDING RIVETS

- MAINTAIN INTEGRITY IN CASE OF RSI CRACKS

- -250°F (117°K) TO $+350^{\circ}$F (450°K) PRIMARY STRUCTURE TEMPERATURE EXTREMES

- EASY INSTALLATION, REMOVAL, INSPECTION AND GAP/HEIGHT ADJUSTMENT

- RESTRICT FLOW BEHIND TILES

ENVIRONMENTS

- DIFFERENTIAL PRESSURES; $+6.0$ PSI (41.4×10^3 N/M^2), -4.5 PSI (-31.0×10^3 N/M^2) ULTIMATE

- VIBRATION; 30 g

- ACOUSTICS; 160 dB

- TEMPERATURE; 2300°F (1535°K) PEAK

Figure 2

THREE ATTACHMENT LOCATIONS CONSIDERED

(Figure 3)

Screening studies were conducted to aid in selecting a mechanical attachment concept for detailed evaluation. Eighteen concepts were evaluated. Screening studies are summarized in the following figures.

Mechanical attachment concepts were separated into three categories; edge, corner, and bottom attachments. Edge attachments engage on two sides of each tile. Corner attachment concepts are located at the intersection of three tiles. The majority of the attachment concepts fall in the category of bottom attachments. Typical examples from each category are illustrated in figure 4.

THREE ATTACHMENT LOCATIONS CONSIDERED

○ ATTACHMENT LOCATION

EDGE

CORNER

BOTTOM

1035
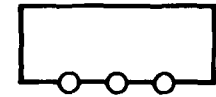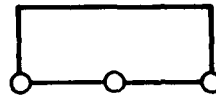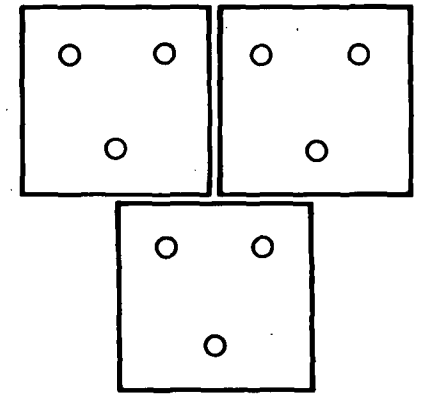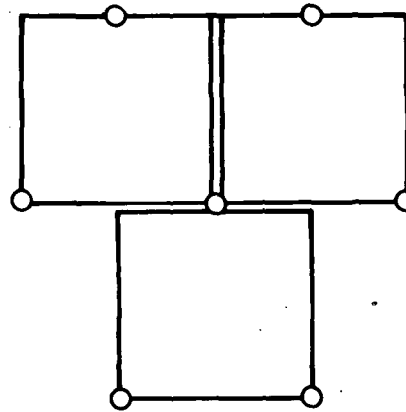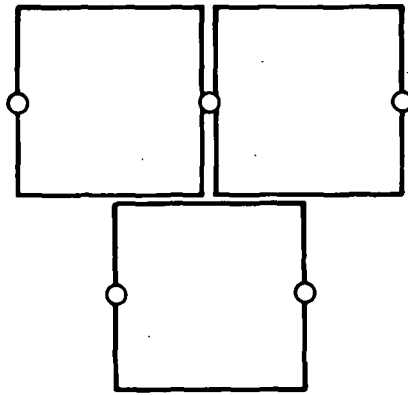
Figure 3

TYPICAL CONCEPTS

(Figure 4)

Eighteen attachment concepts were evaluated. Six typical concepts are shown on this chart as examples. Edge attachment concepts are accessible through tile gaps. In general, edge attachments are not as reliable as corner or bottom attachments, and it is difficult to control gap size and tile height of edge attached tiles. Access to corner attachments is provided either through tile gaps or with the use of removable plugs. Corner attachment concepts are relatively complex since three different tiles engage in each attachment. Complexity results from individual strain isolation and adjustment requirements for each tile. Bottom attachment concepts such as the snap spring and ball joint concepts are simple, easily adjusted, and reliable. The ball joint concept, which is discussed in detail in figure 5, was selected for detailed evaluation.

TYPICAL CONCEPTS

(18 CONCEPTS EVALUATED)

EDGE
- ELASTOMERIC SILL

TILE

PRIMARY
STRUCTURE — SILL
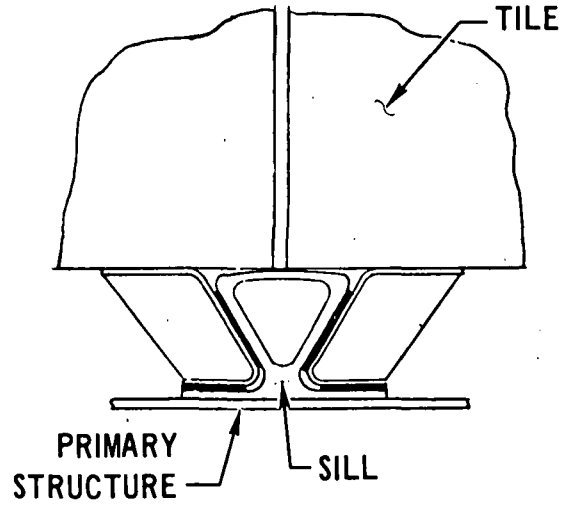
- SPRING CLIPS

CLIP
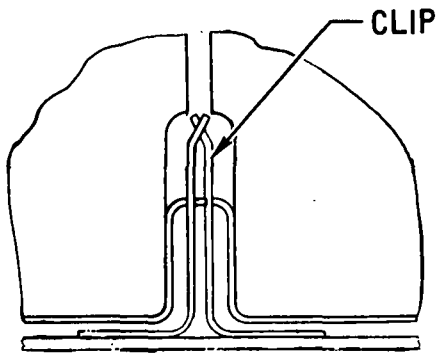
CORNER
- CORNER PLUG

PLUG — TILE
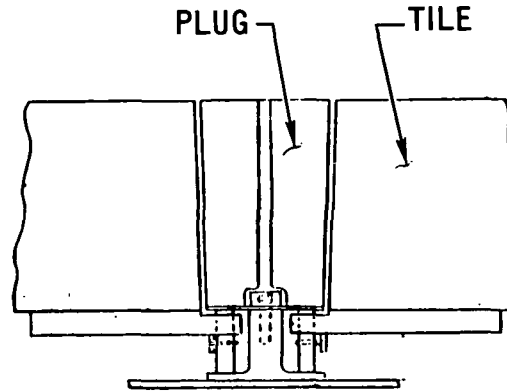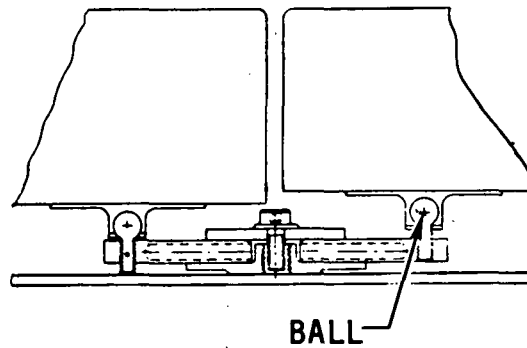
- BALL JOINT

BALL

BOTTOM
- SNAP SPRING

TILE

PIN
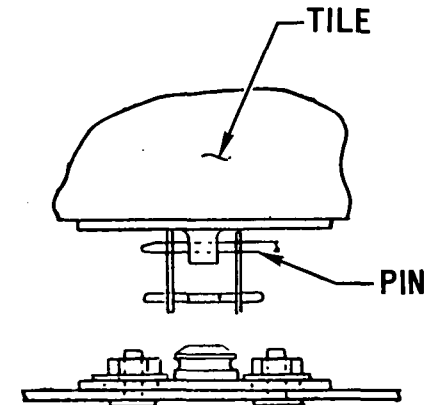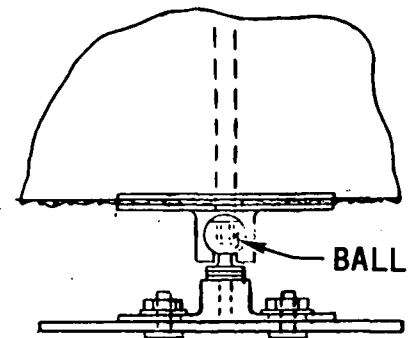
- BALL JOINT

BALL

Figure 4

BALL JOINT CONCEPT SELECTED

(Figure 5)

The ball joint attachment concept selected for detailed evaluation is illustrated in this figure. It is a three-point bottom attachment concept consisting of small ball joints engaged in sockets bonded to the inboard side of tiles. Ball joints slide and rotate within sockets to provide strain isolation. Each socket is bonded to a washer, which distributes attachment loads into the RSI. A titanium screen is bonded to the backside of the tile. This screen aids in maintaining RSI tile integrity in case the tile cracks or is damaged. For loss of a complete tile, the titanium screen retains the insulation package.

The ball is machined on one end of a threaded stud. To install a tile the three balls are aligned with the threaded fittings, and an allen wrench is used to thread each ball into the fittings. Small holes in the tile allow the allen wrench to engage the top of each ball. Tile height adjustment is provided by spacers between the ball and fitting. Tile gap adjustment is accomplished by adjusting the fittings attached to the primary structure.

A low density insulation package is placed between the tile and primary structure. This insulation package reduces TPS weight by allowing the tile backface to reach 590°K (600°F), while the primary structure temperature does not exceed 450°K (350°F). The insulation package also provides a hot gas barrier behind tiles.

BALL JOINT CONCEPT SELECTED

1039

RSI TILE

INSULATION PACKAGE

1.0 IN. (2.54 CM)

6.0 IN. (15.2 CM)

6.0 IN.
(15.2 CM)

ACCESS HOLE IN HCF

RIVETS

RTV 560 ADHESIVE

14 MESH TITANIUM SCREEN

BALL

WASHERS

SOCKET

PRIMARY STRUCTURE

FITTING
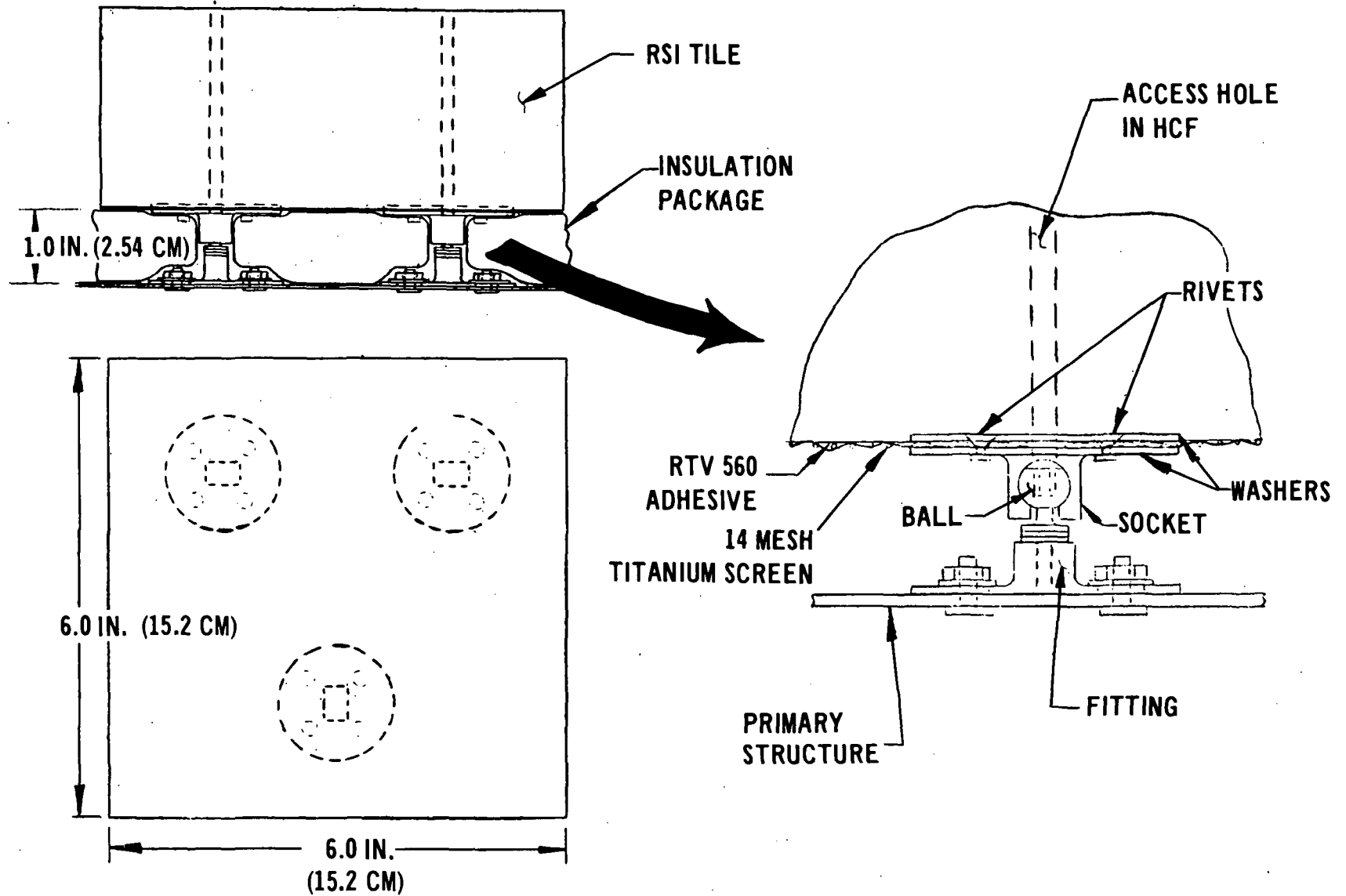
Figure 5

NUMBER OF ATTACHMENTS PER TILE SELECTED

(Figure 6)
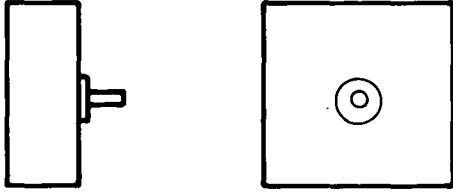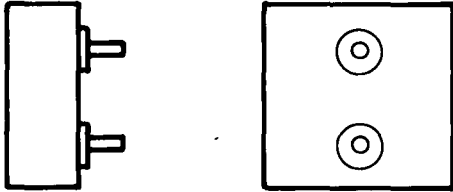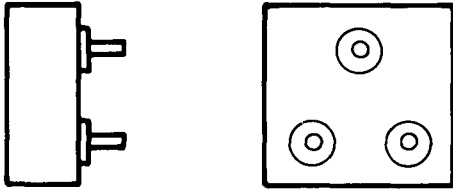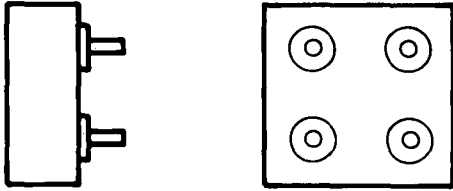
The objective of this program is to determine the feasibility of the mechanical attachment concept. Conventional materials were used to accomplish this objective. It is recognized that further weight savings could be achieved using other materials such as advanced composites. Results of trade studies to optimize the selected ball joint concept are summarized on the following charts.

One-, two-, three-, and four-point attachment arrangements were evaluated. One- and two-point attachment concepts are lightweight and easily installed but do not provide adequate support for lateral loads applied to tiles. Torsional stiffness is required to survive dynamic environments that could cause tiles to contact each other along edges. Torsional natural frequencies of one- and two-point attachments were found to be 53 Hz and 75 Hz, respectively. Since torsional natural frequencies above 100 Hz are required to prevent cross coupling with the natural frequency of the primary structure panels, one- and two-point attachments were dropped from further consideration.

The four-point attachment is the heaviest concept considered but has the obvious advantage of providing redundancy if a fastener fails. The major disadvantage of this concept is difficulty of installation. If all attachments do not lie in the same plane it is difficult to engage fasteners without imposing high stresses on RSI tiles.

The three-point attachment concept offers the best compromise. It has acceptable weight, provides high torsional stiffness, and is easily installed.

NUMBER OF ATTACHMENTS PER TILE SELECTED

NUMBER OF ATTACHMENTS	SKETCH	ADVANTAGES	DISADVANTAGES
ONE		• LIGHTWEIGHT • EASY INSTALLATION	• LOW TORSIONAL STIFFNESS • HIGH HCF STRESSES DUE TO PRESSURE LOADS • SINGLE ATTACHMENT FAILURE CAUSES LOSS OF TILE
TWO		• INTERMEDIATE WEIGHT • EASY INSTALLATION	• LOW TORSIONAL STIFFNESS • FAIRLY HIGH HCF STRESSES DUE TO PRESSURE LOADS
THREE		• EASY INSTALLATION • LOW HCF STRESSES DUE TO PRESSURE LOADS	
FOUR		• LOW HCF STRESSES DUE TO PRESSURE LOADS • FAILURE OF ONE ATTACHMENT DOES NOT CAUSE LOSS OF TILE	• HEAVY • DIFFICULT TO INSTALL

Figure 6

TITANIUM SCREEN CARRIER PLATE SELECTED
(Figure 7)

A carrier plate is bonded to the backside of each RSI tile with RTV-560 adhesive. This plate aids in maintaining RSI integrity in case a tile cracks or is damaged. For loss of a complete tile the carrier plate retains the packaged insulation, thereby providing some thermal protection to the primary structure.

Trade studies of various carrier plate materials were conducted. Weights are summarized on this chart. The titanium screen carrier plate was selected. It is slightly heavier than the beryllium plate but allows inspection of the RTV-560 bond line through the titanium screen. Other carrier plates, including beryllium, could be made lighter by perforating the plates. This would also allow inspection of the bond line. Selection of size and distribution of perforations requires further study.

TITANIUM SCREEN CARRIER
PLATE SELECTED
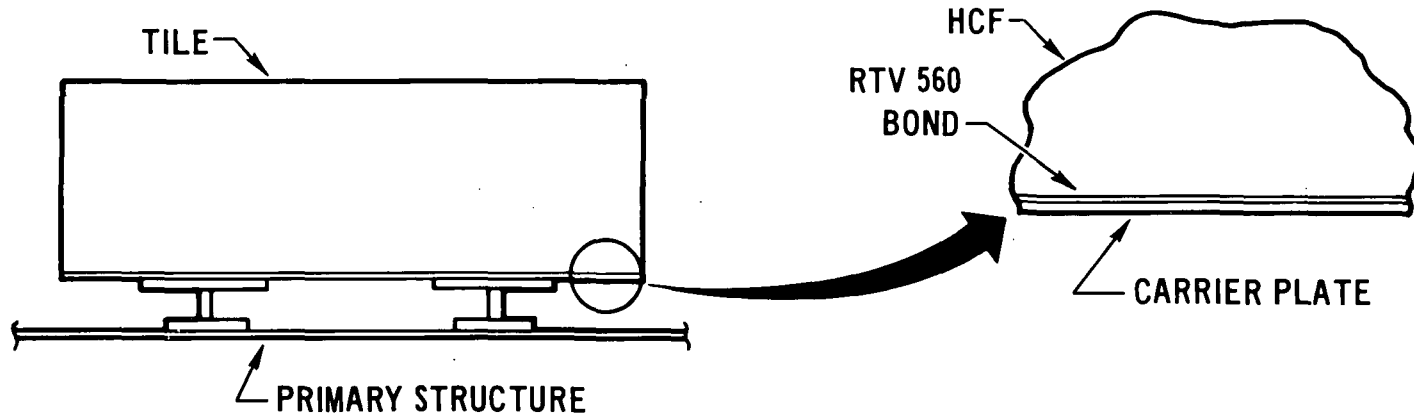
CARRIER PLATE MATERIAL	PLATE THICKNESS IN. (a)	PLATE + ADHESIVE WEIGHT LB/FT^2 (b)
TITANIUM	0.008 (0.020)	0.39 (1.91)
BERYLLIUM	0.008 (0.020)	0.31 (1.52)
INVAR	0.008 (0.020)	0.49 (2.39)
GRAPHITE POLYIMIDE	0.010 (0.025)	0.35 (1.71)
COLUMBIUM	0.008 (0.020)	0.58 (2.84)
TITANIUM SCREEN	14 MESH	0.34 (1.66)

(a) UNITS IN PARENTHESES ARE CM

(b) UNITS IN PARENTHESES ARE Kg/M^2

TITANIUM WASHER DISTRIBUTES ATTACHMENT LOADS
(Figure 8)

Washers distribute attachment loads to the RSI. Washer stiffness requirements are summarized on charts that follow. Three washer concepts were evaluated: solid washers, honeycomb, and integral rib washers. All three concepts can be configured to provide adequate stiffness. The solid washer concept was selected based on considerations of material availability, simplicity, and fabrication cost. In addition, the socket is integrally machined with the washer to simplify fabrication.

Several washer materials were evaluated. Aluminum was eliminated because of the 590°K (600°F) bond line temperature requirement. Beryllium and magnesium are the lightest weight washer materials. Titanium was selected for this program primarily because of material availability. Further analyses are required to develop washer concepts using either magnesium or beryllium. Magnesium has limited corrosion and wear resistance. The low ductility of beryllium subjected to biaxial stresses requires careful design of the lug.

TITANIUM WASHER DISTRIBUTES ATTACHMENT LOADS
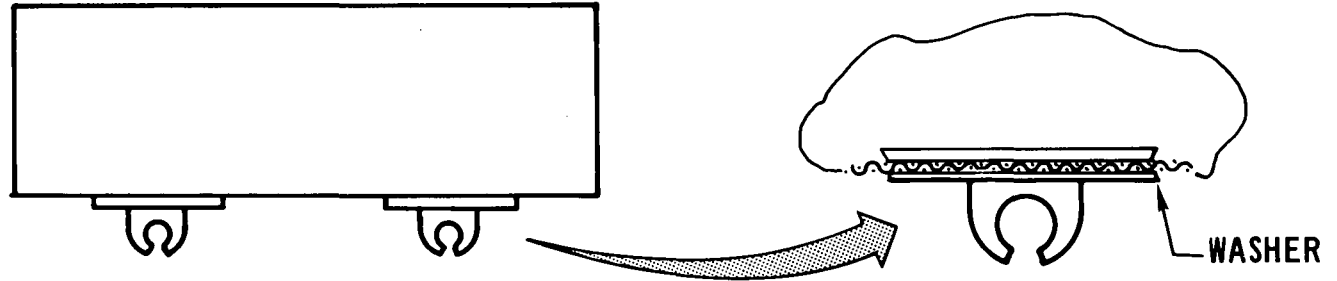
WASHER

CONCEPTS

√. SOLID WASHER

• HONEYCOMB
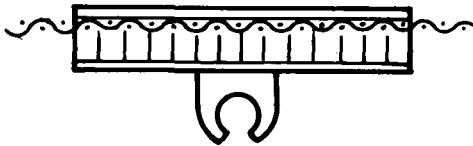
• INTEGRAL RIBS
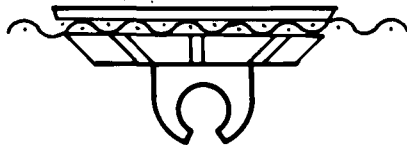
WASHER WEIGHTS

MATERIAL	THICKNESS IN. (a)	WEIGHT LB/FT^2 (b)
BERYLLIUM	0.076 (0.193)	0.14 (0.69)
MAGNESIUM	0.142 (0.361)	0.25 (1.23)
TITANIUM	0.102 (0.260)	0.45 (2.20)
STEEL	0.086 (0.218)	0.66 (3.23)
COLUMBIUM	0.098 (0.250)	1.02 (5.00)

(a) UNITS IN PARENTHESES ARE CM
(b) UNITS IN PARENTHESES ARE Kg/M^2

Figure 8

ANALYTICAL MODEL FOR ATTACHMENT STRESSES

(Figure 9)

A study was conducted to determine washer stiffness requirements for minimizing high concentrated loads in HCF at attachments. The use of thin washers results in high peaking stresses in the HCF near the center of the washers. The approach was to determine a peaking factor (ratio of peak stress to average stress) using a two-dimensional finite element model and applying this peaking factor to the average stress obtained for a circular washer. The analysis utilized the "Computer Aided Structural Design" computer program. The two-dimensional finite element model of RSI and mechanical attachment is illustrated in this chart. The model contains shear panels and axial elements to represent RSI, RTV-560 adhesive and titanium washer. A unit load was applied to the model as illustrated in the chart to determine transverse tensile stresses in the RSI.

ANALYTICAL MODEL FOR ATTACHMENT STRESSES

ATTACHMENT GEOMETRY

1 LB (0.453 kg)

FINITE ELEMENT MODEL

HCF

SHEAR
PANEL (TYP)

RTV–560

WASHER
(TITANIUM)

1 LB (0.453 kg)

AXIAL
MEMBER (TYP)
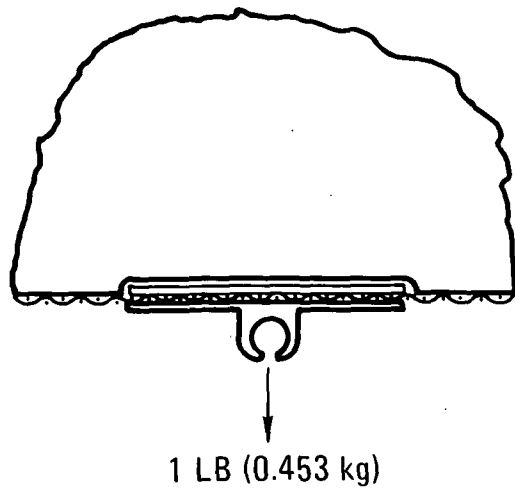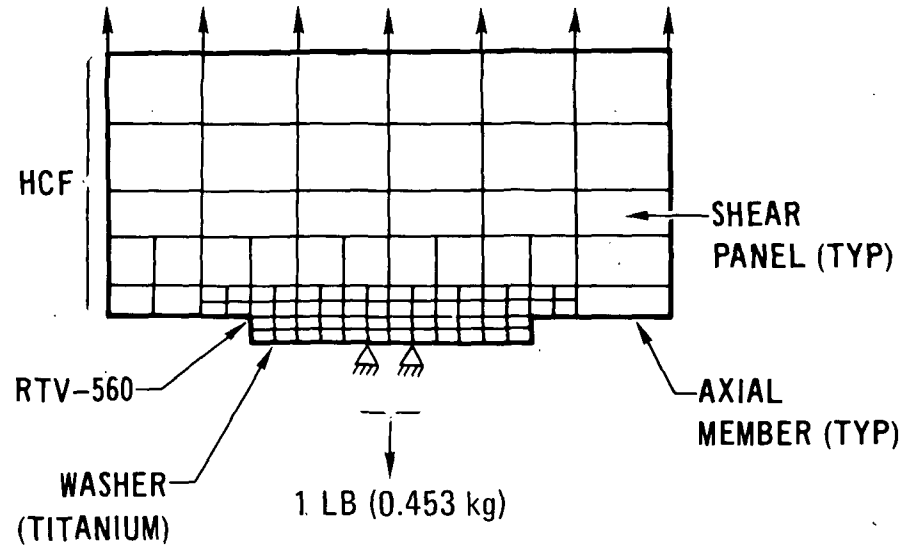
Figure 9

MINIMUM WEIGHT WASHER SELECTED TO LIMIT PEAKING STRESS IN HCF
(Figure 10)

Several washer diameters and washer thicknesses were analyzed. In all cases the maximum RSI transverse tensile stress occurs immediately above the RTV-560 and in line with the sides of the socket. A plot of RSI transverse stress divided by average transverse stress at the RTV-560 bond line as a function of distance from the washer centerline is shown on this chart. Peaking stresses are highest for thin washers. The curves shown are for a washer diameter of 4.57 cm (1.8 inch). Similar curves were obtained for other washer diameters. Peaking stresses obtained using the two-dimensional analytical model are conservative since the washer actually behaves as a plate instead of a beam.

These data were used to determine minimum washer weight as a function of diameter. The 24.4 kg (54 lb) load results from a 31.0×10^3 N/m^2 (4.5 psi) ultimate burst pressure applied to a 15.2 cm x 15.2 cm (6 inch x 6 inch) tile and reacted equally by three attachments. Results are shown on the right of this chart. The curve was obtained by calculating the weight of the thinnest washer for a given diameter that will limit RSI peaking stress to 207×10^3 N/m^2 (30 psi). The minimum weight washer is one of approximately 4.31 cm (1.70 inch) diameter.

MINIMUM WEIGHT WASHER SELECTED TO LIMIT PEAKING STRESS IN HCF
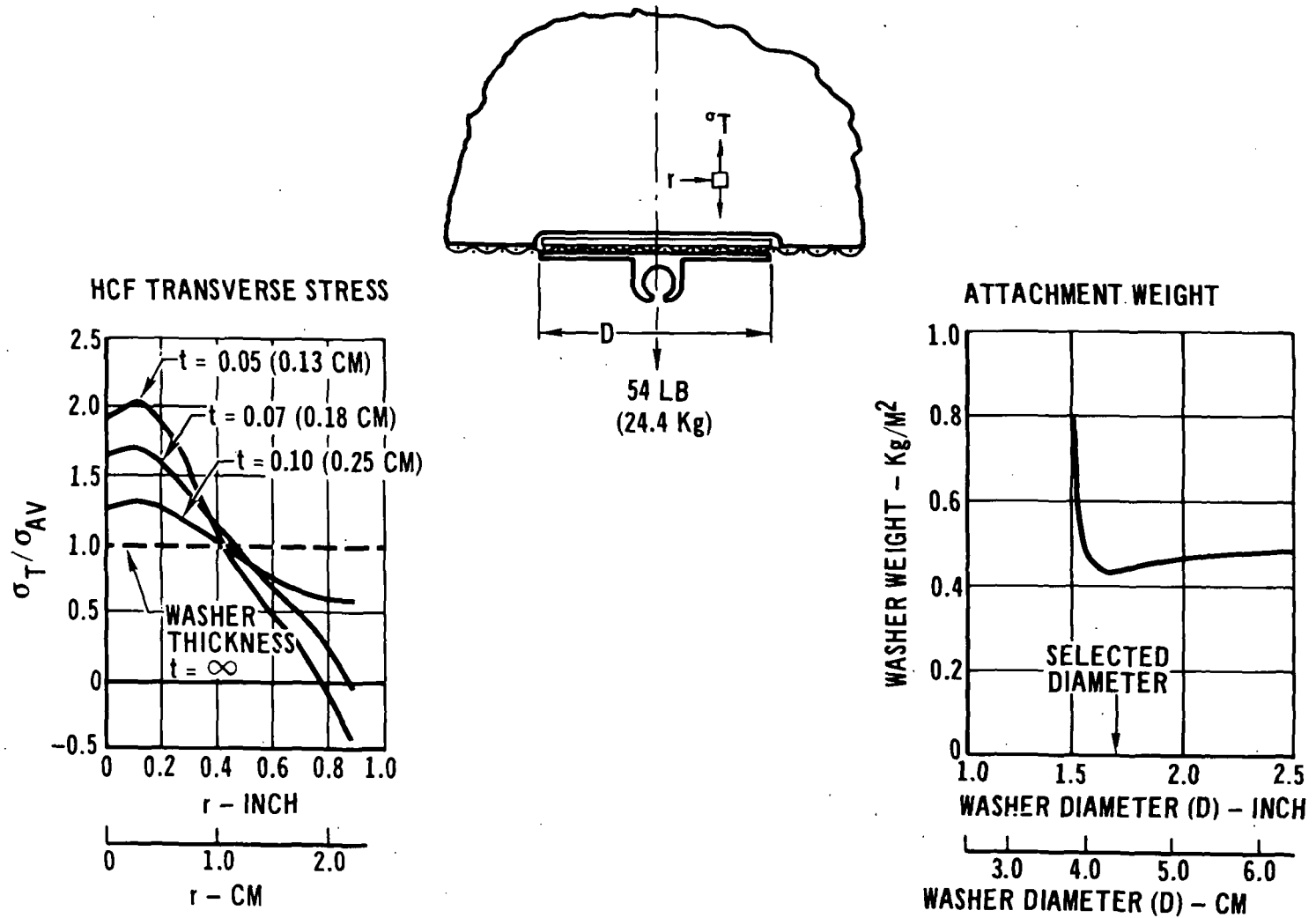
Figure 10

STRAIN ISOLATION REQUIREMENTS

(Figure 11)

Low allowable strain of RSI materials requires that tiles be isolated from thermal and mechanical strains in primary structure. Strain isolation requirements depend on tile size, attachment location, temperatures, mechanical loads, and material properties.

Strain isolation requirements are summarized on this chart. Requirements were obtained by combining tile and structure thermal strains and primary structure mechanical strains resulting from in-plane loads. Two initial temperatures, room temperature and 117°K (-250°F), were investigated. Significant strains and rotations were found to occur at four times during energy; 0, 1200, 2600, and 3600 seconds. Maximum requirements for strain isolation are obtained by combining the 0.0392 cm (0.0154 inch) expansion with the 0.0305 cm (0.0120 inch) contraction for a total sliding requirement of 0.0696 cm (0.0274 inch). The ball joint attachment concept can accommodate these motions easily.

STRAIN ISOLATION REQUIREMENTS
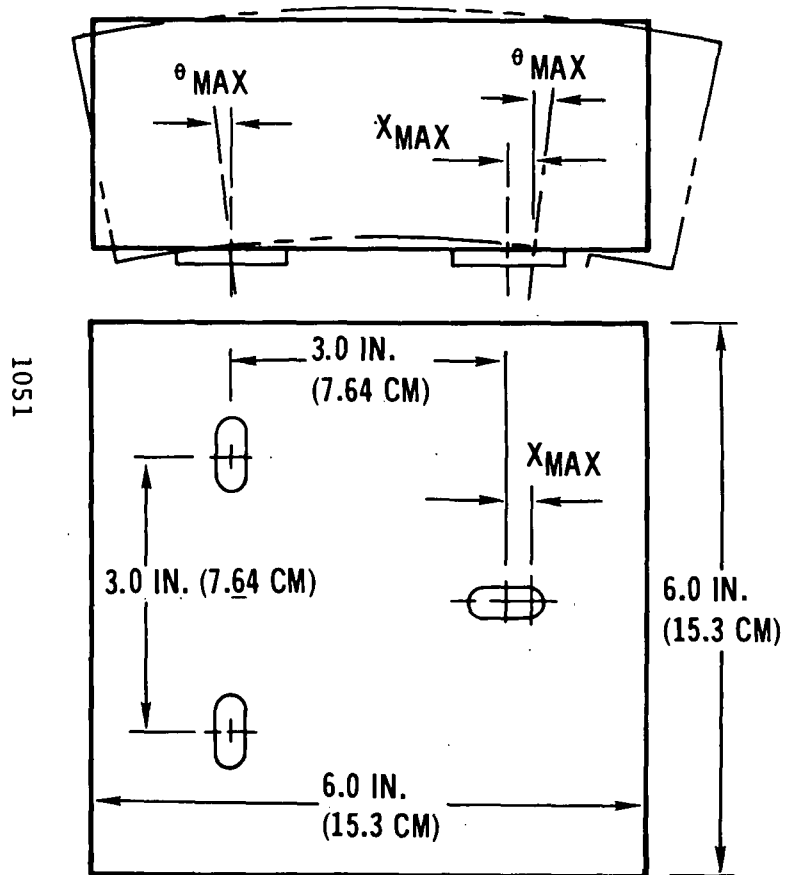
INITIAL TEMPERATURE (°F)	ENTRY TIME (SEC)	$X_{MAXIMUM}$ IN. (a)	θ MAXIMUM (DEG)
RT	0	0	0
	1200	0.0019 (0.0048)	0.13
	2600	0.0082 (0.0021)	0
	3600	0.0154 (0.0392)	−0.03
−250 (117°K)	0	−0.0120 (−0.0305)	0
	1200	−0.0093 (−0.0246)	0.15
	2600	−0.0090 (−0.0229)	0.03
	3600	−0.0113 (−0.0283)	0

TOTAL SLIP = 0.0154 − (−0.0120) = 0.0274 IN. (0.0696 CM)
(a) UNITS IN PARENTHESIS ARE CM

Figure 11

ATTACHMENT STRENGTH TESTS

(Figure 12)

Static load, acoustics, and vibration tests were conducted to determine the integrity of the ball joint concept. Results of tests are summarized in the following figures.

The ball joint attachment concept was strength tested. Attachments were loaded to failure in tension, compression, and shear. All specimens withstood loads greater than they were designed for. Failing loads are summarized in figure 12 and compared with design ultimate loads. Tension and compression design loads result from 31.0×10^3 N/m^2 (4.5 psi) ultimate burst pressure and 41.4×10^3 N/m^2 (6.0 psi) collapse pressure applied to a 15.2 cm x 15.2 cm (6 inch x 6 inch) tile. The design shear load is based on a 30 g side load applied to a tile.

Ultimate strengths were considerably greater than design loads. The difference between the two may have been due to a combination of the following reasons.

- HCF transverse strength may have been greater than assumed.
- Membrane forces in titanium screen react some loads.
- RTV-560 adhesive impregnates HCF and increases effective tension and shear area.
- Predicted peaking stresses using two-dimensional analytical model are conservative.

ATTACHMENT STRENGTH TESTS
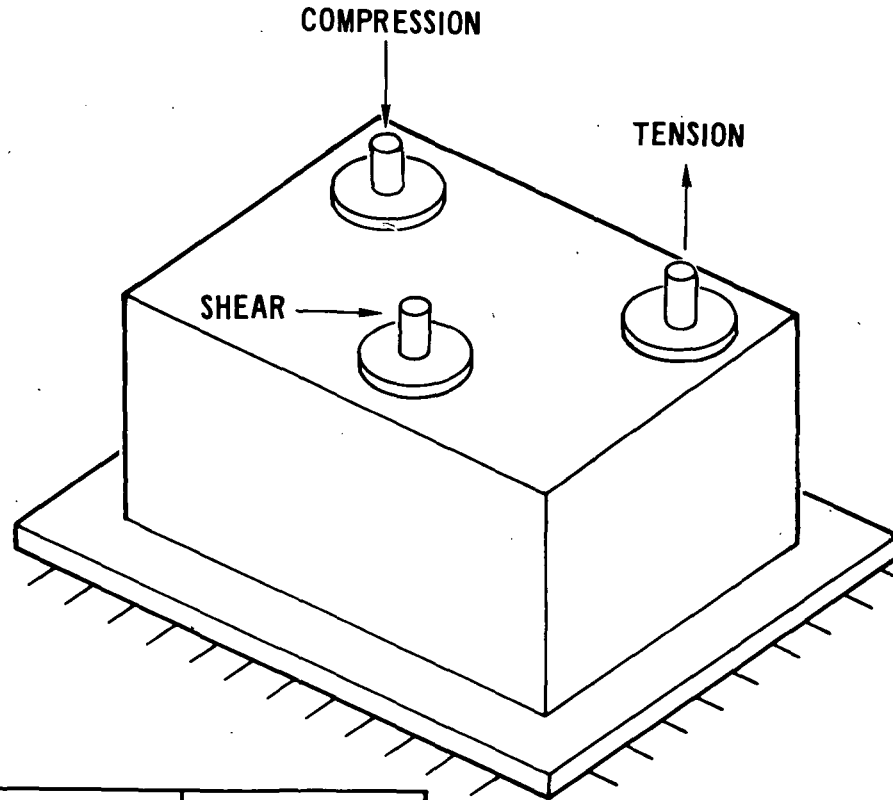
TEST	ULTIMATE STRENGTH LB (a)	DESIGN LOAD LB (a)
TENSION	159 (72)	54 (24)
COMPRESSION	328 (148)	72 (33)
SHEAR	177 (80)	32 (15)

(a) UNITS IN PARENTHESIS ARE Kg

Figure 12

TILE ACOUSTIC TEST

(Figure 13)

A 15.2 cm x 15.2 cm x 7.0 cm (6 inch x 6 inch x 2.75 inch) thick RSI tile was exposed to a 160 dB acoustic environment for 50 minutes to simulate 100 Shuttle flights. The tile was mechanically attached to a support fixture. An insulated box surrounded the tile, providing a 0.254 cm (0.10 inch) gap between tile and insulation box. Microphones were located on both sides of the tile to measure acoustic attenuation through RSI. The tile survived the 160 dB environment without evidence of damage.

1054

TILE ACOUSTIC TEST

TEST SETUP

MICROPHONE

0.10 (TYP)
(0.254 CM)

RESPONSE
ACCELEROMETER

TILE

INSULATION
PACKAGE

BALL JOINT
ATTACHMENT

SUPPORT
FIXTURE

MICROPHONE

1055

ENVIRONMENT

OCTAVE BAND SOUND PRESSURE LEVEL
(VE 0.0002 DYNES/CM^2)

OVERALL – 160 dB

150

145

140

16   31.5   63   125   250   500   1000   2000   4000   8000

OCTAVE BAND CENTER FREQUENCIES – Hz
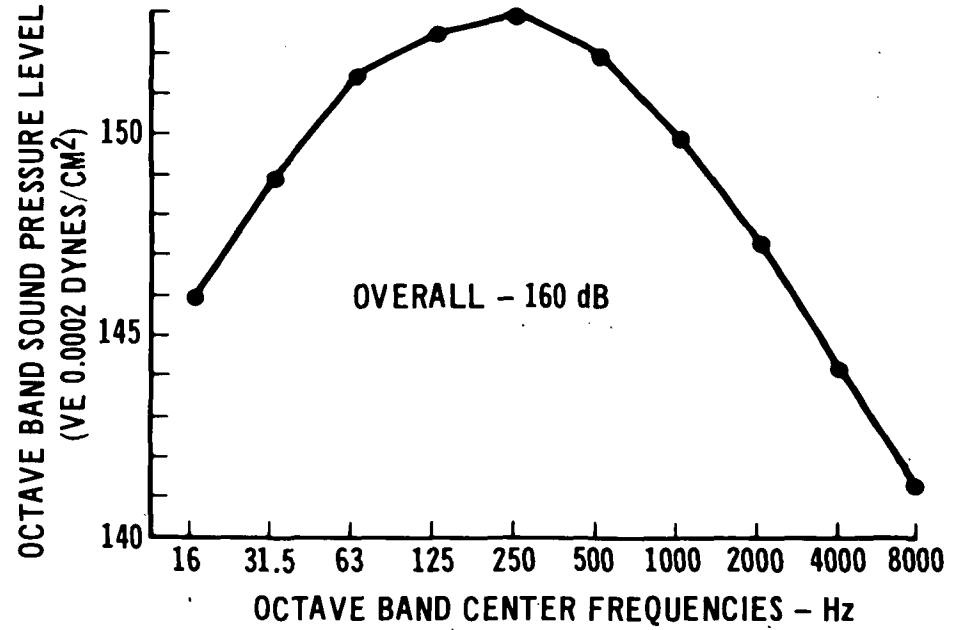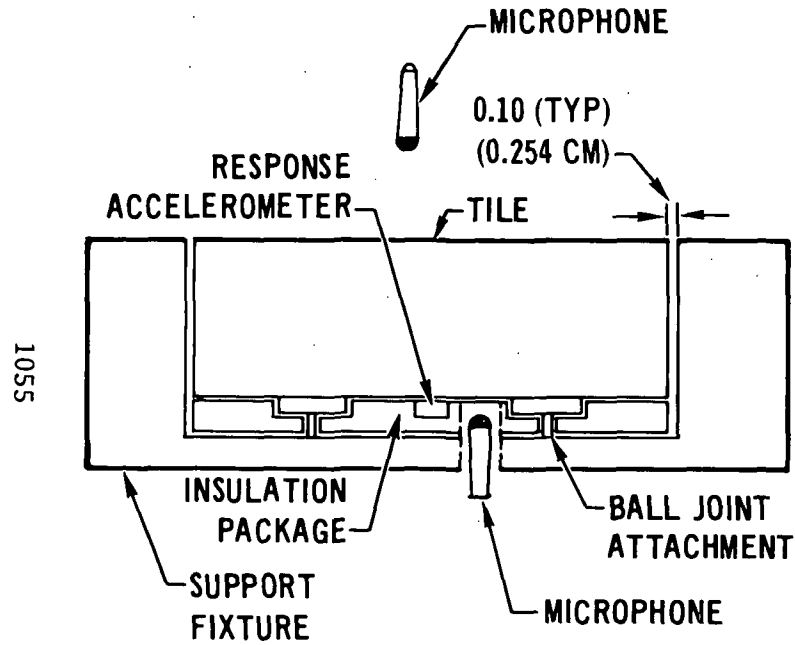
Figure 13

VIBRATION TEST

(Figure 14)

Response of a typical Shuttle primary structure panel to the acoustic environment was calculated. The calculated panel response was then used as input to the random vibration test. A 15.2 cm x 15.2 cm x 7.0 cm (6 inch x 6 inch x 2.75 inch) thick tile was mechanically attached to an aluminum plate, which was in turn bolted to a shaker table. Tile response was measured with an accelerometer bonded to the backside of the tile. Fifty minutes of testing was selected to represent 100 Shuttle flights.

The HCF failed at the bond line after 42 minutes of the planned 50 minute test. Examination of the test specimen revealed the following two possible causes of failure. Weight of the RTV-560 bond line on the test specimen was unusually low, which may have led to the premature failure. In addition, significant wear was noted on the balls and sockets. The wear may have caused the tile to rattle, leading to a premature failure. This problem could be minimized by coating the titanium, using a larger ball to reduce bearing stresses or replacement of balls prior to 100 flights.

VIBRATION TEST

TEST SETUP

RESPONSE ACCELEROMETER

MECHANICAL ATTACHMENT

HCF TILE

BASE PLATE

INPUT ACCELEROMETER

VIBRATOR EXCITER

1057

ENVIRONMENT

POWER SPECTRAL DENSITY – g^2/Hz

OVERALL – 29.4 g's RMS

1.0 g^2/Hz

0.5 g^2/Hz

0.5 g^2/Hz

0.2 g^2/Hz

20   40   200 300 800   2000

10   100   1000

FREQUENCY – Hz
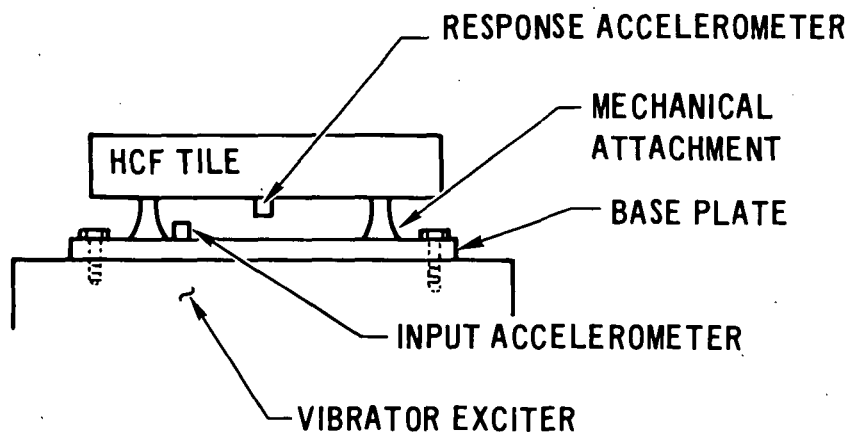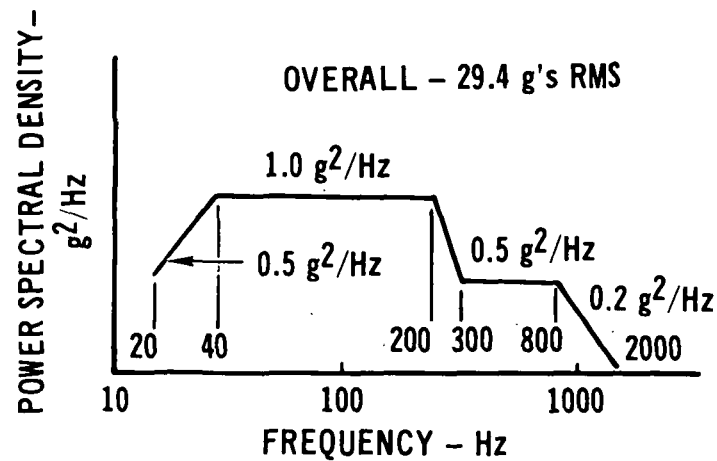
Figure 14

WEIGHT COMPARISON - MECHANICAL ATTACHMENT VERSUS DIRECT BONDED TILES

(Figure 15)

The mechanical attachment concept is slightly lighter than direct bonded tiles. Mechanical attachment hardware and adhesive weights are measured values. Insulation and tile weights are theoretical and will be verified on the current program. Direct bond weights are measured values obtained from out Phase 2 RSI study.

For production hardware it may be possible to reduce the weight of the mechanical attachment concept to about 23.5 kg/m^2 (4.8 lb/ft^2) by proper selection of materials. For example, use of beryllium washers reduces the weight by 1.5 kg/m^2 (0.3 lb/ft^2). Using 128 kg/m^3 (8 pcf) MIN-K insulation instead of 56.1 kg/m^3 (3.5 pcf) TG-1500 insulation results in reduced HCF thickness and a weight savings of 1.0 kg/m^2 (0.2 lb/ft^2). However, further analyses are required to substantiate these weight savings.

WEIGHT COMPARISON — MECHANICAL ATTACHMENT VERSUS DIRECT BONDED TILES

	kg/m^2	lb/ft^2
MECHANICAL ATTACHMENT		
HARDWARE	3.56	0.73
INSULATION	1.95	0.40
TILE	19.17	3.92
ADHESIVE	1.41	0.29
	26.09	5.34
DIRECT BOND		
TILE	23.41	4.79
0.25 IN. SPONGE	3.08	0.63
ADHESIVE	1.85	0.38
	28.34	5.80

Figure 15

CONCLUSIONS

(Figure 16)

Mechanical attachment concept is nearly 2.45 kg/m^2 (0.50 lb/ft^2) lighter than direct bond. The ball joint mechanical attachment concept has withstood tensile, compressive, and shear forces in excess of design loads. A tile has survived a typical Shuttle acoustic environment. Another tile survived a vibration environment equivalent to 84 shuttle flights. The ball joint attachment concept is easy to install, remove, inspect, and adjust.

1060

CONCLUSIONS

- MECHANICAL ATTACHMENT CONCEPT IS LIGHTER THAN DIRECT BOND

- SURVIVED STRENGTH, ACOUSTIC AND VIBRATION TESTS

- SURVIVED VIBRATION ENVIRONMENT EQUIVALENT TO 84 SHUTTLE FLIGHTS

- STRAIN ISOLATION ACCOMPLISHED

- FLOW BEHIND TILE RESTRICTED

- EASY INSTALLATION, REMOVAL, INSPECTION AND ADJUSTMENT

- CARRIER PLATE AND INSULATION PROVIDE SOME PROTECTION IF RSI IS LOST

1061

Figure 16

OPTIMUM TPS DESIGN WITH REI-MULLITE

BY

T.E. HESS, R.J. MICHALAK, R.A. BREWER

GENERAL ELECTRIC CO.
RE-ENTRY, AND ENVIRONMENTAL SYSTEMS DIVISION
PHILADELPHIA, PENNSYLVANIA

1063

32

INTRODUCTION

Stringent requirements have been placed upon the design of the Shuttle Orbiter thermal protection system (TPS). Design safety factors must be used to prevent failure of the insulator, its attachment system, and its coating. The system must be capable of withstanding temperature extremes from 1644° K (2500° F) to 116° K (-250° F) and remain waterproof for 100 mission reuses. In addition, it must be capable of enduring a variety of environmental exposures including salt spray, humidity, rain, acoustics, and the temperature/vacuum extremes of orbital flight.

This paper discusses factors important to the design of a Reusable External Insulation TPS, REI-Mullite, that meets these requirements. Successful thermostructural design requires consideration of the characteristics of the TPS components as well as the complex structural interactions. Included in the latter is the level of stress and strain developed in the coating, insulation, and attachment system; the effect of residual stresses and creep on system performance and design; and the effect of material shrinkage on the system capability.

One of the more severe design conditions for a bonded system is that of on-orbit cold soak in which temperatures as low as 116° K (-250° F) are experienced. Being below the glass transition temperature of the silicone polymer class of materials used for attachment, this can result in high stresses in both the insulator and the bond since the coefficient of expansion of the bond is two orders of magnitude greater than the insulator and one order of magnitude greater than the substructure. TPS configurations have been analyzed and tested for this condition. These tests have served to demonstrate that the adhesive bond attachment systems developed by General Electric Company (GE-RESD) can be successfully designed for use under these conditions, but that special analytical treatment is necessary to account for the unusual behavior of the bond material as it becomes cold and highly stressed. System and subsystem test results are discussed as well as their correlation with the thermostructural analyses. TPS configuration limitations are defined for this 116° K (-250° F) on-orbit cold soak situation.

While design optimization has been pursued on both a technology level as part of NASA-MSC contract activity and on an Orbiter design application level for the North American Rockwell Corporation as part of their Phase B Space Shuttle activity, this paper concentrates on the former. The analyses and trades presented here are based on Area 1 and Area 2P NASA-MSC defined heating and loading levels and, where the analyses depend on tile size, it is done for the 0.2 x 0.2 m (8 x 8 in.) tile size selected for use in prototype hardware to be supplied on the contract.

The severe operational requirements set forth for the TPS, which require capability over a temperature range from 116° to 1644° K (-250° F to 2500° F), can be met with REI-Mullite. This is a material system, developed by the General Electric Company, that is considered to be near optimum for meeting the Shuttle Orbiter 1644° K (2500° F) multimission requirement.

MOD IB REI-MULLITE MEETS REQUIREMENTS

(Figure 1)

It will be shown in this paper that the GE-RESD MOD IB REI-Mullite TPS can be used to surface temperatures of 1644° K (2500° F) with adequate margins of safety based on minimum strengths or strains of the material. This includes entry from the cold start condition of 116° K (-250° F).

A new lightweight foam bond strain isolator has been developed and utilized in the design studies and test hardware. This bond is compatible with the 116° K (-250° F) cold orbital soak condition and has been shown both analytically and experimentally to have structural integrity for this condition.

MOD IB REI-MULLITE MEETS REQUIREMENTS

1067

- CAN WITHSTAND REPEATED USE AT 1644°K (2500°F)

- CAN ENDURE THERMAL STRESSES OF ENTRY HEATUP WITH ADEQUATE MARGINS

    - FACTOR-OF-SAFETY OF 1.5
    - BASED ON MINIMUM STRENGTH OR STRAIN
    - COLD START OF 116°K (-250°F)

- FOAM BOND SYSTEM IS COMPATIBLE WITH 116°K (-250°F) COLD SOAK CONDITION

(FIGURE 1)

MAJOR DESIGN REQUIREMENTS

(Figure 2)

The GE-RESD Space Shuttle TPS design activities have emphasized the use of direct bonding as the method of attachment of the insulation to the orbiter structure. These activities have been directed toward meeting a set of requirements, the major points of which are summarized here. Multimission reuse, while remaining waterproof after exposure to temperature extremes from 116° K (-250° F) to 1644° K (2500° F), is a severe requiremei t that affects all aspects of the TPS design.

1068

MAJOR DESIGN REQUIREMENTS

- 1644°K (2500°F) MAXIMUM TEMPERATURE

- 1922°K (3000°F) OVERSHOOT

- 116°K (-250°F) COLD SOAK

- 100 MISSION REUSE

- WATERPROOF

(FIGURE 2)

1069

TYPICAL ISOTHERMS/THERMAL PROTECTION NR/SD SHUTTLE ORBITER
(Figure 3)

Figure 3 illustrates a map of typical isotherms developed on the North American Rockwell Corporation (NR/SD) Shuttle Orbiter. These isotherms are based on a nominal high, cross-range trajectory.

1070

TYPICAL ISOTHERMS/THERMAL PROTECTION
NR/SD SHUTTLE ORBITER

RCC ☐

REI-M ☐

REI-E ☐

1461°K
(2170°F)
(BOOST)

728°K
(850°F)

616°K
(650°F)

728°K
(850°F)

728°K
(850°F)

1644°K
(2500°F)

616°K
(650°F)

616°K
(650°F)

728°K
(850°F)

728°K
(850°F)

1905°K
(2970°F)

616°K
(650°F)

1311°K
(1900°F)

1533°K
(2300°F)

1533°K
(2300°F)

1644°K
(2500°F)

1311°K
(1900°F)

1644°K
(2500°F)

1644°K
(2500°F)

1071
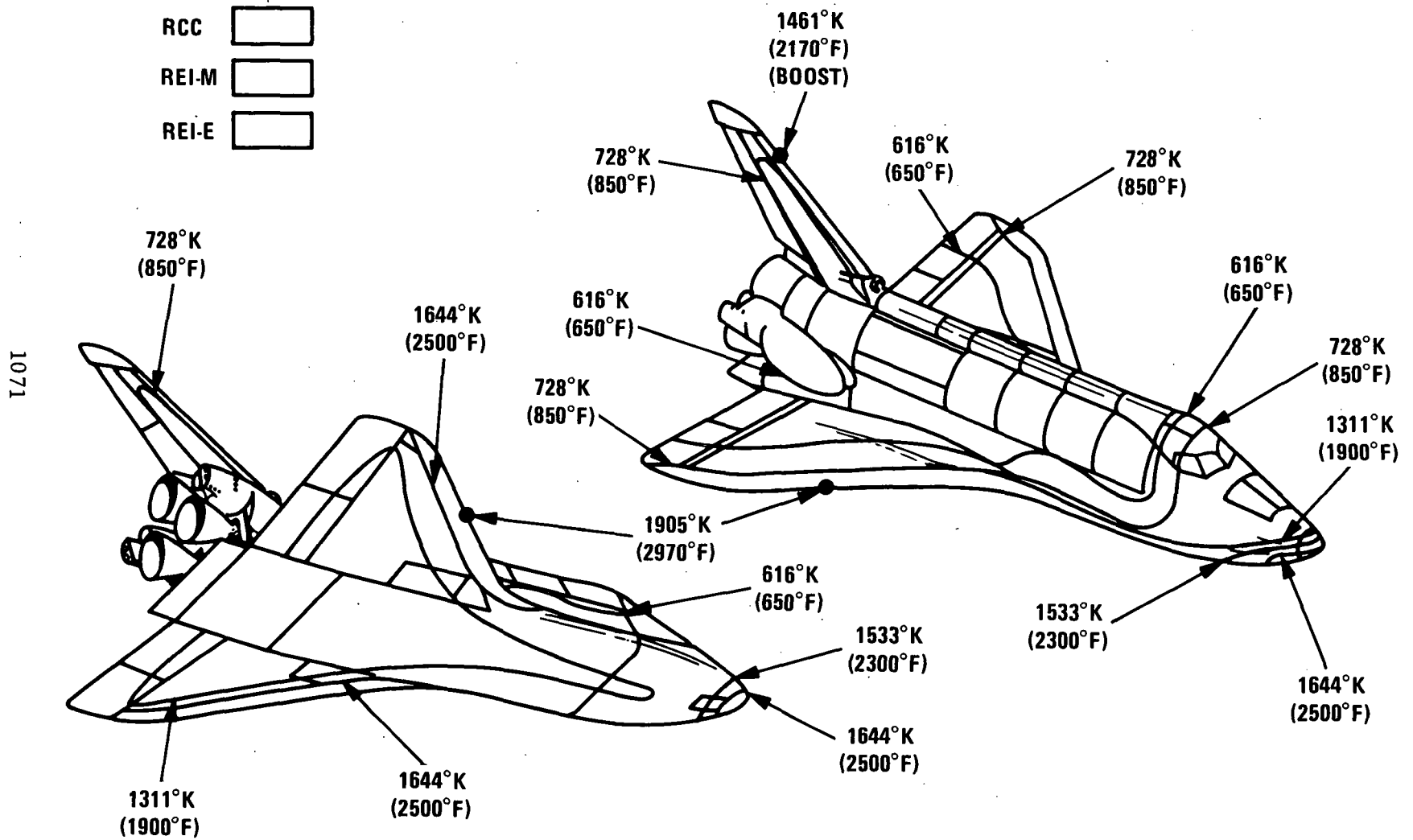
(FIGURE 3)

STRUCTURAL ANALYSIS METHODOLOGY
(Figure 4)

The primary structural analysis tool being used in the TPS studies is the finite element technique. Two-dimensional plane stress analysis has been used extensively to date and analyses using three-dimensional modeling are currently being performed. In addition, certain aspects of the TPS behavior require special treatment in these analyses. This results from: (1) the fact that the bond goes through its glass transition phase during orbital cold soak and creeps in the process; and (2) the existence of residual stresses at room temperature in the coated tiles due to the elevated temperature firing cycles.

Particular attention has been given to comparing the analyses to experimental test results so that the determination of an optimum design is based on a realistic prediction of its response to mission environments. These comparisons are discussed later in this paper.

STRUCTURAL ANALYSIS METHODOLOGY

- **FINITE ELEMENT TECHNIQUES**

  - GE ORTHOSAFE PROGRAM

    - 2-D – PLANE STRESS

    - 3-D – HIGHER ORDER ELEMENTS

- **SPECIAL CONSIDERATIONS**

  - GLASS TRANSITION OF PD-200 FOAM BOND

  - BOND CREEP

  - RESIDUAL STRESS IN REI AND COATING

- **EXPERIMENTAL CALIBRATION OF ANALYSIS**

(FIGURE 4)

1073

TYPICAL FINITE ELEMENT MODELS

(Figure 5)

Figure 5 illustrates typical two- and three-dimensional finite element models. The 2-D models contain approximately 1400 elements and the 3-D models 1600 elements. Most of the analyses have been with the 2-D analysis with special effects and details not considered in the 2-D analysis being treated with the 3-D analysis. These analyses used orthotropic and temperature dependent properties.

1074

TYPICAL FINITE ELEMENT MODELS

2D

3D

SR2-HF1 COATING

REI—MULLITE

PD200 BOND

STRUCTURE

1075
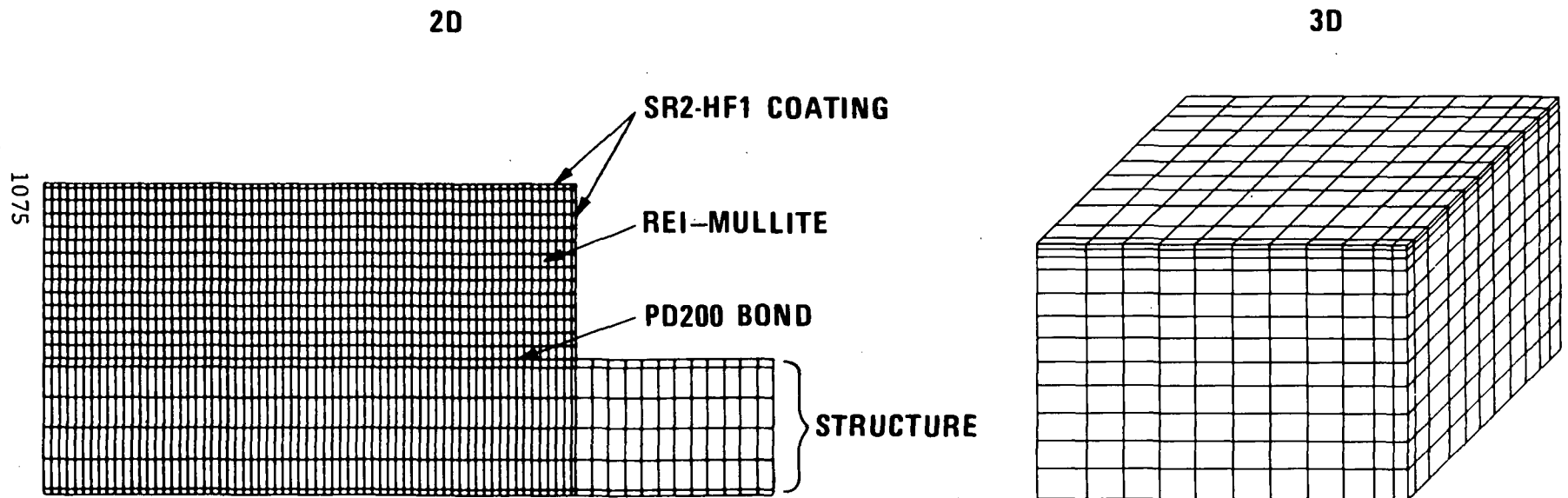
(FIGURE 5)

CALIBRATION OF ANALYTICAL TECHNIQUES
(Figure 6)

Comparison of analytical predictions and test results have been made using three types of tests. These are:

1. Residual coating strain measurements made on room temperature specimens

2. Cold soak subsystem tests made using tiles bonded to aluminum substrates

3. Tests on specimens especially designed to make correlations for the cold soak condition

These tests are discussed in Figures 7 through 11.

CALIBRATION OF ANALYTICAL TECHNIQUES

- COLD SOAK INSTRUMENTED MODELS

- COLD SOAK SUBSYSTEM TESTS

- RESIDUAL STRAIN TESTS

1077

(FIGURE 6)

COLD SOAK SANDWICH BEAM TEST

(Figure 7)

Analyses for the 116° K (-250° F) cold soak condition predicted failure in the bond and in the REI-Mullite, whereas the cold soak tests produced no failures. To resolve this apparent discrepancy a test specimen was designed with which actual strain measurements could be made to investigate postulated creep behavior. This specimen is shown in Figure 7 and consists of a sandwich beam with thin aluminum faces and a PD 200-16 core bonded with thin film layers of RTV 560. Several of these specimens were cooled to 116° K (-250° F), and the strains in the aluminum sheets were monitored throughout the cycle.

COLD SOAK SANDWICH BEAM TEST

STRAIN GAGE

0.00041m (0.016 IN.) ALUMINUM

PD-200-16 FOAM BOND

0.00041m (0.016 IN.) ALUMINUM

0.0145 m (0.57 IN.)

116°K
(-250°F)

TEMPERATURE, °K

TIME, HOURS

1079
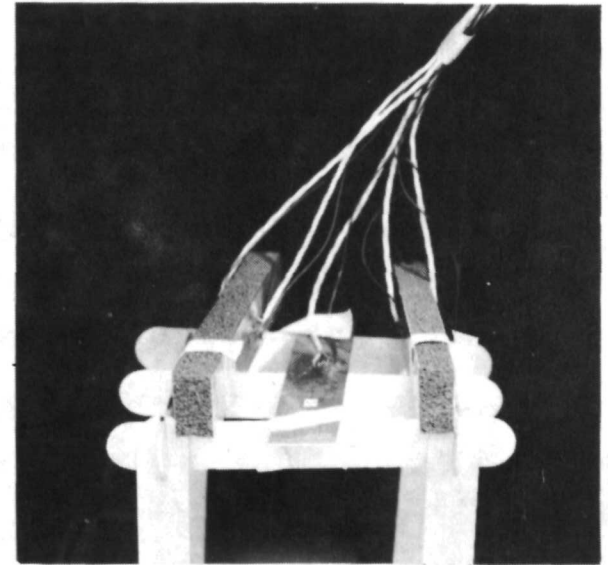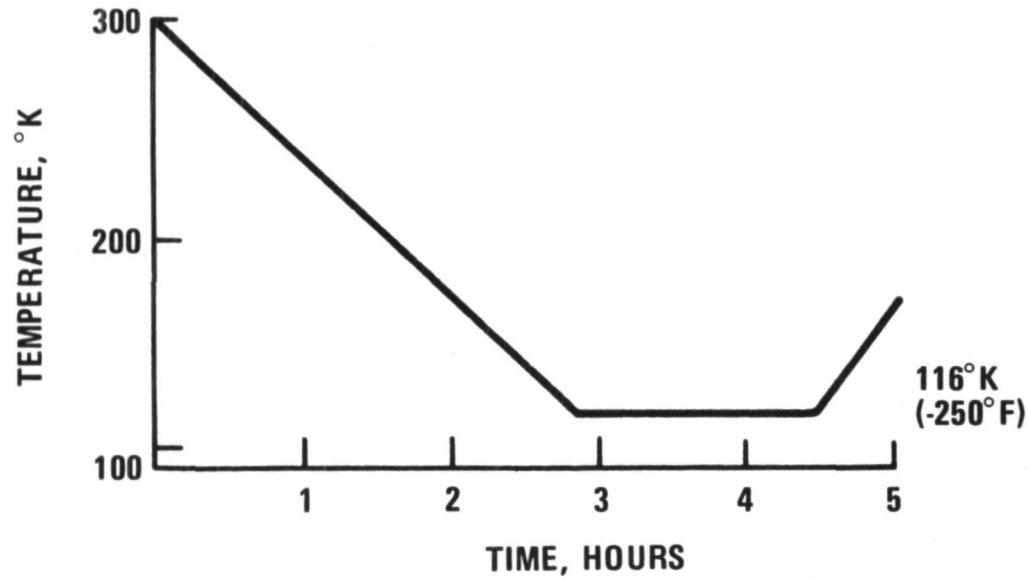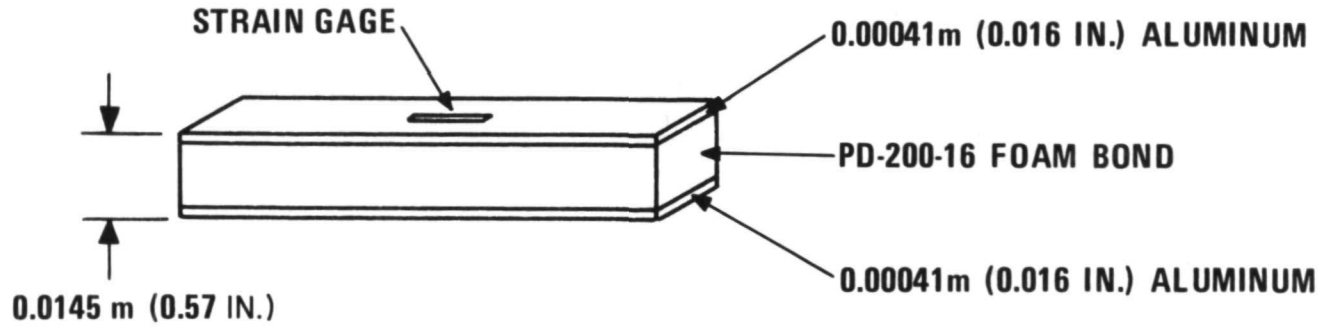
(FIGURE 7)

SANDWICH BEAM TEST RESULTS

(Figure 8)

These sandwich beam specimens were also analyzed using finite element techniques to predict the strain in the aluminum at 116° K (-250° F). The tests produced strains in the aluminum face sheets of about -275 microstrain (10^{-6} m/m/(in/in)) while the predicted value was -2280 microstrain. It was suspected that this difference could be caused by creep of the bond, which would relieve the general state of stress in the specimen. Creep tests were run on the PD 200-16 at room temperature and at 180° K (-135° F). These tests showed that cooling to 116° K over a several hour period produced enough creep to explain the difference between analyses and test results. Creep effects were subsequently included in the modified analysis method to predict the performance of bonded tiles in subsystem tests.

SANDWICH BEAM TEST RESULTS

STRAIN IN ALUMINUM

-275 AVERAGE

O SPECIMEN 1
□ SPECIMEN 2

116°K
(-250°F)

STRAIN, 10^{-6} m/m (IN./IN.)

TEMPERATURE, °K

PD 200-16 CREEP TESTS

180°K

300°K

CREEP, % PER HOUR

STRAIN, %

1081
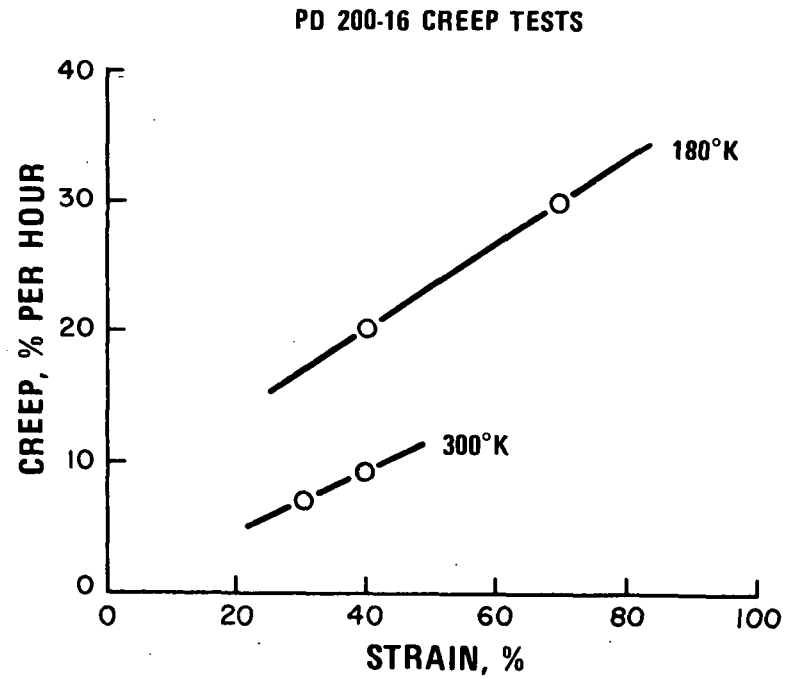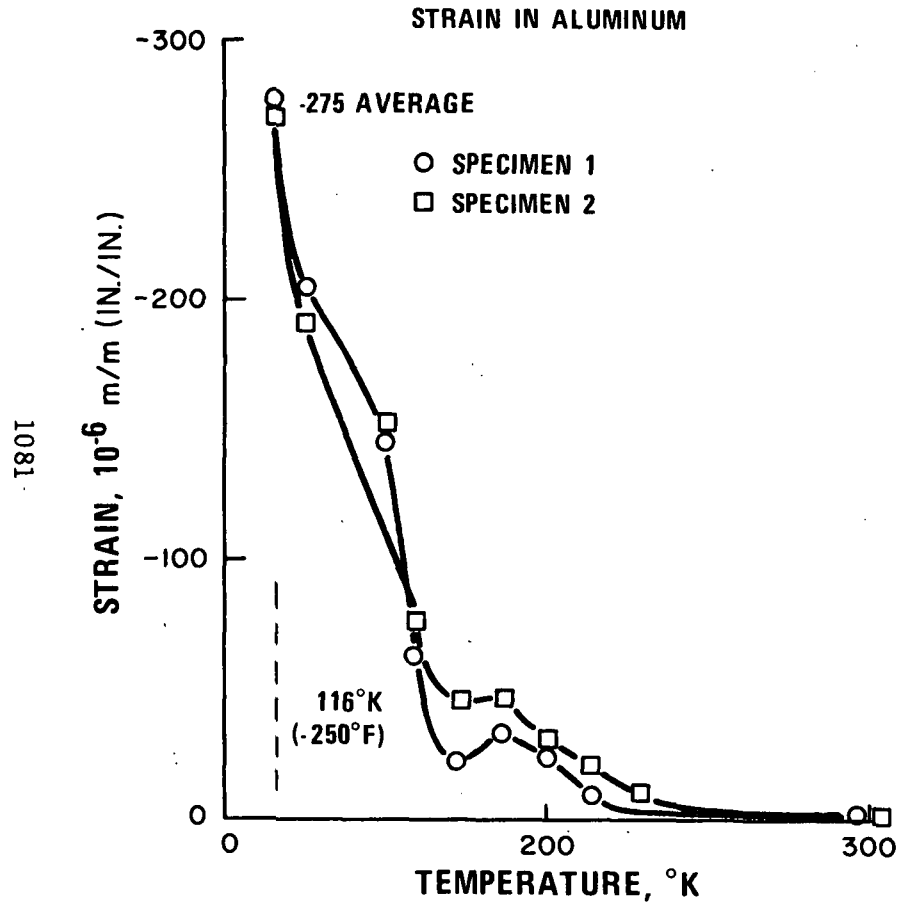
(FIGURE 8)

COLD SOAK SUBSYSTEM TESTS

(Figure 9)

The subsystem tests consisted of cooling 0.20 x 0.20 m (8 x 8 inch) tiles to 116° K (-250° F) and 89° K (-300° F). The tiles were bonded to aluminum substrates with the PD 200-16 foam bond. Using the analysis technique previously described, which includes bond creep, it was predicted that no failures would occur in these tests and no failures did occur in either the bond or the REI-Mullite. Although no meaningful instrumentation could be used for strain measurements in these tests, the results served to provide additional confidence in the methodology developed for analyzing cold soak conditions.

COLD SOAK SUBSYSTEM TESTS

- 0.20 m x 0.20 m (8 IN. x 8 IN.) TILES

- 0.00625 m (.25 IN.) BOND — 256 Kg/m^3 (16 LB/FT^3)

- 116°K (-250°F), 89°K (-300°F) SOAK

- PREDICTION — NO FAILURES

- TEST RESULTS — NO FAILURES

1083

(FIGURE 9)

RESIDUAL COATING STRESSES
(Figure 10)

Since the REI-Mullite has a slightly greater expansion coefficient than the SR2-HF1 coating system, a compressive prestrain in induced in the coating as the tile cools from the 1644° K (2500° F) firing temperature used in its fabrication. A review of the characteristics of the coating and the REI-Mullite as they cool has led to the assumption that 1367° K (2000° F) is the zero stress temperature for the tile. All subsequent environmental conditions were analyzed with this as a reference condition for the coating and the REI-Mullite.

The presence of these residual stresses are accounted for in the analytical modeling by shifting the expansion curve (αT) for the coating so that it is equal to that for the REI-Mullite at 1367° K (2000° F). Room temperature isothermal soak analyses result in compression in the coating and tension in the REI-Mullite.

RESIDUAL COATING STRESSES

1085
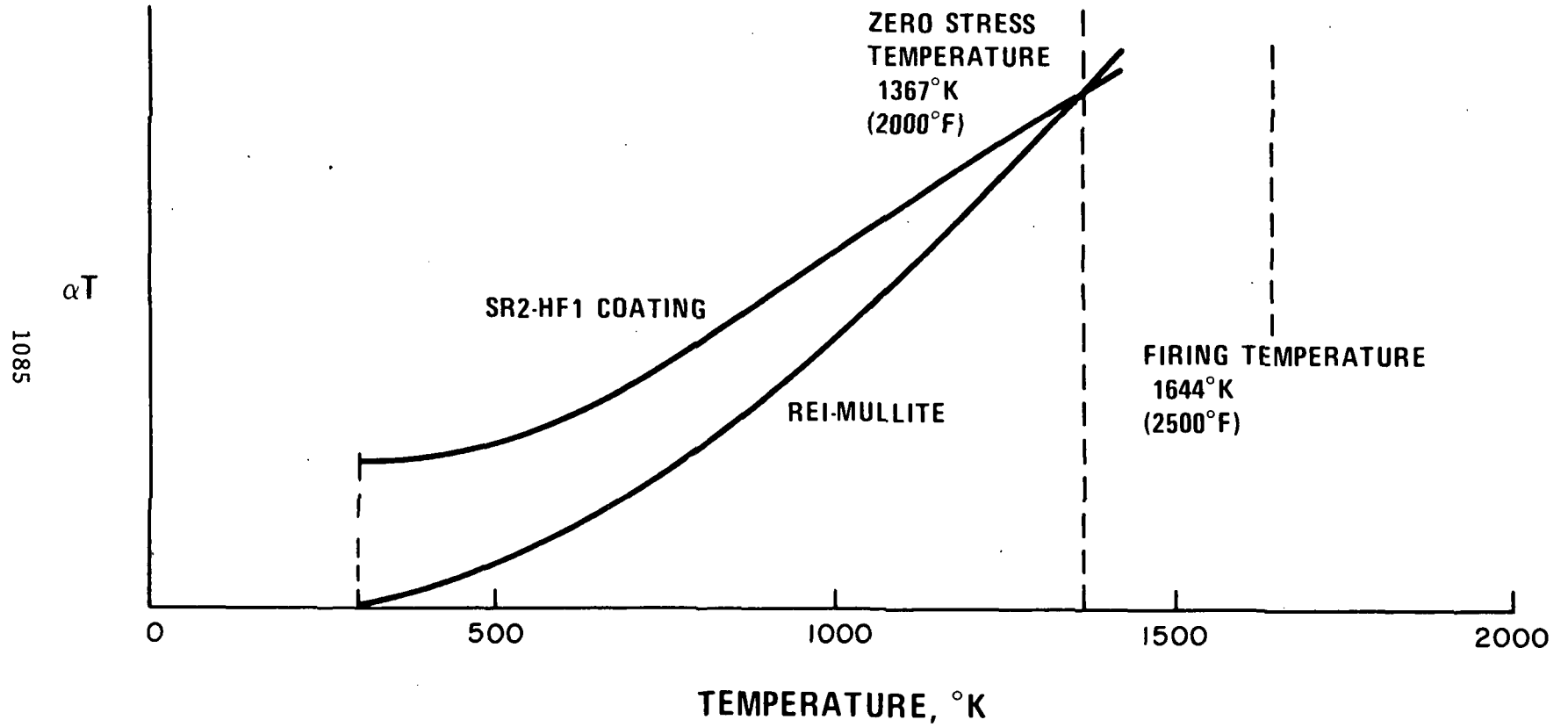
(FIGURE 10)

COMPARISON OF RESIDUAL STRAIN MEASUREMENTS TO PREDICTIONS

(Figure 11)

Tests were performed to measure the room temperature residual strain in the coatings in order to verify the residual strain effects. The specimens used were 0.051 m (2.0 inches) thick and 0.2 m (8 inches) long. Parametric 2-D finite element analyses as a function of REI-Mullite thickness were also performed for a room temperature soak to determine the residual strain state in the tile. Zero stress temperatures of both 1367° K (2000° F) and 1644° K (2500° F) were analyzed. The results of this analysis including a strain distribution through the thickness of the tile for the 1367° K (2000° F) zero stress temperature are shown. Test data fall between the analytical points representing the two zero stress temperatures. Use of the lower zero stress temperature, 1367° K (2000° F), for analyses is conservative.

Other tests have also been performed that give higher values of prestrain. These were tests on pieces cut from a five-sided coated tile in which the side coating has an effect on residual strain. Correct prediction of the prestrain in these tiles requires 3-D analyses. Correlation of the 3-D analysis with test results is currently underway.

COMPARISON OF RESIDUAL STRAIN MEASUREMENTS
TO PREDICTIONS

COATING RESIDUAL STRAIN
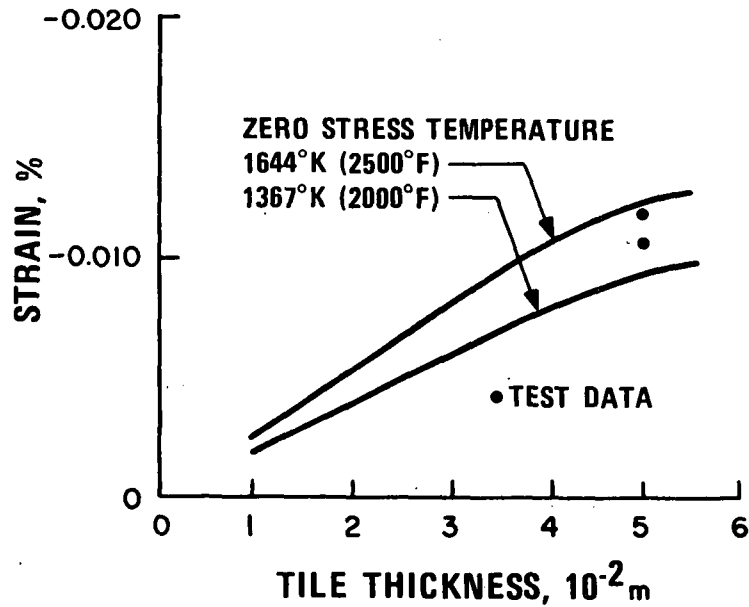
RESIDUAL STRAIN DISTRIBUTION
THROUGH TILE 1367°K (2000°F)

ZERO STRESS TEMPERATURE
1644°K (2500°F)
1367°K (2000°F)

• TEST DATA

STRAIN, %

TILE THICKNESS, 10⁻²m

COATING

REI
MULLITE

DISTANCE FROM SURFACE, 10⁻²m

STRAIN, %

1087
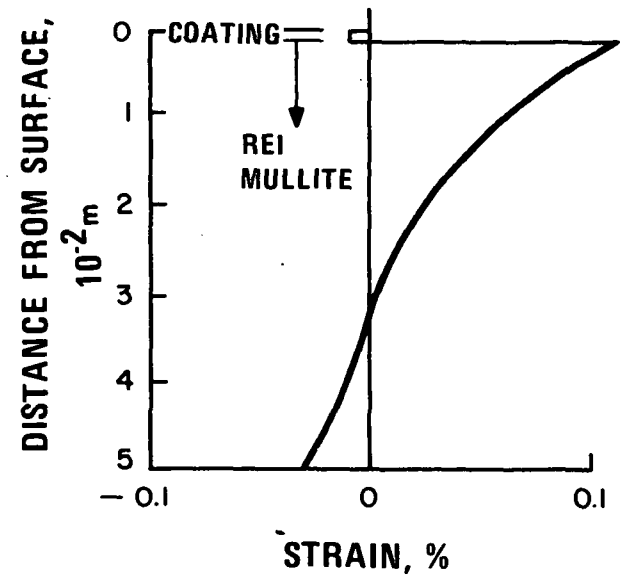
(FIGURE 11)

THERMOSTRUCTURAL TRADES
(Figure 12)

The thermostructural optimization of the REI-Mullite TPS system has been extensively investigated. The major objective of these studies has been to define the minimum weight combination of REI-Mullite and PD-200 bond system that meets the thermal and structural requirements. These trades have been pursued on two fronts; namely, for the NASA-MSC point designs on the Phase 2 and Phase 2 follow-on technology contracts, and the NR/SD orbiter designs as part of GE-RESD's contribution to the NR/SD Phase B Study. Aside from the fact that the NR/SD trades considered a much broader range of heating rates, the main differences were that the NASA-MSC point designs involved thicker substrates with lower temperature limits than the NR/SD trades.

The results are based upon the technology contract studies, although the trends and many of the results are equally applicable to the NR/SD orbiter.

Analyses were performed for (1) the orbital cold soak condition of 116° K, (2) entry heatup with the cold start condition, and (3) for post entry with start temperatures at both extremes of the temperature range. It was previously pointed out that the warm start post entry produces maximum bond temperature, whereas the cold start post entry produces a bond that is partially "soft" and partially "hard" and feels the effects of maximum structural loading.

THERMOSTRUCTURAL TRADES

- **OBJECTIVE**

  - MINIMUM WEIGHT COMBINATION OF REI-MULLITE AND PD200 BOND WHICH MEETS THERMAL AND STRUCTURAL REQUIREMENTS

- **CONDITIONS CONSIDERED**

  - ORBITAL COLD SOAK, 116°K (-250°F)
  - ENTRY HEATUP, COLD START
  - POST ENTRY, COLD START
  - POST ENTRY, WARM START

- **NASA MSC POINT DESIGNS**

  - AREA 1, 977°K (1300°F), 7.9 x 10^7 JOULES/m^2 (6900 BTU/FT^2)
  - AREA 2P, 1533°K (2300°F), 30.1 x 10^7 JOULES/m^2 (25,500 BTU/FT^2)
  - 422°K (300°F) MAXIMUM ALUMINUM SUBSTRATE TEMPERATURE
  - 706,000 N/m (4000 LB./IN.) STRUCTURE LINE LOAD

(FIGURE 12)

TRADE RESTRAINTS-REI THICKNESS VS BOND THICKNESS

(Figure 13)

For the NASA-MSC point design trades, combinations of REI-Mullite and PD-200 bond thicknesses were considered that limit the aluminum substrate temperature to a maximum of 422° K (300° F). In Area 1, there is an increase in weight as the bond thickness increases and corresponding REI-Mullite thickness decreases. However, in Area 2P there is very nearly a one-to-one trade with almost no weight difference for any combination of REI-Mullite and PD-200 bond. These weights do not include coating weight. The effect of coating weights will be shown later.

The curves shown in Figure 13 include the maximum temperature at the REI/bond interface. Since the temperature of the bond is being limited to 589° K (600° F), that limitation must be placed on the trade results generated.

TRADE RESTRAINTS –
REI THICKNESS VERSUS BOND THICKNESS

AREA 1
0.0038m (0.15 IN.) ALUMINUM
311°K (100°F) INITIAL TEMPERATURE

AREA 2P
0.0034m (0.132 IN.) ALUMINUM
311°K (100°F) INITIAL TEMPERATURE
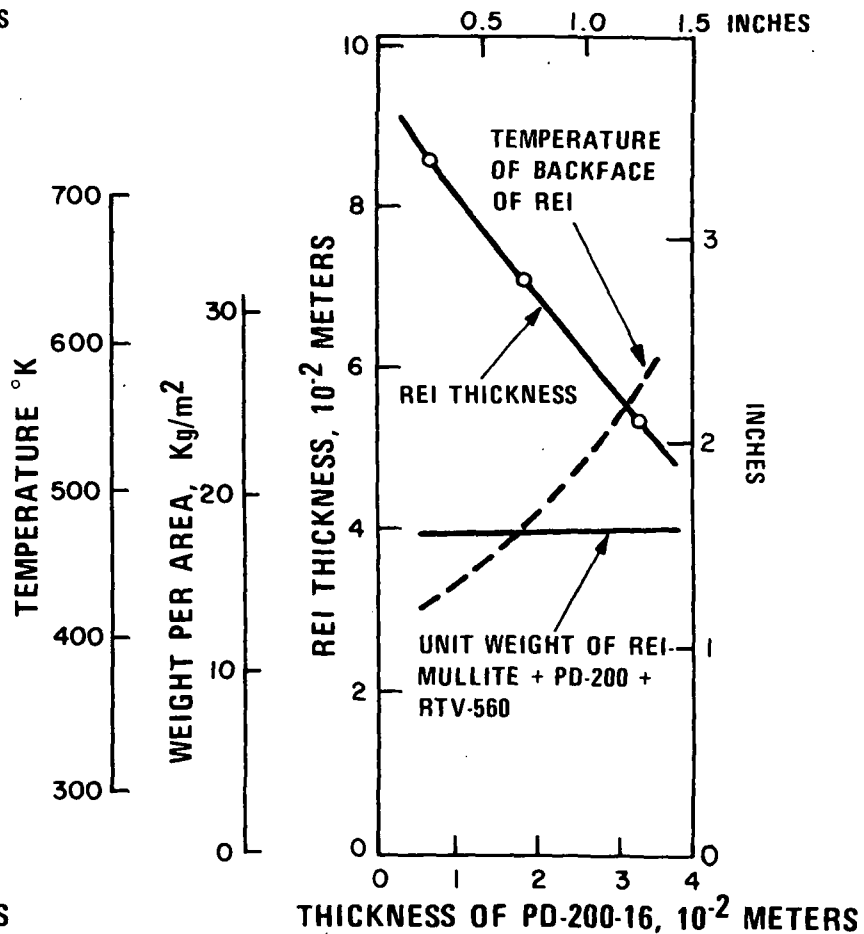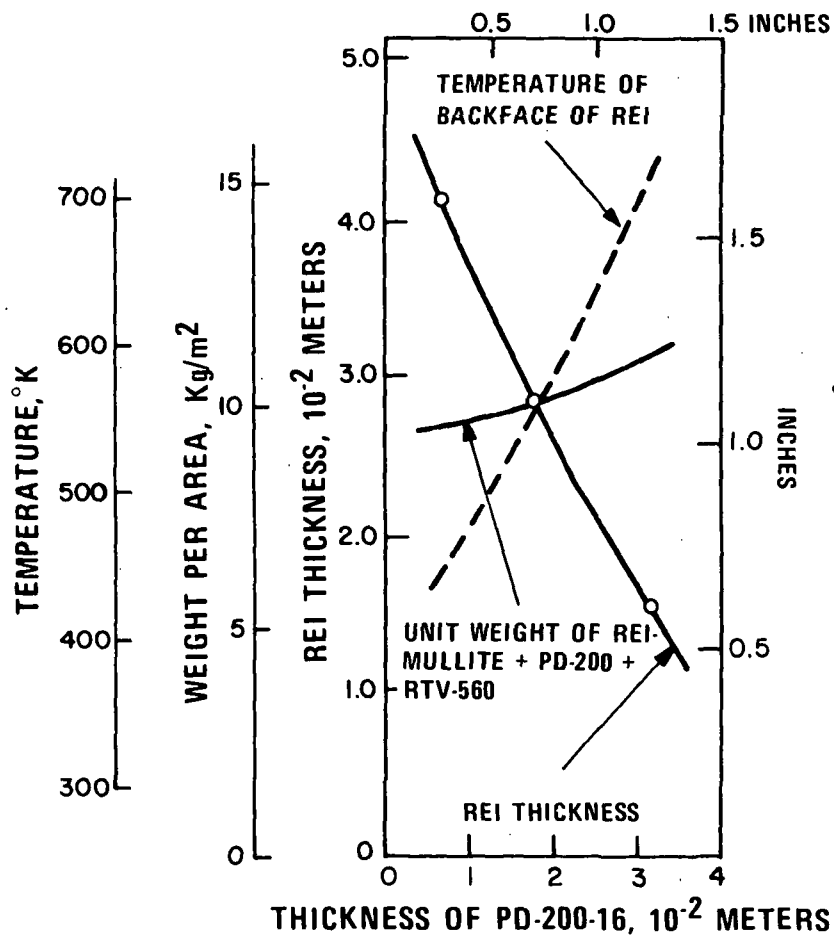
(FIGURE 13)

THERMAL GRADIENTS

(Figure 14)

Typical thermal gradients are given here for Area 1 and Area 2P. Critical conditions occur during

heatup in the 200 to 500 second time period and during post entry in the 2700 to 3600 second time

period. Heatup gradients are worse for the cold start condition, while post entry has critical

conditions in both cold start and warm start conditions. In the former case, part of the PD-200 foam

pad bond thickness is still below its glass transition temperature in the high structural load part

of the flight (2700 to 3600 seconds), while in the latter case the bond reaches its maximum temperature

level.

THERMAL GRADIENTS

AREA 1
0.041m (1.6 IN.) REI-MULLITE
0.0063m (0.25 IN.) PD-200-16

AREA 2P
0.083m (3.26 IN.) REI-MULLITE
0.009m (0.35 IN.) PD-200-16

(FIGURE 14)

1093
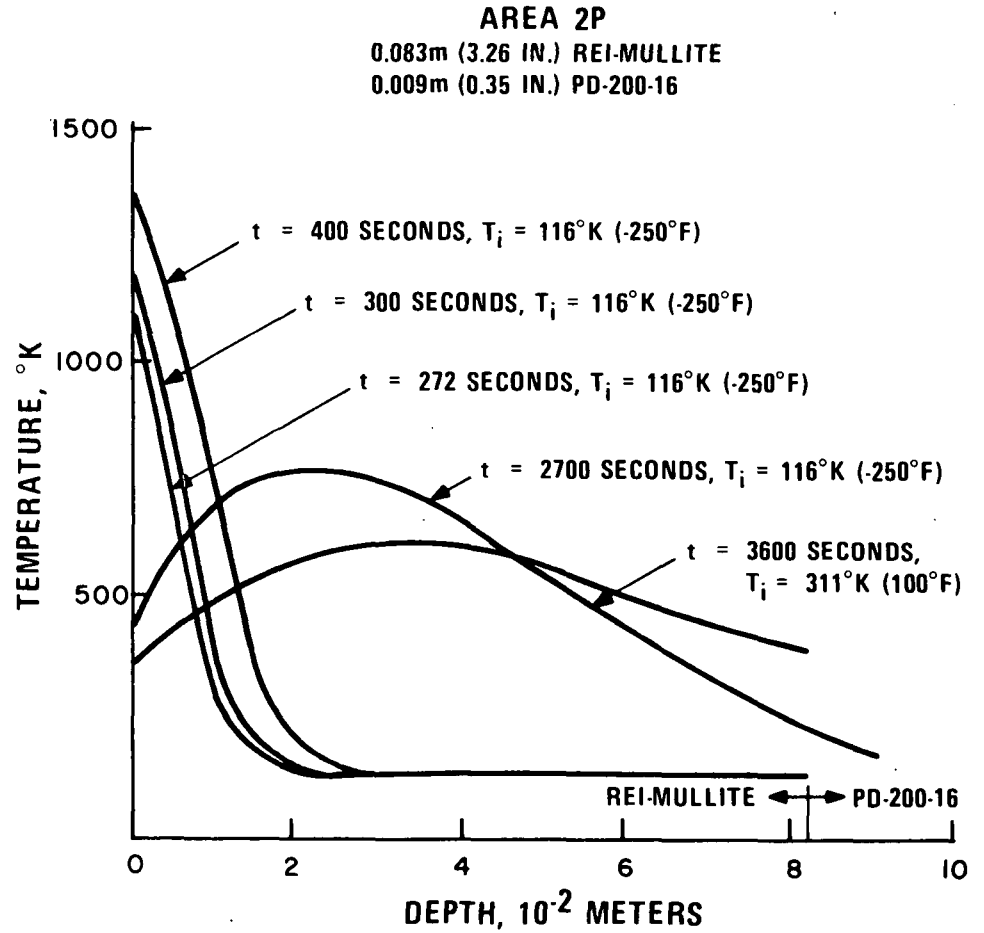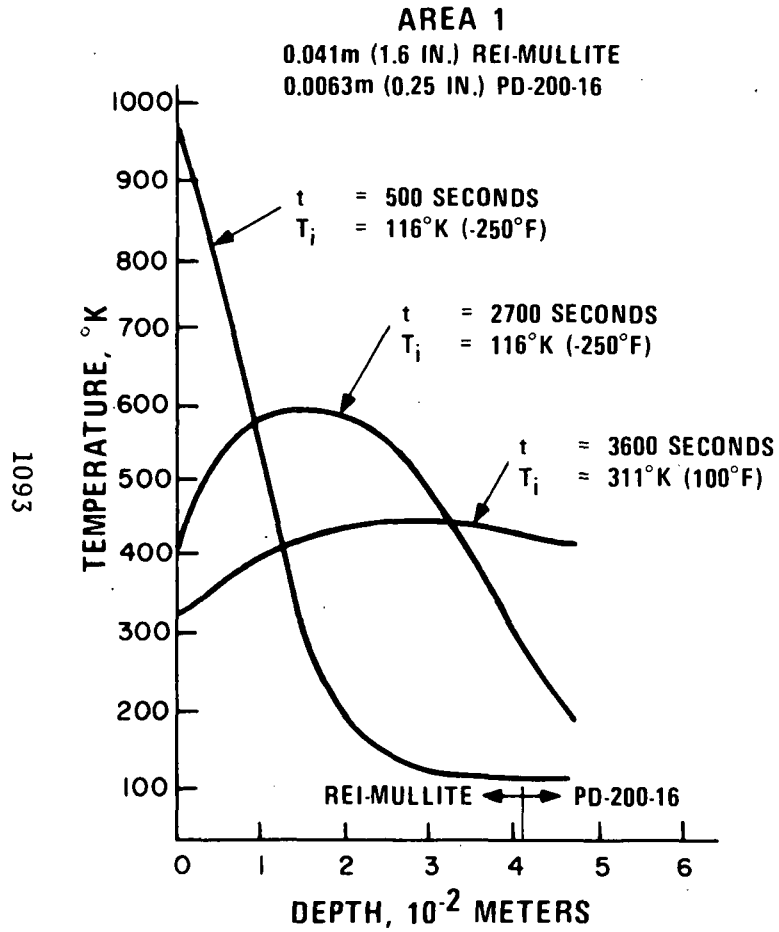
SIDEWALL COATING GRADIENTS

(Figure 15)

The temperature gradients down the coating sidewall are critical to the thermostructural design of the tile. In order to assure that realistic gradients were used in the analyses, a series of tests were performed with various sidewall configurations. A representative transient gradient is shown here together with the maximum temperature reached as a function of distance from the surface of the .05 m (2.0 inch) thick tiles that were tested. These results are compared to the temperatures predicted in the center of the tile using one-dimensional thermal analysis and the temperatures measured in the center of the panel. It can be seen that the coating temperatures run as much as 28° K (50° F) hotter than the 1-D prediction in the transient case and 83° K (150° F) hotter in the soak case.

SIDEWALL COATING GRADIENTS
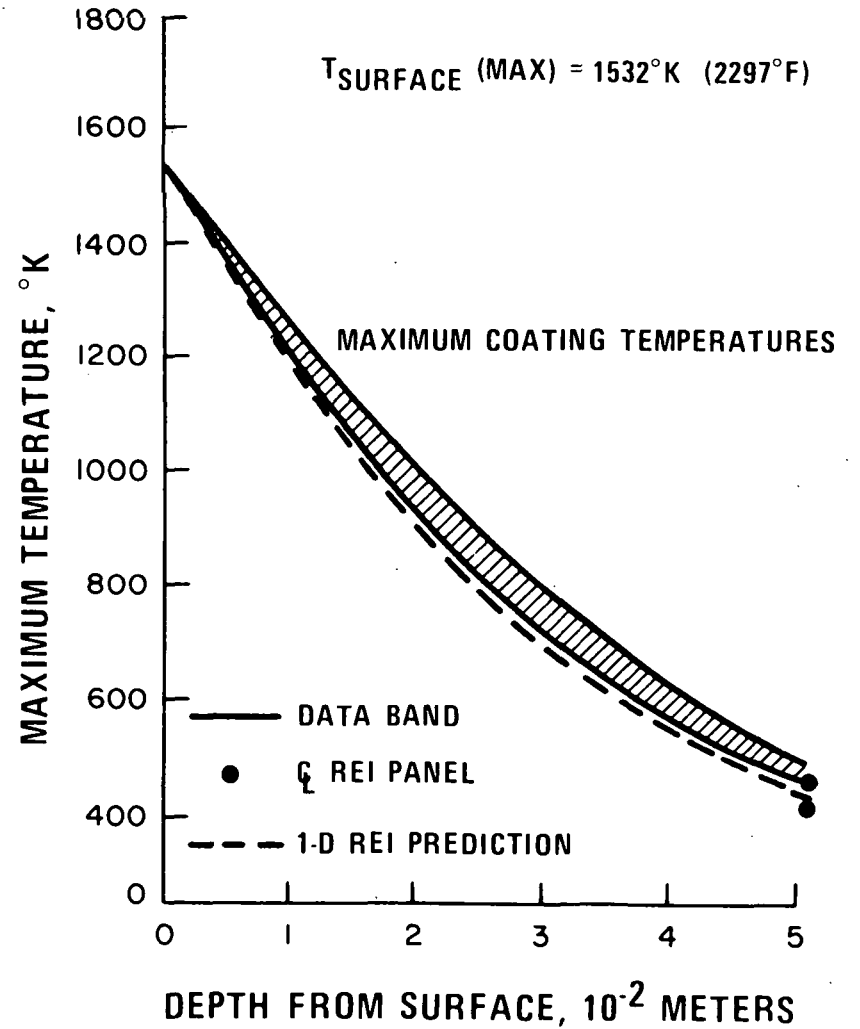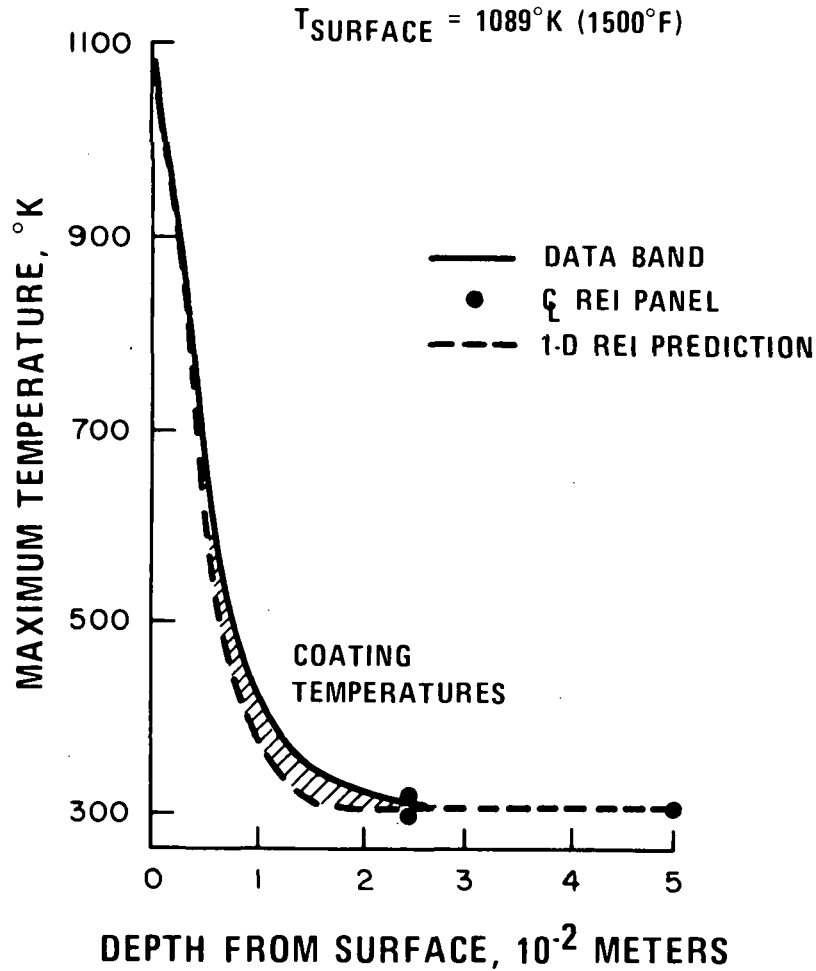
(FIGURE 15)

SUMMARY OF TPS PROPERTIES USED IN ANALYSIS
(Figure 16)

Figure 16 presents a summary of the TPS material properties used in these analyses and trades. Except for the PD-200 only room temperature data are presented here. However, variation in properties with temperature were measured and the temperature dependent properties were used in the analyses.

1096

SUMMARY OF TPS PROPERTIES USED IN ANALYSIS

COMPONENT	IN-PLANE		TRANSVERSE		SHEAR		EXPANSION
	MODULUS	STRAIN %	MODULUS	STRAIN %	MODULUS	STRAIN %	α T(RT→T)
MOD IB REI MULLITE (ROOM TEMPERATURE)	331×10^6 N/m^2 (48000 PSI)	0.25	48.3×10^6 N/m^2 (7000 PSI)	0.50	9.6×10^6 N/m^2 (1400 PSI)	10.0	5.20×10^{-3} AT 1368°K (2000°F)
SR2-HF1 COATING (ROOM TEMPERATURE)	44.8×10^9 N/m^2 (6.5×10^6 PSI)	0.03	44.8×10^9 N/m^2 (6.5×10^6 PSI)	0.03	–	–	3.95×10^{-3} AT 1368°K (2000°F)
PD200-16 BOND (ROOM TEMPERATURE)	95.1×10^3 N/m^2 (13.8 PSI)	55	95.1×10^3 N/m^2 (13.8 PSI)	55	64.1×10^3 N/m^2 (9.3 PSI)	90	80×10^{-3} AT 600°K (620°F)
116 °K (-250°F)	302×10^6 N/m^2 (43800 PSI)	0.60	302×10^6 N/m^2 (43800 PSI)	0.60	17.2×10^6 N/m^2 (2500 PSI)	0.55	36×10^{-3} AT 116°K (-250°F)

(FIGURE 16)

RESULTS OF STRUCTURAL TRADES
(Figure 17)

The structural trade analyses showed that the stresses produced during entry heatup with a cold start, the bond being at $116°$ K, are equal to or greater than those developed in an isothermal soak of $116°$ K. Cold soak, therefore, is treated as part of the cold start entry heatup condition and not as a separate case. Other general conclusions are given in this chart and detailed elaboration is given in Figures 17 through 22.

RESULTS OF STRUCTURAL TRADES

- **COLD SOAK AT 116°K (-250°F)**

    - STRESSES ARE EQUAL TO OR LESS THAN
      HEATUP GRADIENTS WITH COLD START

- **ENTRY HEATUP**

    - MAXIMUM STRAIN CONDITIONS (AREA 2P) OCCUR FOR SURFACE
      TEMPERATURES BETWEEN 1089°K (1500°F) AND 1367°K (2000°F)

    - MAXIMUM STRESS/STRAIN PARAMETERS

        - REI IN-PLANE TENSION
        - BOND TENSION
        - COATING TENSION

- **POST ENTRY**

    - STRESSES LOW FOR WARM START
    - MAXIMUM STRESS CONDITION IS COLD START

        - BOND TENSION
        - BOND SHEAR

(FIGURE 17)

1099

ENTRY HEATUP TRADES
(Figure 18)

The in-plane tensile strain in the REI-Mullite is shown in Figure 18 as a function of bond thickness (and, therefore, REI thickness) and REI-Mullite modulus of elasticity. The curves on the left are based on an in-plane modulus in the mullite of $331 \times 10^6 \, N/m^2$ (48,000 psi). In the hotter Area 2P the strain in insensitive to tile thickness, but a slight sensitivity exists in Area 1. As modulus increases the strain developed increases and vice-versa. The REI-Mullite has an adequate margin-of-safety based on mi. ....um material strain-to-failure data. Test data reveal that the value of this strain-to-failure is also modulus dependent.

ENTRY HEATUP TRADES

REI-MULLITE ULTIMATE IN-PLANE TENSILE STRAIN
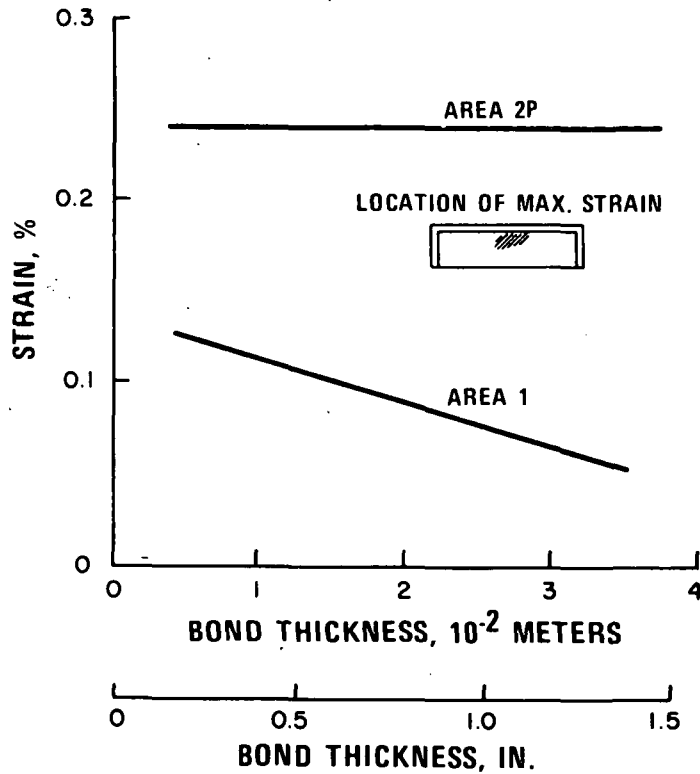
VARIATION WITH MODULUS
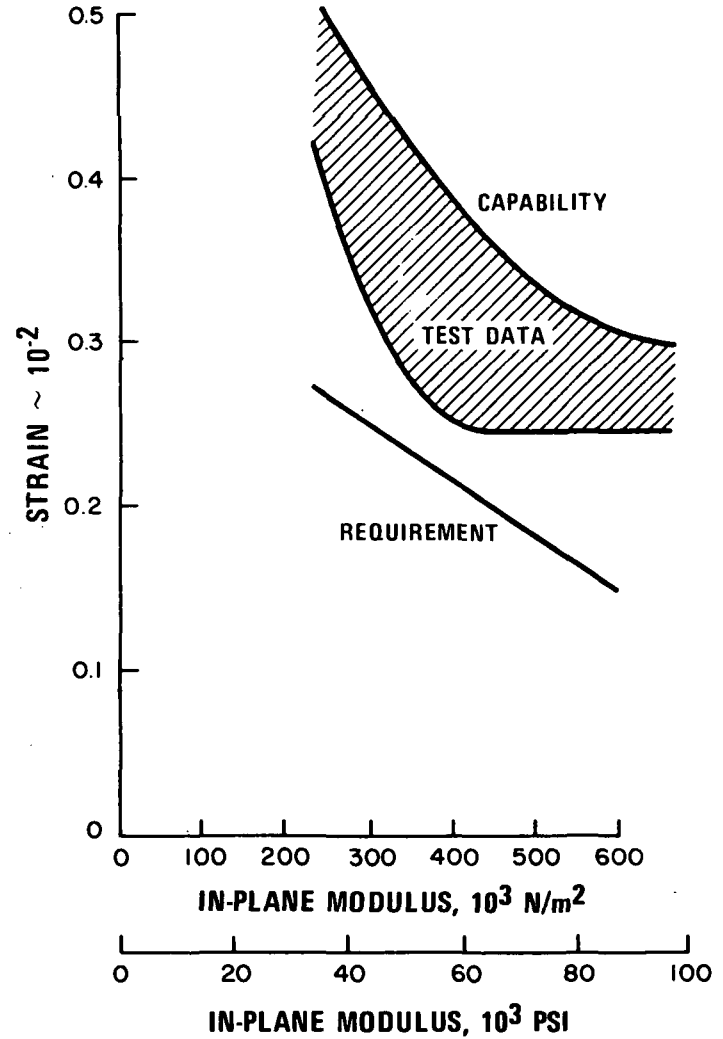
(FIGURE 18)

ENTRY HEATUP TRADES
(Figure 19)

The most important conclusion resulting from the entry heatup/cold soak trades is that the bond tension stress reaches critical levels because of the cold temperature of $116°$ K involved. The results show that in order to maintain adequate margins the bond thickness in Area 1 must be kept below 0.0076 m (0.3 in) and in Area 2P below 0.01 m (0.4 in).

The maximum strains in the coating as determined from two-dimensional finite element analysis is also shown here. Although high tensile strains are developed, the temperature of the coating is high enough that it has adequate capability due to the increased elongation at the higher temperatures.

ENTRY HEATUP TRADES
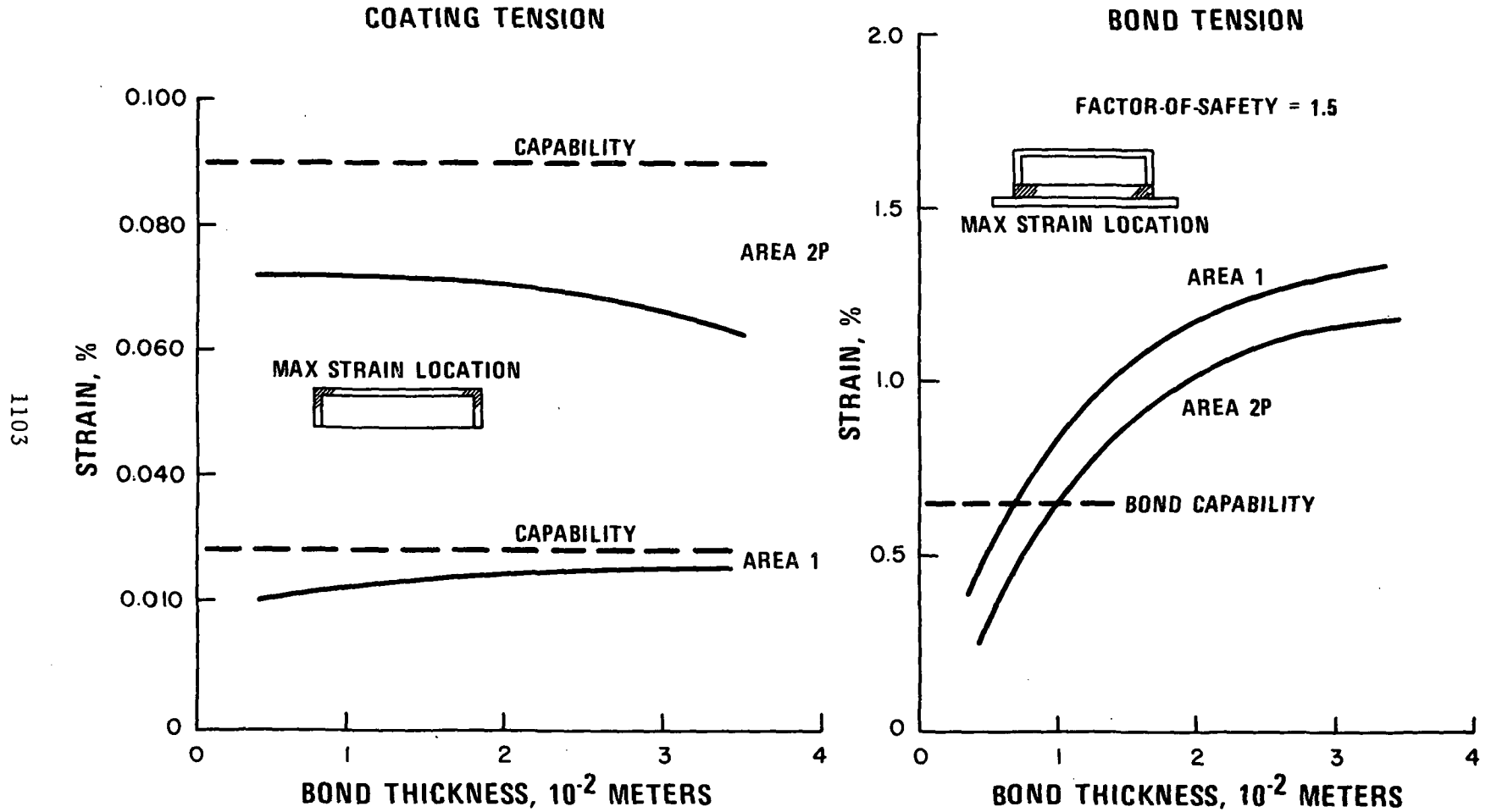
(FIGURE 19)

COATING CRACKING TENDENCIES
(Figure 20)

Although Figure 19 indicated that the coating has adequate strain capability, cracking has been experienced on the top and sidewall coatings. During plasma arc and entry simulation tests this cracking has been seen in both in-house tests and in the tests on the GE-RESD prototype panels supplied to NASA-MSC.

This tendency for coating cracking has been thoroughly investigated including the conduction and of three-dimensional analyses. These analyses indicate that the coating in the corner of the tile runs about $110°$ K $(200°$ F) cooler than the rest of the coating on the top surface. This results in an incremental increase in tension at this point which aggravates the corner strain condition. In addition, the tensile strains predicted for the sidewall near the top of the tile from the 3-D modeling are higher than those which had been predicted using two-dimensional modeling due to the ability of the 3-D model to analyze the critical plane.

It is felt based on these improved analyses and the test experience, that the tendency for sidewall cracking is most pronounced during heatup. The tensile strains subsequently induced in the tile during cool down caused these cracks to propagate and the incremental tension in the cooler corner causes additional cracks to form. Detailed examination of NDE records indicates a definite relationship between the sidewall cracks and the top surface cracks, indicating that crack propagation occurred.

COATING CRACKING TENDENCIES

- TEST HARDWARE HAS EXPERIENCED TENDENCY FOR TOP AND SIDEWALL CRACKING

    - NASA MSC PROTOTYPE PANELS
    - IN-HOUSE TESTS

- 3D THERMOSTRUCTURAL ANALYSIS HAS SHOWN

    - COATING RUNS COOLER AT CORNER OF TILE PRODUCING A TENSILE STRAIN INCREMENT
    - 3D MODELING OF TILE INCLUDES EFFECTS NOT INCLUDED IN 2D MODELING AND RESULTS IN HIGHER SIDEWALL STRAINS

- COATING CRACKING SEQUENCE

    - *SIDEWALL CRACKS DEVELOP DURING HEATUP* ①
    - SIDEWALL CRACKS PROPAGATED DURING COOL DOWN ②
    - CORNER CRACKS DEVELOP DURING COOL DOWN ③

- TEMPERATURE DISTRIBUTION   STRAIN DISTRIBUTION   STRAIN DISTRIBUTION
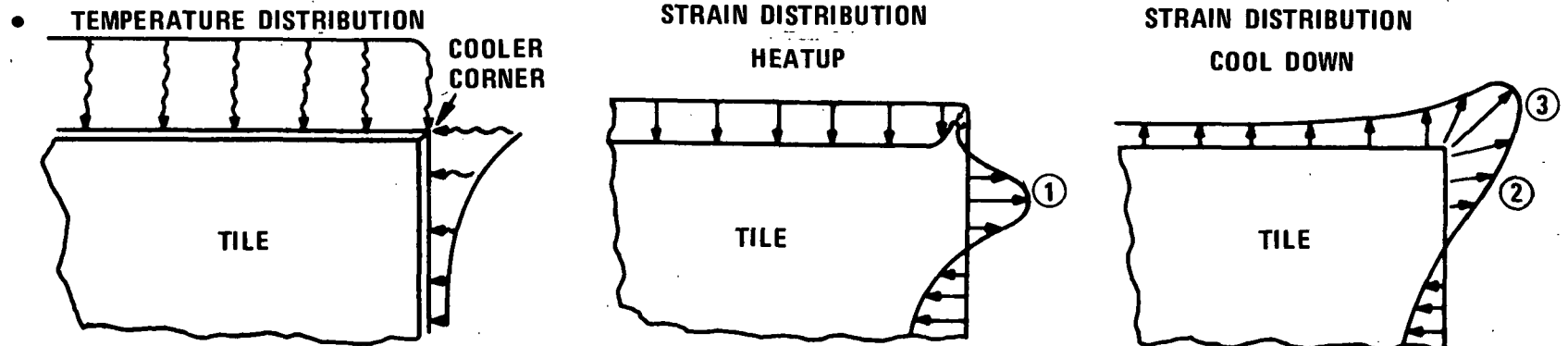
(FIGURE 20)

COATING CRACKING SOLUTION

(Figure 21)

Analyses indicate that to eliminate the coating cracking tendencies, the tile stiffness must be increased. This reduces both the residual and flight contributions to the maximum tensile strains in the coating. Furthermore, contouring of the coating sidewall provides either flexibility and/or stiffness where required and further reduces the level of maximum tensile strains in the coating.

Tiles have been designed incorporating these approaches and are now in environmental tests. Preliminary results from these tests indicate that the coating cracking can be eliminated by proper design. Also it is planned that the changes will be incorporated in fabrication of future prototype hardware.

COATING CRACKING SOLUTION

- **CORRECTIVE ACTION**

  - **REDUCE MAXIMUM RESIDUAL AND ENVIRONMENTAL TENSILE STRAIN BY:**

    - **INCREASING TILE STIFFNESS**
    - **COATING SIDEWALL TAILORING FOR OPTIMUM STIFFNESS**
    - **PARTIAL DEPTH COATING**

- **TYPICAL REDESIGN NOW IN RE-ENTRY SIMULATION TESTING**

- **REDESIGN CONFIGURATIONS**

  - **COATED FIVE & SIX SIDES**
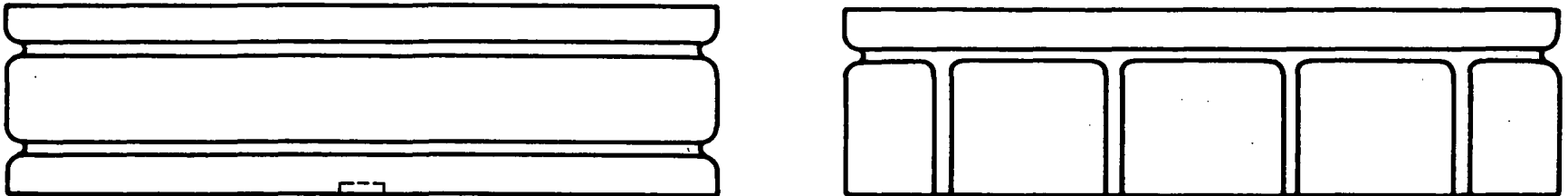
(FIGURE 21)

POST ENTRY TRADES

(Figure 22)

In post entry, large margins exist due to the low level of stress/strain developed. Some difference in the coating strain exists between Area 1 and Area 2P, but the REI-Mullite in-plane strain is about the same for Area 1 and Area 2P and independent of bond thickness.

POST ENTRY TRADES
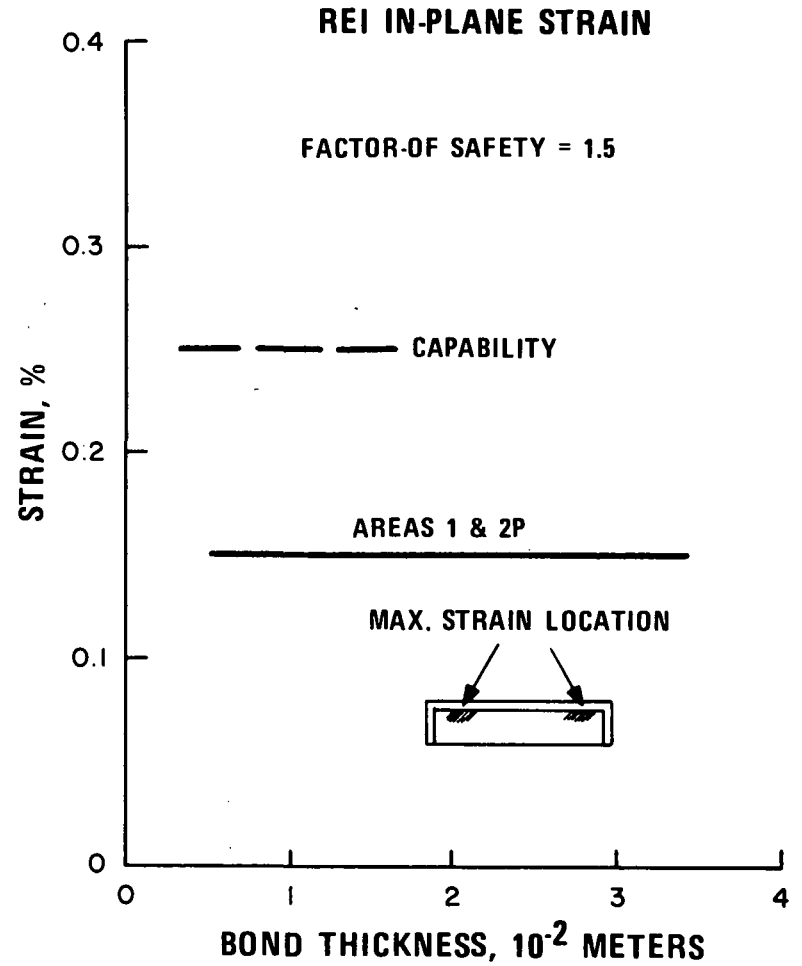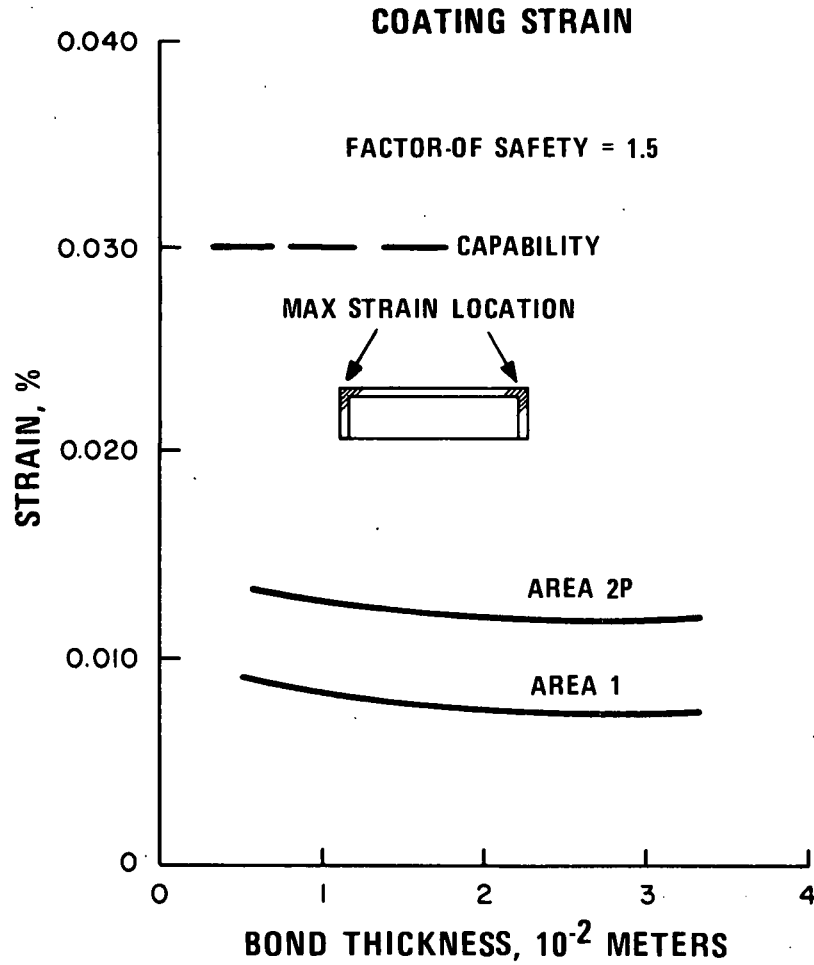
(FIGURE 22)

SUMMARY OF SYSTEM RESTRAINTS
(Figure 23)

The major TPS system restraints are due to the entry heat/cold soak and result from the bond tensile stresses. These restraints result in the maximum bond thicknesses defined here.

1110

SUMMARY OF SYSTEM RESTRAINTS

- ENTRY HEATUP/COLD SOAK

- BOND TENSILE STRESS

- MAXIMUM BOND THICKNESS

    AREA 1 — 0.0076 m (0.3 INCH)

    AREA 2P — 0.0101 m (0.4 INCH)

(FIGURE 23)

COMPARATIVE SYSTEM WEIGHTS – AREA 1
(Figure 24)

Figure 24 gives the variation of the Area 1 TPS system weight (insulation, coating, and bond) as a function of tile size, tile thickness and bond thickness. Both fully coated and partially coating sidewalls are considered. In the case of the partial coating, a waterproofing spray is proposed for use from the point where the coating ends (corresponding to the $700°$ K ($800°$ F) isotherm) to the bottom of the tile.

In both cases, the largest size tiles are lighter due to coating weight considerations. As the tile size decreases, the bond thicknesses corresponding to minimum weight increases for the fully coated tiles but remain constant for the partially coated tiles. The minimum weight for a 0.2 m (8 inch) square tile is for a thickness of .041 m (1.6 inch) with a 0.0064 m (0.25 inch) bond. The minimum weight for a partially coated tile is about 0.5 Kg/m^2 (.1 lb/ft^2) lighter and is 0.046 m (1.8 inch) thick on a .0025 m (0.1 inch) bond. For purposes of the NASA–MSC sponsored technology program, 0.2 m by 0.2 m (8 inch by 8 inch) tiles were selected since that size was compatible with testing requirements and was the subject of the most testing experience. Other sizes can be used in the orbiter TPS depending upon location and heating rates consistent with thermostructural limitations.

It can be seen that even with the previously established maximum bond thickness restraint a design can be selected that is not penalized from a weight standpoint.

COMPARATIVE SYSTEM WEIGHTS
(TILE SIZE AND COATING DEPTH) AREA 1
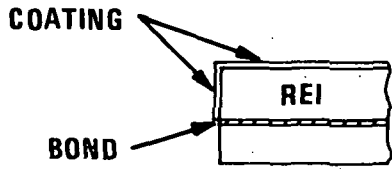
(FIGURE 24)
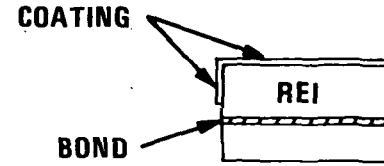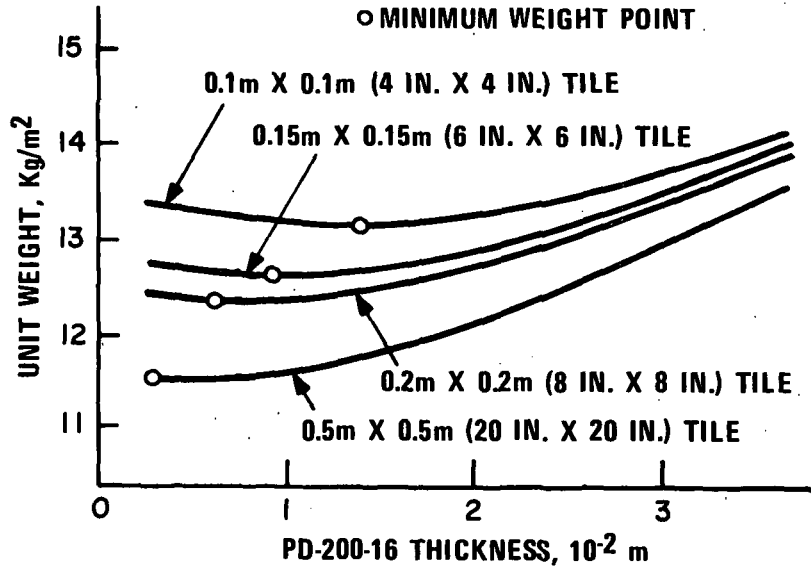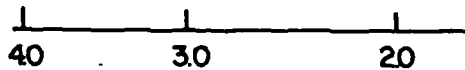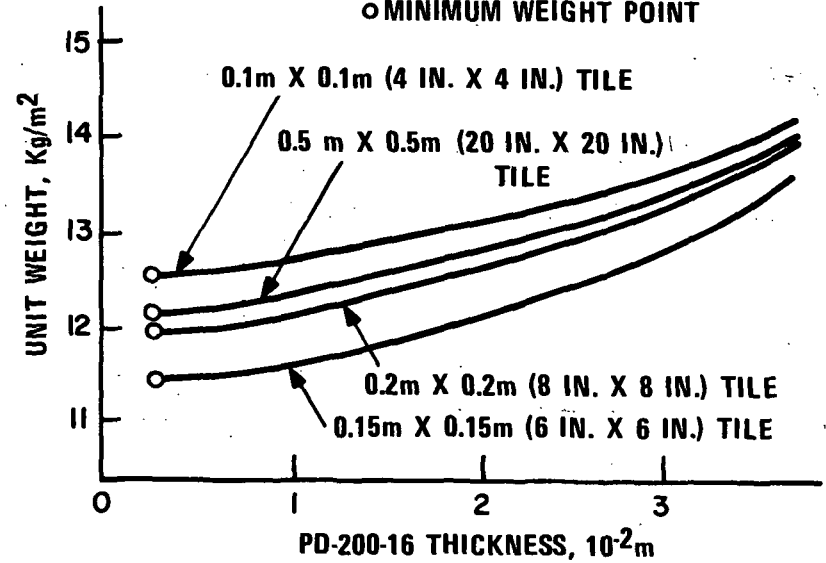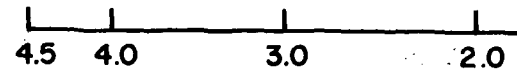
COMPARATIVE SYSTEM WEIGHTS — AREA 2P
(Figure 25)

The main difference between the optimum weight trends for the hotter area, Area 2P, and the cooler Area 1 is that the minimum weight configurations swing toward greater bond thicknesses. This is more pronounced for fully coated tiles than for partially coated tiles with the difference again being about 0.5 kg/m^2 (0.1 lb/ft^2) for the 0.2 m (8 inch) square tiles. The imposition of the maximum bond thickness restraint causes a 0.5 kg/m^2 (0.1 lb/ft^2) penalty for fully coated tiles but no penalty for partially coated tiles.

COMPARATIVE SYSTEM WEIGHTS
(TILE SIZE & COATING DEPTH) AREA 2P
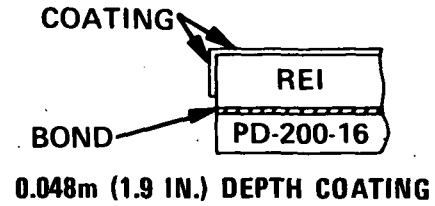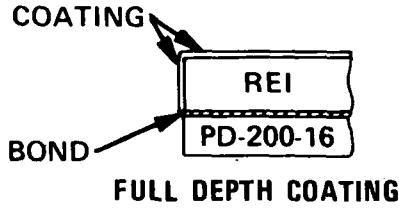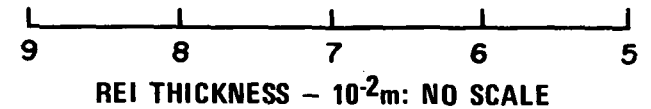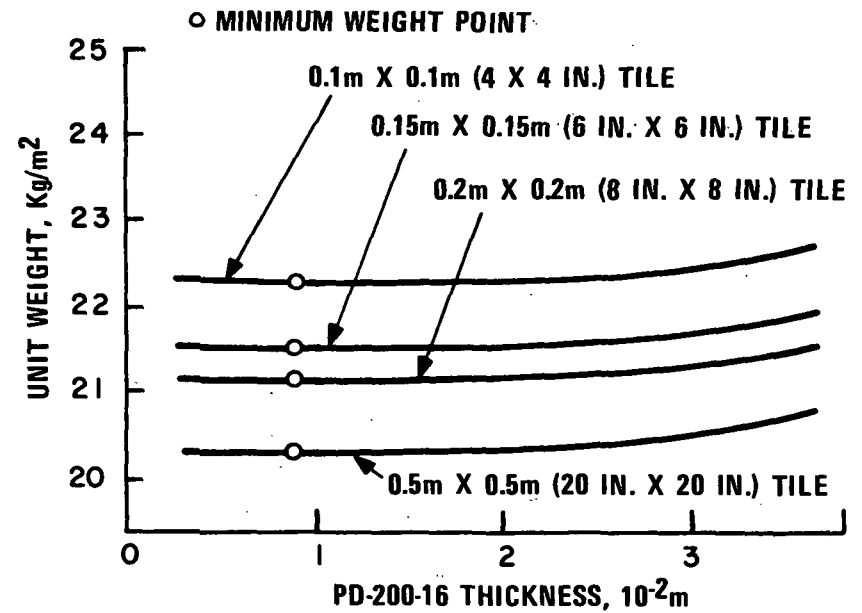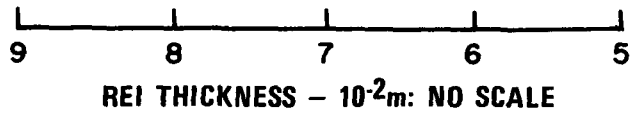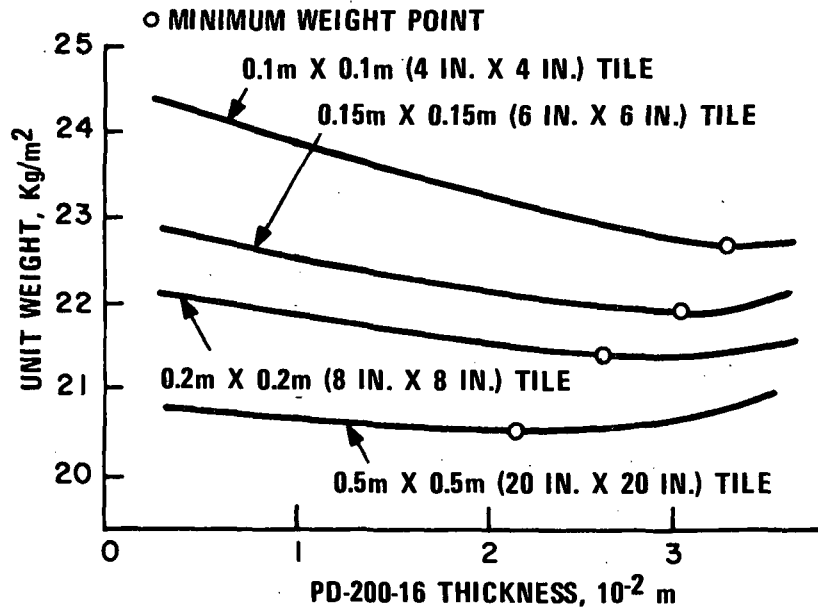
(FIGURE 25)

COMPARATIVE WEIGHTS

(Figure 26)

Figure 26 demonstrates that today's MOD IB REI-Mullite system weights for representative low and high temperature areas 977° K (1300° F) and 1533° K (2300° F) are significantly less than those previously reported[1] despite the fact that the system is now designed for the more severe orbital cold soak and cold start entry conditions, and minimum material strengths are being used to determine margins-of-safety. It is also to be noted this chart reflects configurations for the NASA-MSC technology program. Sizes and thicknesses for an actual orbiter application may differ from these values depending upon specific requirements.

COMPARATIVE WEIGHTS

- ADDITIONAL REQUIREMENTS: 116°K (-250°F) COLD SOAK & COLD START ENTRY; MINIMUM PROPERTIES
- WEIGHT REDUCTION ACHIEVED THROUGH USE OF LIGHTER BOND, MOD IB MULLITE

ITEMS	SR-2 MOD IA PD-200-28 φ 2 PROTOTYPES				SR-2 – HF1 MOD IB PD-200-16 φ 2 F/O BASELINE FULLY COATED				SR-2 – HF1 MOD IB PD-200-16 φ 2 F/O BASELINE PARTIAL DEPTH COATING			
	THICKNESS		WEIGHT		THICKNESS		WEIGHT		THICKNESS		WEIGHT	
	m	IN.	Kg/m²	LB/FT²	m	IN.	Kg/m²	LB/FT²	m	IN.	Kg/m²	LB/FT²
AREA 1 TILE SIZE 0.2m X 0.2m (8 IN. X 8 IN.)												
REI MULLITE	0.043	1.7	8.3	1.70	0.041	1.6	7.80	1.60	0.041	1.6	7.80	1.60
COATING DEPTH	0.043	1.7	2.5	0.52	0.041	1.6	1.95	0.40	0.025	1.0	1.61	0.33
STRAIN ISOLATION*	0.002	0.08	1.7	0.34	0.0064	0.25	2.34	0.48	0.0064	0.25	2.34	0.48
TOTAL			12.5	2.56			12.09	2.48			11.75	2.41
AREA 2 TILE SIZE 0.2m X 0.2m (8 IN. X 8 IN.)												
REI MULLITE	0.051	2.0	9.75	2.00	0.083	3.26	15.90	3.26	0.083	3.26	15.90	3.26
COATING DEPTH	0.051	2.0	2.73	0.56	0.083	3.26	2.83	0.58	0.048	1.90	2.10	0.43
STRAIN ISOLATION*	0.028	1.1	13.28	2.72	0.009	0.35	2.98	0.61	0.009	0.35	2.98	0.61
TOTAL			25.76	5.28			21.71	4.45			20.98	4.30

REI MULLITE DENSITY – 196 Kg/m³ (12 PCF)
STRAIN ISOLATION DENSITY: PD200-28 449 Kg/m³ (28 PCF); PD200-16 256 Kg/m³ (16 PCF)
  *STRAIN ISOLATION WEIGHTS INCLUDE TWO RTV FILM LAYERS.

(FIGURE 26)

SUMMARY

(Figure 27)

In conclusion, it has been shown that the MOD IB REI-Mullite has adequate margins-of-safety based on minimum strengths for the critical thermostructural conditions of the shuttle mission. Furthermore, the introduction into the design of the new lower density PD-200 foam bond material provides cold soak and cold entry capability at 116° K (-250° F). Finally, design solutions to the coating cracking tendencies have been identified and the solution analytically verified with three-dimensional thermostructural analyses. Experimental verification through entry simulation testing is now underway.

SUMMARY

- **MOD IB REI-MULLITE HAS FACTORS-OF-SAFETY $\geq$ 1.5 BASED ON MINIMUM PROPERTIES FOR SHUTTLE MISSION ENVIRONMENTS**

- **PD-200-16 LIGHTWEIGHT FOAM BOND PROVIDES STRAIN ISOLATION FOR THE 116°K (-250°F) COLD SOAK CONDITION**

- **TILE CONFIGURATIONS NOW IN TEST WILL RESULT IN A SOLUTION TO COATING CRACKING TENDENCIES.**

1119

(FIGURE 27)

REFERENCE

1. GE-RESD Final Report on NASA-MSC contract NAS-9-12084 dated May 1972 entitled "Final Report for Reusable Surface Insulation Thermal Protection System Development Program."

SILICA RSI
FOR APPLICATION
TO THE
SHUTTLE ORBITER

K. J. Forsberg, J. Jue, M. H. Kural, and F. A. Velligan
LOCKHEED MISSILES & SPACE COMPANY. INC.

INTRODUCTION
(Figure 1)

There are three key TPS technical problem areas that must receive concentrated attention: cold soak condition, thermodynamic effect of gaps and steps, and aerodynamic effect of gaps and steps. All three areas have direct impact on the tolerance requirements for the gaps and steps of the installed tiles. From a practical standpoint the tolerances must be as large as possible to facilitate assembly and to minimize manufacturing costs. On the other hand, gap heating effects may be so severe that certain joint concepts become impractical. Such design information is required as soon as possible. Tests now under-way at various NASA Centers will provide key data in this area.

The major consideration in the Space Shuttle Program is to develop a reliable, reusable orbiter at minimum cost. The impact of the orbiter TPS on total program weight and cost is so strong that TPS weight must be given more emphasis as a major discriminator between candidate material systems.

INTRODUCTION

KEY TPS ISSUES

- COLD SOAK CONDITION

- THERMODYNAMIC EFFECT OF GAPS AND STEPS

- AERODYNAMIC EFFECT OF GAPS AND STEPS

- TPS WEIGHT/COST RELATIONSHIP

1123

Figure 1

COLD SOAK
(Figure 2)

Direct bonding is the most promising method of attaching the RSI to the orbiter structure. To function properly the bond must have a low modulus of elasticity [less than 6.9×10^5 N/m^2 (100 psi)] in order to isolate the RSI from the primary structure deformation. Several bond systems (e.g., RTV-560) work well in the range 172° K to 533° K (-150° F to + 500° F). However, below 172° K (-150° F) the bond undergoes a transition and the modulus increases as much as three orders of magnitude.

A foam bond (such as PD-200 or RL1973) may well provide the necessary strain isolation at 116° K (-250° F) (tests indicate that tiles survive cold soak when bonded with RL1973), but present property data are inadequate to analytically predict the tile and bond performance.

A new concept, called the strain arrestor plate by its creator, Mr. Murat Kural, provides a means of solving the cold soak attachment problem.

COLD SOAK

● CRITICAL DESIGN CONDITION FOR DIRECT BOND SYSTEMS:

$$T < 144^{\circ}K \ (-200^{\circ}F)$$

● PROBLEM:

GLASSY TRANSITION OF BOND
MODULUS OF ELASTICITY INCREASES BY FACTOR OF 100 TO 1000

● SOLUTIONS:

STRAIN ARRESTOR PLATE
FOAM BOND

Figure 2

TYPICAL TEMPERATURE/LOAD HISTORY
(Figure 3)

Depending on orbit conditions, the initial temperature at start of re-entry can vary from 394° K (+250° F) down to 116° K (-250° F). The backface temperature history of a typical aluminum structure is shown here for two initial temperatures. The trajectory used here is for 2000 km (1100 nm) crossrange with 3600 seconds from 122 km (400,000 ft) to touchdown. In addition, the substrate load history is superimposed from start of re-entry to touchdown at 3600 seconds. The 116° K (-250° F) cold soak condition has been used for the majority of the strain arrestor plate screening exercises. Other critical conditions at t = 1000 seconds and at touchdown have been considered in the design effort. For screening, it has been shown that the 116° K (-250° F) cold soak condition results in stresses very close to the maximum values; therefore, for ease of computation this condition has been used exclusively. Note that peak temperatures at the bondline occur after touchdown.

TYPICAL TEMPERATURE/LOAD HISTORY

Figure 3

1127
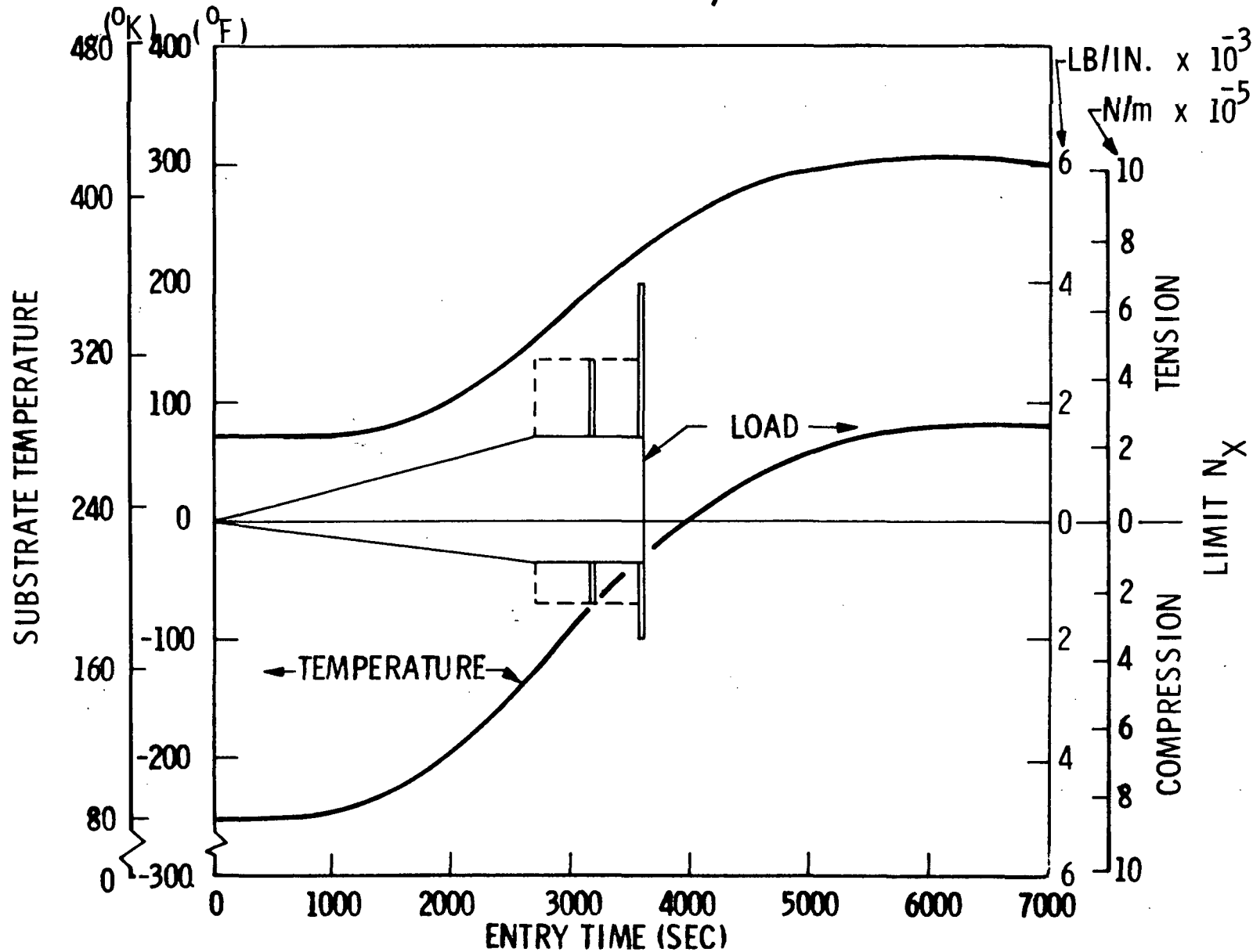
STRAIN ARRESTOR PLATE (SAP) MECHANICS
(Figure 4)

The strain arrestor plate (SAP) is a high-modulus, high-strength, low-thermal-expansion [zero to 5.4×10^{-7} cm/cm/°K (3×10^{-7} in./in./°F)] system bonded between the RSI tile and the foam bond.

In a foam bonded system, loading of the primary structure induces high stresses through the foam and bond lines into the RSI tile, with the peak stress occurring at the corner of the tiles. At 116°K (-250°F), the modulus of the foam bond system has increased to a point that excessive stress is transferred to the RSI tile.

With the SAP, large strains in the primary structure transferred through the foam bond are resisted by the SAP. The high extensional stiffness (modulus) of the plate results in very low SAP strains, thus preventing high stresses in the RSI above it.

STRAIN ARRESTOR PLATE (SAP) MECHANICS

1129

DIRECT BOND

UNLOADED
RSI/STR

DIRECT BOND WITH STRAIN ARRESTOR PLATE

UNLOADED
RSI/STR

RSI

HIGH STRAIN
IN RSI

FOAM
BOND

PRIMARY
STR

RSI

LOW STRAIN
IN RSI

HARD BOND

GRAPHITE
EPOXY SAP

FOAM BOND

PRIMARY STR

UNIT DEFORMATION
OF PRIME STR

UNIT DEFORMATION
OF PRIME STR
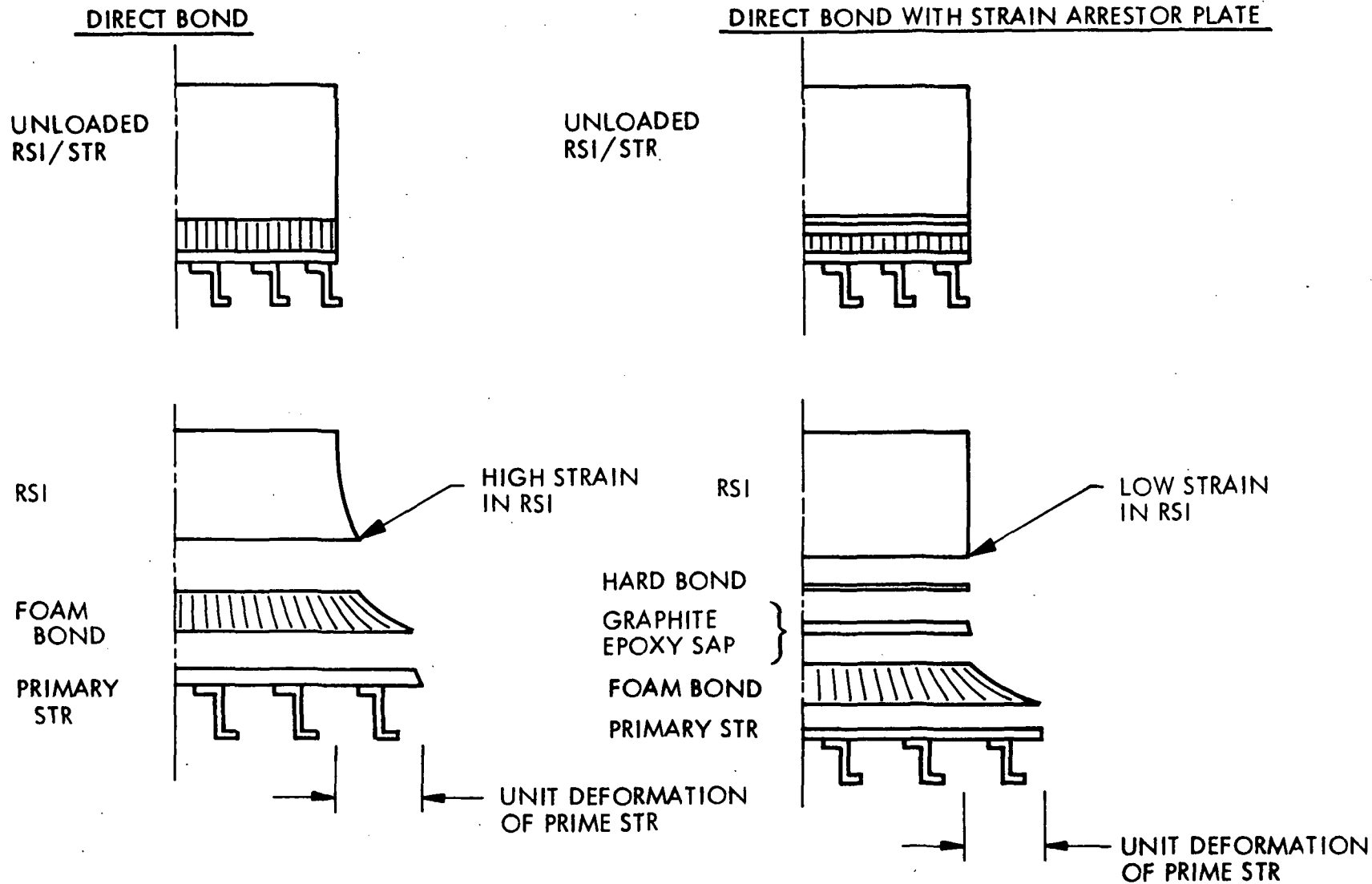
Figure 4

COMPUTER MODELING
(Figure 5)

The model used for the strain arrestor plate investigations considered a skin stringer aluminum primary structure. In modeling, one-half of the panel is analyzed with an area of symmetry at the centerline.

Two models are used in the analysis — stiff direction and weak direction. The stiff direction model is pinned at the fr me support end. Symmetry is simulated at the centerline by lateral and rotational restraints. The resistance of the stringers to bending under the $116^{\circ}K$ $(-250^{\circ}F)$ cold soak condition results in a very stiff substrate.

The weak direction model considers the stresses across the panel. In this model the stiffeners are modeled as springs.

COMPUTER MODELING

Z DIRECTION

R - DIRECTION (STIFF) R - DIRECTION (WEAK)

L

COATING (0042)

LI-900

ARRESTOR PLATE

BOND

SUBSTRUCTURE

FRAME SUPPORT

STIFF DIRECTION

WEAK DIRECTION

FRAME SUPPORT

STIFF DIRECTION

LI-900

0042 COATING

STRAIN ARRESTOR PLATE

BOND

SUBSTRATE

WEAK DIRECTION

LI-900

SPRINGS
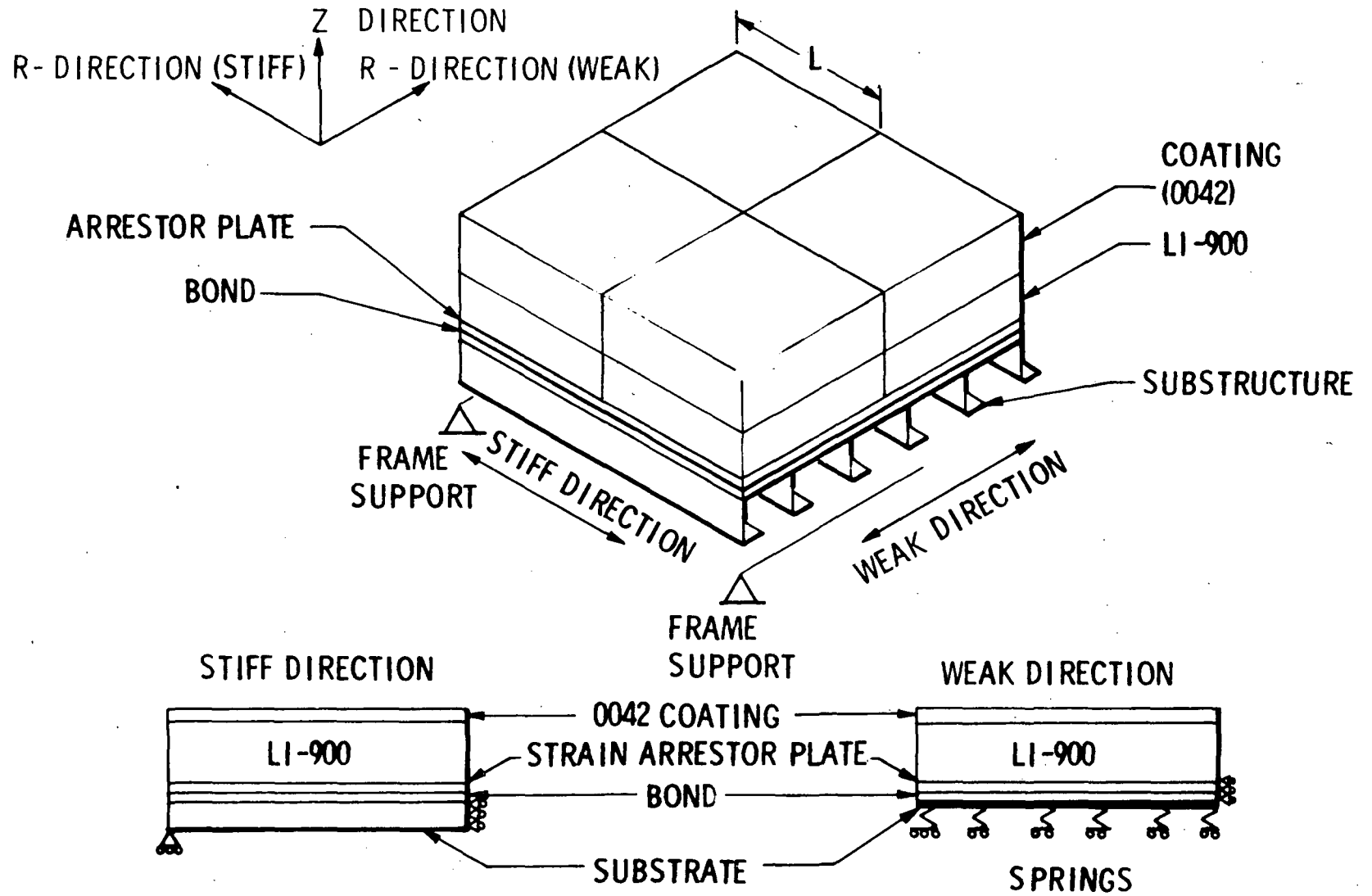
Figure 5

COLD SOAK MECHANICS - INDUCED BENDING
(Figure 6)

The composite is fabricated and assembled at room temperature. The reduction in temperature has little effect on the LI-900 and SAP because of their low coefficient of thermal expansion. The aluminum substrate (and bond), however, contracts a significant amount because of relatively high coefficient of expansion.

This contraction gives rise to high shear stresses, forcing compatibility at layer interfaces of the composite. These shear stresses result in bending of the components and, therefore, induce stresses in the LI-900.

COLD SOAK MECHANICS - INDUCED BENDING

COATING

STRAIN ARRESTOR PLATE

LI-900

BOND

SUBSTRATE

AT ROOM TEMP.

AT 116°K (-250°F)

TILE
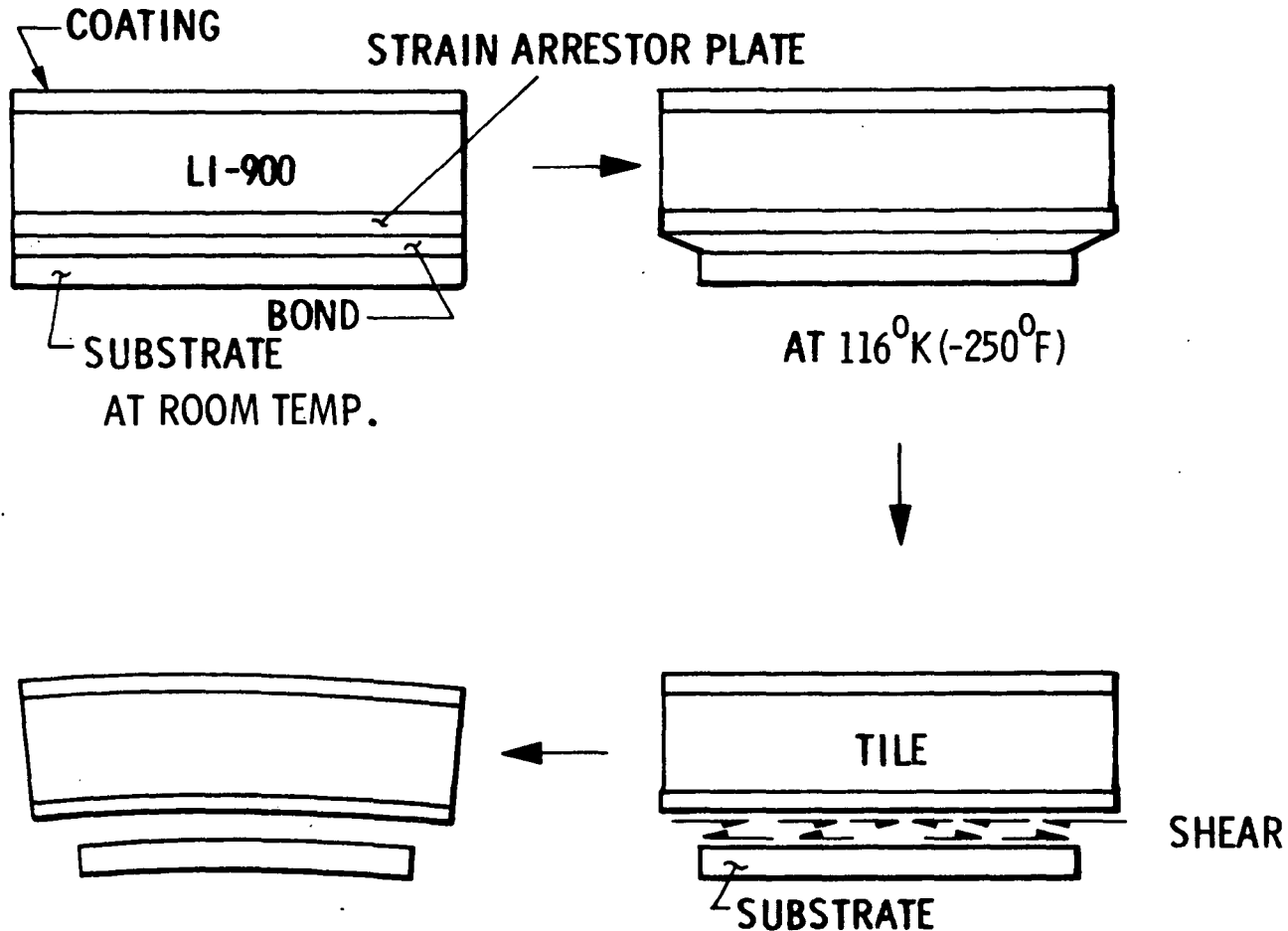
SHEAR

SUBSTRATE

BENDING MOMENTS INDUCED IN THE TILE AND SUBSTRATE DUE TO SHEAR BETWEEN LAYERS CAUSED BY DISSIMILAR THERMAL CONTRACTIONS OF LAYERS.

Figure 6

The amount of bending in the tile-SAP combination is primarily dependent on the extensional SAP stiffness (AE); the bending in the primary structure is dependent on the primary structure bending stiffness (EI).

In the weak direction, the imposed shear loads easily bend the primary structure (1) and (2). A low AE SAP is also easily bent to conform to a large radius. The large radius of curvature results in moderate stresses at the tile edge. Hence, a low AE SAP is desirable (1).

With a high AE (2) and weak primary structure, the low shear stresses near the center of the tile have little effect on the SAP and all compatibility is forced rather abruptly near the edge. This gives rise to high loads in the LI-900 tile.

In the stiff direction, the shear stresses again easily deform a low stiffness SAP (3), but cannot bend the stiff primary structure (high EI). This results in high compression stress at the edge of the tile.

A high AE SAP in conjunction with the stiff primary structure (4) results in little bending of either component, since compatibility at the tile edge is easily achieved. Very low peel stresses result. Hence, a high AE SAP is desirable.

These conflicting requirements were examined to identify favorable tile/SAP designs.

COLD SOAK MECHANICS - MAX STRESS
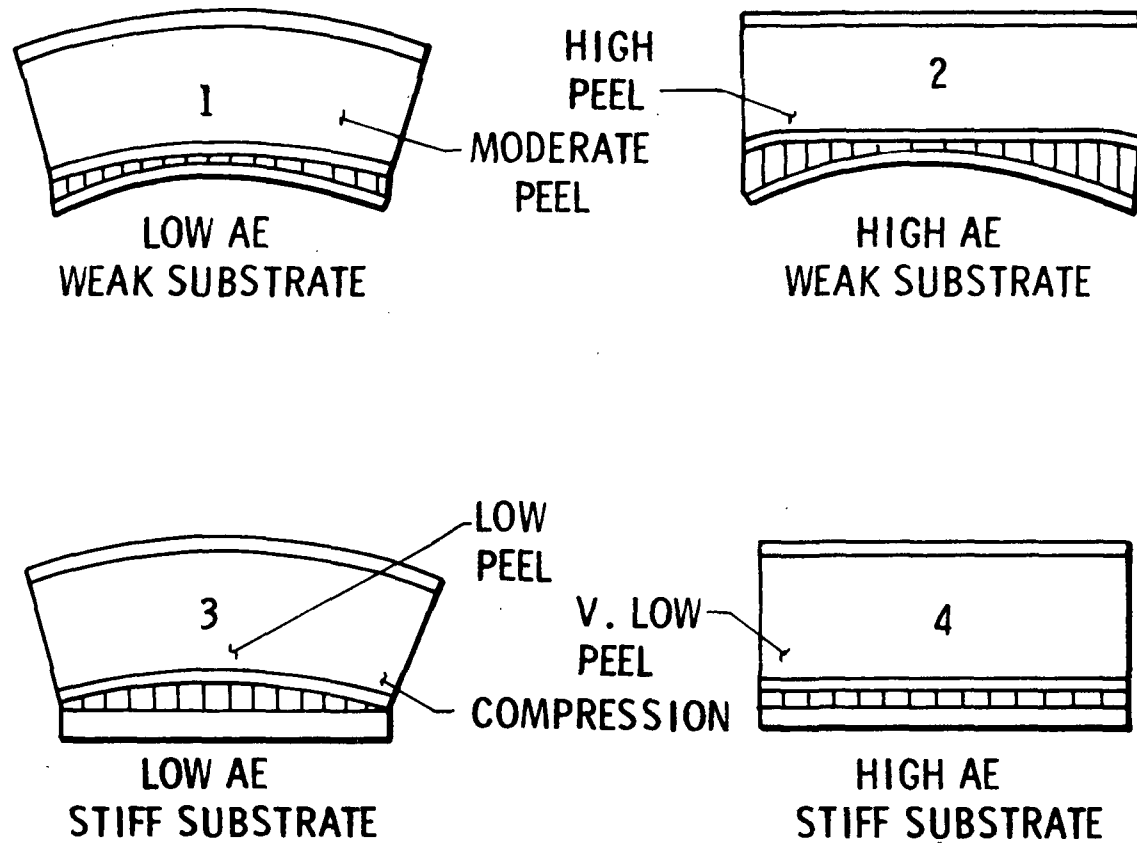
Figure 7

TRENDS OF LI-900 STRESSES VS SAP STIFFNESS
FOR STIFF AND WEAK SUBSTRATES
(Figure 8)

The opposing trends of the LI-900 critical stresses versus SAP stiffness are compared here. The following two charts illustrate the mechanics involved in the composite at the 116^OK $(-250^O$F) soak condition.

TRENDS OF LI-900 STRESS VS STIFFNESS
FOR STIFF AND WEAK SUBSTRATES
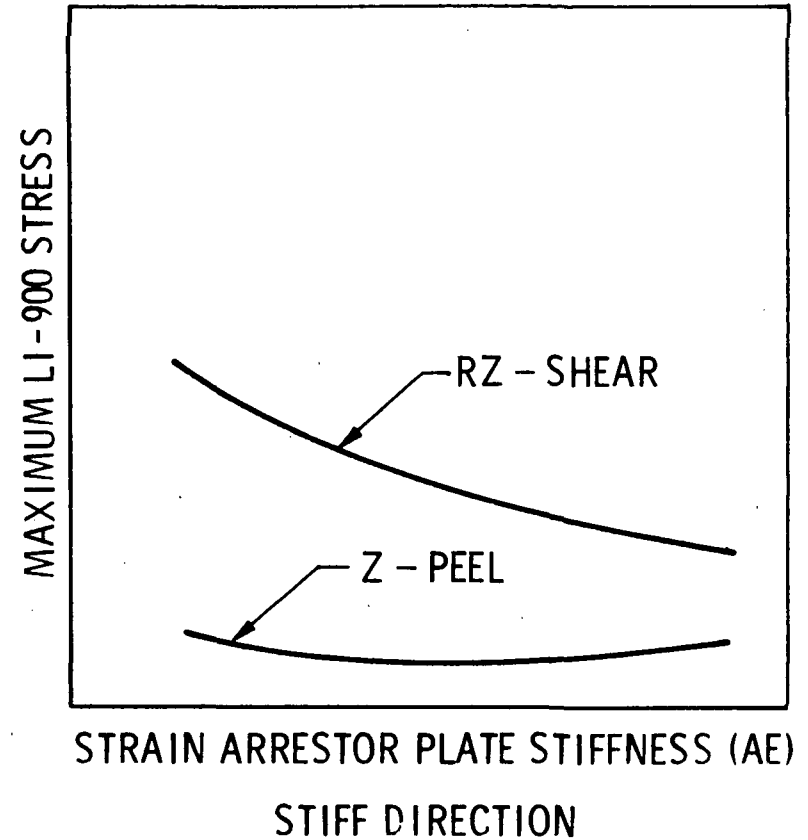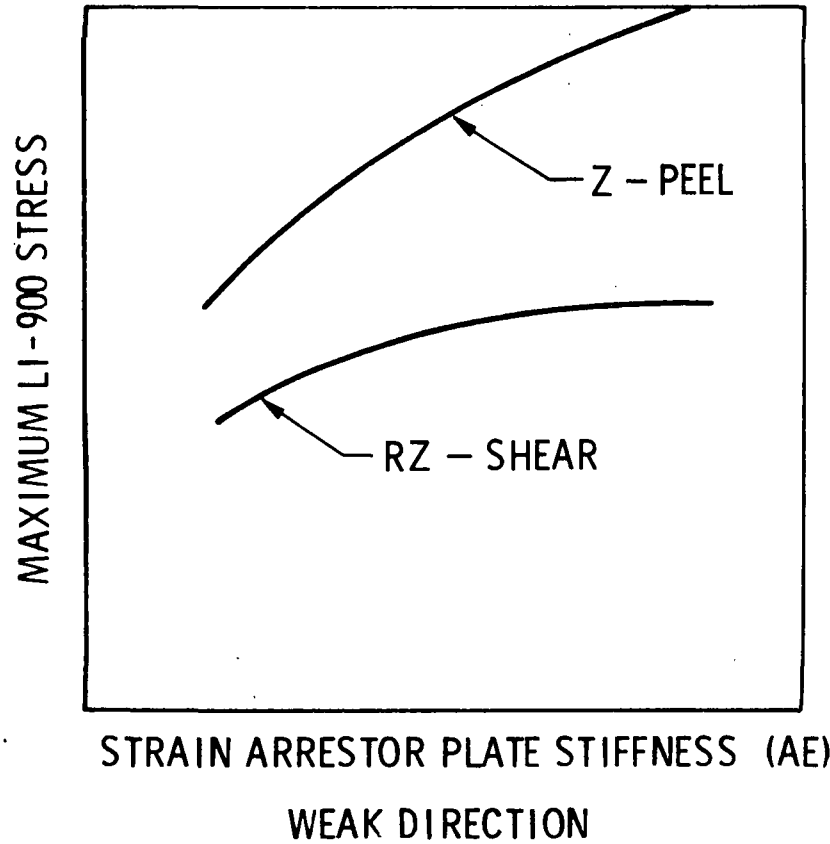
Figure 8

LI-900 STRESS VS TILE LENGTH (WEAK DIRECTION)
(Figure 9)

The tile length in the weak direction was varied to assess the possibility of varying tile dimensions to reduce stress levels in LI-900 tiles using a SAP. The shear stress level was found to be a minimum of approximately 33 cm (13 in.). The peel stress, however, continues to decrease with increasing tile length. This study indicates the possibility of increasing tile length to decrease overall stress levels in the LI-900.

LI-900 STRESS VS TILE LENGTH - WEAK DIRECTION
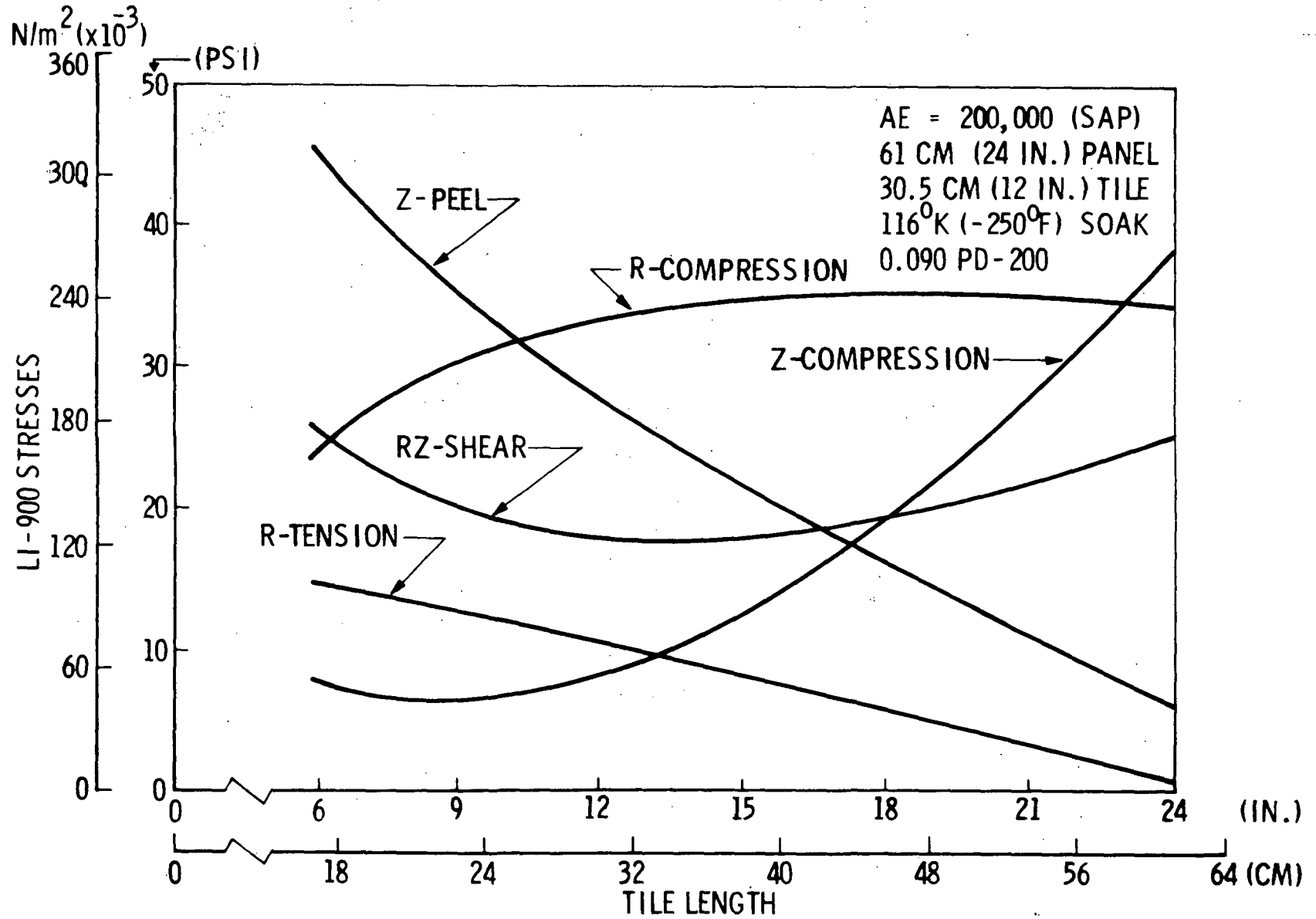
Figure 9

LI-900 STRESS VS TILE LENGTH — STIFF DIRECTION
(Figure 10)

The LI-900 stresses continue to increase with increasing tile length in the strong direction. Again, the opposite trends are seen for the weak and stiff directions. Based on this study, limiting the tile lengths to 30.5 cm (12 in.) would be warranted.

LI-900 STRESS VS TILE LENGTH - STIFF DIRECTION

$N/m^2(x10^3)$ → (PSI)

AE = 200,000
61 CM (24 IN.) PANEL
30.5 CM (12 IN.) TILE
$116^{O}K$ $(-250^{O}F)$ SOAK
0.090 PD-200

LI-900 STRESS

R-COMPRESSION

RZ-SHEAR

Z-COMPRESSION

R-TENSION

Z-PEEL

TILE LENGTH
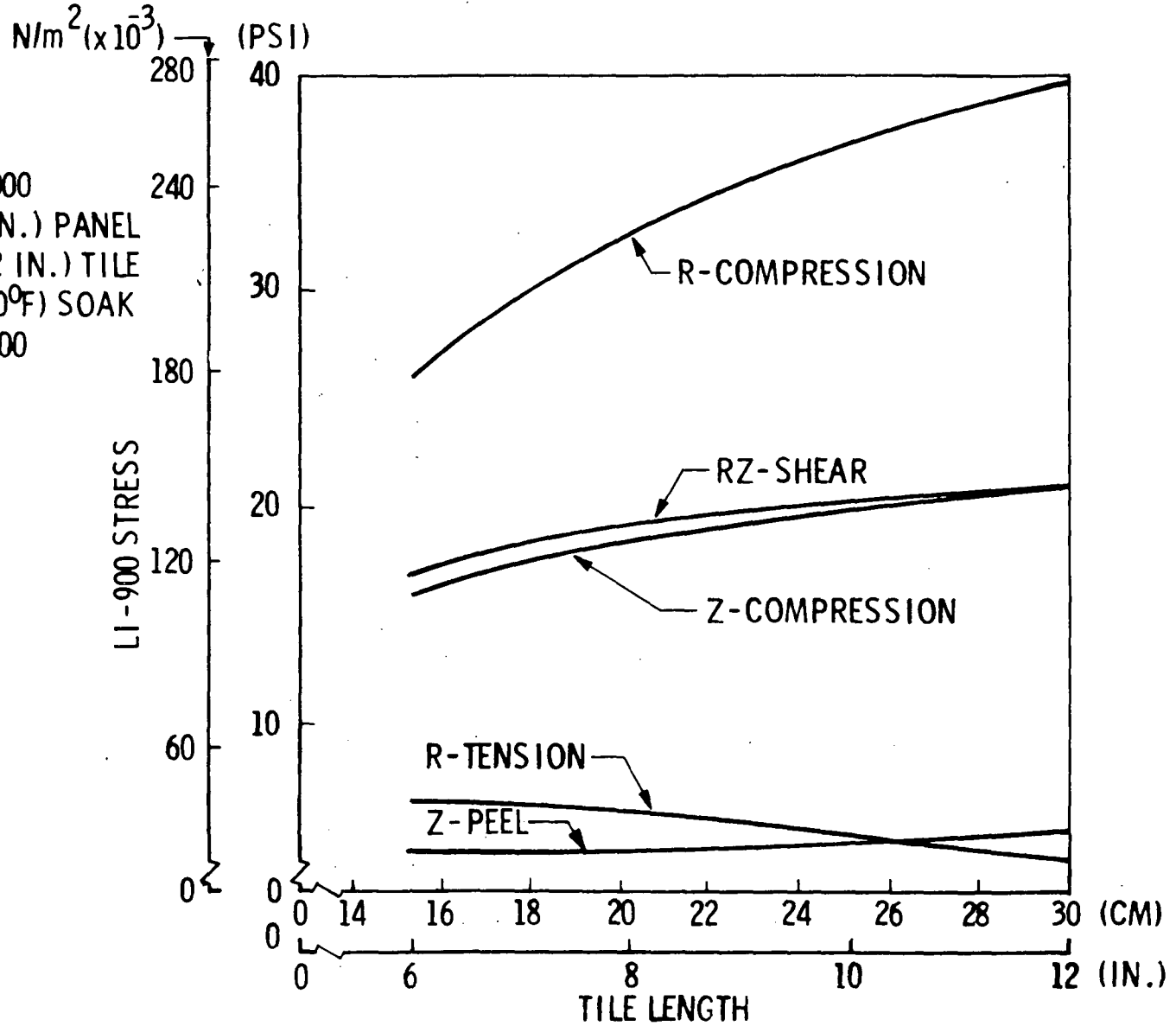
Figure 10

LI-900 STRESSES VS SAP STIFFNESS, PD-200
(Figure 11)

Positive margins are shown for critical RSI stresses with a SAP stiffness of 150,000 and above, when the GE PD-200 foam bond system is used to attach the SAP to the primary structure. A modulus of 82.7×10^6 N/m^2 (12,000 psi) was used for the $116^\circ K$ ($-250^\circ F$) condition. Therefore, considering the available data, PD-200 was selected as the baseline attachment system for the screening analysis. An SAP extensional stiffness of 98,800 kg (200,000 lb) was selected for the tradeoff studies.

LI-900 STRESS VS SAP STIFFNESS

Figure 11

RL-1973 FOAM 116^OK $(-250^O$F) TESTS
(Figure 12)

Data for cryogenic properties of attachment materials are scarce and conflicting. Most reported data on moduli have been taken at high strain rates (up to 50 percent strain reported). In application, however, maximum strains experienced are on the order of 5 percent. To aid in analytical studies and design activities, LMSC has performed a series of -116^OK $(-250^O$F) tests on RL-1973 foam, RL-1973 foam with thin layers of RTV-560 on each surface, and RTV-560 alone. Temperature variations over the specimen length were within 10^OF and strain levels verified within 0.5 percent. Modulus of these specimens was determined over a range of 0 to 5 percent strain.

Specimens were loaded and unloaded at 116^OK $(-250^O$F) and in some cases multiple cycles were performed, with the specimen allowed to warm to ambient temperature between cycles. The RL-1973 silicone foam was found to be generally consistent in behavior, with the exception of two cases where very low moduli were measured. No explanation is attempted for this variation but it was observed that in the second test on one specimen the elastic modulus fell within the scatter of the other tests. These tests indicate that the 116^OK $(-250^O$F) modulus is in the range of 48.2 to 55.8 x 10^6 N/m^2 (7000 to 8100 psi).

Twenty-four (24) tests were performed on seven (7) specimens of RL-1973 with RTV-560. These tests were generally inconclusive, with the composite modulus measurements ranging from 14.5 to 827 x 10^6 N/m^2 (2100 to 120,000 psi).

Seventeen (17) tests were performed on six (6) RTV-560 specimens. Again, these tests were inconclusive, with modulus measurements ranging from 166 to 2420 x 10^6 kg/m^2 (24,000 to 350,000 psi).

RL-1973 FOAM — 116°K (250°F) TESTS

Figure 12

1145

The 116°K (-250°F) cold soak environment imposes the critical design stresses in the RSI tile. Prelimi-
nary tests indicate that use of a foam bond alone may be sufficient to allow the tile to survive this
condition; however, present material data on the available foam bonds are inadequate for design pur-
poses. Moreover, data from available tests indicate that the physical behavior of bond materials at
these temperatures is not well understood.

The strain arrestor plate (SAP) concept provides a means for meeting the design requirements for cold
soak at 116°K (-250°F). Taking advantage of the heat capacitance of the SAP allows a reduction in the
RSI thickness, and thus use of the SAP on the orbiter lower surface does not involve a weight penalty.
However, in lower temperature regimes there is a net weight penalty so that the overall TPS weight may
increase as much as 909 kg (2000 lb).

CONCLUSIONS ON COLD SOAK ENVIRONMENT

- TEMPERATURES BELOW 101°K (-150°F) IMPOSE SEVERE CONSTRAINT ON RSI DESIGN

- FOAM BOND MAY WORK BUT PRESENT MATERIAL CHARACTERIZATION IS INADEQUATE FOR ANALYSIS

- STRAIN ARRESTOR PLATE (SAP) CONCEPT IS SUCCESSFUL IN KEEPING RSI STRESSES BELOW ALLOWABLES AT 116°K (-250°F)

- SAP IMPOSES OVERALL TPS WEIGHT PENALTY 680 TO 909 kg (1500 TO 2000 LB)

- MUST TAKE ACTION TO

    - ENSURE ENVIRONMENT PROPERLY DEFINED

    - CHARACTERIZE BOND MECHANICAL PROP, INCLUDING CREEP AND STRESS RELAXATION BEHAVIOR OVER TEMPERATURE RANGE DOWN TO 116°K (-250°F)

Figure 13

EFFECTS OF GAP HEATING ON TPS
(Figure 14)

Gap heating effects can strongly influence joint design as well as establish manufacturing and installation tolerances. Excessively restrictive tolerances (specified simply to avoid the problem) will have a profound influence on cost. Hence, careful evaluation of gap heating effects is vital. By nature this problem can only be treated semi-empirically. Tests in NASA facilities have recently been completed and present effort is directed at determining the system impact of these results.

EFFECTS OF GAP HEATING ON TPS

- ADDITIONAL HEAT LOAD RESULTS IN PRIMARY STRUCTURE TEMPERATURE INCREASE

- LOCALIZED HEATING OF LI-1500 MATERIAL AT GAP SIDES

- HEATING AT GAP BASE WHICH COULD RESULT IN OVERTEMPERATURE OF JOINT WATERPROOFING

STATUS OF GAP HEATING ANALYSIS

- PRELIMINARY ANALYSIS MADE TO ASSESS EFFECTS OF GAP HEATING UTILIZING CORRELATION OF MSC ARC JET TEST DATA ON LI-1500 JOINT

1149

Figure 14

LI-1500 JOINT GAP HEATING
(Figure 15)

Analysis was made assuming that the convective heating along the gap edge (down a distance equal to the gap width) is equal to the surface convective heat rate. It is also assumed that the convective heating deeper inside the gap is 0.007 times the surface convective heat rate. These assumed values are in close agreement with existing test data. The reduced view factor of the surfaces inside the gap is considered in establishing the radiative heat rate.

The effect of gap heating is to significantly increase the temperature along the gap wall. The bondline temperature also is increased. The impact on TPS design is now under evaluation.

MAXIMUM TEMPERATURE DISTRIBUTION DOWN GAP WALL
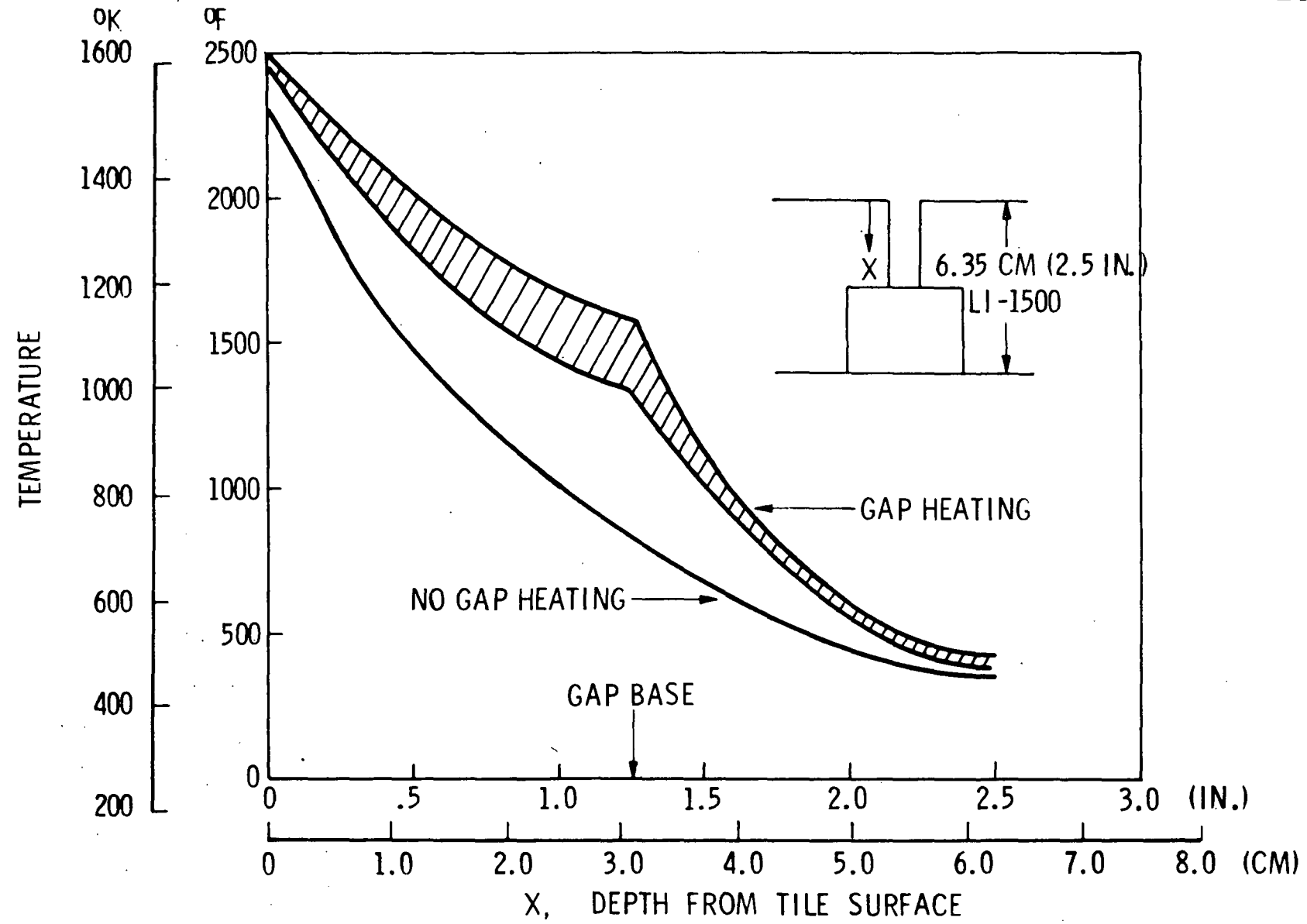
Figure 15

HEAT TRANSFER DATA ON GAP HEATING
(Figure 16)

The heating tests performed to date have given limited insight into TPS gap and slot heating characteristics. Additional testing is needed to aid in refining gap/slot/step heating data as the TPS design progresses.

HEAT TRANSFER DATA ON GAP HEATING

SOURCE	CONFIGURATION	CONDITIONS	STATUS OF DATA
NASA LaRC C. JOHNSON	METALLIC TILES PARALLEL AND STAGGERED TILES GAP SIZE = .16, .32, .48 CM (1/16, 1/8, 3/16 IN.) TILE SIZE = 15.25 x 15.25 x 2.54 CM (6 x 6 x 1 IN.)	LaRC — VDT $M_\infty = 8$ $Re_\infty / M = 0.06 \times 10^6$ TO 3.3×10^6 LAMINAR AND TURBULENT B.L.	AVAILABLE AS OF 26 SEP 1972
NASA LaRC J. DUNAVANT	METALLIC TILES ON CURVED SURFACE PARALLEL TILES GAP SIZE = 0.32 CM (0.125 IN.) TILE SIZE = 15.25 x 15.25 x 2.54 CM (6 x 6 x 1 IN.)	LaRC — CFHT $M_\infty = 10$ $Re_\infty / M = 0.12 \times 10^6$ TO 0.76×10^6 TURBULENT B.L.	TESTS SCHEDULED FOR JAN 1973
NASA LaRC A. CHAPMAN	METALLIC TILE INSERT IN RSI TILE ARRAY TILE SIZE = 15.25 x 15.25 x 5.08 CM (6 x 6 x 2 IN.)	AFFDL 50 MW FACILITY $\alpha = 30$ DEG	TEST SCHEDULED FOR DEC 1972
NASA ARC F. CENTOLANZI (PHASE III MODEL)	20.3 x 25.4 CM (8 x 10 IN.) LI-900 ARRAY JOINT COATING, SURFACE, AND IN-DEPTH T/Cs	TURBULENT B.L. IN DUCT WALL $T_{MAX} = 1533^\circ K$ (2300°F)	TEST SCHEDULED FOR NOV 1972
NASA MSC D. TILLIAN (PHASE III MODEL)	30.5 x 30.5 CM (12 x 12 IN.) LI-900 ARRAY JOINT COATING, SURFACE, AND IN-DEPTH T/Cs	LAMINAR B.L. 10 MW 100 CYCLES	TEST SCHEDULED FOR NOV 1972

Figure 16

TURBULENT DUCT TEST MODEL
(Figure 17)

This model is sized for the heat pulse specified under the Phase III TPS technology contract (monitored by NASA/MSC), and instrumented to provide maximum gap/step joint heating data. A total of 39 thermocouples, including 11 platinum/platinum -13% rhodium surface T/C's, will be installed in the panel. Twenty-four (24) of these will be employed to determine gap temperatures. Five (5) chromel/alumel T/C's will be installed in each of two T/C plugs, and five chromel/alumel T/C's will be attached to the substrate.

OBJECTIVES
- Turbulent convective heating exposure
- Joint, gap, and step heating data
- Thermal response/prediction correlation
- Cyclic effects

TEST CONDITIONS
- Arc-heated air
- Area 2P heat pulse
- Supersonic, turbulent flow
- Minimum five cycles
- NDE procedures every cycle

TURBULENT DUCT TEST MODEL

FLOW

20.1 CM
(7.900 IN.)

25.2 CM ± (9.900
IN. ±)

THERMOCOUPLE
LOCATION (TYP)

0.0508 CM
(0.020 IN.)

TYP

T/C PLUG

SUBSTRATE

9.76 CM
(3.840 IN.)

HONEYCOMB
SUBSTRATE
INSULATOR

MOUNT PLATE
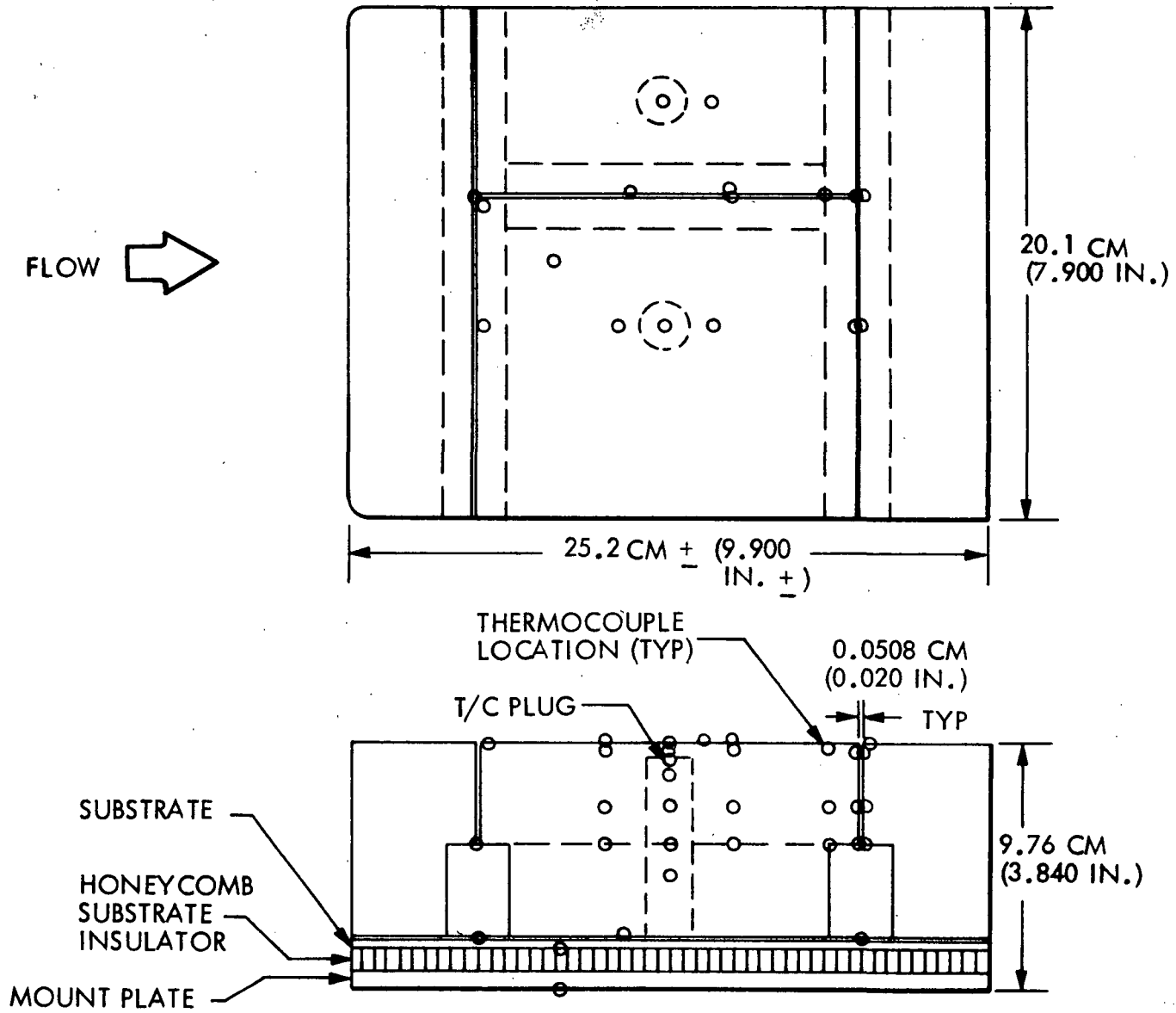
Figure 17

METHODS FOR REDUCING EFFECT OF GAP HEATING
(Figure 18)

A number of design alternatives are being considered to minimize gap heating effects. A partial list is shown.

METHODS FOR REDUCING EFFECT OF GAP HEATING

ON TPS MATERIALS

- REDUCE RATIO OF GAP WIDTH/GAP HEIGHT

- USE OF FILLER MATERIALS

ON PRIMARY STRUCTURE TEMPERATURES

- REDUCE GAP WIDTH

- USE OF FILLER MATERIAL

- INCREASE INSULATION THICKNESS

- INCREASE TILE SIZE

Figure 18

EFFECT OF FORWARD FACING STEPS ON
LOWER SURFACE HEATING
(Figure 19)

Forward facing steps can result in significant increase over surface heating. This curve defines heating increase for both laminar and turbulent flow as a function of the ratio of step height to boundary layer displacement thickness H/ζ^*. Laminar H/ζ^* expected for flight are as shown, resulting in a heating increase of 8 to 25 percent, 283 to 373°K (50 to 150°F) for a 1.27 mm (0.05 in.) step. Turbulent H/ζ^* anticipated for flight results in heating increases of 2 to 5 percent, 272 to 300°K (30 to 80°F).

EFFECT OF FORWARD FACING STEPS
ON LOWER SURFACE HEATING
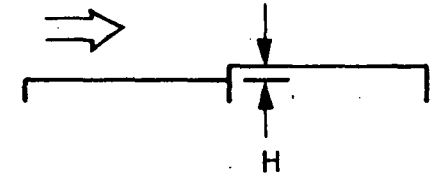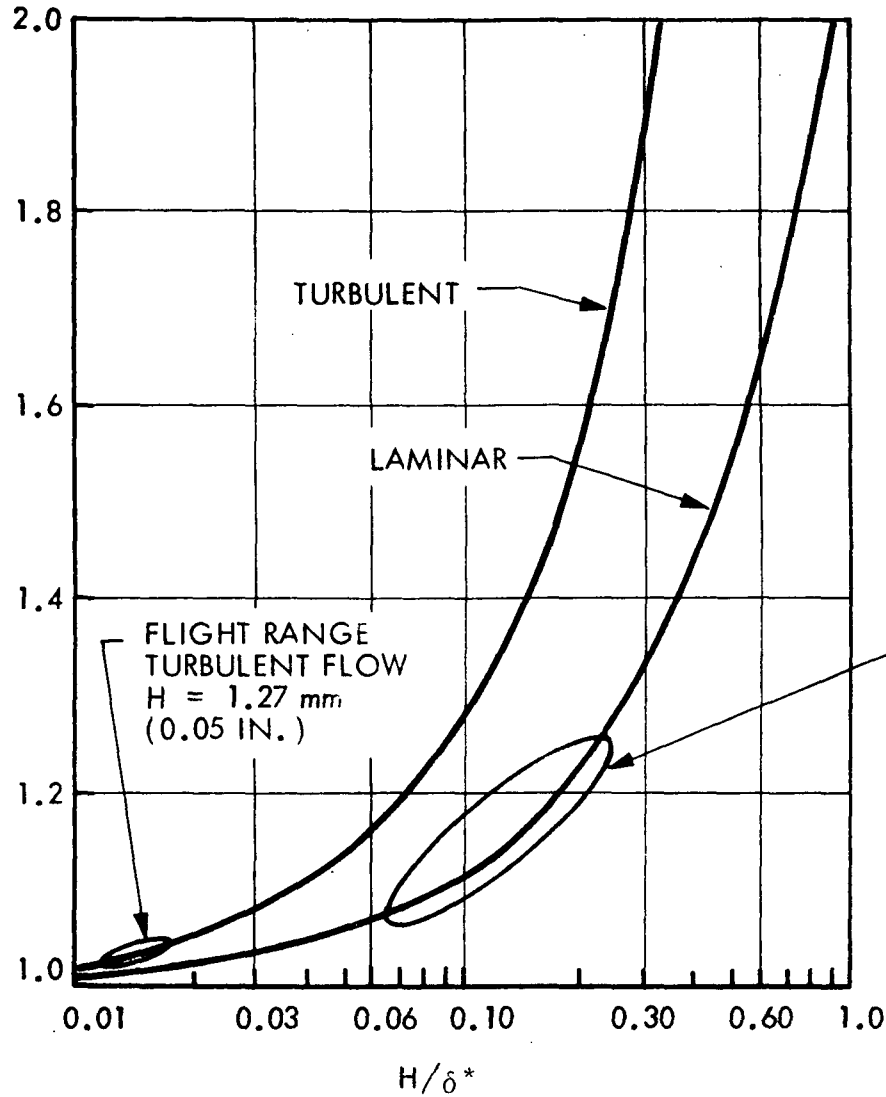
Figure 19

DRAG DATA FOR GAPS, GROOVES, AND STEPS
(Figure 20)

Gaps and steps between adjacent tiles affect aerodynamic as well as thermodynamic design of the vehicle. The effects on drag, L/D, and vehicle stability are of critical importance, particularly in subsonic flight. Aerodynamic considerations may establish manufacturing tolerance constraints; manufacturing limitations may impose performance constraints. These effects must be established as early as possible. Wind tunnel testing on typical configurations is needed to provide precise data, but the magnitude of gap and step effects on aerodynamic factors can be established on the basis of existing information.

DRAG DATA FOR GAPS, GROOVES, AND STEPS

SHALLOW GAPS

$C_{D_\bullet}$ vs e/h

$h = .5e = \frac{\ell}{16} = .24\delta$

DEEP GAPS

$C_{D_\square}$ vs h/e

- SHALLOW TRANSVERSE GAPS HAVE HIGHER DRAG THAN DEEP TRANSVERSE GAPS

$V_{CROSSFLOW}$

$V_{LONGITUDINAL}$

$C_{D_\bullet} = .01$ $C_{D_{Wet}} = .009$

$C_{D_\bullet} = .01$ $C_{D_{Wet}} = .001$

IN CROSSFLOW   IN LONGITUDINAL FLOW

- LONGITUDINAL GROOVES NORMALLY HAVE HIGHER DRAG THAN TRANSVERSE GAPS
- FAIRING GROOVES CAN RESULT IN LOWER DRAG THAN GAPS

$C_{D_\bullet}$ $C_{D_\bullet}$

0.40   0.22

0.11   0.24

V →   ← V

0.04   0.16

0.24   0.24

0.01   0.01

- BUTT JOINTS HAVE LOWEST DRAG
- MOST PROTRUDING AND SHARP-EDGED JOINTS HAVE HIGHEST DRAG
- ROUNDING AND BEVELING REDUCES DRAG

Figure 20

TYPICAL SUBSONIC DRAG BREAKDOWN
(Figure 21)

Surface gaps, 0.229 cm (0.090 in.) contribute an increment of 2 percent of the zero lift drag coefficient. Forward-facing steps [assumed to be .127 cm (0.050 in.) on half of the tiles, zero on the remainder] contribute 5 percent of the zero lift drag coefficient. Skin friction due to (an assumed) 8-mil surface roughness on the tile coating contributes much more (14 percent) to the drag coefficient. Thus, it is clear that the aerodynamic effects of gaps and steps, while important, are not critical to the vehicle design, unless the resulting roughness causes adverse flow separations, or unless the ABES thrust becomes marginal.

TYPICAL SUBSONIC DRAG BREAKDOWN

Figure 21

1163
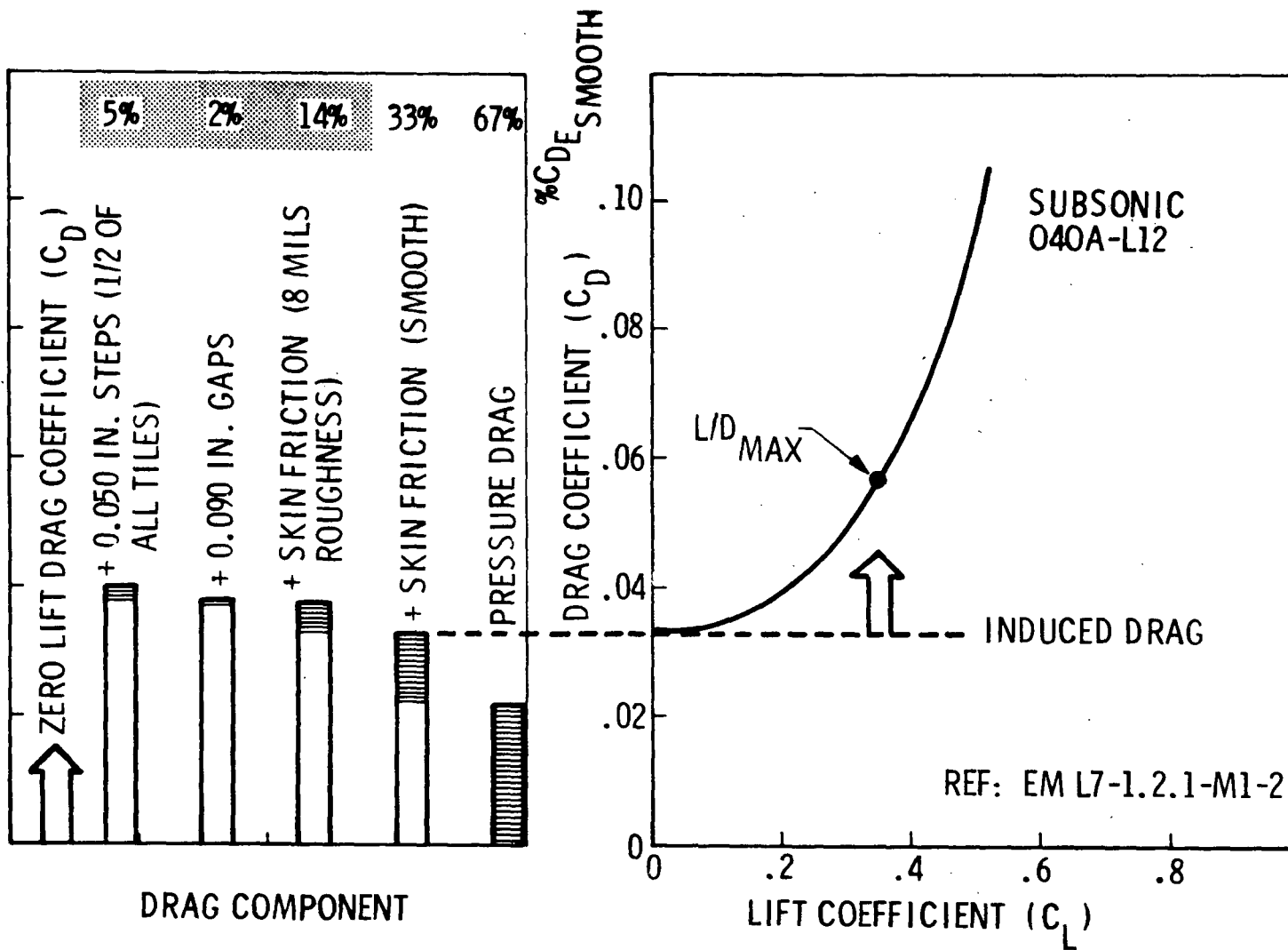
ABLATOR ROUGHNESS EFFECTS ON LIFTING SPACECRAFT
AERODYNAMIC CHARACTERISTICS
(Figure 22)

Although surface roughness effects on the aerodynamic drag must be considered in the
orbiter design, they may not pose a serious problem to the orbiter performance. Studies
performed on the effects of surface roughness of a charred ablator on a lifting body
indicate that there are potentially serious problems in vehicle aerodynamic stability.
Existing data are inadequate to make predictions regarding the effect of TPS gaps and
steps on orbiter stability. It is clear, however, that this is a potential problem requir-
ing early resolution.

ABLATOR ROUGHNESS EFFECTS ON LIFTING SPACECRAFT AERO CHARACTERISTICS
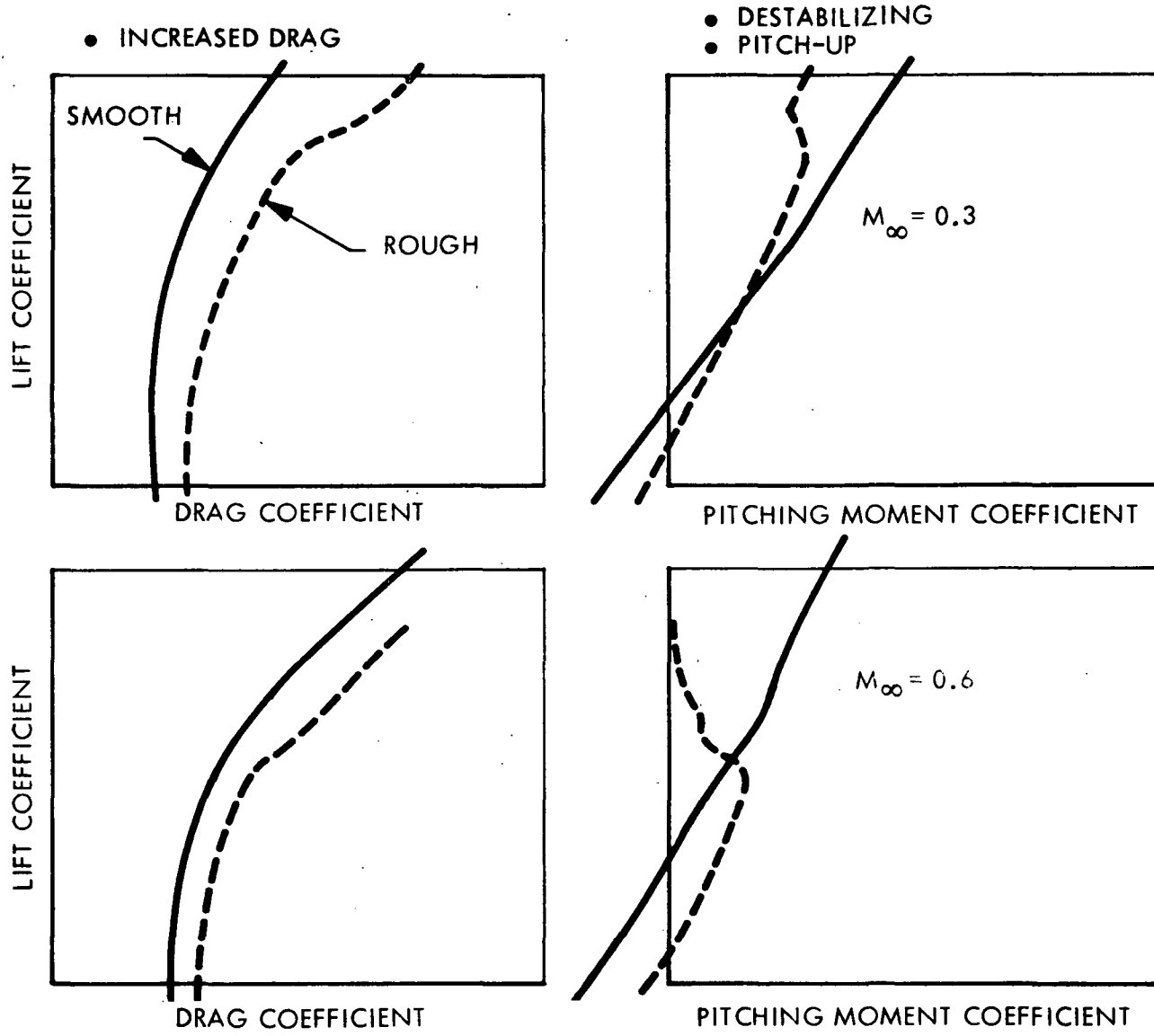
Figure 22

DRAG STUDY SUMMARY
(Figure 23)

Further evaluation is required to verify these conditions. However, such additional work must await wind tunnel test data.

DRAG STUDY SUMMARY

- $\triangle C_{D_0{}_{TPS}} \approx 0.007$ OR 21 PERCENT $C_{D_0{}_{SMOOTH}}$
- TILE SURFACE FINISH MORE IMPORTANT THAN GAPS OR STEPS

- $\triangle C_{D_{TPS}}$ AT $(L/D)_{MAX}$ CAN BE 2 TO 3 TIMES $\triangle C_{D_0{}_{TPS}}$

- EDGE GEOMETRY CAN MINIMIZE DRAG LOSSES

- TPS CAN INDUCE FLOW SEPARATION

RECOMMENDATIONS

- SURFACE ROUGHNESS MEASUREMENT

- DETAIL A WIND TUNNEL PROGRAM TO DEFINE/VERIFY AERO PENALTIES/ IMPROVEMENTS/SCALING LAWS

1167

Figure 23

SQUARE TILE TOLERANCE/GAP RELATIONSHIP
(Figure 24)

One of the primary impacts of the aerodynamic and thermodynamic studies of TPS gaps and steps will be to establish tolerance requirements on the RSI tiles and on the assembled array of tiles. The cold soak condition imposes a minimum gap requirement on silica tiles—0.102 cm (0.040 inch) between 20.0 cm (8-inch) tiles, and 0.076 cm (0.030 inch) between 15.2 cm (6-inch) tiles—and the maximum mechanical loading at temperature imposes another minimum gap requirement depending upon tile size and thickness.

This chart assumes that the tiles are rectangular, deviating from a square only by the amount of the tolerance. Angular tolerances, combined with primary structure tolerances, have not been included in this simplified chart. While LI-1500 tiles have been machined to a tolerance of ±0.13 mm (0.005 inch), a minimum tolerance of ±0.25 mm (0.010 inch) is presently assumed. A ±0.076 mm (0.030 inch) or even larger would significantly reduce installation costs. An effort is currently under way to quantify the cost of achieving a given tolerance over a range of values.

SQUARE TILE TOLERANCE/GAP RELATIONSHIPS
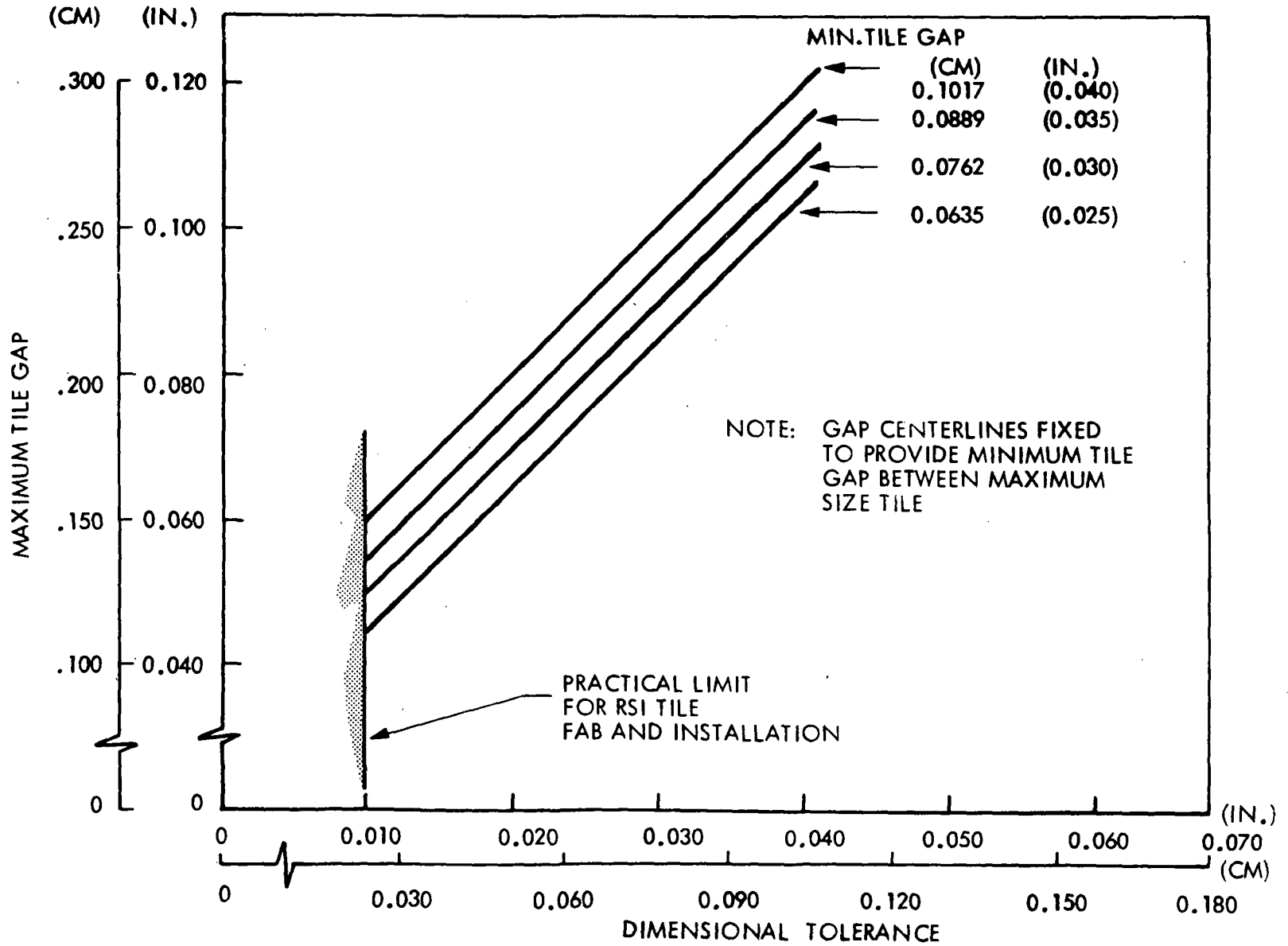
Figure 24

THERMAL-DIMENSIONAL STABILITY, LI-1500/LI-900
(Figure 25)

The aero- and thermodynamic effects of gaps and steps impose restrictions on the dimensional stability of the RSI tiles during their 100-mission life. Results of long time oven exposures of the silica materials at 1648°K (2500°F) have raised false concerns that the shrinkage of silica RSI would create significant growth of gaps between tiles. A 110-mission 1648°K (2500°F) peak temperature, 3000-second pulse test series on LI-1500 has shown the actual dimensional change to be less than 0.1 percent. A similar 100-mission exposure (with a 1533°K, 2300°F, peak) showed that LI-1500 and LI-900 have comparable performance well within the requirements for Shuttle application.

THERMAL-DIMENSIONAL STABILITY LI-1500/LI-900

DISPLAYED IN 100-CYCLE RADIANT HEAT TESTS

NOVEMBER 1971: NOMINAL NAS 9-12083 REENTRY PERTURBED TO 1648°K (2500°F)

SPECIMEN	LENGTH, CM			WIDTH, CM		
	PRE	POST	% CHANGE	PRE	POST	% CHANGE
TT42-5[1]	9.987	9.987	0	9.942	9.942	0
TT42-6[1]	9.967	9.967	0	9.957	9.952	-0.05

OCTOBER 1972: AREA 2P TEMPERATURE–TIME HISTORY 1533°K (2300°F)

SPECIMEN	LENGTH, CM			WIDTH, CM		
	PRE	POST	% CHANGE	PRE	POST	% CHANGE
84-3[2]	12.626	12,619	-0.06	12.637	12.626	-0.08
84-4[2]	12.586	12.558	-0.22	12.588	12.568	-0.16
85-3[1]	12.662	12.639	-0.18	12.619	12.662	-0.02
85-4[1]	12.685	12.705	+0.16	12.715	12.703	-0.10

[1] 240 kg/m^3 (15 PCF) DENSITY SPECIMEN   [2] 144 kg/m^3 (9 PCF) DENSITY SPECIMEN

Figure 25

DOLLAR VALUE OF A POUND SAVED
(Figure 26)

TPS weight has a significant impact on total program costs. If a TPS weight reduction is introduced early enough in the orbiter design (prior to structure ten percent drawing release) the vehicle can be resized to take full advantage of the weight saving, thus obtaining maximum total program cost saving.

DOLLAR VALUE OF A POUND SAVED

PRIOR TO 10 PERCENT STRUCTURE DRAWING RELEASE ON ORBITER

      REDUCTION OF TPS WEIGHT BY 2270 kg (5,000 LB) REDUCES TOTAL PROGRAM
      COSTS BY $174,000,000

AFTER CRITICAL DESIGN REVIEW ON ORBITER STRUCTURE

      REDUCTION OF TPS WEIGHT BY 2270 kg (5,000 LB) REDUCES TOTAL PROGRAM
      COSTS BY $113,000,000

(BASED ON 500-FLIGHT PROGRAM)

Figure 26

SYSTEM WEIGHT CHANGE DUE TO ONE UNIT OF TPS WEIGHT CHANGE

(Figure 27)

A change in the TPS weight will result in a change in the orbiter dry weight if the payload weight capability is kept constant. The on-orbit maneuvering system and reaction control system propellant requirements also change proportionately. Thus for each 0.45 kg (1.0 lb) of change in TPS weight the orbiter vehicle weight will change a total of .74 kg (1.63). As shown in the sketch, the gross liftoff weight (GLOW) will change 24.8 kg (54.53 lb).

If the orbiter design is fixed (e.g., after structure CDR) a decrease in TPS weight could be accepted with no impact on orbiter design. In that case, for a constant payload weight the orbiter weight would drop by 0.51 kg per kg (1.12 lb per lb) reduction in TPS, since OMS and RCS propellant requirements can still change. The impact of orbiter weight change on the external tank and SRM would still be in the same ratio, however. Thus a 1 kg (2.2 lb) decrease in TPS will reduce the GLOW by 17.1 kg (37.6 lb).

Late in the program, when the full advantage of reductions in system weight cannot be realized, TPS weight reduction is still advantageous. Such a weight reduction may offer the capability of restoring a lagging payload capability, or of providing payload or performance capability above the nominal required values.

1174

SYSTEM WEIGHT CHANGE
DUE TO ONE UNIT OF TPS WEIGHT CHANGE

ORBITER

EXTERNAL TANK

Δ TPS

Δ ORBITER DRY

(OMS AND RCS) PROP

1.00
+
0.45
+
0.18

1.63 Δ ORBITER

6.39
+
0.27

Δ TANK PROP

Δ TANK DRY

$$\frac{6.66 \, \Delta \text{TANK}}{8.29 \, \Delta (\text{TANK} + \text{ORB})}$$

SRB

Δ SRB PROP

Δ SRB DRY

41.20
+
5.04

$$\frac{46.24 \, \Delta \text{SRB}}{54.53 \, \Delta \text{GLOW}}$$
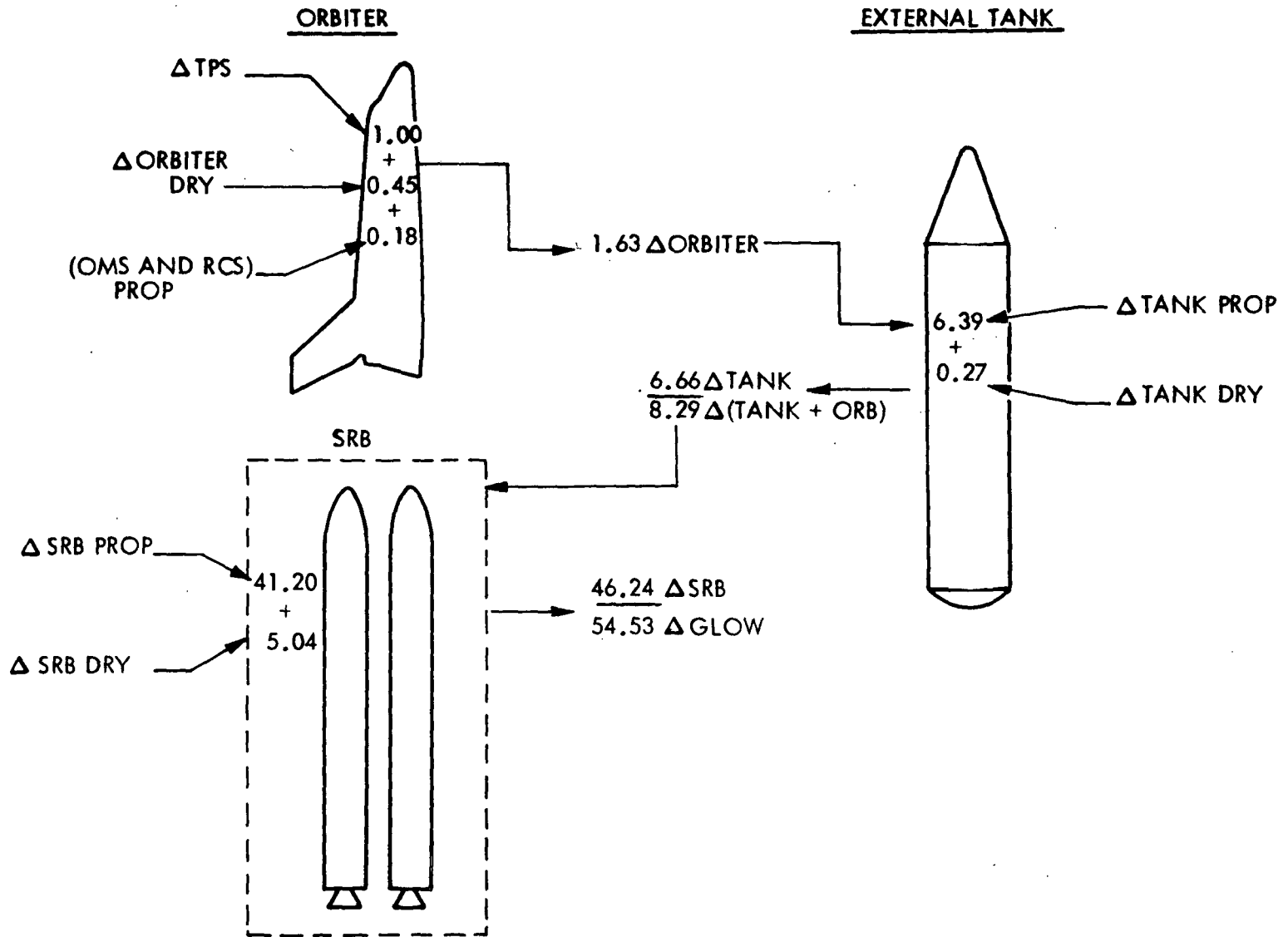
1175

Figure 27

ORBITER TPS WEIGHT COMPARISON
(Figure 28)

TPS weights for the LMSC orbiter were computed by LMSC using four different materials (LI-900, LI-1500, and two mullites). The O40-L12 delta wing orbiter has a 1,170 square meter (12,200 sq ft) surface area and peak lower-surface isotherms of 1533°K (2300°F). Most of the lower surface is above 1423°K (2100°F).

The sizing assumptions were identical for all four materials. A value of 0.9 was assumed for σ/ε, and maximum on-orbit heating was used in TPS sizing. In all cases a 0.080 foam bond with 0.010 RTV-560 was assumed, although it is recognized that the mullite manufacturers used thicker pads in their designs (which will increase the weight somewhat).

Thermal conductivity data were taken from two sources: (1) contractor final reports for the Phase II contracts with NASA-MSC, and (2) the Battelle final report. There is considerable difference in some of the weights, depending upon which source is used.

ORBITER TPS WEIGHT COMPARISON

THERMAL CONDUCTIVITY SOURCE	TPS WEIGHT (kg)			
	LMSC LI-900	LMSC LI-1500	MDC MULLITE	GE MULLITE
CONTRACTOR DATA (NAS 9-12083, NAS 9-12082, NAS 9-12084)	7,160	8,750	13,760	10,400
BATTELLE (NAS 9-10853)	7,640	9,640	13,200	13,950

LMSC ORBITER CONFIGURATION O4OA-L12
1100 NM CROSSRANGE
NOSE CAP AND WING LEADING EDGE IS CARBON-CARBON

*LI-900 CONDUCTIVITY NOT MEASURED BY BATTELLE; ABOVE DATUM
 BASED ON LI-1500 CONDUCTIVITY COMPARISON
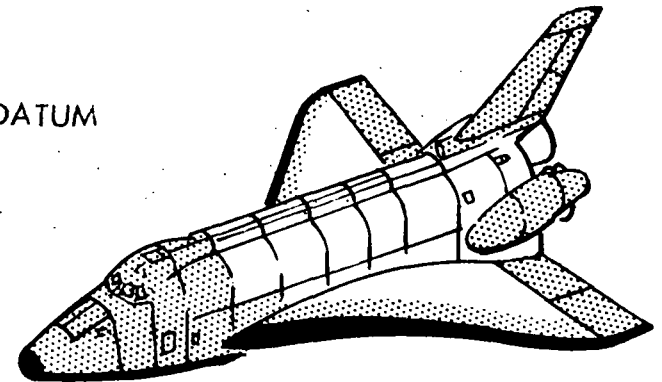
Figure 28

TPS TOTAL PROGRAM COST SENSITIVITIES
(Figure 29)

The dollar value of a kilogram saved is derived from a detailed cost sensitivity study.[1] These total program cost figures are based on an assumed 500-flight program. If the orbiter structure design is frozen, the OMS, RCS, external tank, and SRM propellants can still be altered to take advantage of a TPS weight change. The total dollar value of a kilogram saved will change by 76,600-6, 050/1.45 or $49,300/kg ($22,500/lb).

TPS TOTAL PROGRAM COST SENSITIVITIES

WEIGHT SENSITIVITIES (kg/kg)	INDIVIDUAL COST SENSITIVITIES ($/kg)	COST SENSITIVITIES FOR TPS ($/kg)	
$\dfrac{\partial W_{ORB}}{\partial W_{TPS}} = 1.45$	$\dfrac{\partial \$_{ORB}}{\partial W_{ORB}} = 11,440$	$\dfrac{\partial \$_{ORB}}{\partial W_{TPS}} = (1.45 - 1.0) \times 11,440 =$	\$ 5,050
$\dfrac{\partial W_{PROP}}{\partial W_{TPS}} = 6.39$	$\dfrac{\partial \$_{PROP}}{\partial W_{PROP}} = 13**$	$\dfrac{\partial \$_{PROP}}{\partial W_{TPS}} = 6.39 \times 13 =$	\$ 835**
$\dfrac{\partial W_{TANK}}{\partial W_{TPS}} = 0.27$	$\dfrac{\partial \$_{TANK}}{\partial W_{TANK}} = 21,000**$	$\dfrac{\partial \$_{TANK}}{\partial W_{TPS}} = 0.27 \times 21,000 =$	\$ 5,720
$\dfrac{\partial W_{SRB}}{\partial W_{TPS}} = 41.2$	$\dfrac{\partial \$_{SRB}}{\partial W_{SRB}} = 1,580**$	$\dfrac{\partial \$_{SRB}}{\partial W_{TPS}} = 41.2 \times 1,580 =$	\$ 65,000*

PRE-10 PERCENT DRAWING RELEASE:

$$\frac{\partial \$_{TOTAL}}{\partial W_{TPS}} = \sum \text{OF ABOVE} = \qquad \$\ 76,600**$$

POST ORBITER STR CDR:

$$\frac{\partial \$_{TOTAL}}{\partial W_{TPS}} = 1/1.45\,(76,600 - 5,050) = \quad \$\ 49,300$$

*DIRECT COST FOR ∂W_{TPS} IS ZERO
**BASED ON 500-FLIGHT PROGRAM

Figure 29

ORBITER TPS COST COMPARISON
(Figure 30)

Using the total program cost sensitivity presented earlier $76,600/kg ($34,900/lb), the weight differences presented in the previous chart result in significant cost differences.

The GE mullite weights have been arbitrarily selected as a base for this comparison. These figures clearly show that TPS weight has a profound impact on total program costs, and regardless of which set of cᴏ ᴊuctivity data one wishes to use, the silica RSI results in significantly lower costs.

Since the total DDT&E for TPS is less than $100 million, the total program cost savings can exceed the entire TPS development cost. Clearly, the TPS weight must be used as a major discriminator between competing TPS materials.

ORBITER TPS COST COMPARISON

THERMAL CONDUCTIVITY SOURCE	PROGRAM COST REDUCTION (MILLIONS) COMPARED TO GE MULLITE DESIGN			
	LMSC LI-900	LMSC LI-1500	MDC MULLITE	GE MULLITE
CONTRACTOR DATA (NAS 9-12083, NAS 9-12082, NAS 9-12084)	-$248	-$112	+$261	0
BATTELLE (NAS 9-10853	-$484	-$332	-$58	0

LMSC ORBITER CONFIGURATION O4OA-L12
1100 NM CROSSRANGE
NOSE CAP AND WING LEADING EDGE IS CARBON-CARBON
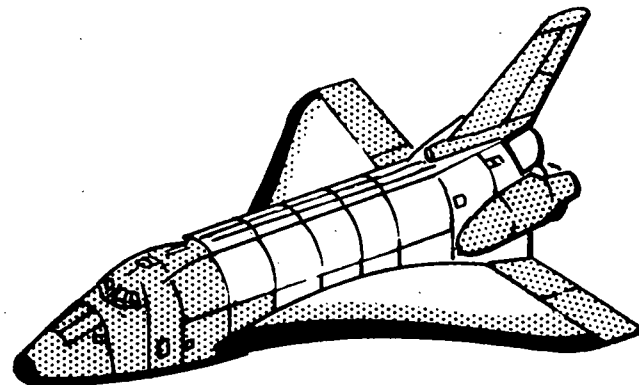
Figure 30

SUMMARY

- CONCENTRATED TECHNICAL EFFORT REQUIRED

    - COLD SOAK CONDITION

    - BOND PROPERTIES AT LOW TEMPERATURE

    - GAP AND STEP HEATING EFFECTS

    - AERODYNAMIC EFFECTS OF SURFACE ROUGHNESS
      (PARTICULARLY AERO STABILITY)

- ABOVE CONDITIONS STRONGLY INFLUENCE TPS WEIGHT AND COST

- TPS WEIGHT HAS SIGNIFICANT IMPACT ON TOTAL PROGRAM COSTS

    - TOTAL PROGRAM COST SAVING OF SILICA (VS MULLITE) EXCEEDS TPS
      DDT&E COSTS

    - TPS WEIGHT IS MAJOR TPS MATERIAL DISCRIMINATOR

    - EARLY INTRODUCTION OF SILICA INCREASES TOTAL PROGRAM COST
      SAVINGS

1182

REFERENCE

1. "Sensitivity of Space Shuttle Weight and Cost to Structure Subsystem Weights," Final Report on Contract NAS 1-11438, August 1972.

1183

A NON RIGID REUSABLE SURFACE INSULATION CONCEPT
FOR THE
SPACE SHUTTLE THERMAL PROTECTION SYSTEM

J. G. ALEXANDER

AVCO SYSTEMS DIVISION

LOWELL, MASSACHUSETTS

INTRODUCTION

The requirement for multiple flight capability of the Space Shuttle has provided impetus for development of high temperature ceramic surface insulations for thermal protection applications previously satisfied by ablative materials. A critical difficulty with rigid ceramic materials in this application is their characteristic low strain to failure and resultant difficulty in maintaining compatibility with deflections of the vehicle structure. A reusable thermal protection system concept, designated 3DSX, was developed that utilizes a flexible, woven ceramic mat insulation beneath an aerodynamic skin and moisture barrier consisting of either a dense ceramic coating or a super alloy metallic foil.

The resulting heat shield material has unique structural characteristics. The shear modulus of the woven mat is very low such that bending and membrane loads introduced into the underlying structural panel remain isolated from the surface skin.

This work was performed under NASA Contracts NAS9-12490 and NAS8-29061.

NOMENCLATURE

E	Tensile or compressive modulus
I	Moment of inertia
G	Shear modulus
k	Transverse extensional stiffness of 3DSX mat (E/d)
D	Flexural stiffness (EI)
h_c	Coating thickness
ΔP	Pressure differential across panel
l	Tile span
l_3	Depth of side coating (Tile thickness)
d	Woven 3DSX mat thickness
β	Stiffness parameter
B_2	Extensional stiffness of coating, $E_2 h_c$
ϵ	Strain

Subscripts

2	Coating
1	Substructure
i	Woven 3DSX mat
e	Edge of tile
c	Center of tile

SCHEMATIC 3DSX WOVEN MAT

(Figure 1)

The flexible mat is fabricated from fibrous ceramic felts compressed to the desired density and held under compression by ceramic yarns laced perpendicular to the felt layers. An outside layer of silica fabric is used to sandwich the felt and to provide a surface to prevent the reinforcement yarns from tearing the felt. The basic configuration utilized all silica components, although fabrication of the mat with other materials such as mullite, and zirconia has been demonstrated. The mat can be readily produced in a variety of densities, but nominal 93 kg/m^3 (6 lb/ft^3) and 150 kg/m^3 (10 lb/ft^3) systems have been fabricated and tested.

Fused silica coatings with high emittance additives or overcoats were developed that provide a moisture impervious surface and surface temperature capability to at least 1200°C (2300°F).

Systems that utilize nickel and cobalt base super alloy foil surfaces are currently being evaluated for use at surface temperatures to 1000°C (1800°F). The foils are stiffened by texturizing and attached to the substructure by wire fasteners that penetrate the woven mat.

SCHEMATIC
3DSX WOVEN MAT

SURFACE FABRIC WOVEN FROM CERAMIC YARNS

DENSE CERAMIC COATINGS PROVIDE MOISTURE BARRIER AND HIGH EMITTANCE

SURFACE FELT

MULTIPLE LAYERS OF COMPACTED CERAMIC FELTS 93 TO 160 Kg/m^3 DENSITY RANGE

VERTICAL REINFORCEMENT CERAMIC YARN

INSULATOR THICKNESS

VERTICAL REINFORCEMENTS ON 0.5 CM CENTERS
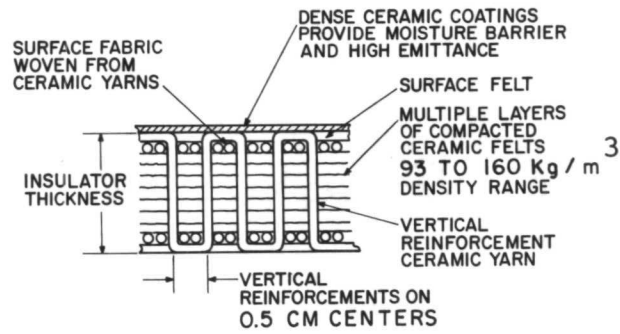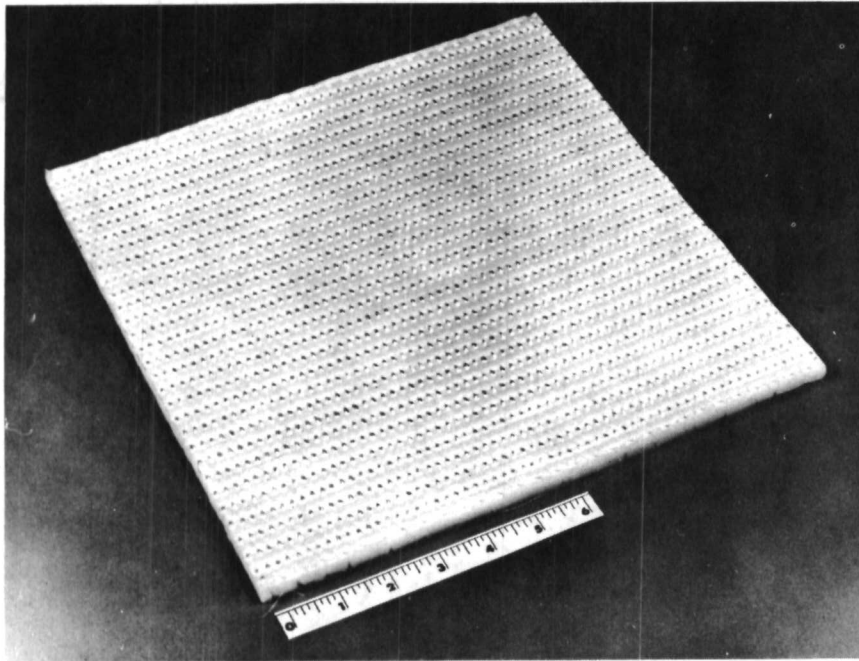
3DSX WOVEN MAT

SILICA COATED 3DSX PANEL

1189
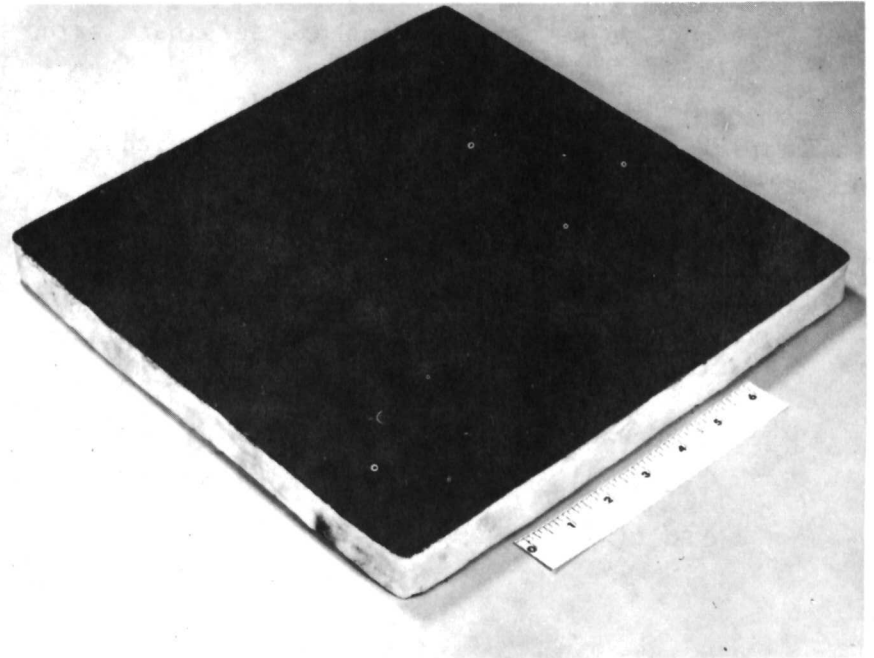
Figure 1

THERMAL CONDUCTIVITY OF 3DSX CERAMIC INSULATION

(Figure 2)

The figure presents measured values of thermal conductivity of a 93 kg/m^3 (5.8 lb/ft^3) 3DSX woven mat. The conductivity values and functional behavior relative to temperature and pressure are not unique but are generally consistent with other low density fibrous materials. The sharp knee occurring at 1000 N/m^2 in the 449°C (840°F) curve is evidence of a transition to a "free-molecule flow" regime where energy transfer occurs primarily by gas/solid molecule collisions rather than by gas/gas collisions. This knee corresponds to a state condition for air characterized by a mean free path of 16 microns, which correlates well with the actual fiber spacing, which averages about 30 microns. The "knee" locations for the other curves were predicted using the 16 micron mean free path as the correlating parameter. The apparent merging of the free molecule regime boundary is coincidental for this particular material configuration.

A major portion of the shuttle re-entry heating pulse occurs at pressures in excess of 2500 N/m^2 therefore, the free molecule regime does not have a significant effect for this material. However, the correlation suggests that reduction in mean fiber spacing achievable by reducing the fiber diameter would shift the free molecule regime toward higher pressures where the phenomenon could be important.

Thermal conductivity data for a 150 kg/m^3 (9.4 lb/ft^3) mat also exhibited the expected trends. Reduction of fiber spacing by the additional compaction of the material shifted the 449°C (840°F) knee to a pressure of about 3333 N/m^2.

THERMAL CONDUCTIVITY OF 3DSX CERAMIC INSULATION
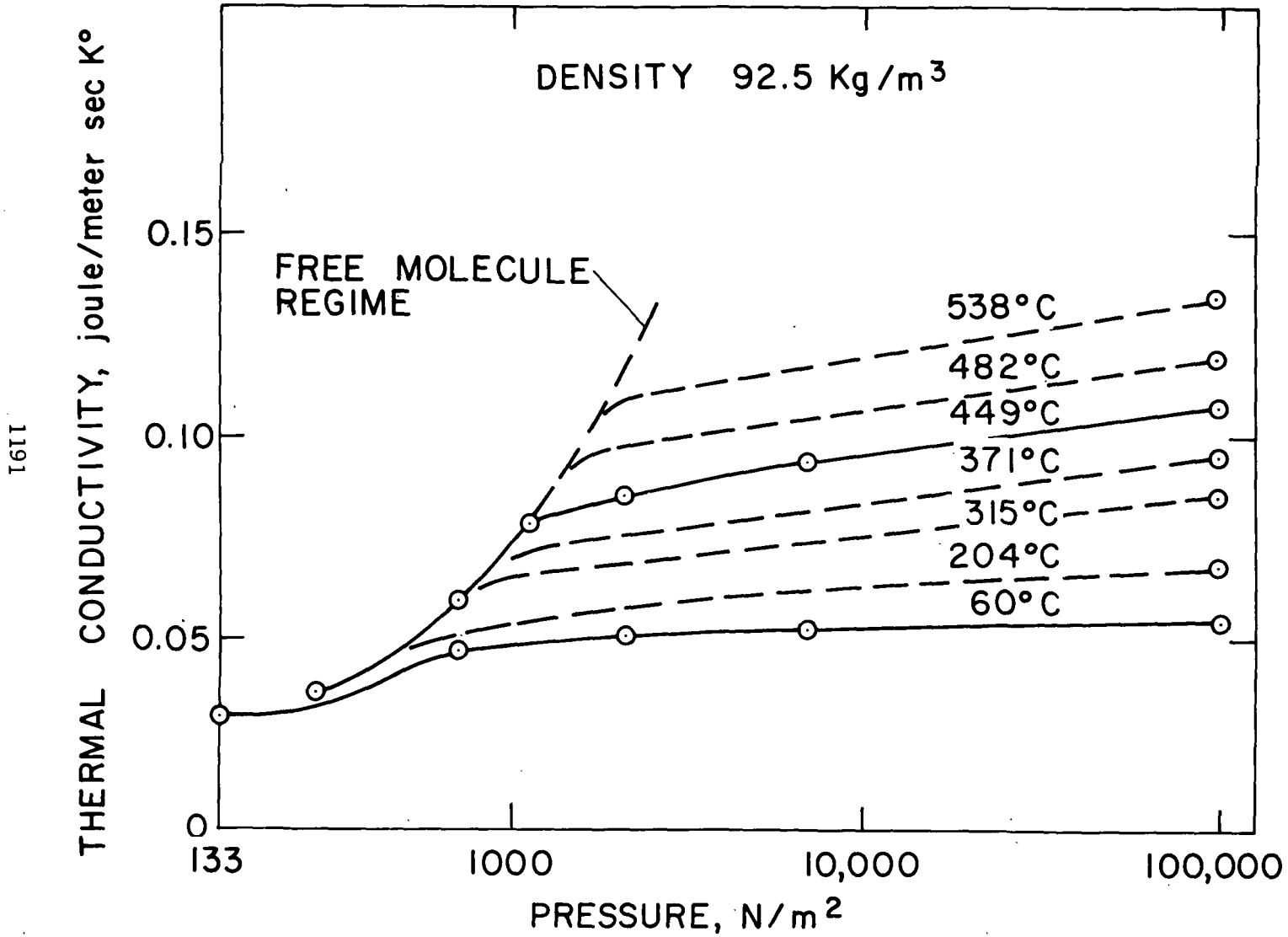
Figure 2

TENTATIVE THERMAL PROPERTY MODEL FOR 3DSX MAT

(Figure 3)

Heat shield sizing studies were performed utilizing the thermal model presented in figure 3. Conductivity values at temperatures greater than 530°C (1000°F) were based on correlation of data for similar materials and are not yet supported by firm data on 3DSX.

TEMPERATURE °C	SPECIFIC HEAT joule/kg - °C	THERMAL CONDUCTIVITY AT ONE ATM. joule/meter sec °K	
		92.5 kg/m^3 MATERIAL	150.0 kg/m^3 MATERIAL
27	796	0.057	0.059
93	838	0.061	0.061
260	1006	0.074	0.071
538	1131	0.133	0.107
816	1215	0.214	0.163
1093	1258	0.313	0.243
1371	1300	0.427	0.360

PRESSURE MULTIPLIER FOR THERMAL CONDUCTIVITY

PRESSURE N/M^2	MULTIPLIER
133	0.55
1,333	0.65
13,333	0.90
101,308	1.00

Figure 3

1193

3DSX WEIGHT MODEL
(Figure 4)

The weight of a 3DSX heat shield cannot be simply characterized by a density-volume product since the weight associated with the dense surface coating is a significant fraction of the total. For use in thermal sizing, the "density" associated with the thermal conductivity has been defined as the weight per unit volume of the compressed felts plus the Z-component of the lacing yarns. This density is 93 kg/m^3 (5.8 lb/ft^3) and 150 kg/m^3 (9.4 lb/ft^3) for the two configurations studied. For the purpose of weight management, the weights associated with the surface coating, surface fabric, and the X-Y yarn component at the surface are defined in terms of a weight per unit area. A similar definition is applied to the sealed sides of the specimen.

3DSX WEIGHT MODEL

DENSE SURFACE COATING
1.71 TO 3.42 Kg/m^2

SURFACE FELT 0.0815 Kg/m^2

SURFACE FABRIC PLUS
SURFACE YARNS
0.179 Kg/m^2

WOVEN MAT DENSITY
93 TO 150 Kg/m^3

BOTTOM SURFACE FABRIC
AND SURFACE YARNS
0.179 Kg/m^2

SIDE FABRIC

SIDE FELT

SIDE COATING

1195
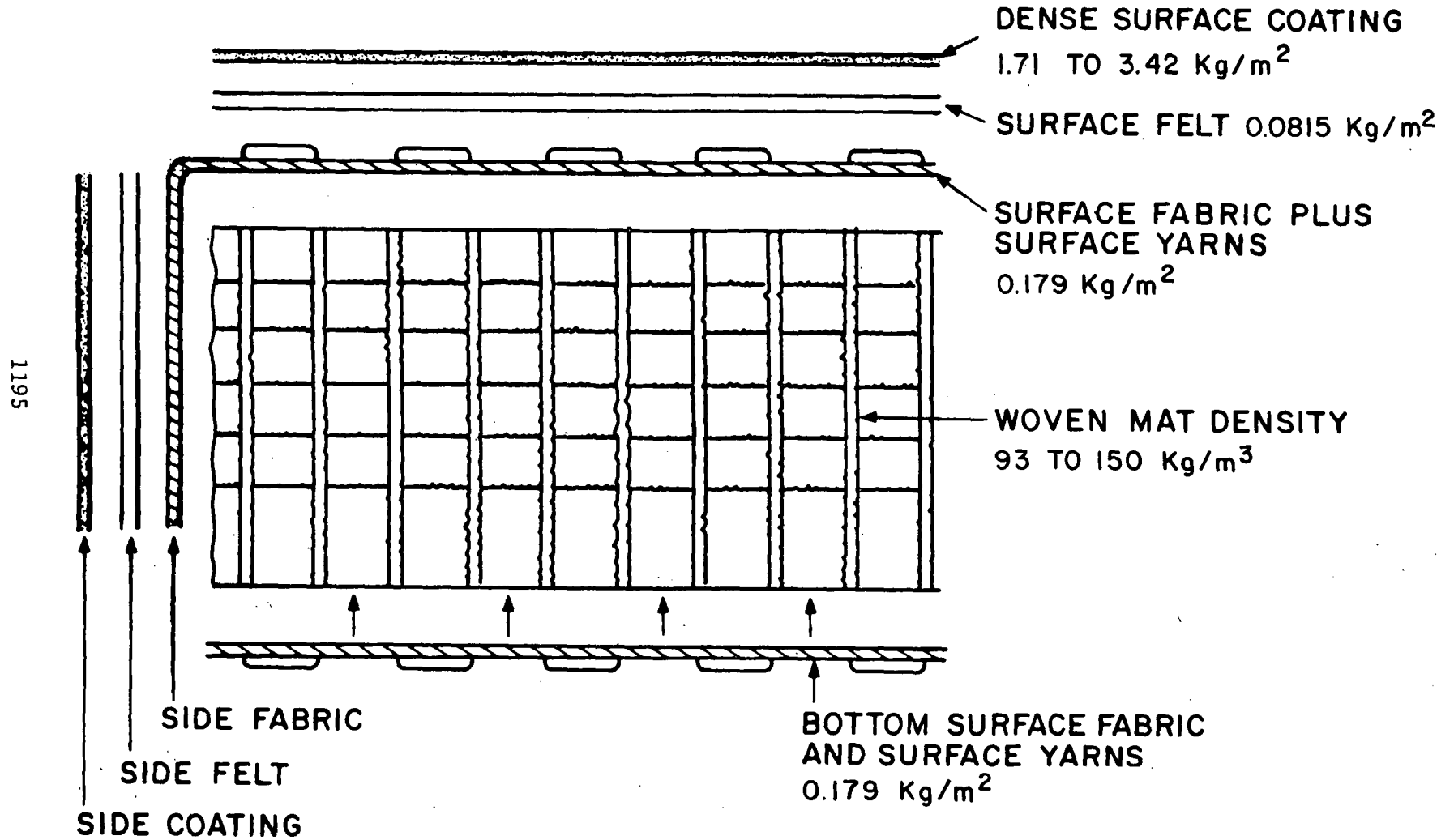
Figure 4

SENSITIVITY OF WEIGHT TO TILE SIZE
(Figure 5)

The heat shield system weight is also sensitive to tile size since the coated area on the side of the tile represents a significant fraction of the total. Larger tiles provide lower weight because of the reduced area of side coating required. The graph illustrates this effect for a reasonable range of tile size parameters. The design point shown represents a maximum local heat shield thickness for a perturbed heating in "region 2" on the underside of the vehicle.

SENSITIVITY OF WEIGHT TO TILE SIZE

COATED TILE WEIGHT, Kg/m²

INSULATION THICKNESS, cm

1.71 Kg/m² COATING WEIGHT
150 Kg/m³ MATRIX DENSITY

TILE SIZE
15.2 x 15.2 cm
30.5 x 30.5 cm
61.0 x 91.5 cm

DESIGN
THICKNESS
AREA 2P

Figure 5

1197
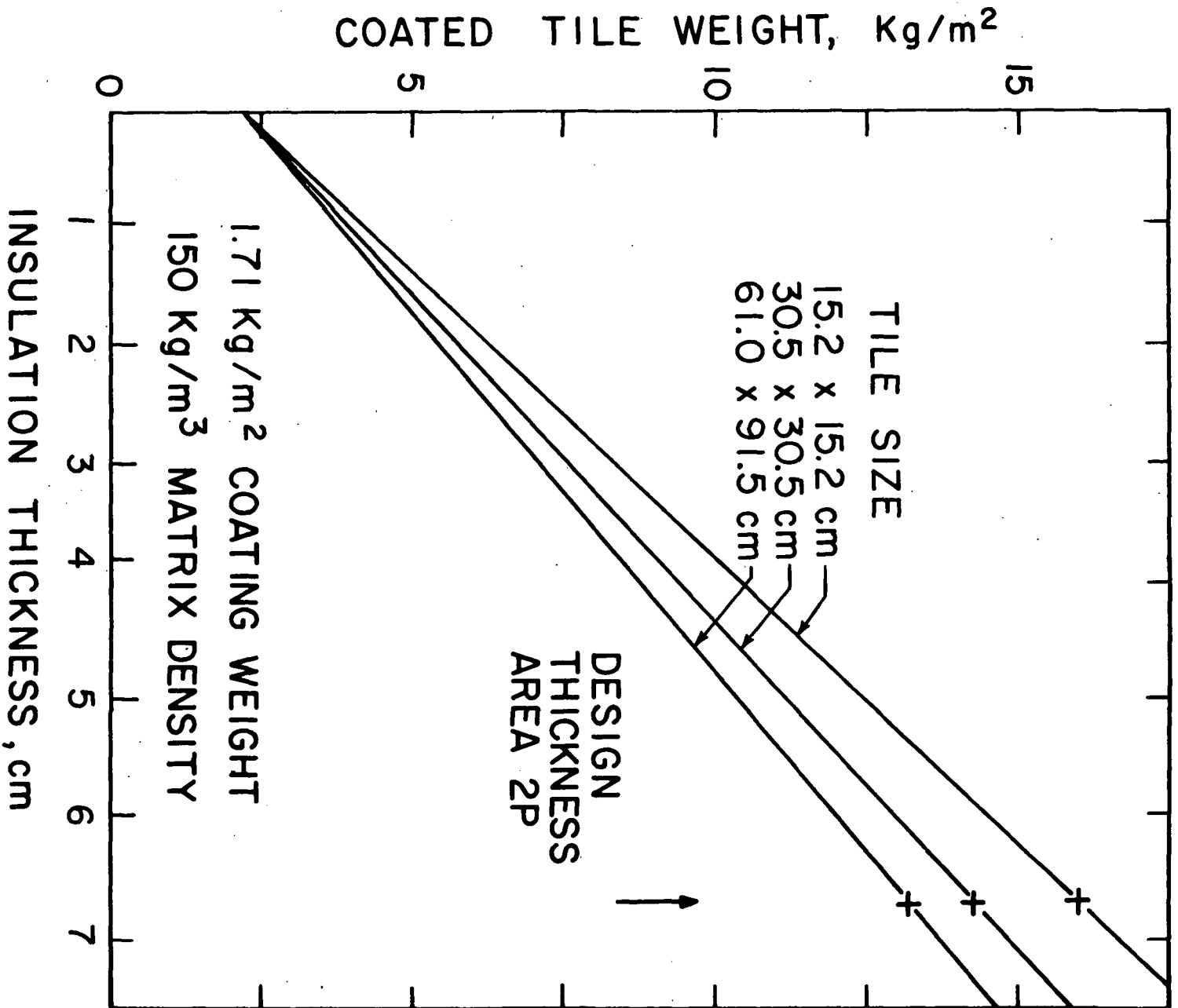
STRUCTURAL PROPERTY DATA

(Figure 6)

As shown in the figure the woven silica mat has a very low shear modulus compared to the tensile and compressive moduli. The tensile modulus is much higher than the compressive modulus because of the resistance of the lacing yarns to tensile loads but not to compressive loads. It will be seen in the discussion of the structural model that the difference in the tensile and compressive moduli is not too important to the behavior of the system because both provide relatively high mat stiffness in the direction of an external pressure loading.

Ultimate strength values of the woven mat are difficult to define because the material exhibits very large nonlinear deflections prior to any apparent failure. The values indicated are approximate yield strengths below which the material will exhibit respectable response to loading.

The silica surface coating properties are "apparent" properties deduced from the measured response of the coating material in a four point flexure test and assuming the coating is a uniform homogeneous material. The flexure stiffness EI/b is more significant to the structural model and was measured to have an average value of 17 meter-Newtons (150 lb-in).

STRUCTURAL PROPERTIES OF 3DSX

WOVEN SILICA MAT	92.5 kg/m^3 MAT	150.0/kg/m^3
TENSILE MODULUS, N/m^2	41.3×10^6	88.9×10^6
COMPRESSIVE MODULUS N/m^2	5.4×10^6	9.8×10^6
SHEAR MODULUS, N/m^2	0.22×10^6	0.65×10^6
TENSILE STRENGTH, N/m^2	17×10^4	17×10^4
COMPRESSIVE STRENGTH, N/m^2	3.4×10^4	8.3×10^4
SHEAR STRENGTH, N/m^2	0.34×10^4	1.4×10^4

SILICA COATING

FLEXURE STRENGTH, N/m^2	10.3×10^6
ELASTIC MODULUS, N/m^2	1.0×10^{10}
STRAIN TO FAILURE, percent	0.13

Figure 6

CONCEPTUAL ILLUSTRATION OF STRUCTURAL BEHAVIOR OF 3DSX WOVEN MAT
(Figure 7)

The structural nature of the woven silica mat is principally characterized by a very low shear modulus as compared to the tensile and compressive moduli. This led to an initial conceptual model depicted in the illustration where the woven mat was represented as a number of independent linear springs connecting the surface coating and substructure. The ends of the springs are pinned (free to rotate). If the springs are very stiff and the coating is thin (low flexural stiffness) the pressure load is transferred directly to the substructure and the coating is forced to assume the same shape as the deflected substructure as shown. In the other extreme, if the springs are very soft and the coating is very stiff the springs will be compressed to resist the pressure load, which will again be transferred to the substructure. The substructure will deflect as before and the springs will adjust their lengths to accommodate the deflection with no strain introduced into the very stiff coating.

CONCEPTUAL ILLUSTRATION OF STRUCTURAL BEHAVIOR OF 3DSX WOVEN MAT
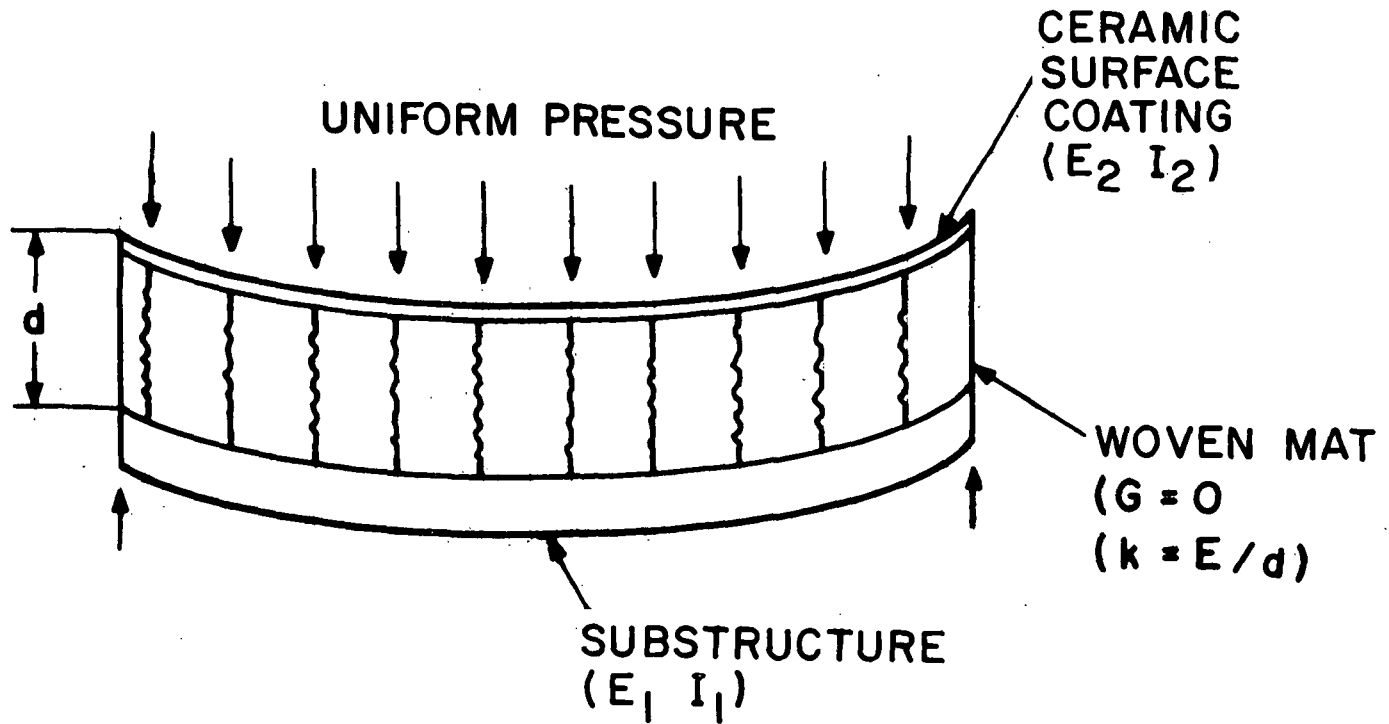
Figure 7

COATING STRAIN IN FLEXURE

(Figure 8)

For the conceptual behavior indicated, the woven mat is characterized by a spring constant and zero shear modulus, and the coating and substructure are characterized by their flexural stiffnesses. Coating strains induced by panel flexure are then described by the relation shown in figure 8.

COATING STRAIN IN FLEXURE
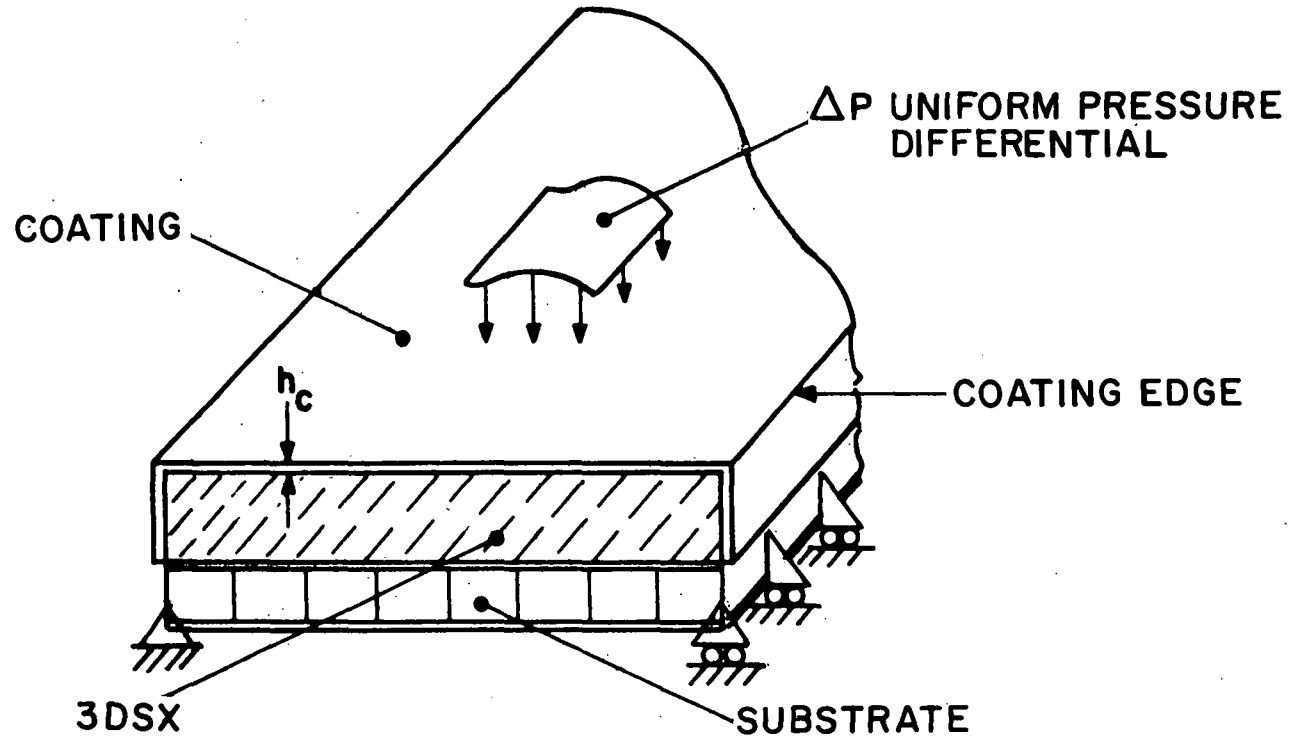
COATING STRAIN (MID-SPAN)

$$\epsilon_c = \frac{2h_c \Delta P \ell^2}{\pi^3 D_1} \cdot \frac{1}{\left[1 + \frac{D_2}{D_1} + 5.279 \frac{D_2 \pi^4}{k \ell^4}\right]}$$

D_1 = FLEXURAL STIFFNESS OF SUBSTRATE

D_2 = FLEXURAL STIFFNESS OF COATING

k = TRANSVERSE EXTENSIONAL STIFFNESS OF 3DSX

Figure 8

STRAIN ISOLATION FOR SIMPLE BEAM IN FLEXURE
(Figure 9)

A more illuminating expression is obtained by deriving the ratio of coating strain to sub-structure strain as in figure 9. The most significant parameter is β which combines the ratio of the woven mat stiffness to the coating stiffness and the span of the beam. Low values of β correspond to the case of a soft spring and stiff coating, while high values of β denote a stiff spring and flexible coating.

Perhaps contrary to intuition, the latter case is representative of practical 3DSX tile configurations. For tile spans of 15.2 to 61.0 cm (6 in. to 2 ft.), tile thicknesses of 2.5 to 7.5 cm (1 to 3 in.), and mat densities of 93 to 150 kg/m^3 (5.8 to 9.4 lb/ft^3), the stiffness parameter takes on values ranging from several hundred to several thousand. The ratio of coating to sub-structure strain $\varepsilon_2/\varepsilon_1$ then approaches the ratio of the coating to substructure thickness h_2/h_1 (or more correctly, the ratios of the distances of the extreme fibers from the neutral axes of the coating and substructure). This is equivalent to stating that the coating assumes the same deflected shape as the substructure but is not shear coupled to the substructure.

Locally higher strain levels may be introduced at the coating edge (intersection of the top and side coating) due to rotational restraints imposed by the woven mat on the side coating. This problem will be addressed in a subsequent section.

STRAIN ISOLATION FOR SIMPLE BEAM IN FLEXURE

$$\frac{\epsilon_2}{\epsilon_1} = \frac{h_2}{h_1} \frac{1}{(1+5.279/\beta)}$$

$$\beta = \frac{k \ell^4}{D_2 \pi^4}$$

Figure 9

1205

3DSX MAT FLEXURE TEST SPECIMEN AND LOADING CONDITION
(Figure 10)

Beam flexure tests were performed to substantiate the predicted behavior. 3DSX specimens
were prepared with a metal sheet simulating the surface coating, and with actual ceramic coatings
applied to the woven mat. These were bonded to an aluminum honeycomb structure. Strain gages
were applied at several span locations to the skin and structure. The structure was loaded with
both positive and negative end moments.

3DSX MAT FLEXURE TEST SPECIMEN AND LOADING CONDITION
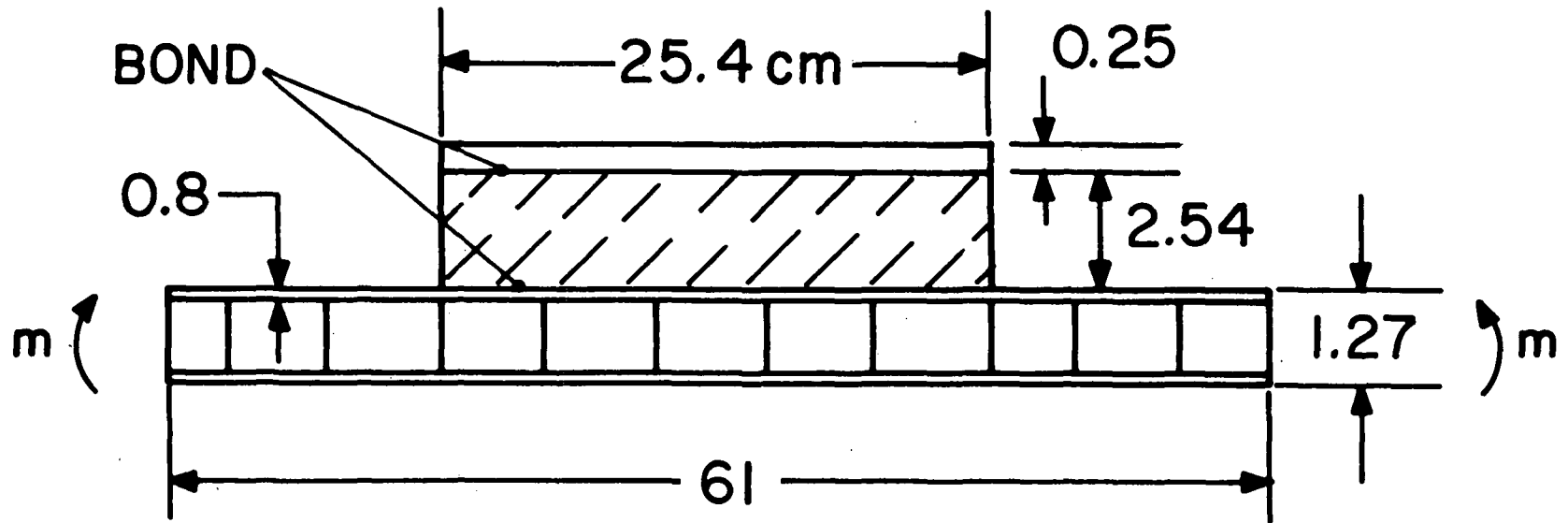
ALUMINUM SKIN
ALUMINUM HONEYCOMB SUBSTRUCTURE

Figure 10

FLEXURE TEST DATA--METAL SKIN

(Figure 11)

The flexure test data presented for the metal skin is a mid-span measurement and shows excellent correlation with the predicted behavior. The stiffness parameter β for this configuration has a value of 200, which is sufficiently high that the stiff spring, flexible coating condition is approached. The measured strain ratios were nearly proportional to the ratio of coating skin to substructure thickness at all span locations.

FLEXURE TEST DATA-METAL SKIN
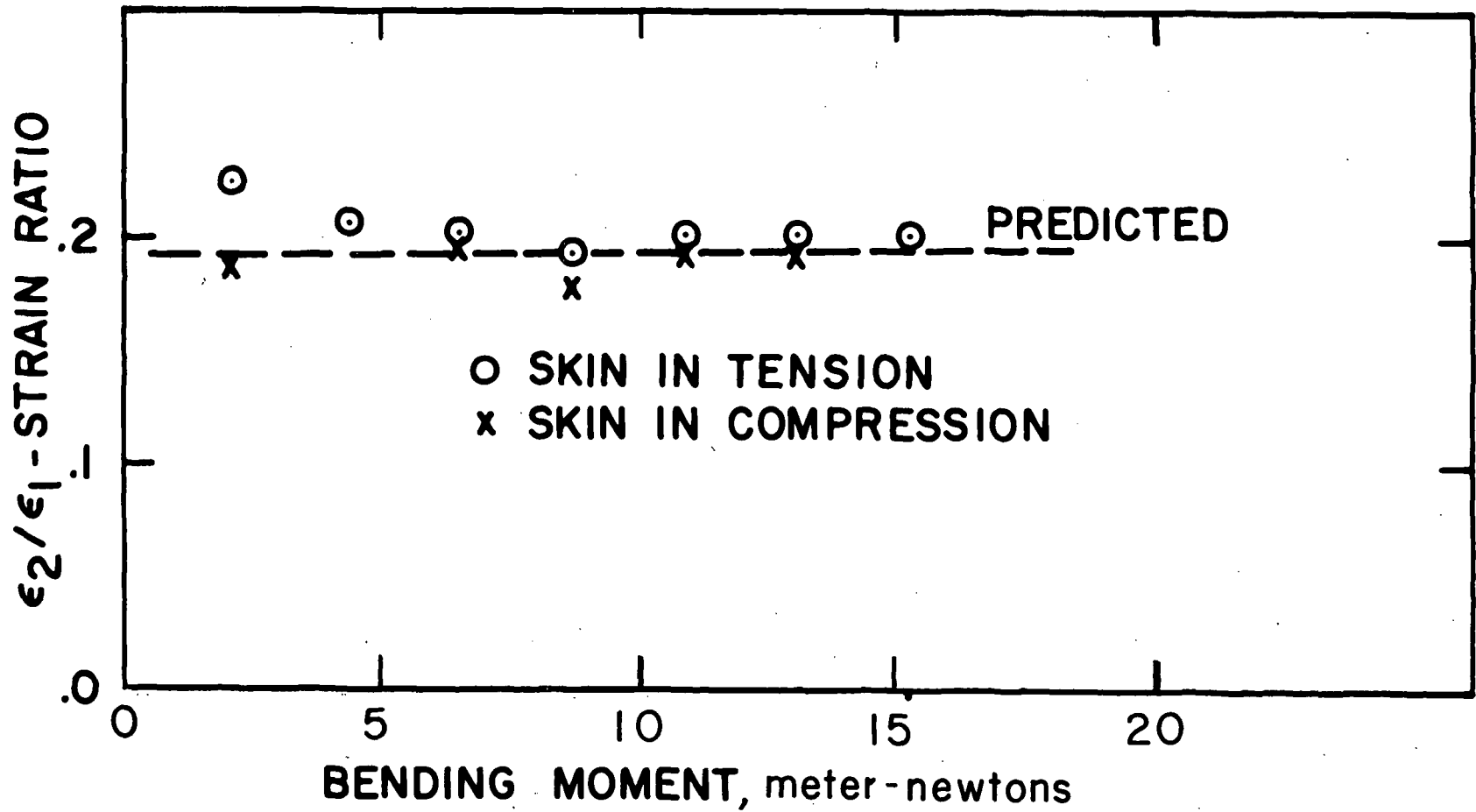
Figure 11

FLEXURE TEST DATA--SILICA COATING

(Figure 12)

The data for the silica coating showed more variation in the strain ratios as load was applied, but after an initial relaxation at low load, the data were entirely consistent with expected behavior. The effective coating thickness implied from the strain data is about 0.10 cm (40 mils), which is consistent with that expected by examination of photomicrographs of typical coating cross-sections.

FLEXURE TEST DATA-SILICA COATING
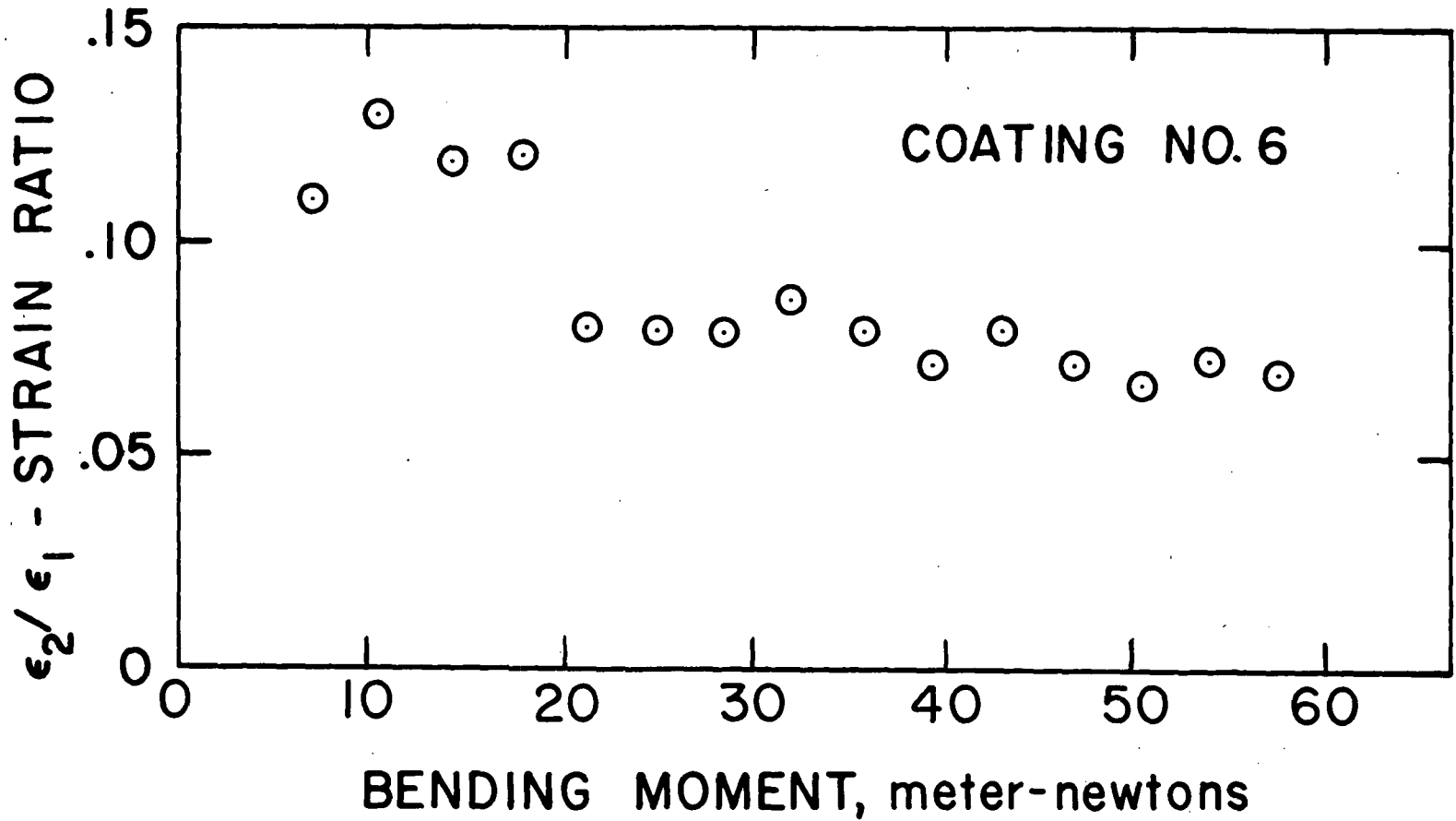
Figure 12

COATING EDGE STRAIN

(Figure 13)

Local high strain levels may be introduced at the intersection of the top and sides of a tile due to rotational restraints imposed on the side coating. The magnitude of this effect is evaluated from the expression in figure 13. The ratio of the edge strain to the midspan strain in the coating $\varepsilon_e/\varepsilon_c$ is seen to be proportional to the tile span 1; and to parameters containing the flexural stiffness of the coating D_2; thickness of the tile l_3; and the elastic moduli of the woven mat E_i and G_i.

COATING EDGE STRAIN

RATIO OF STRAIN AT EDGE TO STRAIN AT CENTER

$$\frac{\epsilon_e}{\epsilon_c} = \frac{\lambda \mathcal{Q}/\pi}{\left\{ 1 + \dfrac{52.5\,\lambda\,D_2\,\ell_3}{3.24\,\sqrt{E_i\,G_i\,\ell_3^3} + 157 D_3} \right\}} \qquad\qquad \lambda = \left(\frac{E_i}{4\,\ell_3 D_2} \right)^{\frac{1}{4}}$$

TYPICAL RANGE FOR BRACKET

$$1.5 < \{\ \ \} < 2$$

Figure 13

COATING EDGE STRAIN FOR TILE IN FLEXURE
(Figure 14)

The function is evaluated for typical tile configurations in the illustration. Predicted local strains at the coating edges are several times higher than at midspan and may be a major factor limiting tile size.

COATING EDGE STRAIN FOR TILE IN FLEXURE

Figure 14

1215
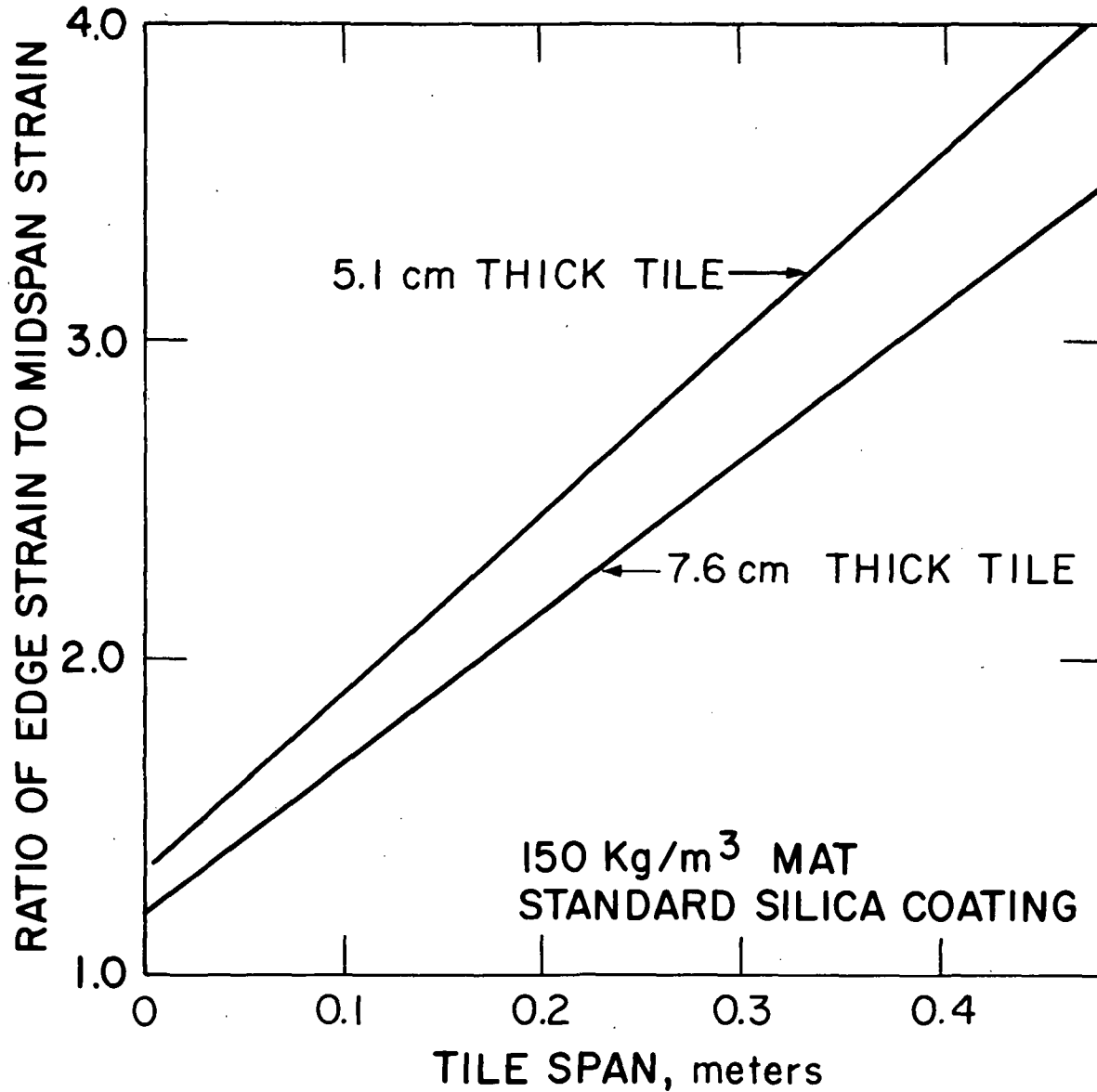
COATING STRAIN DUE TO IN-PLANE SUBSTRUCTURE LOADING

(Figure 15)

Coating strains introduced by in-plane loading of the substructure are related to substructure strains by the relation in figure 15. The expression evaluates the maximum coating strain, which occurs at the center of the panel. The shear modulus of the insulation G_i and the extensional stiffness of the coating B_2 (product of the elastic modulus and coating cross-sectional area) are the significant parameters.

COATING STRAIN DUE TO IN-PLANE SUBSTRUCTURE LOADING
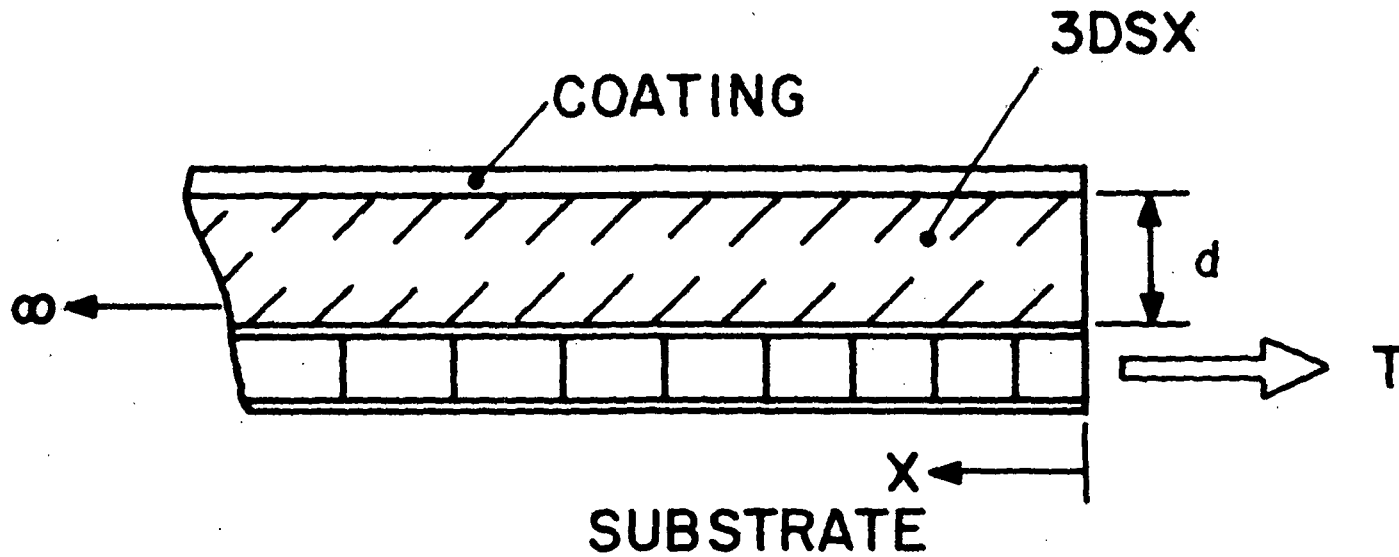
$$\frac{\epsilon_2}{\epsilon_1} = 1 - e^{-\frac{\alpha \ell}{2}}$$

$$\alpha = \sqrt{\frac{G_i}{B_2 d}}$$

Figure 15

COATING STRAIN ISOLATION FOR IN-PLANE LOADING OF SUBSTRUCTURE

(Figure 16)

Figure 16 illustrates a solution of the coating strain isolation for a conservatively low estimate for B_2. Coating strains are predicted to be about 15 to 20 percent of substructure strains for 30 cm (12 inch) tiles with thicknesses ranging from 5 to 7.5 cm (2 to 3 inches).

COATING STRAIN ISOLATION FOR IN-PLANE LOADING OF SUBSTRUCTURE

150 Kg/m^3 MAT
WITH G = 4540 N/m^2
STANDARD SILICA COATING

46 cm TILE

30.5 cm TILE

15.3 cm TILE
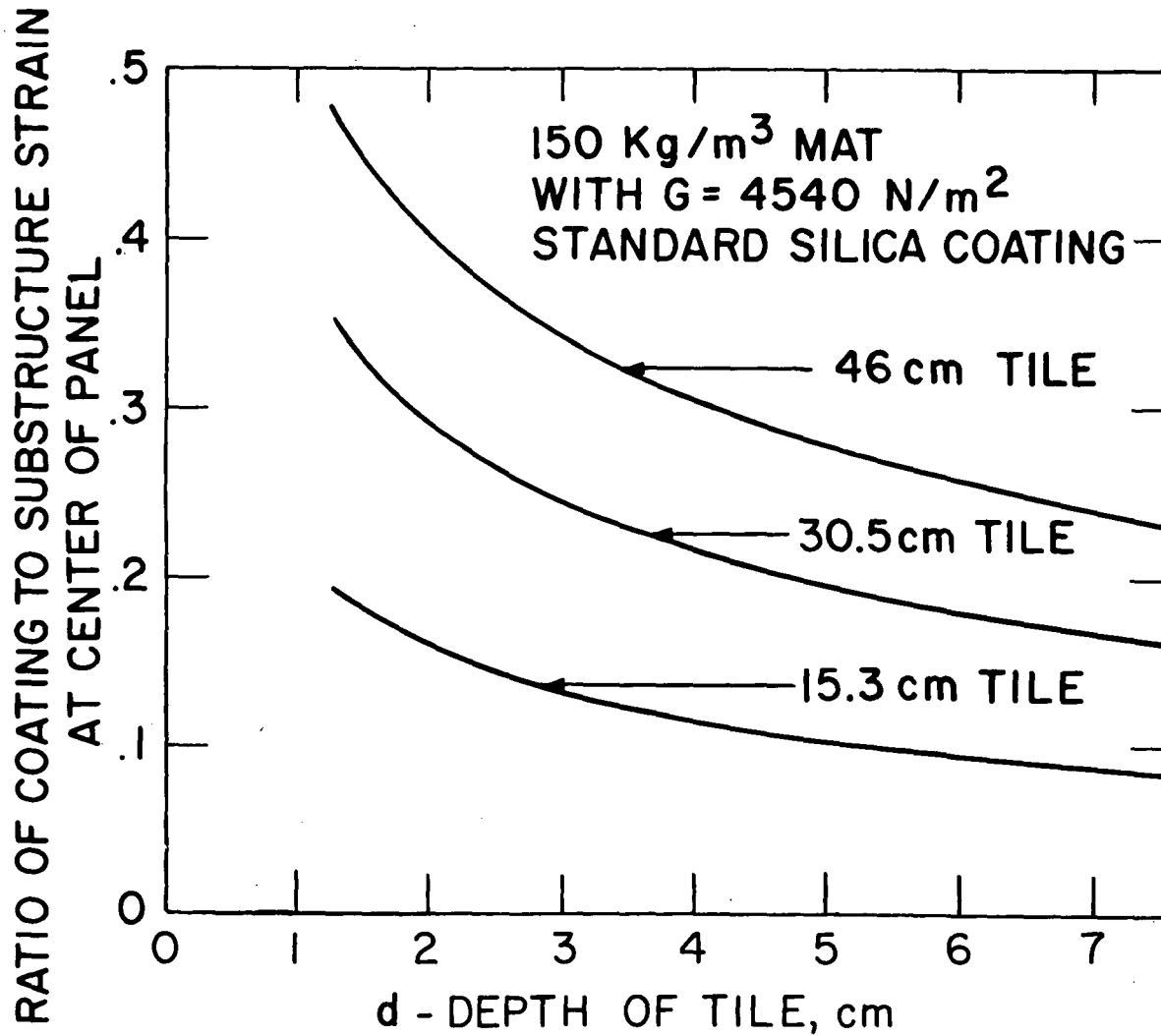
Figure 16

3DSX THERMOSTRUCTURAL TEST PANEL
(Figure 17)

A heat shield panel consisting of four 3DSX tiles covering a   46 x 51 cm   (18 x 20 in.) area of a NASA supplied substructure was fabricated. This panel is scheduled for testing in the near future at the NASA Manned Spacecraft Center under conditions of combined thermal and structural loading. This will be the first experimental evaluation of the 3DSX concept in a realistic heat shield size and configuration.

3DSX THERMOSTRUCTURAL TEST PANEL
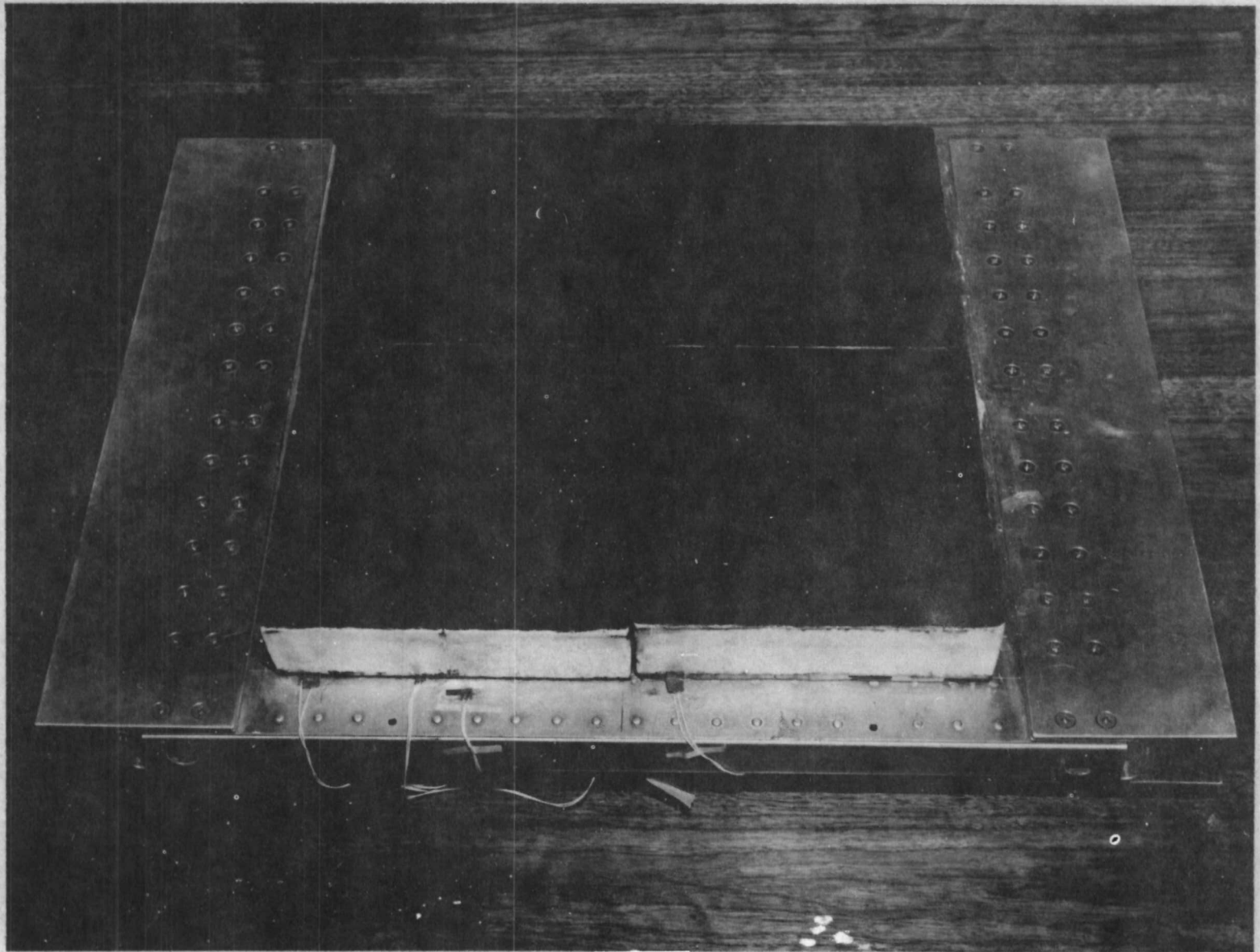
Figure 17

STRAIN PREDICTION FOR DESIGN LOADING
(Figure 18)

Results of an analysis of the design structural loading condition are summarized in the figure. Maximum strain predictions based on the models presented here indicate substantial safety margins.

STRAIN PREDICTION FOR DESIGN LOADING

PRESSURE LOAD , 41300 N/m^2
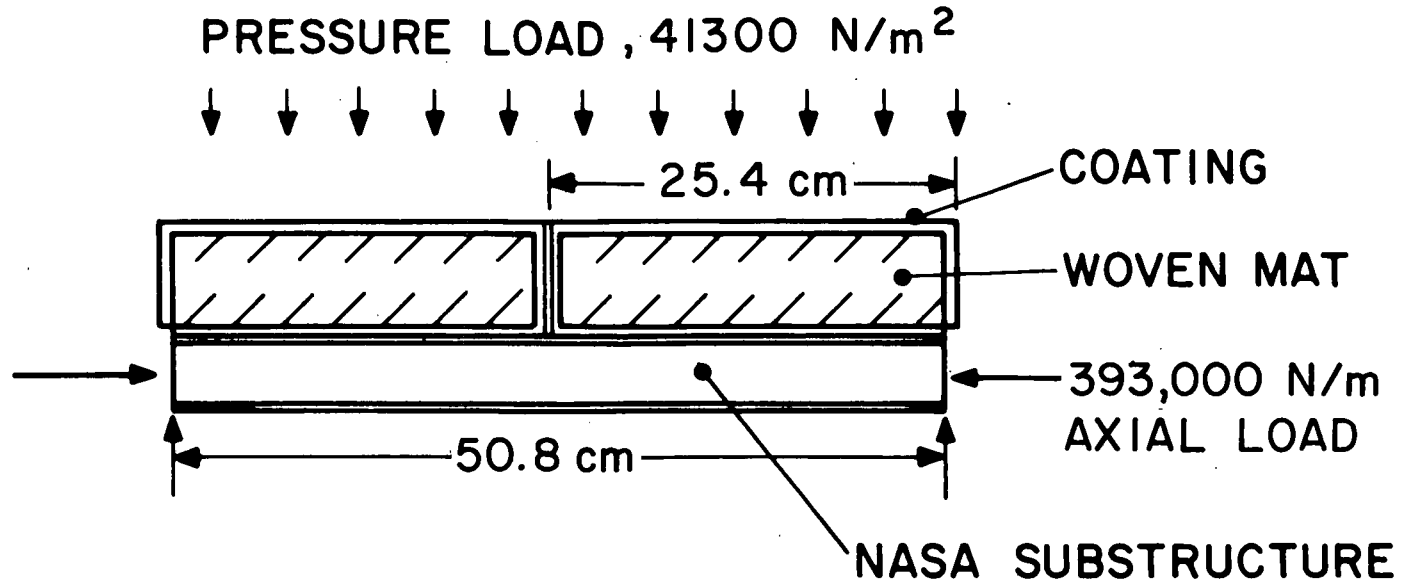
	CALCULATED	ALLOWABLE
COATING STRAIN AT MIDSPAN (PERCENT)	.009	.13
COATING STRAIN AT EDGE (PERCENT)	.067	.13
COMPRESSIVE STRAIN IN WOVEN MAT	.43	>2

Figure 18

FEATURES OF 3DSX

CONCLUDING REMARKS

(Figure 19)

A reusable surface insulation concept is under development which offers several unique features summarized in this figure.

Fabrication processes were established and a limited evaluation of material properties and performance was performed under a recently completed program. Analytical models were developed that predict the thermal and structural performance characteristics. A comprehensive experimental evaluation is now required to verify the anticipated performance levels of the concept.

FEATURES OF 3DSX

LOW SHEAR MODULUS OF WOVEN CERAMIC INSULATION PROVIDES EFFECTIVE STRAIN ISOLATION BETWEEN SURFACE COATING AND SUBSTRUCTURE.

LOW SHEAR MODULUS ALSO ISOLATES INSULATION FROM COATING THERMAL STRAINS.

INSULATIVE MATRIX CAN READILY BE FABRICATED IN VARIABLE DENSITIES AND AS LOW AS 96 Kg/m^3

DEMONSTRATED PURE AMORPHOUS SILICA SYSTEM WITH 1200 °C CAPABILITY.

MATCHING THERMAL EXPANSION OF COATING AND SUBSTRUCTURE.

SYSTEM CAN INCORPORATE MORE REFRACTORY MATERIAL THAN SILICA.

SURFACE CRACKS CANNOT PROPAGATE THROUGH THE INSULATIVE MATRIX. CRACKING DOES NOT CAUSE CATASTROPHIC STRUCTURAL FAILURE.

MINOR SURFACE DAMAGE CAN BE READILY REPAIRED.

Figure 19

RESULTS OF RSI
THERMAL-STRUCTURAL ANALYSIS

by

O.E. Pigg
Manned Spacecraft Center
Houston, Texas

INTRODUCTION
(Figure 1)

The primary objective of this analysis was to compare the structural sensitivity of the prime contending TPS reusable surface insulation (RSI) materials to the entry environment.

The analysis utilized average material moduli derived from test data by the contractors and also bounding moduli derived independently from the data.

The analytical models used were plane stress finite element models, which are presented later. Perfect strain isolation was assumed to eliminate other design parameters. The residual stress due to manufacture was included in the analysis, assuming that the zero stress temperature is 1367°K (2000°F) using contractor coefficient of expansion data.

GE (MOD 1A) and LMSC (LI-1500) materials sized for the Area 2P trajectory and the computed temperature distribution during entry were used for this comparison. A survey was conducted which indicated that peak stresses occurred at approximately 250 seconds. The surface temperature at 250 seconds is approximately 1089°K (1500°F).

Two failure criteria were used to predict margins of safety based on a 1.5 factor of safety. These failure criteria are based on room temperature average properties for the purposes of comparison, although such properties are considered unacceptable for design.

INTRODUCTION

- PRIMARY OBJECTIVE - THERMAL-STRUCTURAL COMPARISON
  OF MULLITE AND SILICA RSI SYSTEM

- MATERIAL PROPERTIES USED IN ANALYSIS
  - MSC DERIVED BOUNDING VALUES
  - CONTRACTOR DERIVED AVERAGE VALUES

- FAILURE CRITERIA
  - COMBINED STRESS - AVERAGE STRENGTH
  - INDIVIDUAL STRESS - AVERAGE STRENGTH
  - AVERAGE STRENGTH USED FOR COMPARISON;
    NOT APPROPRIATE FOR DESIGN

Figure 1

INTRODUCTION (CONT)

- ANALYTICAL MODEL DESCRIPTION
  - 2D - FINITE ELEMENT
  - PLANE STRESS
  - PERFECT STRAIN ISOLATION
  - THERMAL LOADING ONLY, 250 SECONDS INTO ENTRY
  - MATERIALS SIZED FOR AREA 2P TRAJECTORY
    - MULLITE (GE MOD 1A) - 8.92×10^{-2} m (3.51 IN.)
    - SILICA (LMSC LI-1500) - 7.77×10^{-2} m (3.06 IN.)
  - TILE SIZE - 0.152 m (6 IN.)
  - PRESTRESS INCLUDED
    - ZERO STRESS TEMPERATURE - 1367°K (2000°F)

Figure 1 (Concluded)

SILICA

MODULUS OF ELASTICITY VS TEMPERATURE

(Figure 2)

The LMSC LI-1500 in-plane modulus of elasticity derived by LMSC and MSC are presented with test data from LMSC and Battelle. The solid line is the bounding modulus of elasticity vs temperature used in the MSC analyses. The dashed line is average modulus of elasticity vs temperature used in the LMSC analyses.

SILICA MODULUS OF ELASTICITY VS TEMPERATURE
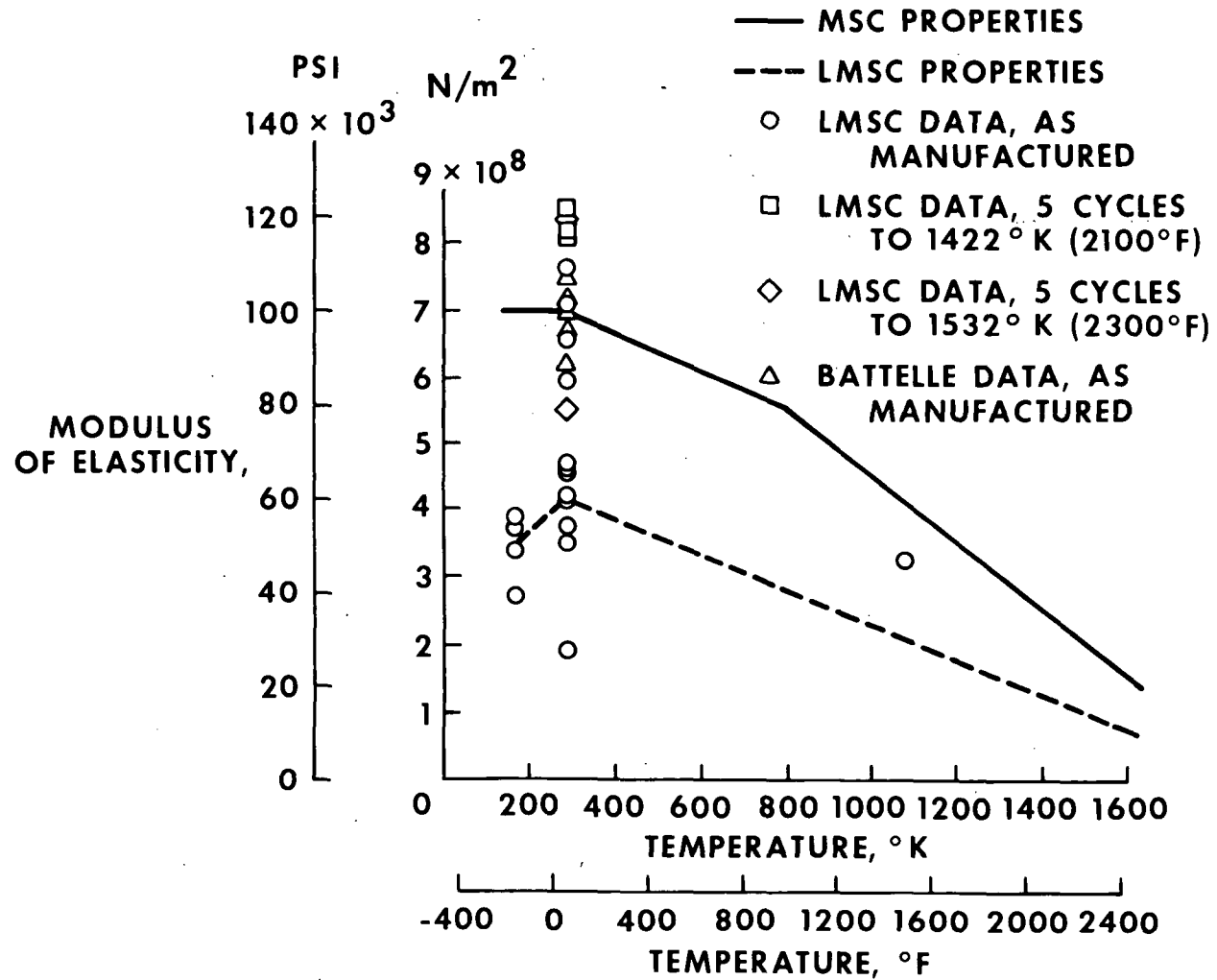
Figure 2

MULLITE

MODULUS OF ELASTICITY VS TEMPERATURE

(Figure 3)

The GE MOD 1A in-plane modulus of elasticity derived by MSC and GE are presented with test data from GE and Battelle. The solid line is the bounding modulus of elasticity vs temperature used in the MSC analyses. The dashed line is the average modulus of elasticity vs temperature used in the GE analyses.

MULLITE MODULUS
OF ELASTICITY VS TEMPERATURE
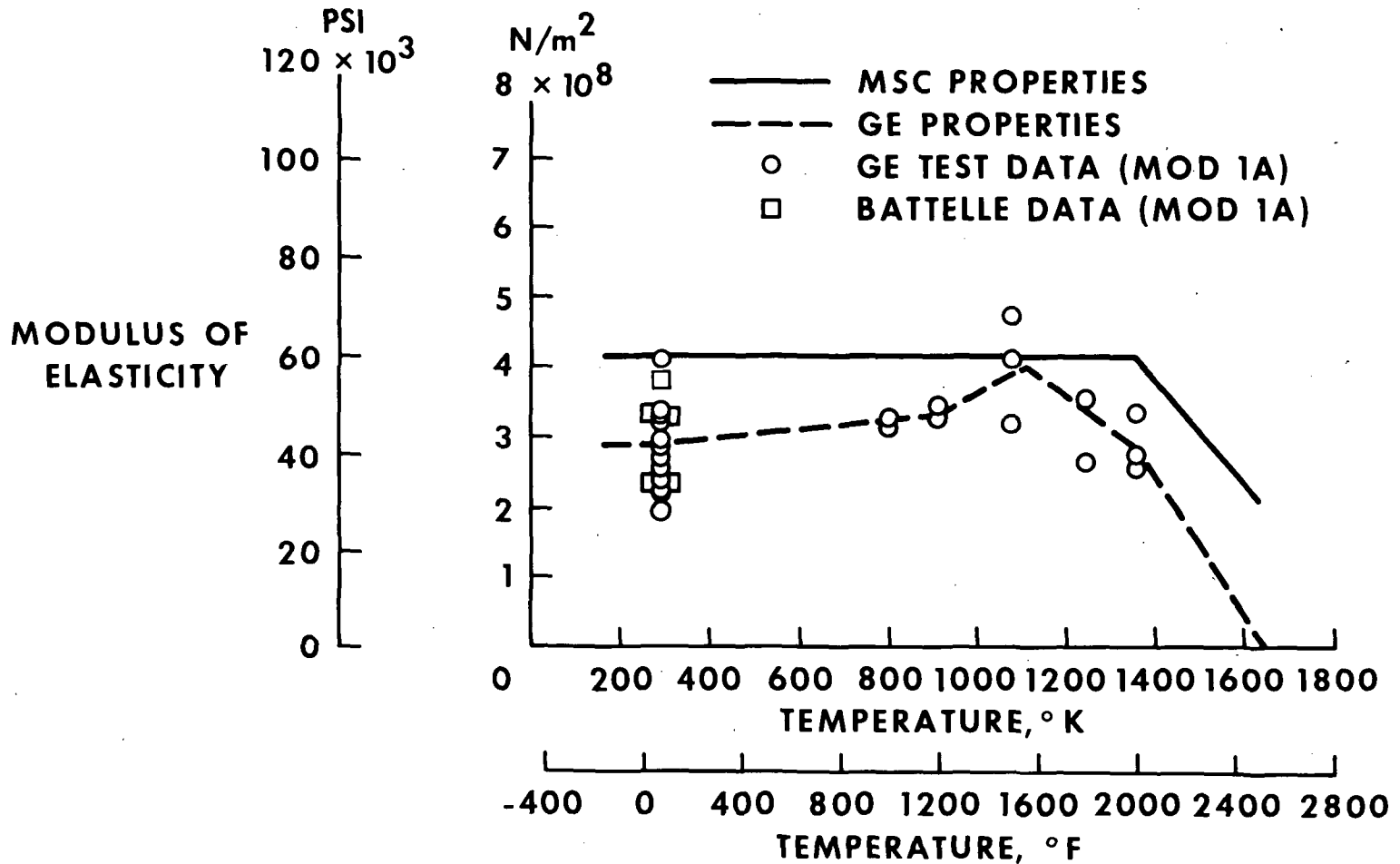
Figure 3

GE COATING
MODULUS OF ELASTICITY VS TEMPERATURE
(Figure 4)

The GE coating modulus of elasticity vs temperature used by MSC and GE are presented with test data from GE and Battelle. The solid line is the modulus of elasticity vs temperature used in the MSC analyses. The dashed line is the modulus of elasticity vs temperature used by GE. The Battelle data are based on the thickness of the vitrified layer only and the GE data include some composite material.

GE COATING MODULUS
OF ELASTICITY VS TEMPERATURE
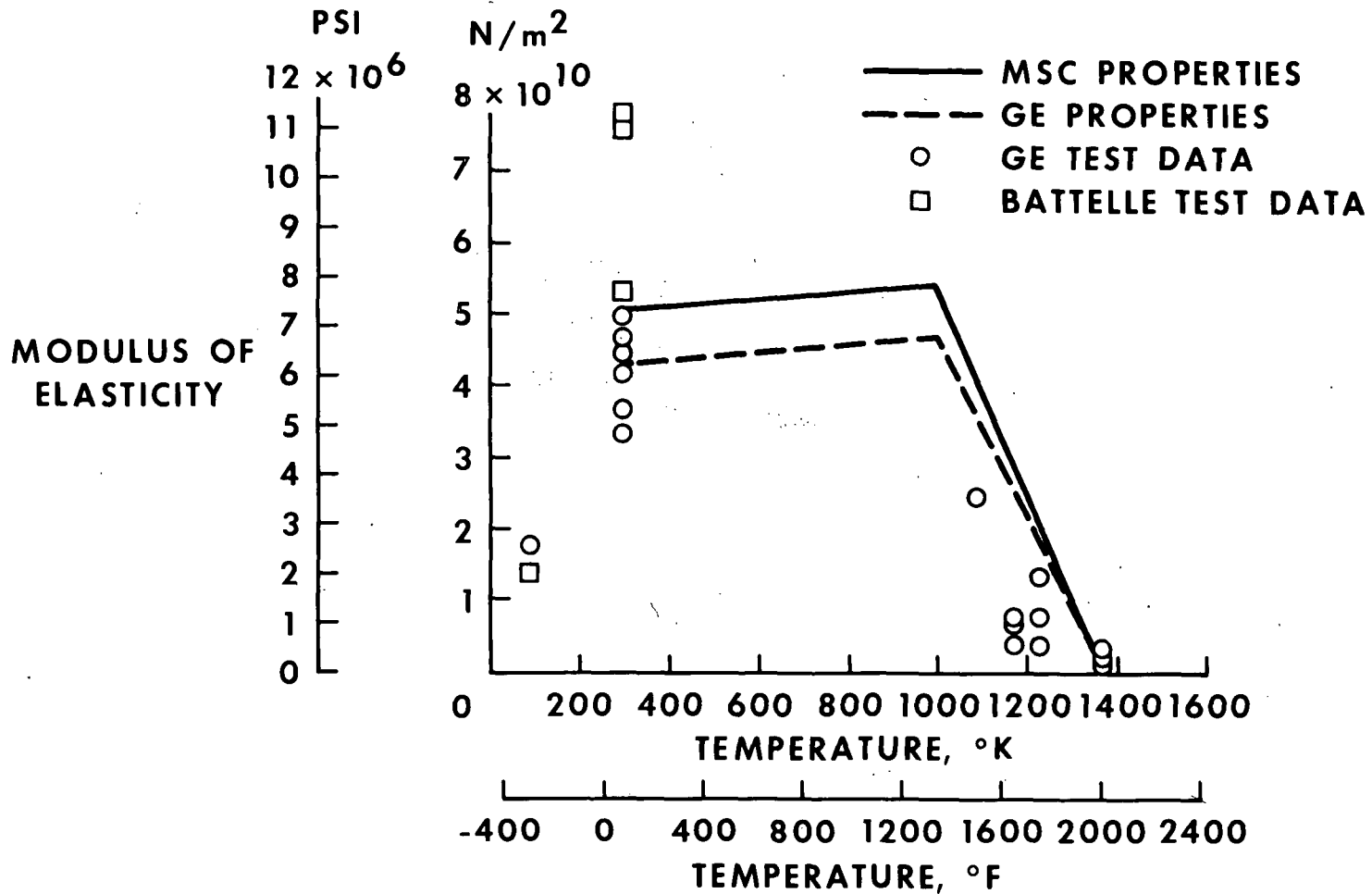
Figure 4

FAILURE CRITERIA
COMBINED STRESS CRITERION
(Figure 5)

A combined failure criterion is presented for transversely isotropic materials. SF1 is the safety factor based on combined stress criterion as shown. The coefficients are defined by ultimate material properties in tension, compression, and shear in the material coordinate directions.*

This criterion was included in the computer program, and MS1 was calculated as shown. The program provides the capability for contour plots of specified stresses. This MSC computer program was modified to provide for contour plots of MS1 specified values, which are presented later.

* For additional information, refer to "The Brittle Strength of Orthotropic Materials," Oscar Hoffman, J. Composite Materials, Vol. 1 (1967), p. 200.

1238

FAILURE CRITERIA

- COMBINED STRESS CRITERION
  - TRANSVERSELY ISOTROPIC MATERIAL

$$SF1 = \left\{ C1\left[(\sigma_{RR} - \sigma_{ZZ})^2 + (\sigma_{ZZ} - \sigma_{\theta\theta})^2\right] + C2(\sigma_{\theta\theta} - \sigma_{RR})^2 + \right.$$

$$\left. C3\left(\sigma_{Z\theta}2 + \sigma_{RZ}2\right) + C4\sigma_{R\theta}2 + C5\left(\sigma_{RR} + \sigma_{ZZ}\right) + C6\sigma_{ZZ}\right\}^{-1}$$

$$C1 = \frac{1}{2\sigma_{ZZ_{UT}}\sigma_{ZZ_{UC}}} \qquad C2 = \frac{1}{\sigma_{RR_{UT}}\sigma_{RR_{UC}}} - \frac{1}{2\sigma_{ZZ_{UT}}\sigma_{ZZ_{UC}}}$$

$$C3 = \frac{1}{\sigma_{Z\theta_U}^2} = \frac{1}{\sigma_{RZ_U}^2} \qquad C4 = \frac{1}{\sigma_{R\theta}2}$$

$$C5 = \frac{1}{\sigma_{RR_{UT}}} - \frac{1}{\sigma_{RR_{UC}}} = \frac{1}{\sigma_{\theta\theta_{UT}}} - \frac{1}{\sigma_{\theta\theta_{UC}}}$$

$$C6 = \frac{1}{\sigma_{ZZ_{UT}}} - \frac{1}{\sigma_{ZZ_{UC}}} \qquad MS1 = \left[\frac{SF1}{1.5} - 1\right]$$

Figure 5

FAILURE CRITERIA
INDIVIDUAL STRESS CRITERION
(Figure 6)

An individual stress failure criterion was also used. The safety factor of each finite element was calculated, as shown, by dividing each stress into its allowable for the material. The minimum safety factor was then tested for each finite element and used to calculate the minimum margin of safety (MS2) as shown. Contours of specified values of MS2 were then plotted and are presented later. Margins based on the individual stress criterion were calculated for comparison with the combined stress criterion because some contractor margins are based on an unacceptable individual stress criterion. A failure criterion must be developed to predict the effect of combined stresses.

FAILURE CRITERIA

● INDIVIDUAL STRESS CRITERION

$$SF2 = \frac{\sigma_{RR_{UT}}}{\sigma_{RR_T}} \; , \; \frac{\sigma_{RR_{UC}}}{\sigma_{RR_C}} \; , \; \frac{\sigma_{ZZ_{UT}}}{\sigma_{ZZ_T}} \; , \; \frac{\sigma_{ZZ_{UC}}}{\sigma_{ZZ_C}} \; , \; \frac{\sigma_{RZ_U}}{\sigma_{RZ}}$$

$$MS2 = \left[\frac{SF2_{MIN}}{1.5} - 1 \right]$$

Figure 6

AVERAGE ULTIMATE STRESSES USED

TO PREDICT MARGINS OF SAFETY

(Figure 7)

The average strengths used to calculate the margins of safety (MS1 and MS2) in the analysis results to follow are presented in this figure. These are room temperature properties and were used over the temperature range of the analysis. Analysis for certification must consider variation of strengths with temperature.

AVERAGE ULTIMATE STRESSES USED
TO PREDICT MARGINS OF SAFETY

	LMSC LI-1500 N/m^2 (PSI)	GE MOD 1A N/m^2 (PSI)
IN-PLANE TENSILE STRESS	482,000 (69.9)	538,000 (78.1)
IN-PLANE COMPRESSIVE STRESS	1,200,000 (174.0)	590,000 (85.5)
TRANSVERSE TENSILE STRESS	96,500 (14.0)	186,000 (27.0)
TRANSVERSE TENSILE STRESS	290,000 (42.0)	290,000 (42.0)
TRANSVERSE SHEAR STRESS	190,000 (27.5)	207,000 (30.0)
	LMSC COATING	GE COATING
TENSILE STRESS	13,800,000 (2000)	13,800,000 (2000)
COMPRESSIVE STRESS	27,600,000 (4000)	27,600,000 (4000)

Figure 7

MULLITE AND SILICA ELEMENT PLOT
(Figure 8)

The plots of the mullite (GE MOD 1A) and silica (LI-1500) undeformed finite element models are presented. The models represent half of a 0.15-meter (6-in.) tile with coating. The insulation thickness is 0.089 meter (3.51 in.) for mullite and 0.078 meter (3.06 in.) for silica. The coating thickness is 0.000762 meter (0.03 in.) for mullite and 0.000381 meter (0.015 in.) for silica. These materials were sized for the Area 2P trajectory.

MULLITE AND SILICA ELEMENT MODEL

HEATED SURFACE OF MULLITE TILE
[.15 m (6 IN.) × .15 IN. (6 IN.)
× 8.92 × 10^{-2} m (3.51 IN.)]

TILE
EDGE

HEATED SURFACE OF SILICA TILE
[.15 m (6 IN.) × .15 m (6 IN.)
× 7.77 × 10^{-2} m (3.06 IN.)]

TILE
EDGE
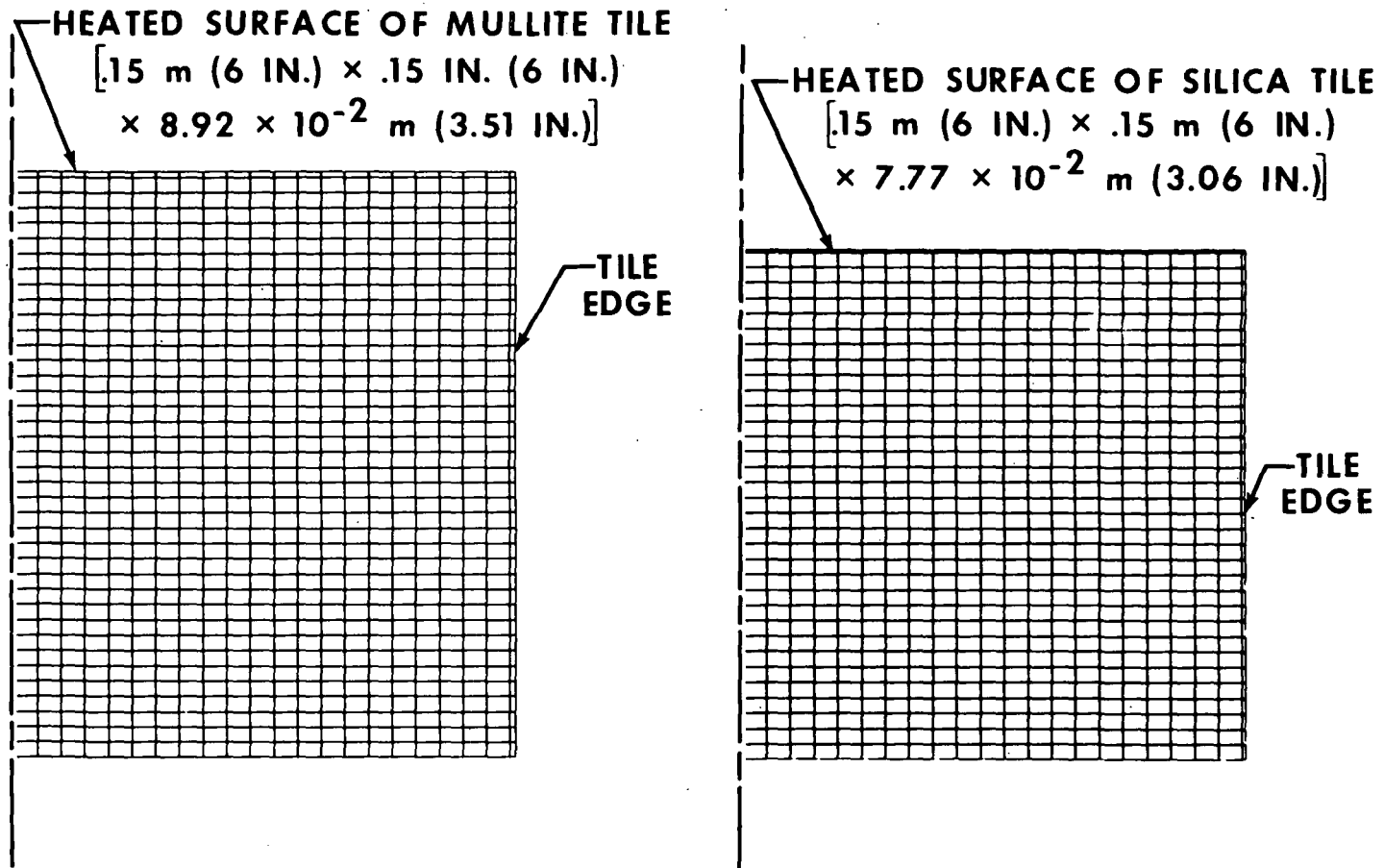
Figure 8

MULLITE AND SILICA DEFORMED ELEMENT PLOT
(Figure 9)

The plots of the mullite (GE MOD 1A) and silica (LI-1500) deformed finite element models are presented. The deformation results from the temperature distribution 250 seconds into entry. The displacements of both models are magnified by a factor of 50. The plots illustrate the effect of the coefficients of thermal expansion of the materials. The temperature at entry initiation was 172°K (-150°F). The surface temperatures of the mullite and silica were 1055°K (1440°F) and 1085°K (1493°F), respectively.

MULLITE AND SILICA
DEFORMED ELEMENT PLOT
250 SECONDS INTO ENTRY
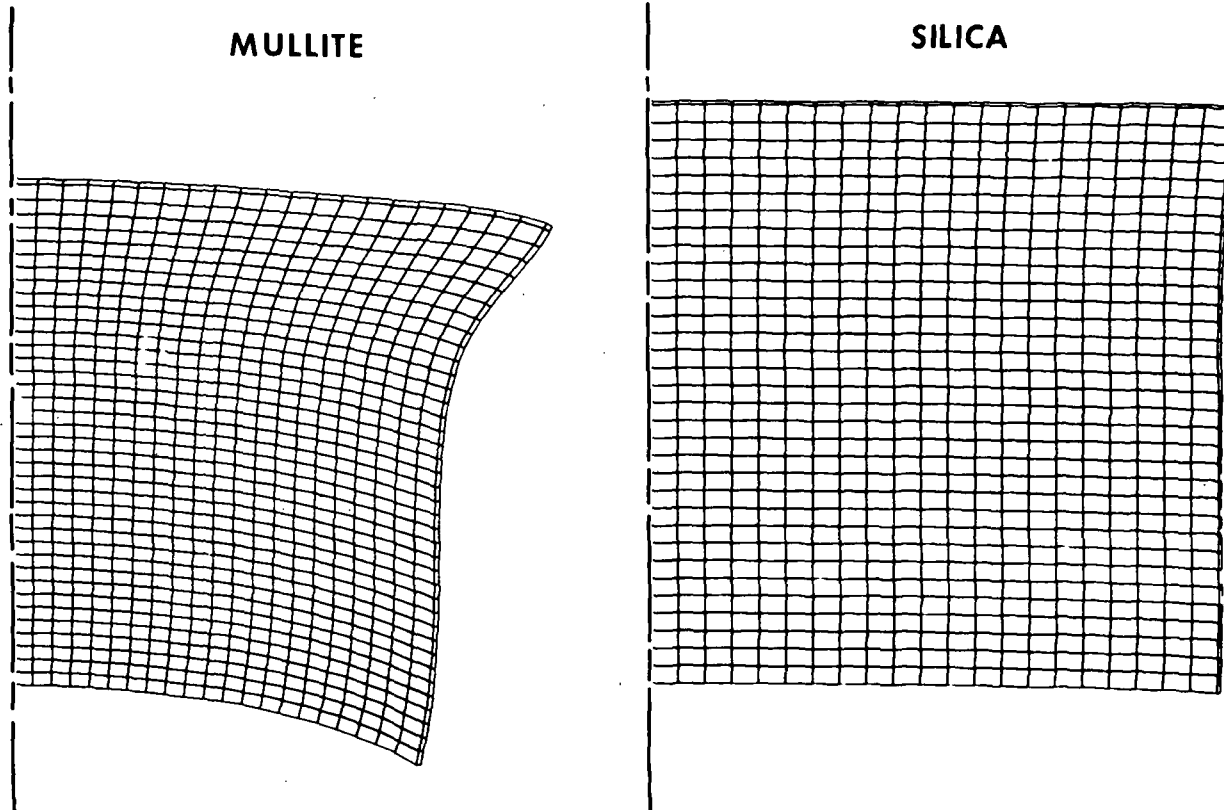
MULLITE

SILICA

Figure 9

CONTOURS OF IN-PLANE TENSILE STRESS
MULLITE AND SILICA
250 SECONDS INTO ENTRY
(Figure 10)

Contours of in-plane tensile stress are presented based on bounding moduli for mullite (GE MOD 1A) and silica(LMSC LI-1500). The contours plotted for silica are from 34,500 N/m² (5 psi) to 69,000 N/m² (10 psi) in 34,500 N/m² (5 psi) increments. The contours plotted for mullite are from 69,000 N/m² (10 psi) to 690,000 N/m² (100 psi) in 69,000 N/m² (10 psi) increments. The contours are plotted on the deformed element plot without the element grid lines.

CONTOURS OF IN-PLANE TENSILE STRESS
MULLITE AND SILICA
250 SECONDS INTO ENTRY

MULLITE

SILICA

$690,000 \ N/m^2$ (100)

$621,000 \ N/m^2$ (90 PSI)

$552,000 \ N/m^2$ (80 PSI)

$483,000 \ N/m^2$ (70 PSI)

$414,000 \ N/m^2$ (60 PSI)

$69,000 \ N/m^2$ (10 PSI)

$345,000 \ N/m^2$ (50 PSI)

$138,000 \ N/m^2$ (20 PSI)

$276,000 \ N/m^2$ (40 PSI)

IN-PLANE TENSILE STRESS

$207,000 \ N/m^2$ (30 PSI)

$69,000 \ N/m^2$ (10 PSI)

$34,500 \ N/m^2$ (5 PSI)

IN-PLANE TENSILE STRESS
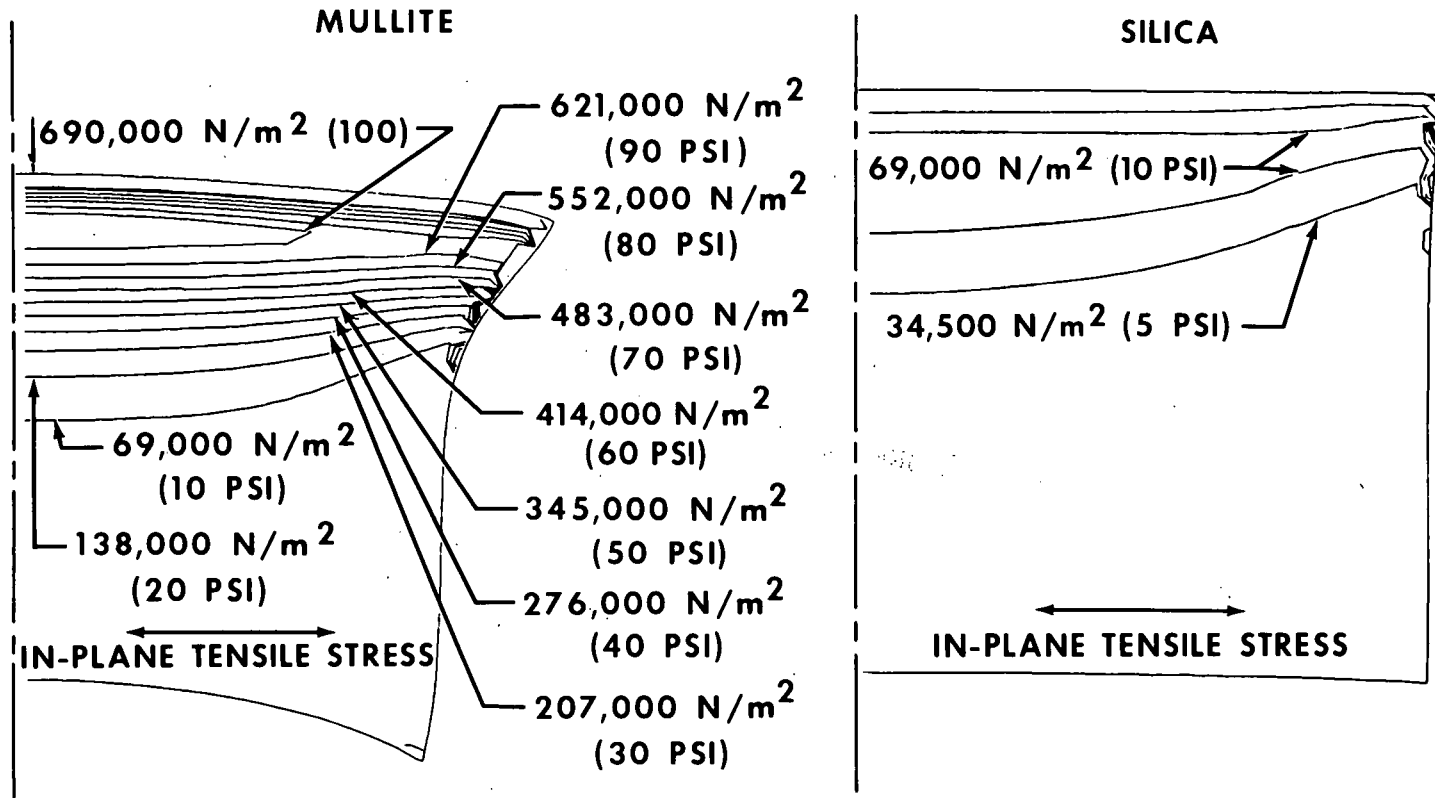
Figure 10

CONTOURS OF TRANSVERSE TENSILE STRESS
MULLITE AND SILICA
250 SECONDS INTO ENTRY
(Figure 11)

Contours of transverse tensile stress are presented based on MSC properties for mullite (GE MOD 1A) and silica (LMSC LI-1500). The contours plotted for mullite are from 34,500 N/m^2 (5 psi) to 241,000 N/m^2 (35 psi). The contours are plotted on the deformed element plot without the element grid lines.

CONTOURS OF TRANSVERSE
MULLITE AND SILICA TENSILE STRESS
250 SECONDS INTO ENTRY
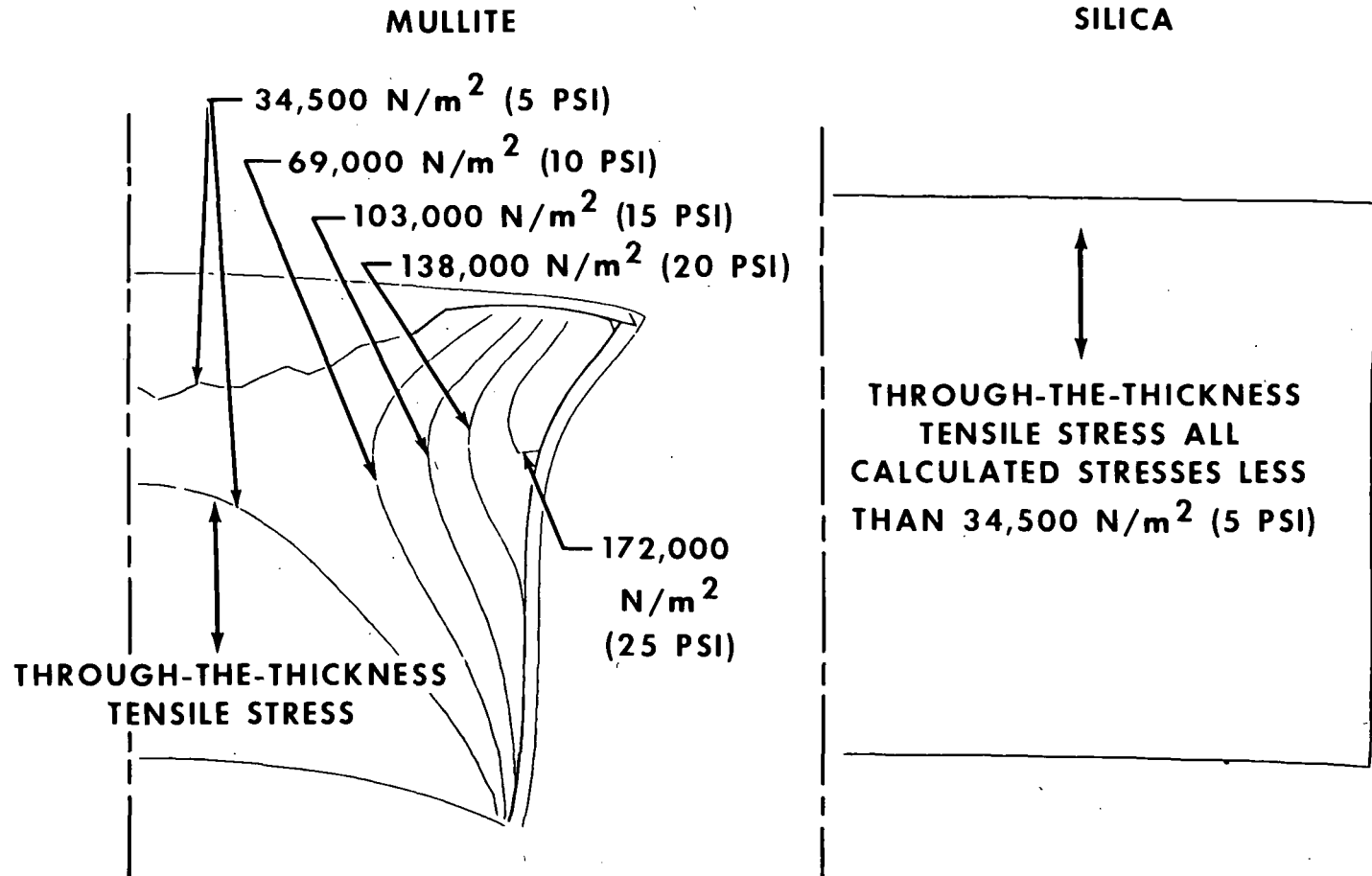
MULLITE

SILICA

34,500 N/m^2 (5 PSI)

69,000 N/m^2 (10 PSI)

103,000 N/m^2 (15 PSI)

138,000 N/m^2 (20 PSI)

172,000 N/m^2 (25 PSI)

THROUGH-THE-THICKNESS
TENSILE STRESS

THROUGH-THE-THICKNESS
TENSILE STRESS ALL
CALCULATED STRESSES LESS
THAN 34,500 N/m^2 (5 PSI)

Figure 11

CONTOURS OF TRANSVERSE SHEAR STRESS
MULLITE AND SILICA
250 SECONDS INTO ENTRY
(Figure 12)

Contours of transverse shear stress are presented based on MSC properties for mullite (GE MOD 1A) and silica (LMSC LI-1500). The contours plotted for silica are shown to 138,000 N/m^2 (20 psi) in 34,500 N/m^2 (5 psi) increments. The contours plotted for mullite are from--138,000 N/m^2 (-20 psi) to 276,000 N/m^2 (40 psi) in 69,000 N/m^2 (10 psi) increments. The contours are plotted on the deformed element plot without the element grid lines. The contours shown for the silica are in the coating. The shear stress are less than 34,500 N/m^2 (5 psi) in the LI-1500.

CONTOURS OF TRANSVERSE
SHEAR STRESS MULLITE AND SILICA
250 SECONDS INTO ENTRY

MULLITE

SILICA

-69,000 N/m^2 (-10 PSI)

-138,000 N/m^2 (-20 PSI)

276,000 N/m^2 (40 PSI)

207,000 N/m^2 (30 PSI)

138,000 N/m^2 (20 PSI)

SHEAR STRESS

69,000 N/m^2 (10 PSI)

34,500 N/m^2 (5 PSI)

69,000 N/m^2 (10 PSI)

103,000 N/m^2 (15 PSI)

138,000 N/m^2 (20 PSI)

SHEAR STRESS

Figure 12

CONTOURS OF MARGIN OF SAFETY (MS1)
MULLITE AND SILICA
250 SECONDS INTO ENTRY
(Figure 13)

Contours of margin of safety (MS1) based on the combined stress criterion and MSC properties are presented for mullite (GE MOD 1A) and silica (LMSC LI-1500). The contours plotted are 0, -0.1, -0.2, and -0.33. The method for calculating MS1 has been discussed previously. The contours are plotted on the deformed element plot without the element grid lines. The lack of any contours in the silica means that all margins (MS1) are positive. This figure demonstrates the structural advantage of silica over mullite systems.

The margins of safety calculated are based on average allowables for comparison, although average allowables are considered inappropriate for design. The margins quoted based on the combined stress criterion are not numerically correct because of the plane stress assumption. The three-dimensional state of stress is required for the correct margin of safety based on the combined criterion.

CONTOURS OF MARGIN OF SAFETY (MS1)
MULLITE AND SILICA
250 SECONDS INTO ENTRY
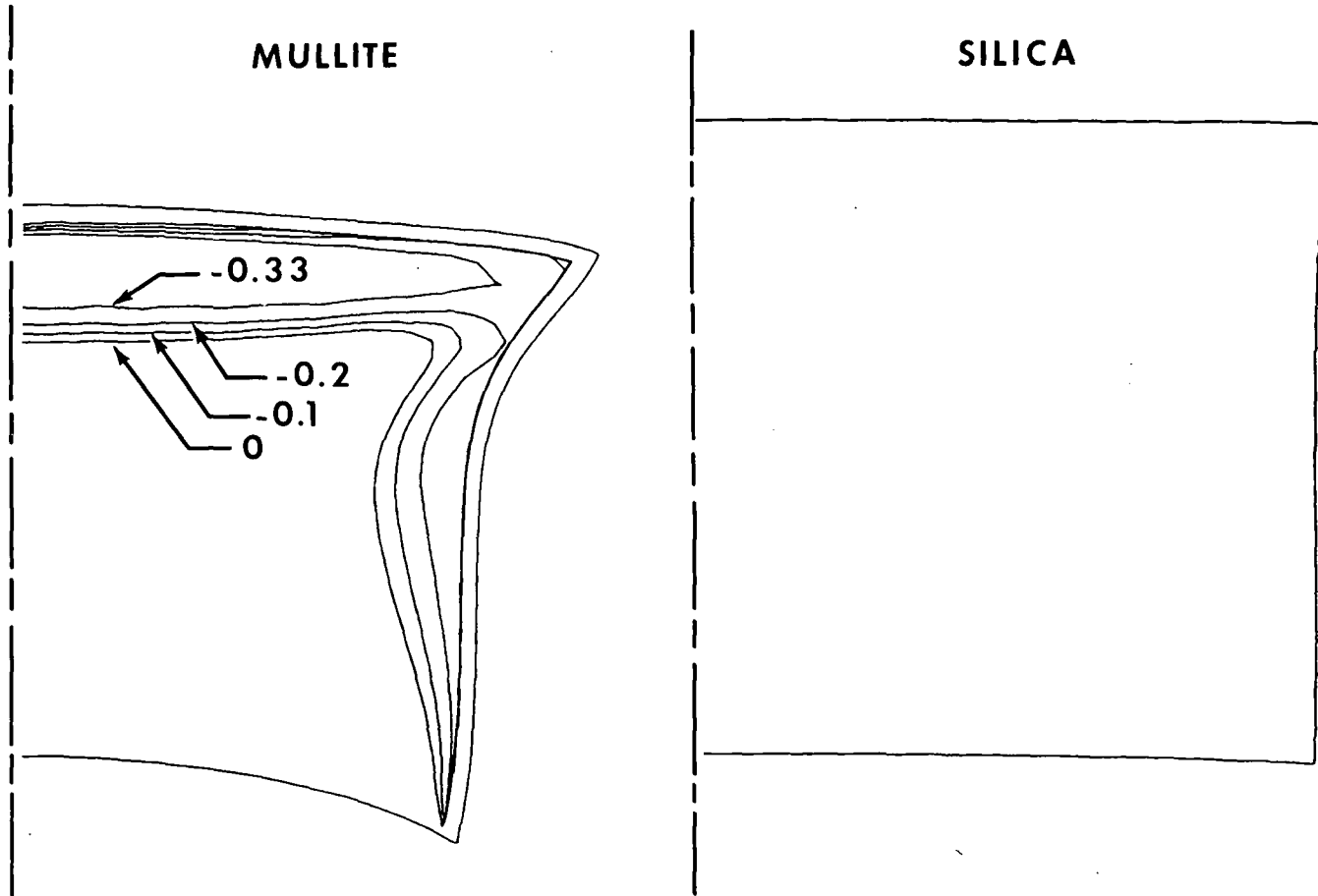
MULLITE

SILICA

-0.33

-0.2

-0.1

0

1255
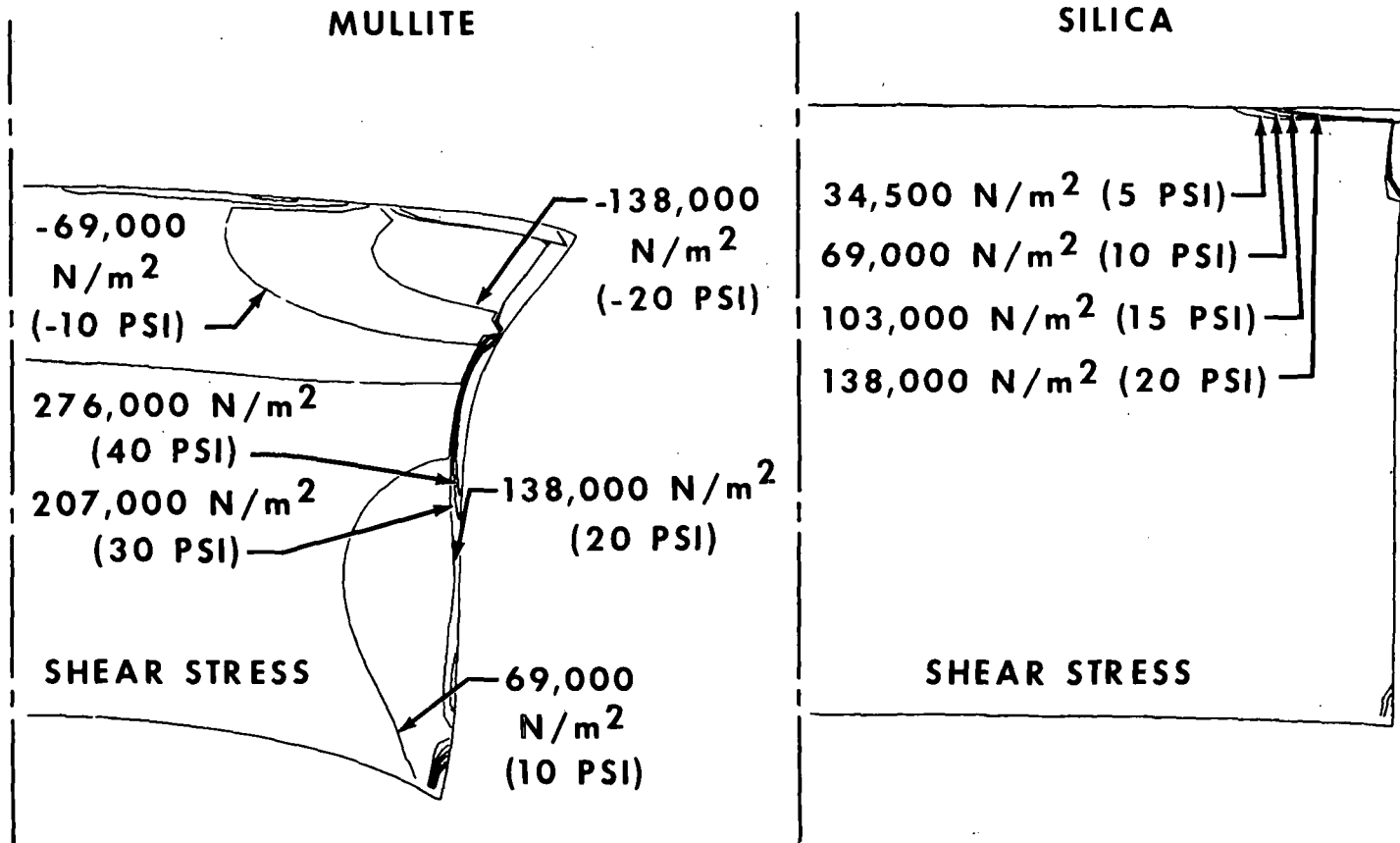
Figure 13

CONTOURS OF MARGIN OF SAFETY (MS2)
MULLITE AND SILICA
250 SECONDS INTO ENTRY
(Figure 14)

Contours of margin of safety (MS2) based on the individual stress criterion and MSC properties are presented for mullite (GE MOD 1A) and silica (LMSC LI-1500). The contours plotted are 0, -0.1, -0.2, and -0.33. The method for calculating MS2 has been discussed previously. The contours are plotted on the deformed element plot without the element grid lines. The lack of any contours in the silica means that all margins (MS2) are positive. This figure demonstrates the structural advantage of silica over mullite systems.

The margins of safety calculated are based on average allowables for comparison, although average allowables are considered inappropriate for design.

CONTOURS OF MARGIN OF SAFETY (MS2)
MULLITE AND SILICA
250 SECONDS INTO ENTRY

MULLITE

SILICA

-0.5   -0.33

-0.2

-0.1

0
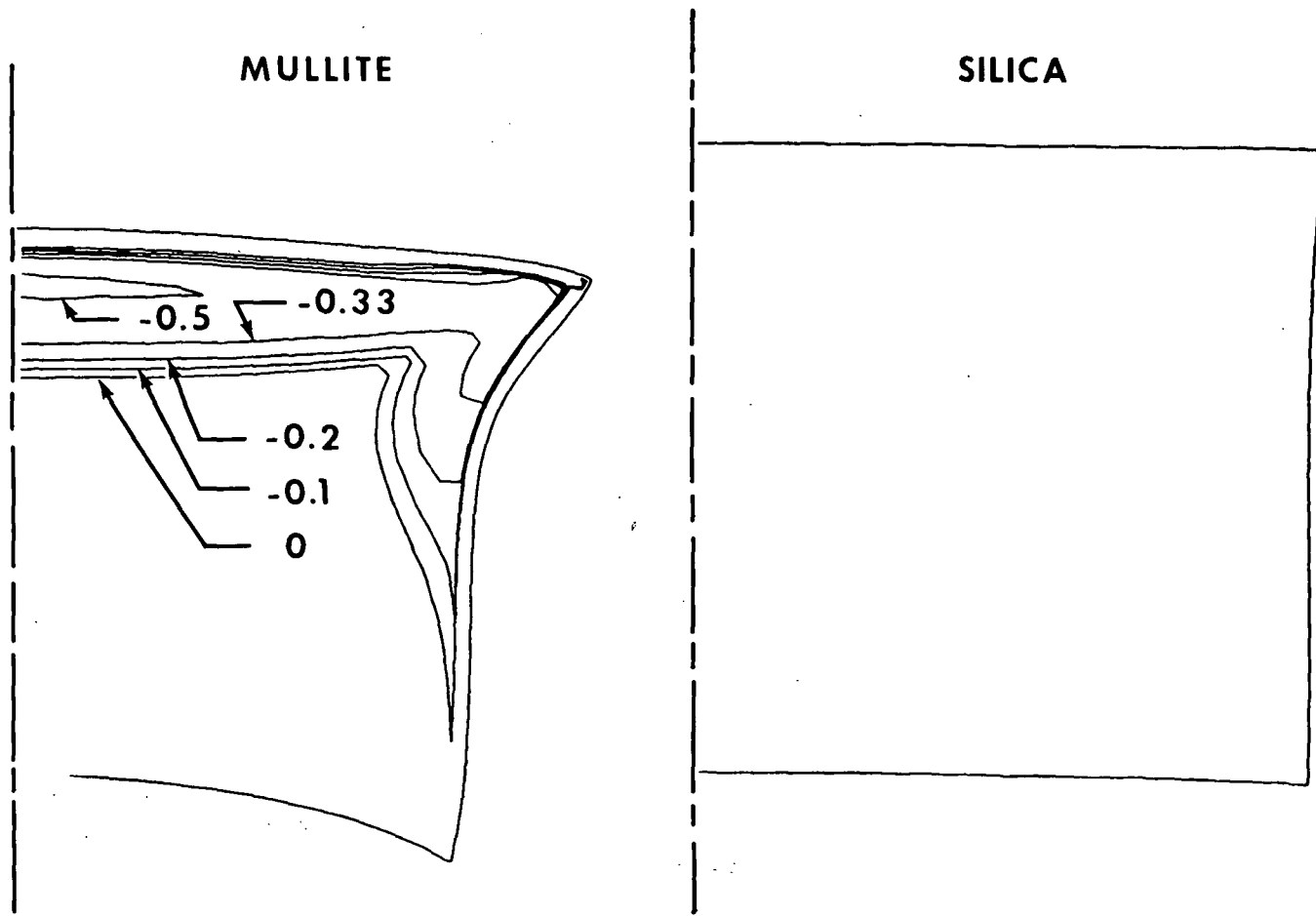
1257

Figure 14

CONTOURS OF MARGIN OF SAFETY (MS1)
MSC AND GE PROPERTIES
MULLITE (GE MOD 1A)
(Figure 15)

Contours of combined stress criterion margin of safety (MS1) based on MSC and GE properties are presented as a comparison. These margins are based on average allowables, presented before, which are considered unacceptable for design.

CONTOURS OF MARGIN OF SAFETY (MS1)
MSC AND GE PROPERTIES MULLITE (GE MOD 1A)
250 SECONDS INTO ENTRY

AVERAGE MODULI

BOUNDING MODULI

-0.33

-0.2

-0.2

0

-0.1

-0.1

0
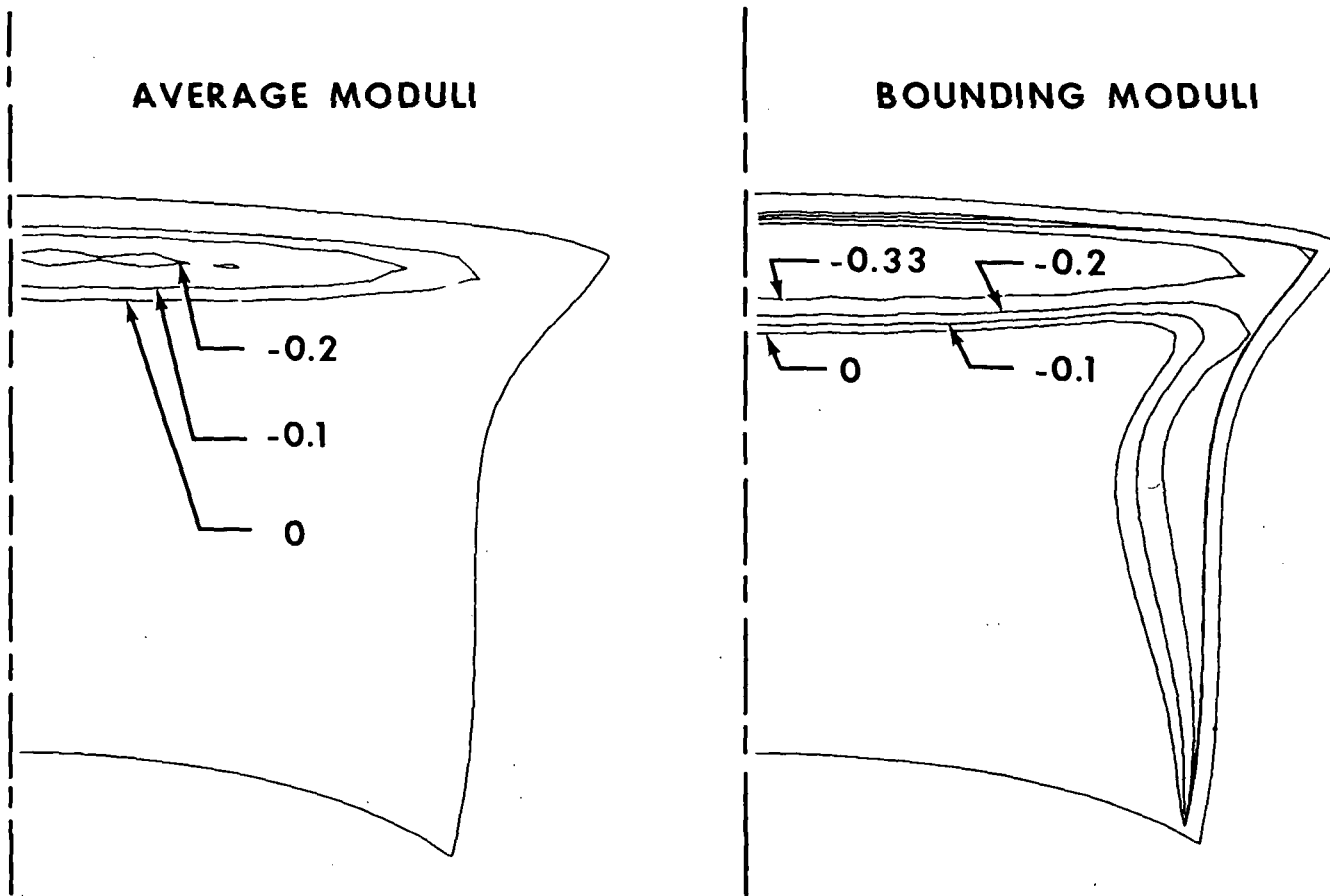
Figure 15

CONTOURS OF MARGIN OF SAFETY (MS2)
MSC AND GE PROPERTIES
MULLITE (GE MOD 1A)
(Figure 16)

Contours of individual stress criterion (MS2) based on MSC and GE properties are presented as a comparison. These margins are based on average allowables, presented before, which are considered unacceptable for design.

CONTOURS OF MARGIN OF SAFETY (MS2)
MSC AND GE PROPERTIES MULLITE (GE MOD 1A)
250 SECONDS INTO ENTRY

AVERAGE MODULI

BOUNDING MODULI
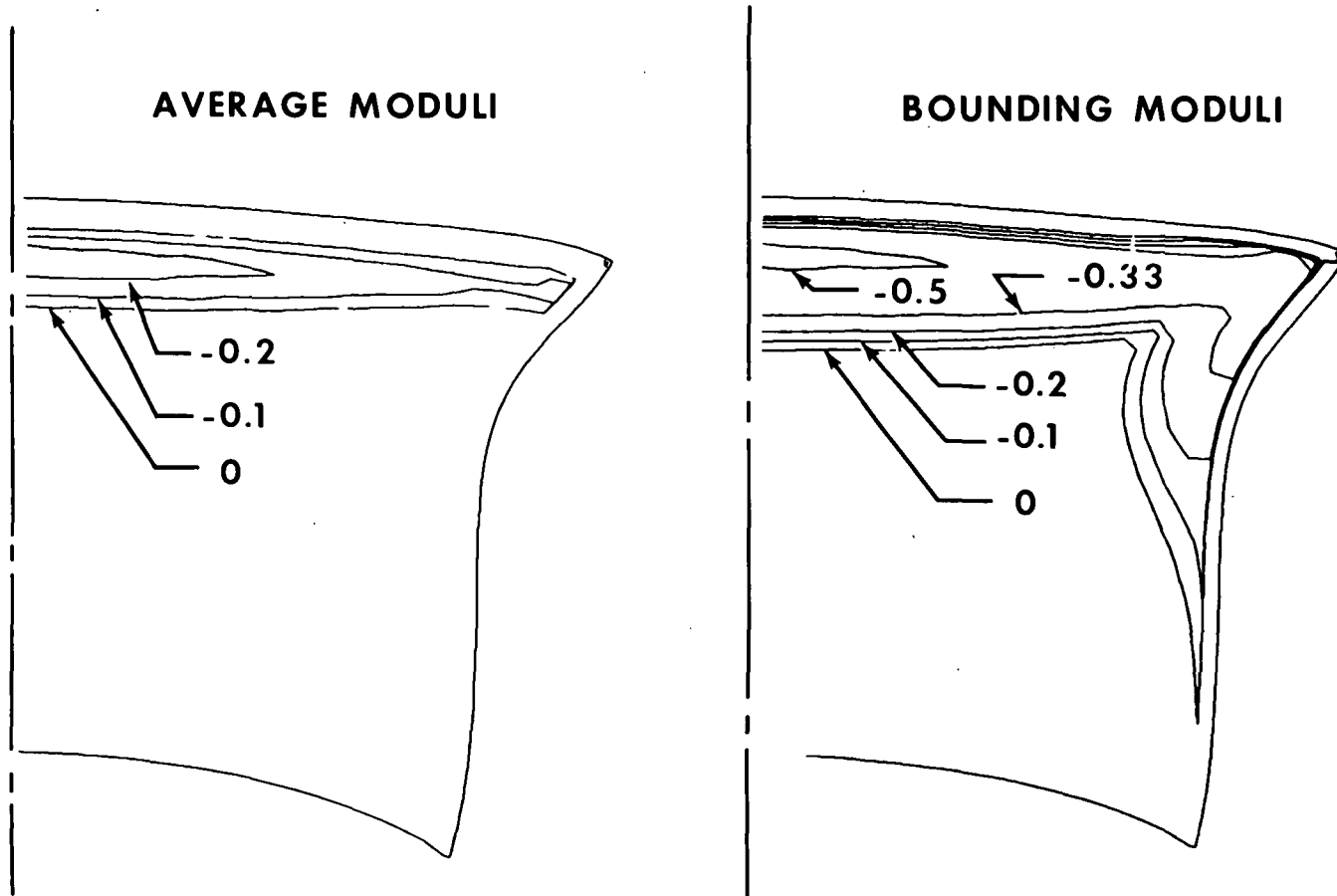
Figure 16

ULTIMATE AND PREDICTED LIMIT STRESSES FOR SILICA
MSC PROPERTIES, 250 SECONDS INTO ENTRY
(MAX SURFACE TEMPERATURE - 1085°K [1493°F])
(Figure 17)

The LMSC and Battelle in-plane ultimate tensile strength test data are presented showing the test data scatter in relation to predicted limit stresses using MSC properties. A comparison of this figure with figure 18 shows the distinct structural advantage of silica over mullite.

ULTIMATE AND PREDICTED LIMIT TENSILE STRESSES FOR SILICA
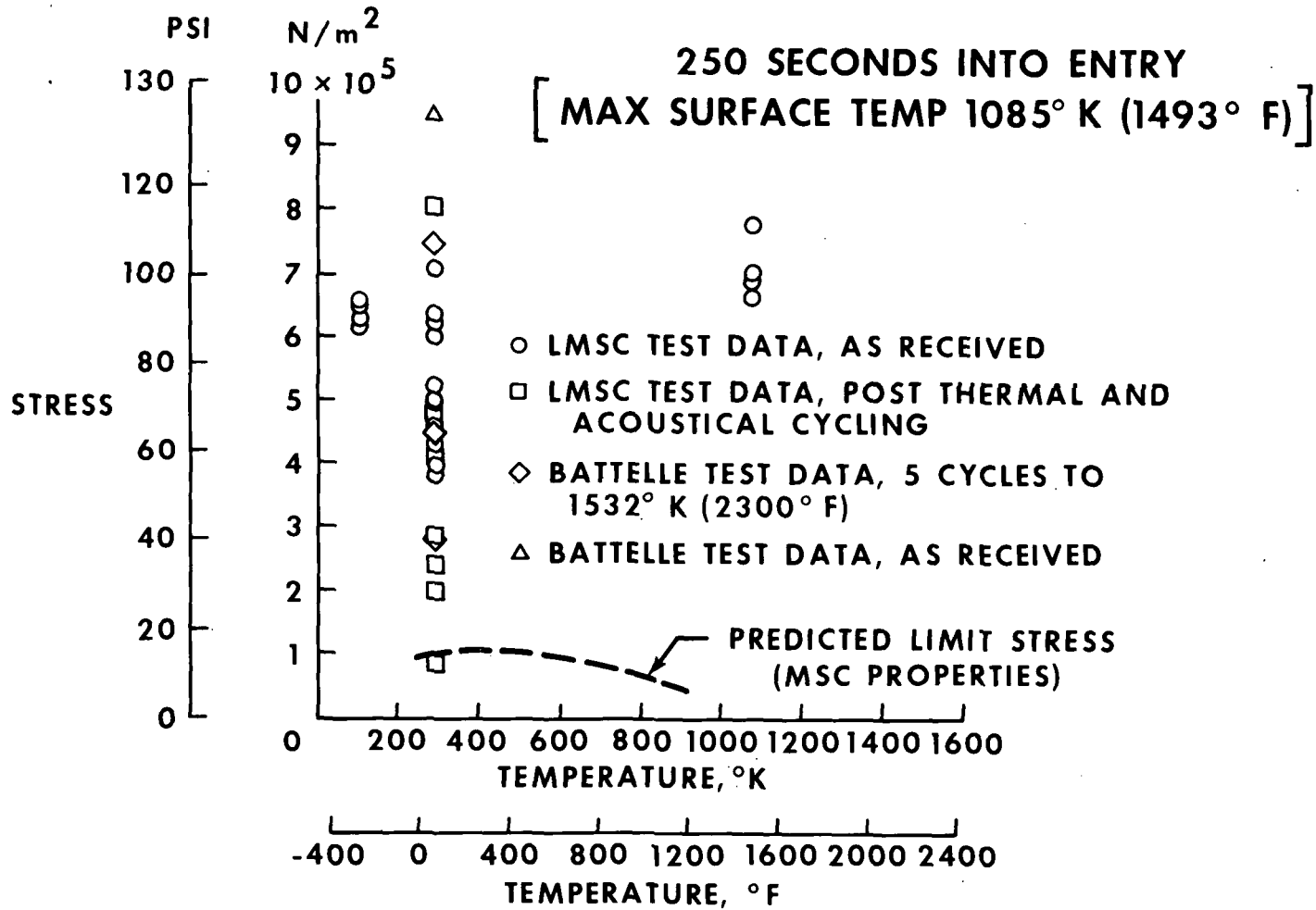
Figure 17

MULLITE
IN-PLANE ULTIMATE AND PREDICTED LIMIT TENSILE STRESSES
MSC AND GE PROPERTIES
250 SECONDS INTO ENTRY (MAX SURFACE TEMP 1055°K [1440°F])
(Figure 18)

The GE and Battelle in-plane ultimate tensile strength test data vs temperature for GE MOD 1A is presented showing the data scatter in relation to limit stresses predicted using both average and bounding moduli. This chart illustrates that the limit stresses using either properties are within the test data scatter.

Based on the bounding value of modulus, the predicted limit stresses indicate that the allowable ultimate in-plane tensile stress required for the mullite to exhibit a 1.5 factor of safety is approximately 1,103,000 N/m² (160 psi).

IN-PLANE ULTIMATE AND PREDICTED LIMIT TENSILE STRESSES FOR MULLITE
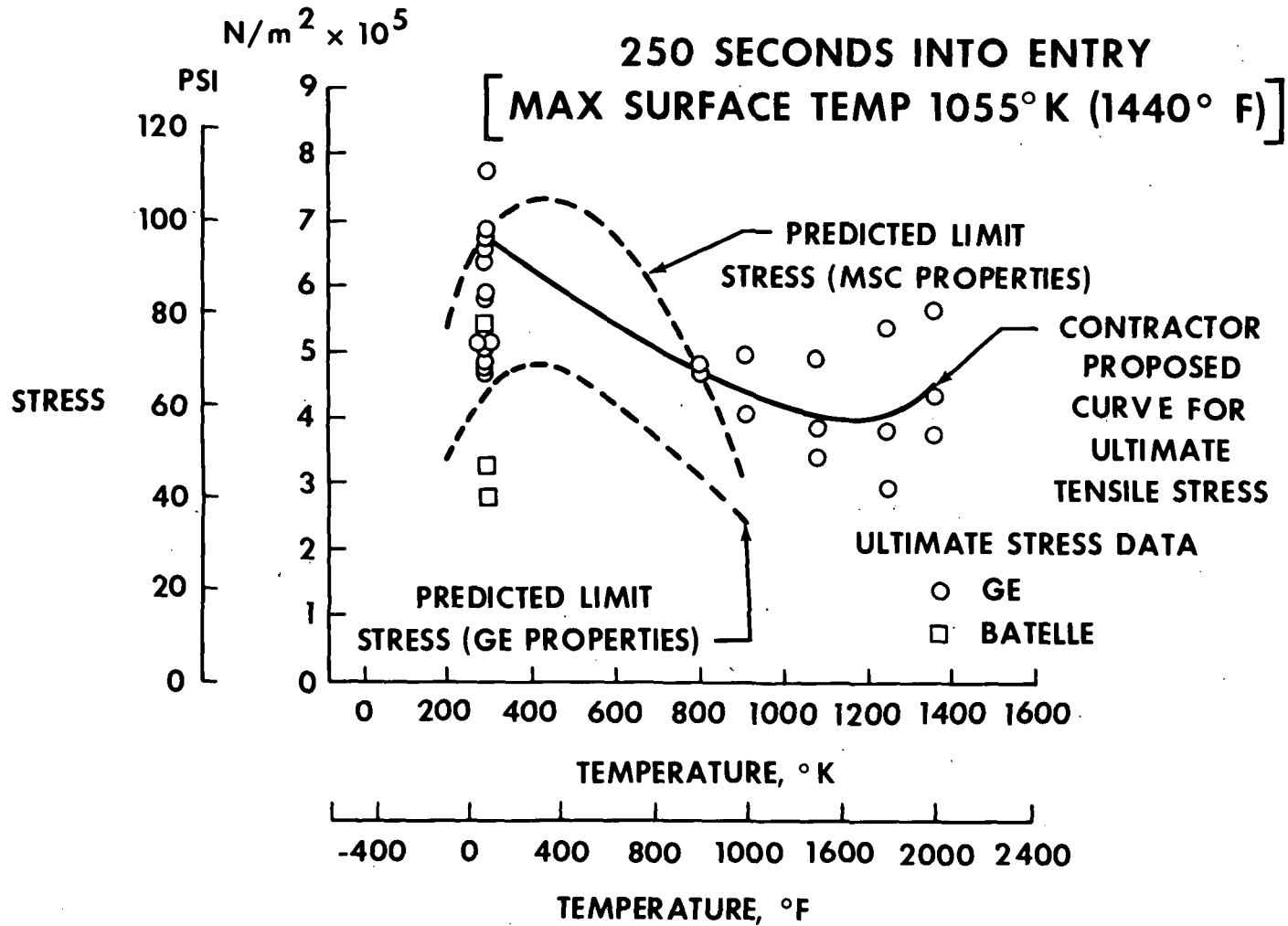
Figure 18

CONCLUSIONS
(Figure 19)

Based on the MSC analysis, the GE MOD 1A mullite system is unacceptable for shuttle trajectories because of predicted failure occurring early in entry. The primary reason for difference between MSC and contractor analysis is the use of average material moduli versus the use of bounding values of material moduli by MSC.

For the shuttle trajectories, thermal shock sensitivity has been identified and shown analytically to be a significant problem for the RSI materials especially for the mullites. The silica system is superior to the mullites for the entry environment.

Factors not discussed for the RSI systems are the edge coating cracking due to thermal gradients and potential coating cracking due to in-plane thermal gradients.

Additional failure criteria work and material property definition is required for the candidate RSI materials.

CONCLUSIONS

- THE MOD IA MULLITE SYSTEM IS NOT ADEQUATE FOR CURRENT
  SHUTTLE TRAJECTORIES BECAUSE OF THE HIGH STRESSES
  OCCURING EARLY IN ENTRY

- THE SILICA SYSTEM IS SUPERIOR TO MULLITE FOR THE THERMAL
  STRESSES ENCOUNTERED DURING ENTRY

- PRIMARY REASON FOR DIFFERENCE BETWEEN THE CONTRACTOR
  AND MSC ANALYTICAL RESULTS IS THE USE OF AVERAGE
  MODULI BY THE CONTRACTOR, VS BOUNDING MODULI BY MSC

- ADDITIONAL FAILURE CRITERIA WORK AND MECHANICAL
  PROPERTY DEFINITION ARE REQUIRED

- FACTORS NOT DISCUSSED ARE EDGE COATING STRESSES AND
  STRESSES DUE TO IN-PLANE THERMAL GRADIENTS

- THERMAL SHOCK SENSITIVITY IS SHOWN TO BE A SIGNIFICANT
  PROBLEM FOR RSI AND PARTICULARLY FOR THE
  MULLITE SYSTEMS

Figure 19

INTERFERENCE HEATING TO CAVITIES BETWEEN SIMULATED RSI TILES

Charles B. Johnson

NASA-Langley Research Center
Hampton, Virginia

INTRODUCTION

One of the largest problems facing the designers of the Space Shuttle involves the thermal protective coatings, which are tentatively to be made up of RSI tiles approximately 20.32 cm (8 inch) square. One of the problems associated with the placing of tiles on the surface of the shuttle is the heating in the small thermal-expansion gaps between the tiles [about .3715 cm to .635 cm (1/8 to 1/4 inch) wide]. Some of the problems associated with heating to the gaps are: (1) high heating rates in the gaps (flow reattachment); (2) radiation blockage, which could increase the equilibrium surface temperature; and (3) a short heat path, which would increase the bond line temperature.

In order to evaluate the interference heating in the cavities between the tiles, tests were made on simulated RSI tiles in the Langley Mach 8 variable density tunnel. The simulated tiles were mounted in a curved plate, which was tested with a thick and thin boundary layer over the tiles. The boundary layer thickness was varied by testing the plate in the free stream and also testing it flush to the nozzle wall. The simulated tiles were tested in both positions with either an "in-line" or a "staggered" orientation.

This paper presents the highlights of a few of the most significant results of the test. A complete set of the over 2,000 data points has been incorporated into the Space Shuttle SADSAC system.

SCHEMATIC OF TUNNEL WALL TESTS

(Figure 1)

Figure 1 is a sketch of the method of testing the plate flush to the tunnel wall. The plate also was tested in the free stream. The model was tested in both positions over a unit Reynolds range of 1.1×10^6 to 40.0×10^6 per meter. With the model flush to the nozzle wall, the boundary-layer thickness over the tiles varies from 10 cm to 5 cm for this Reynolds number range. The boundary-layer thickness was determined from experimental pitot and temperature profiles as described in NASA TN D-5433. The seal below the model is removed for the tests in the free stream.

The heat transfer tests were made with the model initially at room temperature. The model was injected into the tunnel test section from a vacuum chamber that had been evacuated to the test-section stream static pressure. Approximately 0.05 second was required for the model to leave the chamber and enter the uniform test-flow region. The heat transfer data were obtained from a temperature time history of each thermocouple as recorded at either 40 or 20 points per second. The data records were evaluated over a one second interval as soon as there was a constant increase in the thin skin wall temperature. No conduction corrections have been applied to the heat transfer data, but the early time at which the data were evaluated should minimize the conduction error.

SCHEMATIC OF TUNNEL WALL TESTS

$$1.1 \times 10^6 \leq R_\infty/m \leq 40 \times 10^6$$

2.9535 m (116.28 inch)

TEST PLATE

MACH 8 FLOW

3.175 mm

THROAT

δ

NOZZLE WALL

SHARP LEADING EDGE OF PLATE

SEAL

(5 cm $\leq \delta \leq$ 10 cm)

INJECTION MECHANISM

1271
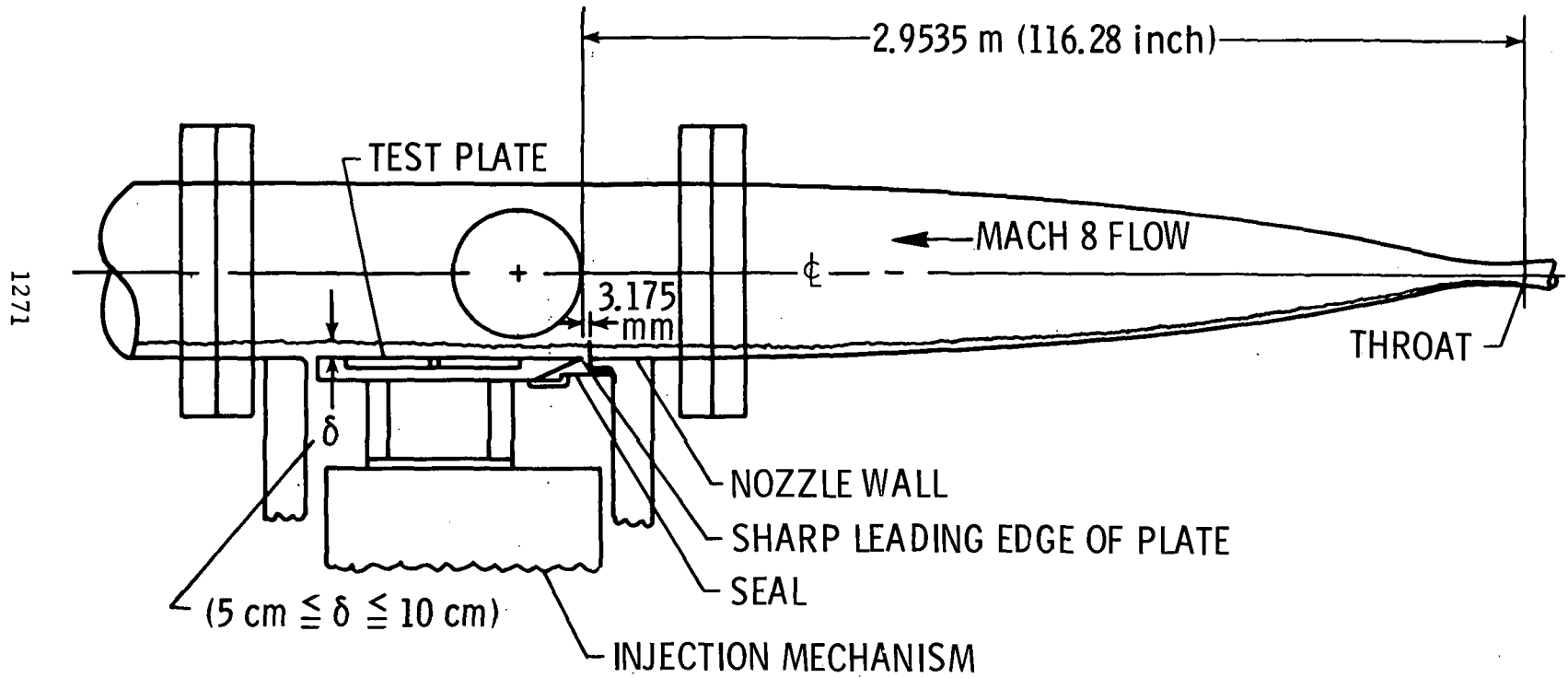
Figure 1

THERMOCOUPLE INSTALLATION

(Figure 2)

The thermocouple installation for the in-line and staggered tiles are shown in figure 2. The triangular marks at the edge of the tiles indicate a vertical row of thermocouples on the wall of the cavity. The four rows of thermocouples on the forward face of the tile in staggered orientation contain eight thermocouples per row. The six rows on the forward faces of the two tiles in the in-line orientation contain five thermocouples per row, and the remaining 22 rows contain three thermocouples per row. The in-line orientation was used to compare the interference heating on three longitudinal gaps, 0.1587 cm (1/16 inch), 0.3175 cm (1/8 inch), and 0.4762 cm (3/16 inch); and two spanwise gaps, 0.1587 cm (1/16 inch), and 0.3175 cm (1/8 inch). The gaps for both tile orientations are 2.54 cm (1.0 inch) deep. Twelve thermocouples on the tile surface, for both tile orientations measure the surface heating to the tile. The simulated tiles are made of 304 stainless steel and have a wall thickness of 0.4064 mm (0.016 inch). The tiles are instrumented with 36 gage-0.127 mm (0.005 inch) diameter iron-constantan thermocouple wire.

THERMOCOUPLE INSTALLATION
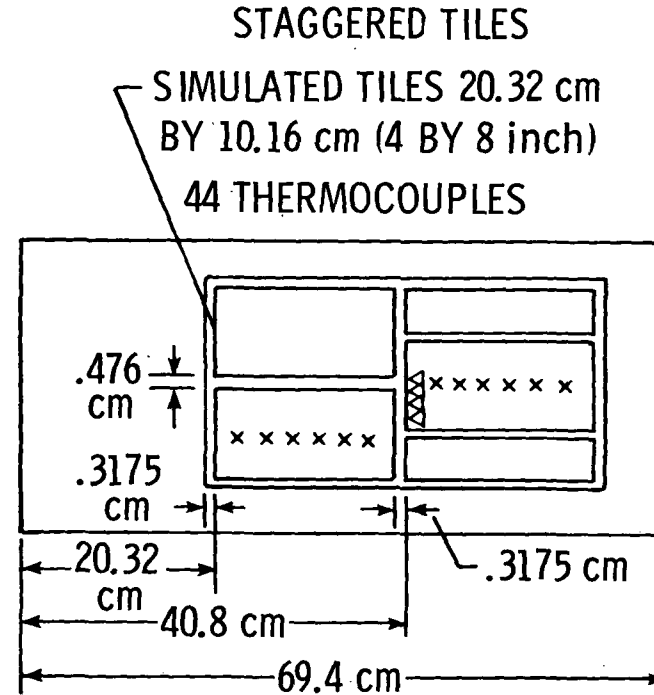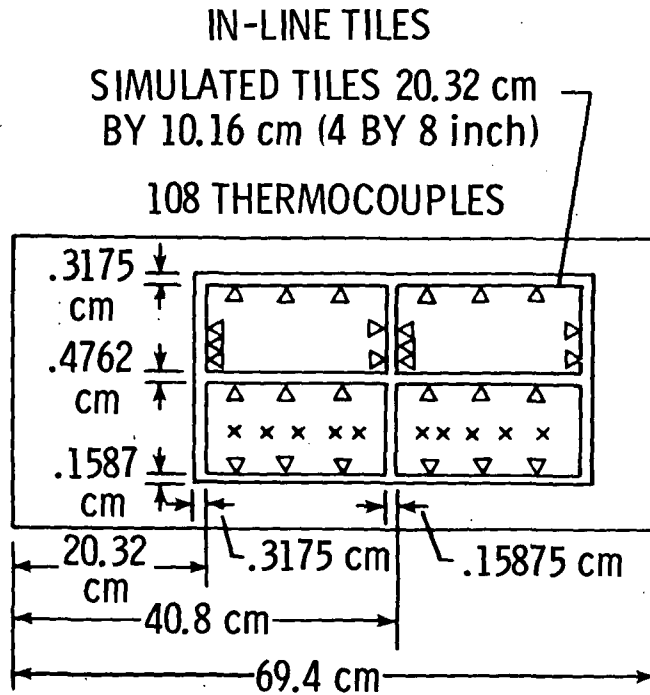
Figure 2

THE EFFECT OF TILE ORIENTATION AND GAP SIZE ON INTERFERENCE HEATING

(Figure 3)

Some of the most significant results of the tests with the plate positioned flush to the tunnel wall are shown in figure 3. The tests were made at a length Reynolds number of 136×10^6. The heating results are presented as $\bar{h}$, which is the ratio of local heating on the cavity wall (0.4762 cm from the surface of the tile) to the measured heating on the surface of the tile. The most significant result is found from comparison of the results on the forward face of a 0.3175 cm (1/8 inch) spanwise gap for the staggered and in-line tile, which show that downstream of the longitudinal gap, the staggered tile orientation has a heating rate about 4.5 times that of the in-line orientation. At a distance of about 2.54 cm (1.0 inch) away from the longitudinal gap, the heating on the forward face is about the same for both the in-line and staggered tiles, with a noticeable increase in heating near the corner of the forward face. It should be noted that the peak heating for the staggered tile directly downstream of the longitudinal gap is $\bar{h} \approx 3.6$ at a distance of 0.2381 cm from the surface. The effect of longitudinal gap size is shown on the in-line orientation, with the highest heating being found for the 0.3175 cm (1/8 inch) gap, the next highest for the 0.4762 cm (3/16 inch) gap and the lowest for the 0.1587 cm (1/16 inch) gap. The effect of spanwise gap size is seen on the in-line orientation with nearly an order of magnitude reduction in heating when the gap size is reduced from 0.3175 cm (1/8 inch) to 0.1587 cm (1/16 inch).

THE EFFECT OF TILE ORIENTATION AND GAP SIZE ON INTERFERENCE HEATING

$$R_{\infty,x} = 136 \times 10^6 - \text{TUNNEL WALL}$$
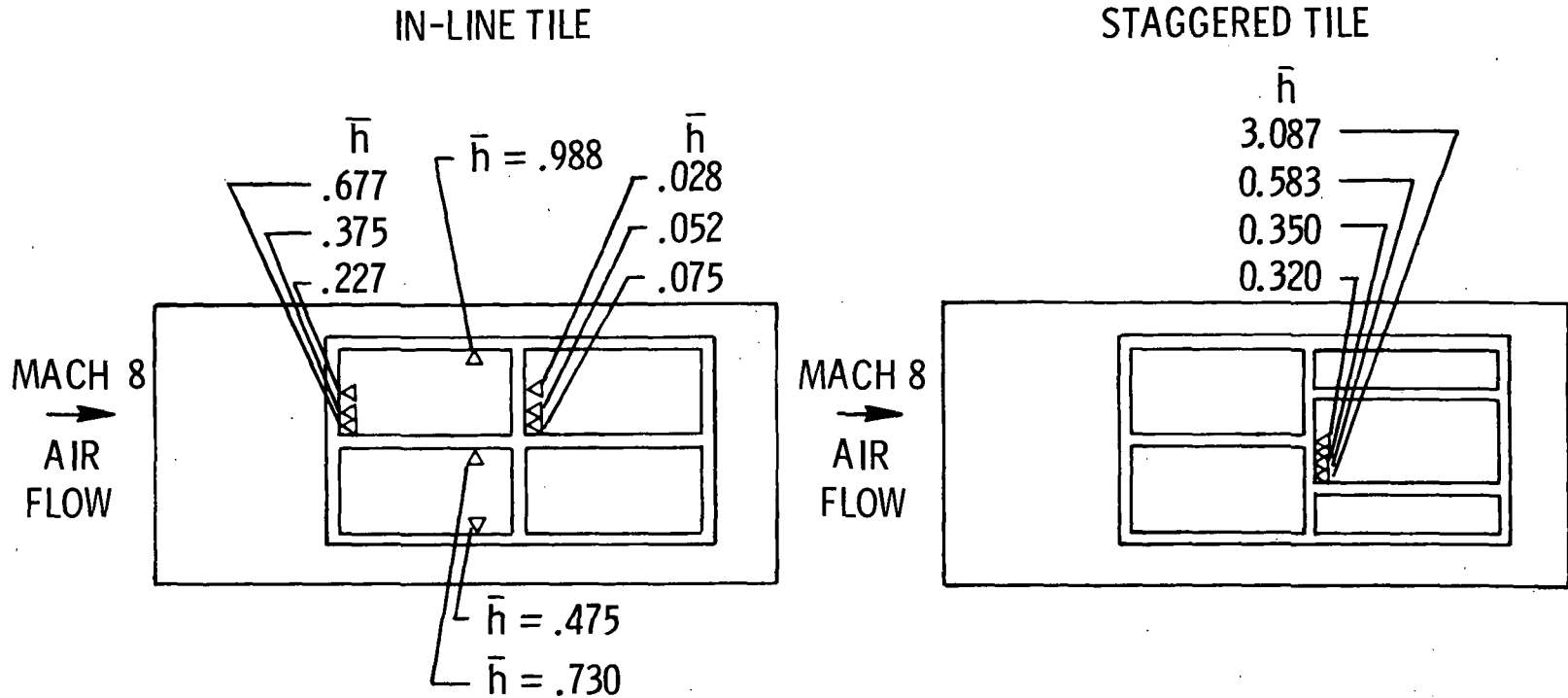
Figure 3

CONCLUDING REMARKS

The entire program of tests of the full-scale simulated RSI tiles on both the tunnel wall and in the free stream, for the in-line and staggered tile orientations, has generated over 2,000 data points, which have been put into the Space Shuttle SADSAC system. Even with the large number of points generated, some of the major trends and significant results found for tunnel wall tests at a length Reynolds number of 136 million have been shown, and are summarized as follows:

1. The staggered tile orientation has heating on the forward face which is a factor of 4.5 times higher than the heating to the forward face of the in-line tile orientation.

2. The longitudinal gap heating was the highest for the 0.3175 cm (1/8 inch) gap and the lowest for the 0.1587 cm (1/16 inch) gap. A 0.4762 cm (3/16 inch) longitudinal gap had a level of heating that fell between the level of the above two gaps.

3. There was an order of magnitude decrease in the heating on the forward face of a spanwise gap when the gap size was decreased from 0.3175 cm (1/8 inch) to 0.1587 cm (1/16 inch).

EFFECT OF CRISTOBALITE ON THE MECHANICAL

PROPERTIES OF SILICA RSI MATERIALS

by

Pramod K. Khandelwal and William D. Scott

Ceramic Engineering Division
Department of Mining, Metallurgical and Ceramic Engineering
University of Washington
Seattle, Washington 98195

1277

37

ABSTRACT

Cristobalite is the common crystallization product from vitreous silica. One would expect cristobalite to be detrimental to the strength of RSI materials because of thermal contraction stresses between the crystalline and glassy phases and because of the beta to alpha cristobalite phase transition, which occurs at about 523°K (482°F) with a 5.4% volume change.

The strength of silica (Lockheed 1500 type) RSI materials was measured after high temperature heat treatment to develop substantial crystalline phases and after low temperature thermal cycling through the alpha-beta cristobalite transformation.

An early Lockheed LI-1500 type material developed 76% cristobalite after one hour at 1533°K (2300°F) and the tensile strength dropped from 544×10^3 N/m^2 (79 psi) to 159×10^3 N/m^2 (23 psi). One low temperature cycle through the alpha-beta transformation temperature further reduced the strength to 103×10^3 N/m^2 (15 psi) and a second low temperature cycle caused spontaneous cracking.

Lockheed LI-1525 developed only 13% cristobalite in the same heat treatment, and there was no significant decrease in strength after five additional low temperature cycles. Lockheed LI-1542 did not crystallize at all and the strength increased from 676×10^3 N/m^2 (98 psi) to 951×10^3 N/m^2 (138 psi) after one hour at 1533°K (2300°F) and further increased to 1055×10^3 N/m^2 (153 psi) after five one-hour cycles at 1533°K (2300°F).

It appears that the presence of cristobalite in the structural elements (the fibers) is highly detrimental to tensile strength. When crystallization does not occur in silica RSI material, the strength improves with heat treatment.

PART I: STABLE AND METASTABLE STATES OF SILICA

Fused silica at room temperature is a glass, a solid material with disordered liquid-like structure, which exists at low temperatures in a permanent metastable state. At high temperatures where some atom mobility is possible, the glass tends to devitrify or revert to a crystalline phase that is thermodynamically more stable. In the case of fused silica, the devitrification occurs at temperatures between about 1100°C and the equilibrium freezing point of cristobalite, 1723°C.

Crystalline silica exists in many polymorphic modifications,[1] but the two forms of interest in the present application are quartz and cristobalite. A third form, trimite, also exists, but does not form under the short term heating situations encountered in this study of silica fiber insulation.

# FREE ENERGY VERSUS TEMPERATURE FOR VARIOUS FORMS OF SILICA
(Figure 1)

A schematic diagram of the free energy relationships between glass, quartz, and cristobalite is shown in figure 1.[2,3]   In this figure, the phase with the lowest free energy is the thermodynamically stable phase at any particular temperature. This does not mean that phases with a higher free energy cannot exist at a particular temperature. For example, glass at 600°C has a higher free energy than either quartz or cristobalite, yet it exists indefinitely because atom mobilities are too low at this temperature to permit rearrangement into a crystalline form.

The quartz cristobalite and cristobalite liquid transitions are very slow because they involve the breaking of silicon-oxygen bonds and rearrangement of SiO_4^{4-} tetrahedra into new configurations. This has two effects: (1) a high temperature form, either liquid or cristobalite can easily be cooled and retained in a metastable state at room temperature; and (2) once a particular crystalline phase (cristobalite or quartz) is nucleated and begins to form in the glass at high temperatures, it continues to grow even though some other crystalline form may be thermodynamically more stable. Thus, according to figure 1, a glass held at temperature between 1025°C and the one marked T_m could lower its free energy by crystallizing to either quartz or cristobalite. Although cristobalite has the lowest free energy, the phase that actually forms depends on which one is nucleated.

At temperatures between T_m and 1725°C, the glass can only lower its free energy by forming cristobalite, and this is the usual devitrification product at high temperatures.

The temperature T_m is where crystalline quartz has the same free energy as glassy silica; i.e., it is the melting point of crystalline quartz. This temperature has been estimated to be below 1450°C and possibly above 1400°C.[4,5]   An interesting situation arises if quartz that has formed in a glass at $T < T_m$ is raised to a higher temperature $T > T_m$. The quartz now has the choice of two reconstructive transformations to lower its free energy, viz., transformation to glass or cristobalite, with cristobalite being the lower energy state. One finds that the actual transition that occurs is quartz to glass, followed possibly by a crystallization of glass to cristobalite. This is reasonable since there is already some glass present from the parent phase, and because the formation of cristobalite directly would involve a new, and difficult, nucleation step.[6,7]   This behavior has been observed in silica RSI materials where extended heating at 1260°C reduced the quartz content from 15% to 5%, while the cristobalite, apparently present as an independent subsystem, increased only 6%.[8]   In order to form a new crystalline phase in a glass, an energy barrier must be overcome to create the first nucleus of the new phase. In most systems, the nucleation step is heterogeneous; i.e., the nucleus originates on the same foreign body or some outside source. In glasses, nucleation usually occurs at the surface and crystal growth proceeds inwards. Scott [9] has shown that water vapor reactions will cause the nucleation of α-sodium disilicate ($Na_2Si_2O_5$) crystals in a glass of the same composition, and Brown [10] in studying the growth of cristobalite in fused silica introduced surface nucleation with short water immersion.

FREE ENERGY VERSUS TEMPERATURE FOR VARIOUS FORMS OF SILICA.
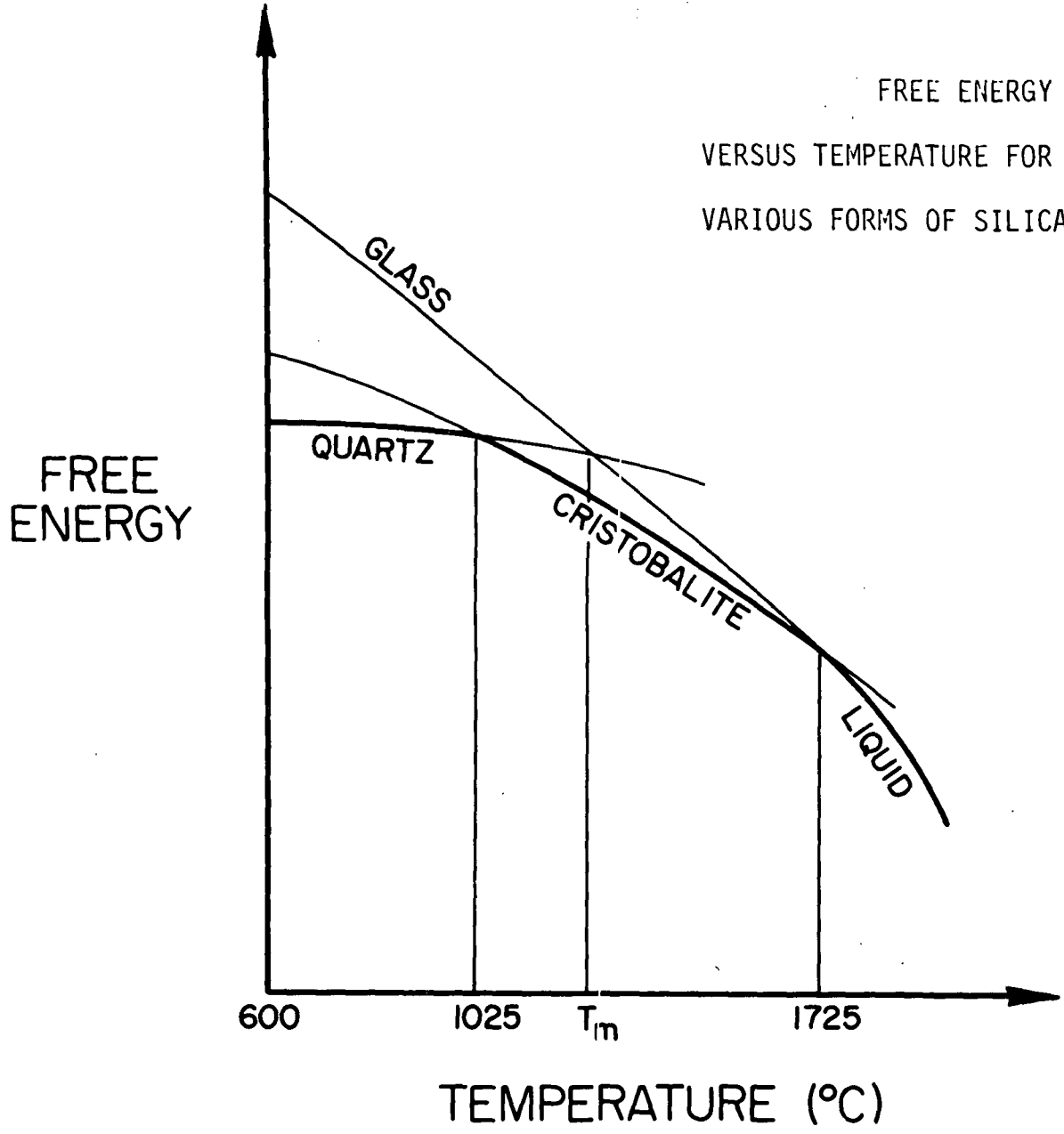
Figure 1

Substantial variation in the crystallization behavior of silica RSI materials has been observed. Variations in purity and pretreatment of the fibers resulted in compacted insulation materials that would form as much as 4% quartz and 64% cristobalite after five minutes at 1260°C or as little as 3% cristobalite and no quartz after seven hours at 1260°C.[4] The latter material was made from the highest purity fibers. In some recent studies on uncompacted (Lot 2002) silica fibers in this laboratory, we have produced as much as 50% quartz and 45.5% cristobalite with heat treatment at 1260°C for two hours. [11]

In addition to the reconstructive transformations discussed above, both quartz and cristobalite undergo displacive transformations at low temperature. These are rapid changes in the crystal structure, which occur at well defined temperatures on heating and cooling and are difficult if not impossible to suppress. In quartz, the transformation from the low temperature alpha form to the high temperature beta form occurs at 573°C. The corresponding transformation from alpha cristobalite to beta cristobalite occurs on the range of 200 to 270°C.[1]   Both the quartz and cristobalite transformations produce substantial volume changes of 2.5% and 2.2%, respectively.

PART II: CRYSTALLIZATION AND MECHANICAL PROPERTIES

Introduction

The low temperature displacive transformations of quartz and cristobalite cited above introduce large mechanical stresses in a polycrystalline or glass-crystalline composite material. These stresses result from the large volume changes involved and from the anisotropic linear dimension changes. Furthermore, it has been shown that some silica RSI materials develop substantial amounts of cristobalite upon treating at 1260°C for 30 minutes to four hours.[8]

The investigation described in this paper was undertaken to see if the presence of cristobalite and in particular cycling through the alpha-beta cristobalite transformation temperature was detrimental to the strength of silica RSI materials.

Procedure: Materials and Tensile Testing

The material used in this study was one of the early hard compacted fiber insulation tiles made by Lockheed Missiles and Space Division and designated as LI-1500 type.* It was made from relatively impure silica fibers about 1.2 μm diameter.

Tensile tests were made on one inch cubes cut from the large tile. Pulling grips were T-shaped aluminum blocks fastened to the cubes with epoxy cement. The tensile stress was applied parallel to the plane of the tile, i.e., in the strong (x,y) directions. Tests were done in an Instron machine using a crosshead speed of 0.01 cm/mm.

The percent crystalline content was determined using quantitative X-ray diffraction. Appropriate standards were made up and quantitative calibration curves constructed based on the peaks for quartz and cristobalite.[12]

* The crystallization and strength behavior of this material is not characteristic of later modifications from this manufacturer.

EFFECT OF HEAT TREATMENT AND CRISTOBALITE CONTENT ON STRENGTH OF SILICA TILES
(Figure 2)

The experimental conditions, cristobalite content and strength are summarized in figure 2. Each entry is discussed below-along with the reasons for the particular experimental conditions.

The baseline strength in the as-received condition was 544 kN/m^2 (79 psi). This material contained 11% quartz and 3% cristobalite.

The as-received material was cycled five times and ten times through 350°C, which is above the α-β cristobalite transition temperature but below the α-β quartz transition. The average strength of the 5 and 10 cycle specimens was nearly the same, 421 and 427 kN/m^2 (61 and 62 psi), respectively. The strength of these specimens was less than the average for as-received cycled material.

After the as-received material was heated to 1260°C for one hour, it contained 76% cristobalite, and the average strength declined to 159 kN/m^2 (23 psi).

Low temperature cycling of this heat treated material (containing 76% cristobalite) further reduced the strength to 103 kN/m^2 (15 psi) after one cycle and to essentially zero (spontaneous cracking) after two cycles to 350°C.

Another similar material (LI-1525) was heated 16 times for one hour at 1260°C and developed 61% cristobalite and 5% quartz. This treatment plus one low temperature cycle to 350°C disintegrated the specimen.

A third high purity silica material (LI-1542) did not develop any cristobalite after five one-hour cycles to 1260°C. The strength of this material increased more than 50% on heat treatment.

One anomalous result is shown in figure 2. The LI-1525 tile showed a strength decrease from 627 to 276 kN/m^2 after one hour at 1260°C during which the crystalline content changed from 5 to 15% quartz and 4 to 13% cristobalite. However, five additional low temperature cycles to 350°C increased the strength to 589 kN/m^2 (81 psi).

Effect of Heat Treatment and Cristobalite Content on Strength of Silica Tiles

Treatment	Early LI-1500		LI-1525		LI-1542	
	% Cristobalite	Ave. Tensile Strength	% Cristobalite	Ave. Tensile Strength	% Cristobalite	Ave. Tensile Strength
As Received	3	(79 psi) 544 kN/m^2	4	(91 psi) 627 kN/m^2	0	(98 psi) 675 kN/m^2
As Received plus 5 cycles to 350°C (662°F)	Same as Above (3%)	(61 psi) 421 kN/m^2	--	--	--	--
As Received plus 10 cyles to 350°C (662°F)	Same as Above (3%)	(62 psi) 427 kN/m^2	--	--	--	--
1 Cycle to 1260°C (2300°F)	76	(23 psi) 159 kN/m^2	13	(40 psi) 276 kN/m^2	0	(138 psi) 951 kN/m^2
1 cycle to 1260°C plus 1 cycle to 350°C	Same as Above (76%)	(15 psi) 103 kN/m^2	13	81* 589 kN/m^2	--	--
1 Cycle to 1260°C plus 2 cycles to 350°C	Same as Above (76%)	(0.5 psi) (cracked <4. kN/m^2	--	--	--	--
5 cycles to 1260°C (2300°F)	--	--	--	--	0	(153 psi) 1055 kN/m^2
16 cycles to 1260°C plus 1 cycle at 350°C	--	--	61	Extensive Cracking	--	--

* 5 cycles to 350°C (662°F)

Figure 2

TENSILE STRENGTH OF SILICA RSI MATERIALS AFTER VARIOUS
HIGH TEMPERATURE AND LOW TEMPERATURE HEAT TREATMENTS
(Figure 3)

The results of tensile strength tests for three different silica RSI materials are summarized in figure 3.

Figure 3

TENSILE STRENGTH OF SILICA RSI MATERIALS AFTER VARIOUS HIGH TEMPERATURE AND LOW TEMPERATURE HEAT TREATMENTS
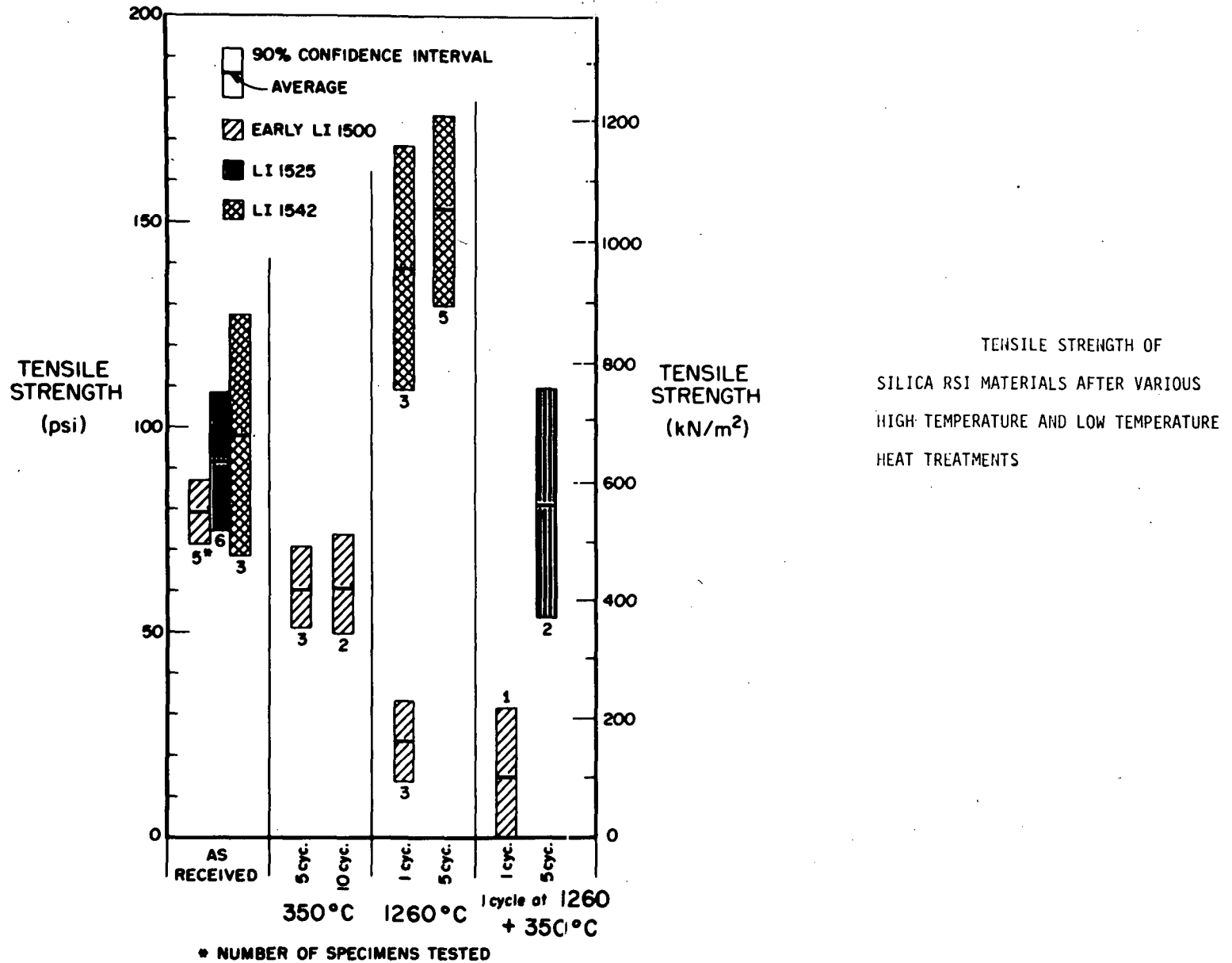
CONCLUSIONS

Different silica fiber materials behave quite differently in their devitrification behavior. When cristobalite forms as the devitrification product and is present at levels of 60% or greater, the tensile strength of the compacted tile is substantially reduced. Furthermore, cycling the cristobalite through its low temperature (200-250°C) inversion further reduced the tensile strength and will ultimately cause spontaneous cracking. High purity silica materials are much more resistant to devitrification and in fact show a strength increase on cyclic heat treatment.

REFERENCES

1. Robert B. Sosman, The Phases of Silica, 388 pp. Rutgers University Press, 1965.

2. I bid., p. 41

3. S. B. Holmquist, "Conversion of Quartz to Tridymite" J. Amer. Ceram. Soc. 44 (2) 82-86, 1961.

4. Op. Cit. R. B. Sosman, pp. 158-167.

5. J. D. Mackenzie, "Fusion of Quartz and Cristobalite," J. Amer. Ceram. Soc. 43 (12) 615-620, 1960

6. A. D. C. Chaklader and A. L. Roberts "Transformation of Quartz to Cristobale," J. Amer. Ceram. Soc. 44 (1), 1961.

7. A. C. D. Chaklader, "Particle Size Dependence of the Quartz Cristobalite Transformation," Trans. Brit. Ceram. Soc. 63 (6) 289-300, 1964.

8. James I. Mueller, Principal Investigator, "Fundamental Research on the Nature and Properties of Ceramic Fiber Insulation," University of Washington, Seattle, Fourth Quarterly Progress Report, June 30, 1972, NASA Contract NAS 2-6541.

9. W. D. Scott and Joseph A. Pask, "Nucleation and Growth of Sodium Disilicate Crystals in Sodium Disilicate Glass," J. Amer. Ceram. Soc. 44 (4) 181-187, 1961.

10. S. D. Brown and S. S. Kistler, "Devitrification of High S_1O_2 Glasses of the Systems Al_2O_3 S_1O_2 J. Amer. Ceram. Soc. 42 (6), 263-270, 1959.

11. L. W. Smiser, University of Washington, Seattle.

12. Op. Cit. J. I. Mueller, 2nd Quarterly Progress Report, December, 1972.

EMITTANCE OF RSI COATINGS DETERMINED FROM RADIATION
MEASUREMENTS IN ARC JET TESTS

by

R.M. Wakefield and D.A. Stewart

Ames Research Center
Moffett Field, California

ABSTRACT

Simultaneous measurements were made of total surface radiation and radiation at discrete wavelengths between 0.88 and 4.5 microns. The (McDonnell Douglas) HCF-MOD III ($M5_{23}A7P_{700}$ coating) radiated all the applied heat at convective heat rates of 204 and 295 kw/m^2 (18 and 26 Btu/ft^{2}sec). Radiation from (General Electric) REI-MOD 1A (SR2/XSR2 coating) was 170 kw/m^2 (15 Btu/ft^{2}sec) at a heat rate of 352 kw/m^2 (31 Btu/ft^{2}sec), and (Lockheed) LI-1542 radiated 295 kw/m^2 (26 Btu/ft^{2}sec) at a heat rate of 454 kw/m^2 (40 Btu/ft^{2}sec). Effective total emissivity and spectral emissivity were evaluated. All three coatings were significantly non-grey. Effective total emissivity values were 0.79 for HCF, 0.50 for REI and 0.78 for LI-1542.

INTRODUCTION

Surface radiation characteristics of reusable surface insulation (RSI) materials are important in both applications and studies of these materials. Radiation of imposed heating is a primary mode of energy accommodation by the RSI and thus, must be accurately determined for entry performance predictions. In tests of RSI materials, radiation properties are critical to analysis and understanding experimental results. Due to the importance of the radiation properties, determination of these properties should be performed on RSI samples with a surface condition as in a flight application. However, the chemical makeup of RSI surfaces changes due to repeated exposure to convective heating.[1] It is therefore desirable to evaluate the radiation characteristics of RSI materials by performing the required radiation measurements on materials at operating temperatures in a convective heating environment that will provide duplication of the material flight condition.

Surface radiation properties of three RSI materials have been determined from in-situ measurements performed during arc jet material tests. The total radiation and the radiation at discrete wavelengths were measured. These results directly indicate the fraction of the imposed heating that is accommodated by surface radiation, and the effective total emissivity and spectral emissivity of the RSI materials are provided by analysis of the radiation measurements. The effective emissivity values are needed to determine radiated energy in RSI entry performance analysis. In wind tunnel tests, the effective emissivity values have application in surface catalyticity studies, and spectral emissivity values are needed in pyrometry to determine true surface temperatures.

The radiation measurements were made during the tests described in reference 2. The test materials were McDonnell Douglas HCF-MOD III with $M5_{23}A7P_{700}$ coating, General Electric REI-MOD 1A with SR2/XSR2 coating, and Lockheed LI-1542.

INSTRUMENTATION AND DATA PROCESSING
(Figure 1)

Radiation measurements were performed with a multi-channel radiometer system depicted in figure 1. The radiometer was mounted on the wind tunnel wall and viewed the RSI sample surface by means of a front-surface silver mirror. Energy radiated by the sample surface was measured with a "total radiation" channel that is uniformly sensitive to all radiation in the spectral region from 0.4 to 9 microns, which encompasses 95 percent or more of the black body emission at the RSI operating temperatures. There are also two filter radiometer channels to measure surface radiation in discrete spectral regions. Spectral radiation data were obtained from 0.88 to 1.62 micron with one radiometer, and from 2.0 to 4.5 microns with the other. The radiometer also has a pyrometer channel for surface temperature measurement that is sensitive to radiation at 0.4 microns. (In some tests, the pyrometer data were questionable because the temperatures were near the sensitivity threshold of the pyrometer channel.) Simultaneous measurements were performed by all radiometer channels at a rate of 20 samples per second, and the filter radiometers completed a scan in 0.5 sec. In each test, data were taken for a 10 to 20 second period. Calibration of the multichannel radiometer over the temperature range of the RSI measurements was made with a black body radiation source using an optical pyrometer standard with a calibration traceable to the NBS. Accuracy of emissivity determined with this system is ± 0.05°; surface temperature accuracy is discussed later.

An automated data system was used to process the test data. Radiometer signals were recorded (during tests) on a magnetic tape analog recorder. Following a test, the analog records were input to a digital converter and tape recorder. The digitized data records were utilized in the data reduction calculations performed on a computer.

The comparisons and analyses of the radiation measurements were based on the usual assumption of Lambertian (or diffuse) radiation from the surfaces, because all the radiation measurements were made at a view angle approximately 45° from the surface normal. The absence of significant specular effects in radiation and pyrometer measurements is commonly accepted as a reasonable assumption in materials tests, although the validity has not been demonstrated.

INSTRUMENTATION AND DATA PROCESSING
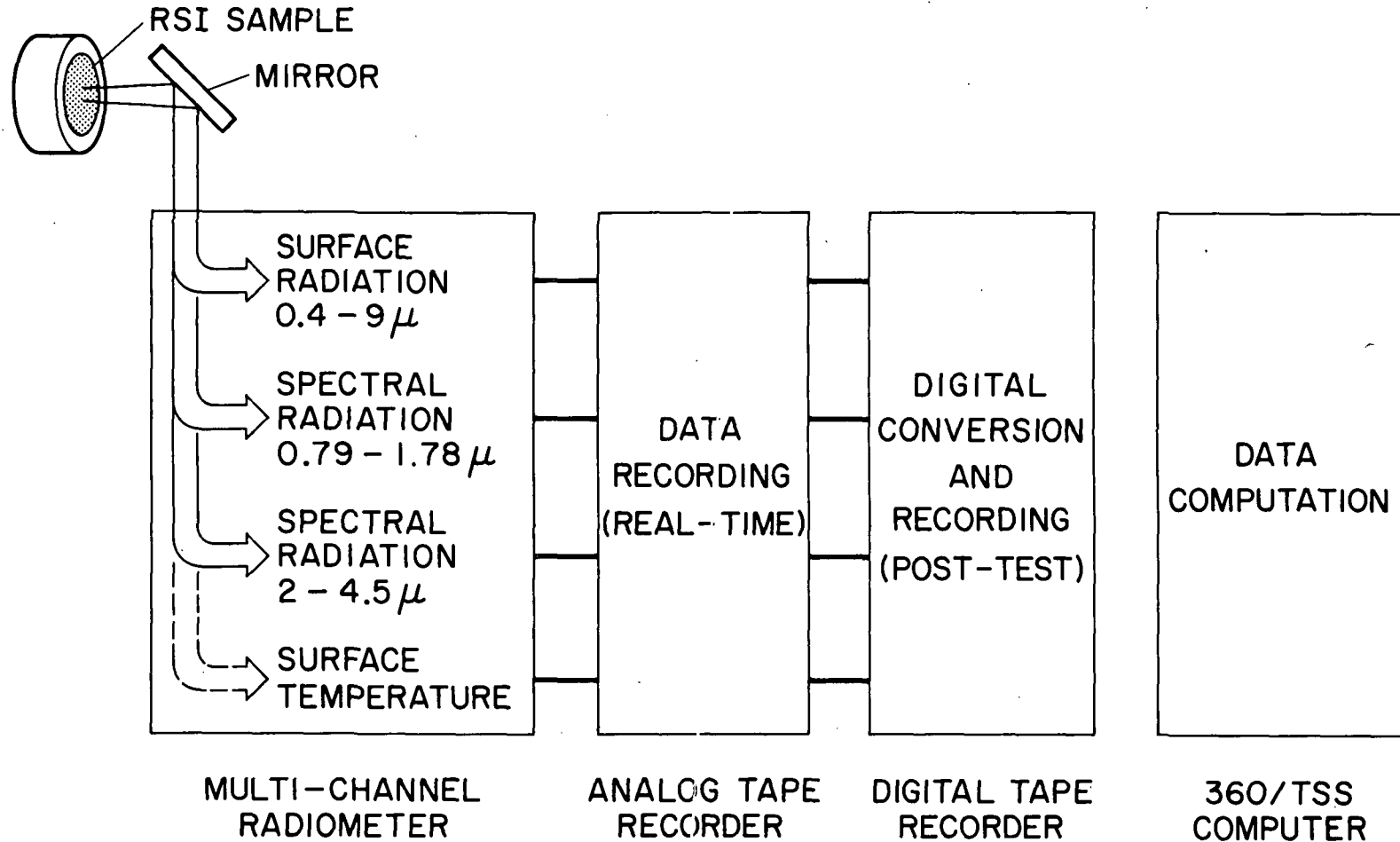
1295

Figure 1

TEST MEASUREMENTS AND DATA

(Figure 2)

The RSI materials, test results, and related information are tabulated in figure 2. The radiation measurements were performed during the 8th cycle at 204 kw/m^2 (18 Btu/ft^{2}sec) and the 5th cycle at 295 kw/m^2 (26 Btu/ft^{2}sec) on the HCF samples, during the 5th and 9th cycles of the RSI sample at 352 kw/m^2 (31 Btu/ft^{2}sec) and during the 1st test cycle of the LI-1542 sample at 454 kw/m^2 (40 Btu/ft^{2}sec).*

A comparison of the imposed heat rates and surface radiation demonstrates basic differences in coating performance. Surface radiation, the primary mode of energy accommodation by the RSI material, was 90 to 100% of the convective heating in these HCF tests. (The 20 kw/m^2 anomaly in the lower heat rate test of HCF is within the combined uncertainty of the two measurements.) However, the REI and LI-1542 surface radiation levels were 50 and 65% of the convective heating, respectively. This phenomenon has been observed previously[2] and is attributed to the effect of a partially noncatalytic surface inhibiting recombination of the dissociated stream gases. Present measurements interpreted in this way indicate that the HCF coating is highly catalytic, and the REI and LI-1542 are significantly less catalytic in the test environment. For all three materials, spectral detail of approximately 70% of the surface radiation will be provided by the spectral radiation data.

The pyrometer data, from the pyrometer measurements at 0.4 micron, is considered a limiting upper value of the RSI surface temperature because of the possibility the pyrometer channel may also have sensed radiation from the test stream. Instead of relying only on one pyrometric measurement for determination of surface temperatures, all the radiation measurements have been utilized to establish upper and lower limits of the true surface temperatures.

The spectral emissivity and total effective emissivity have been determined from the spectral and total radiation data. Spectral emissivity is the ratio of the surface spectral radiation intensity to the spectral intensity of a black body at the same temperature. The effective total emissivity (ε_{eff}) is used to calculate radiation from a non-grey body by the Stefan-Boltzman relation,

$$\text{Surface radiation} = \varepsilon_{eff} \times \text{constant} \times (T/1000)^4.$$

If T is the true temperature in degrees K, the radiation units are kw/m^2, and the constant is 56.7. If T is in degrees R, the radiation units are Btu/ft^{2}sec and the constant is 0.483.

---

* Listed heat rates are calorimeter measurements corrected for "hot-wall" effects.

TEST MEASUREMENTS AND DATA

SAMPLE MATERIAL	HCF	HCF	REI	LI-1542
SAMPLE TEST HISTORY	7 cycles (10 min ea)	4 cycles (15 min ea)	488 cycles (10 min ea)	NONE
CONVECTIVE HEAT RATE, kW/m^2	204	295	352	454
MEASURED SURFACE RADIATION, kW/m^2	227	306	170	295

SPECTRAL RADIATION DATA, WAVELENGTH, microns (ALL MATERIAL)

0.88, 1.0, 1.12, 1.26, 1.42, 1.62, 2.0, 2.25, 2.42, 2.83, 3.18, 3.56, 3.90, 4.50

PYROMETRIC DATA (ALL MATERIAL)

UPPER LIMIT VALUE OF SURFACE TEMPERATURE

Figure 2

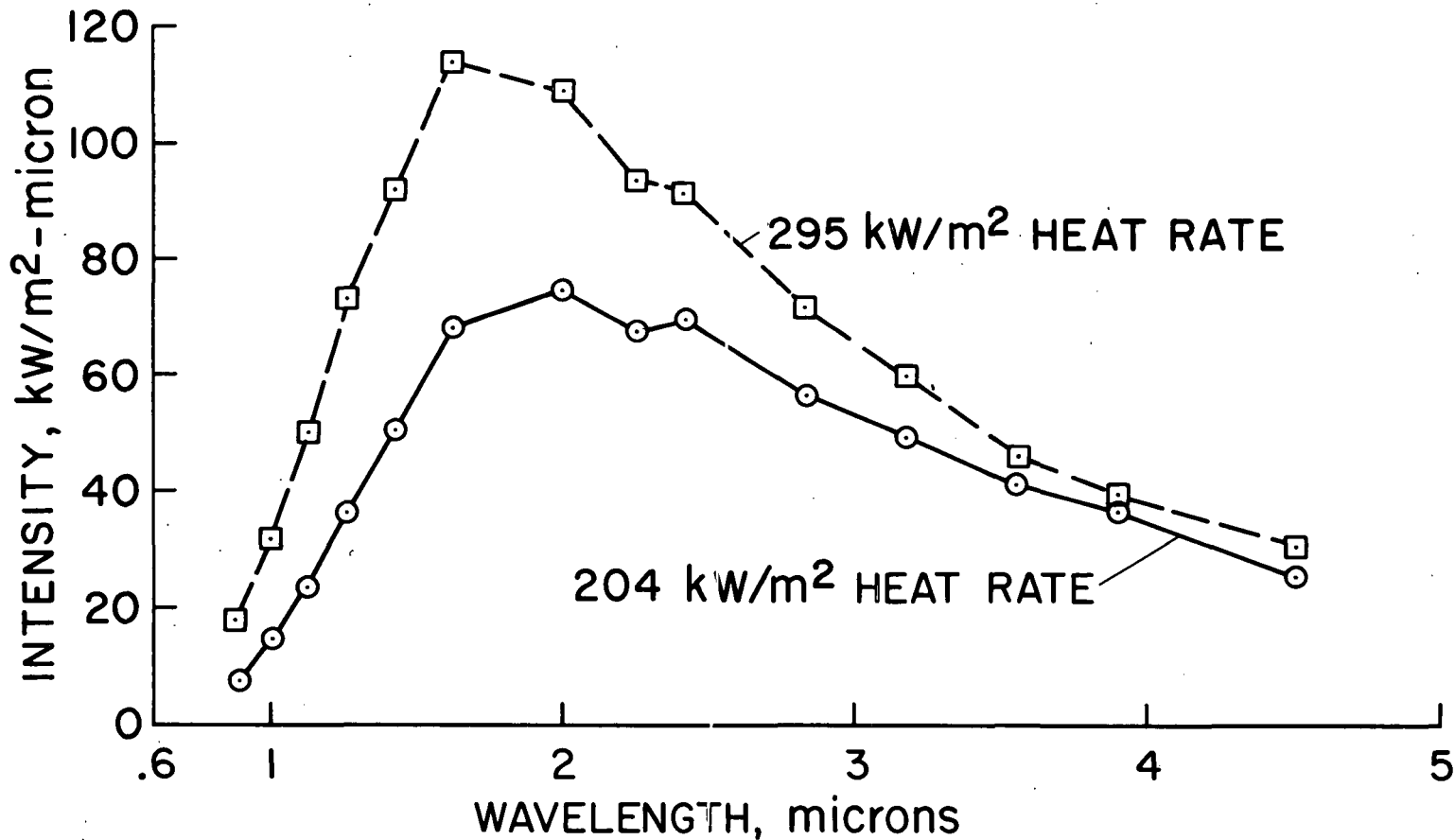SPECTRAL RADIATION INTENSITY

HCF-MOD III

(Figure 3)

The spectral radiation measurements for each of the three materials (HCF, REI, and LI-1542) are presented in the next three figures. In general, the data show that the characteristics of the surface radiation vary with the RSI surface. The data are plotted at the center wavelength of each respective filter optical bandpass, and the width cf the bandpass for each filter is nominally 10% of the filter center wavelength.

The HCF-MOD III results are presented in figure 3. The results for both heating rates have a generally "grey-body" shape, except for the decrease at 2.25 microns. Results from the 295 kw/m^2 test have an apparent "grey-body" peak at a shorter wavelength and a higher value of integrated energy than results from the lower heating rate test.

SPECTRAL RADIATION INTENSITY

HCF MOD III
M5 23 A7P 700 COATING

Figure 3

SPECTRAL RADIATION INTENSITY

REI-MOD 1A

(Figure 4)

The REI-MOD 1A results presented in figure 4 are appreciably different from grey-body radiation due to the depressed intensity in the 2.25 to 3.56 micron region. However, intensity of the REI radiation at 0.88, 1.0, 3.9, and 4.5 microns was comparable to HCF radiation in the 204 kw/m^2 test. Also, the agreement between the spectral data from the two REI tests indicates good measurement repeatability with the radiometer system.

SPECTRAL RADIATION INTENSITY
REI MOD IA
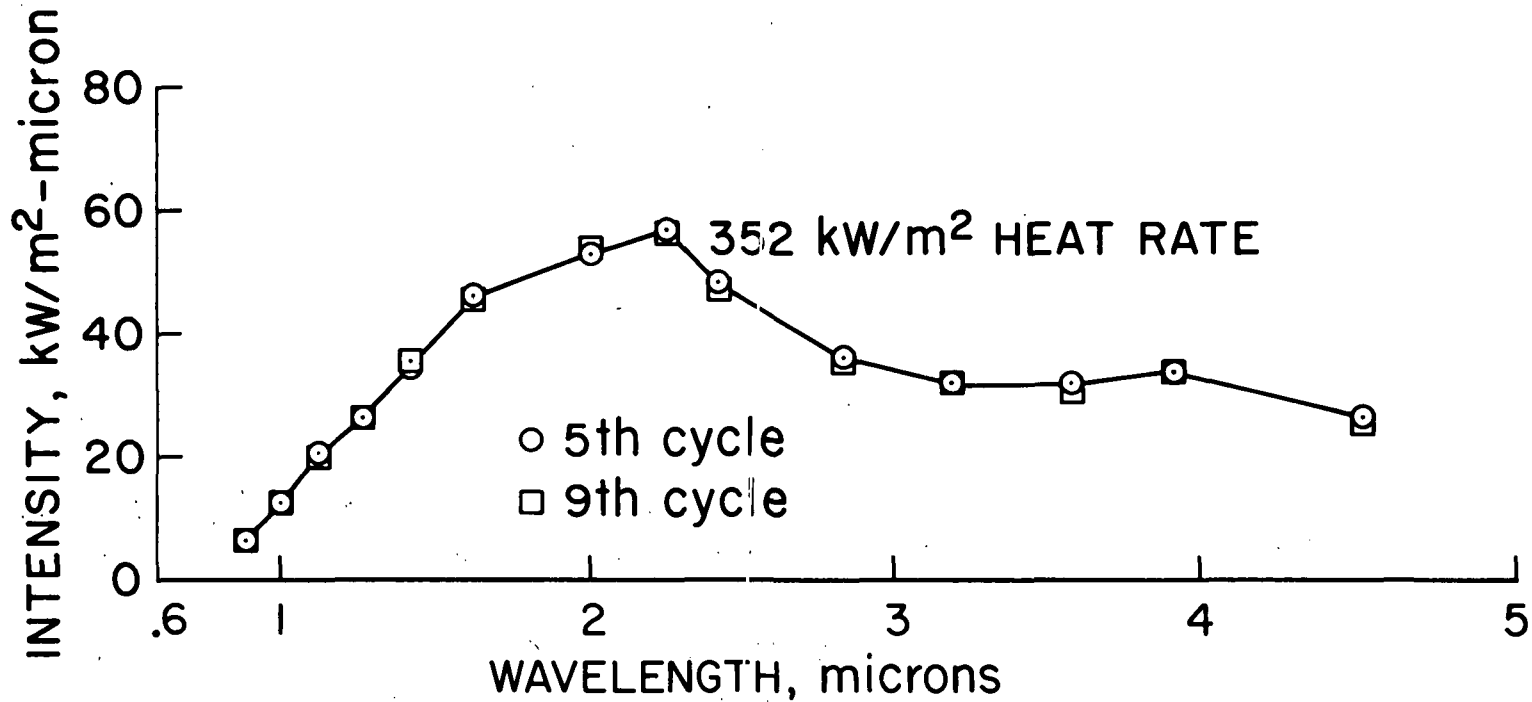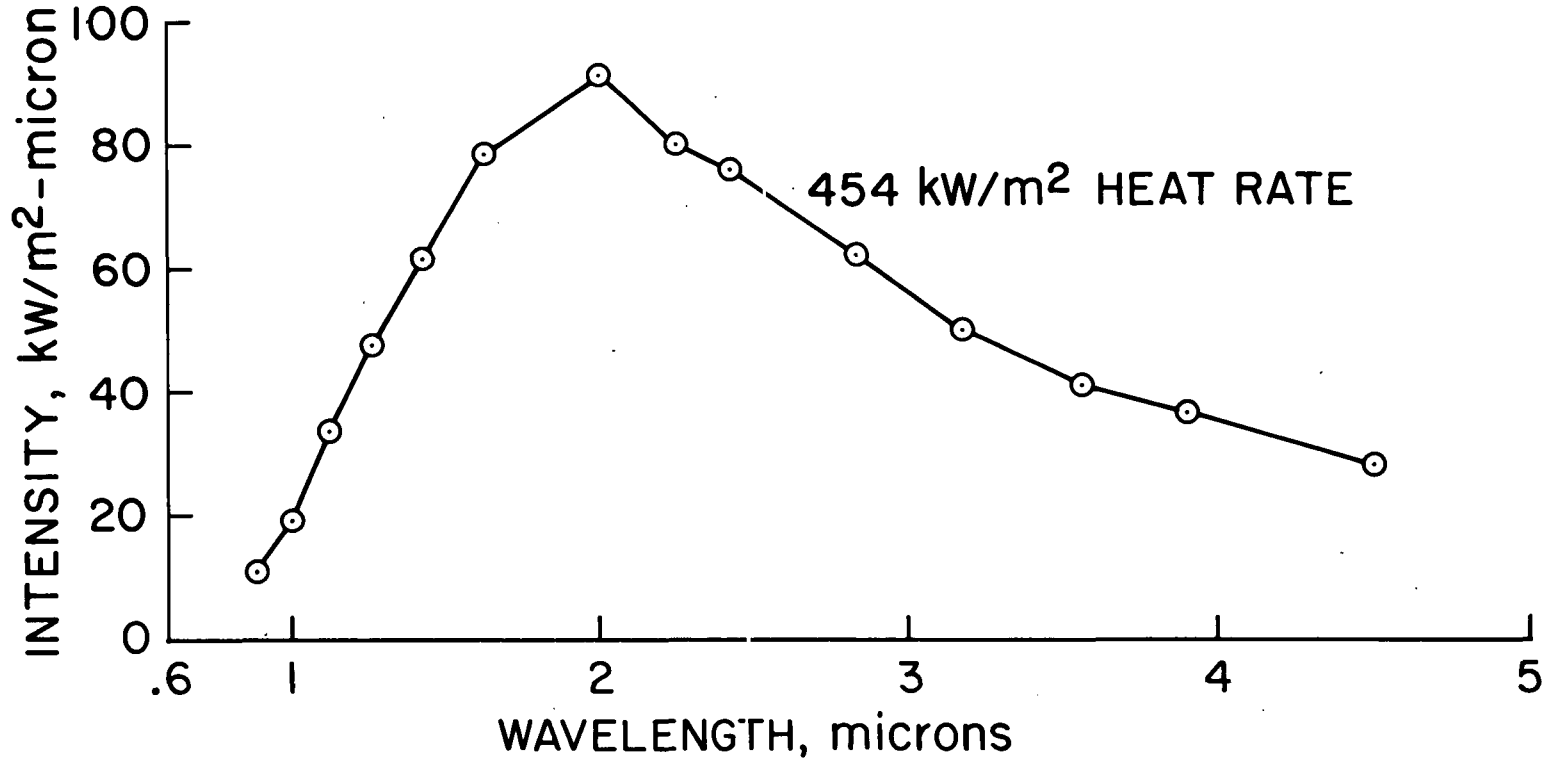## SR2/XSR2 COATING

Figure 4

SPECTRAL RADIATION INTENSITY
LI-1542
(Figure 5)

The LI-1542 spectral data have a smooth variation, but the slope at wavelengths below 2.0 microns appears lower than black or grey-body radiation.

SPECTRAL RADIATION INTENSITY
LI-1542

454 kW/m² HEAT RATE

Figure 5

EMISSIVITY

HCF-MOD III

(Figure 6)

The spectral and total effective emissivity were determined from the radiation measurements at surface temperatures of 1490 and 1630°K (2220 and 2475°F) for the 204 and 295 kw/m^2 tests, respectively, and are shown in figure 6. The spectral emissivity (the filled symbols) for both runs matches in the region of the common depression at 2.25 microns observed in the spectral radiation intensity. Effective emissivity values have the same level as the spectral emissivity in the 1.8 to 3.5 micron region in which most of the surface radiation occurs. Also, the same value of spectral emissivity at 0.65 microns was determined from comparison of the true temperatures and optical pyrometer readings taken in each test.

The correlation of the total radiation, spectral radiation, and optical pyrometer measurements is lost if the emissivities are evaluated at temperatures differing by more than 3 percent from the values used. In the 295 kw/m^2 test, the pyrometer channel indication of the maximum possible true temperature was within the 3 percent limit. In the lower heating rate test, analysis assuming temperatures below the 3 percent limit results in emissivities exceeding unity at some wavelengths.

The spectral emissivity determined from reflectometer measurements at room temperature on the same samples with approximately the same number of test cycles, (described in reference 2) are also shown. Reflectometer results for wavelengths above 2 microns are in reasonable agreement with results from the radiation measurements. At shorter wavelengths, reflectometer results fall above emissivities from the radiation measurements. The differences may result from either changes in the RSI surface optical properties at elevated temperature, or from the assumptions involved in the use of reflection measurements.

If the differences result from changes in optical properties, the values determined from the spectral intensity data are proper for evaluation of material performance at high temperatures. However, the occurrence of transmission in the reflectometer tests would also result in the difference in emissivity results as shown. (In calculation of emissivity from reflectivity data, the assumption of an opaque material is required.) If the surfaces are not opaque in the wind tunnel tests, the total and spectral emissivities from the radiation measurements are valid at least in the range of these surface temperatures.
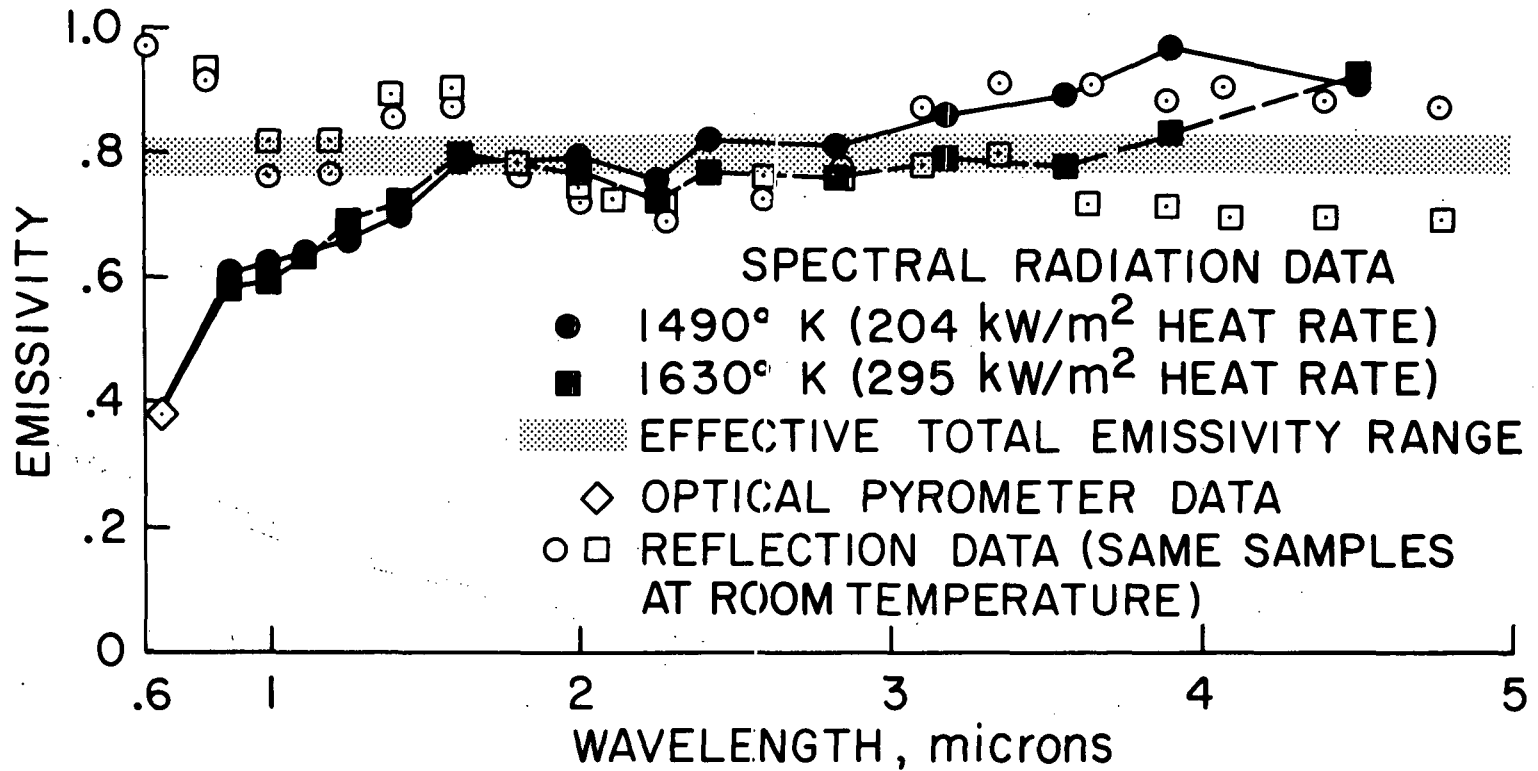
EMISSIVITY
HCF MOD III
M5 23 A7P 700 COATING

Figure 6

EMISSIVITY

REI-MOD 1A

(Figure 7)

Emissivities for REI were determined for a surface temperature of 1495°K (2230°F) and are presented in figure 7. The spectral emissivities for the two tests match, and the total effective emissivity has   the same level as spectral emissivity in the 1 to 3.5 micron region.

In the REI analysis, limiting maximum and minimum values of the true surface temperature have been estimated. The spectral intensities at 0.88, 3.9, and 4.5 microns in both sets of test results equal the levels for a black body at a temperature of 1465°K, thus defining the lower temperature limit. An upper temperature limit cannot be so readily established. In the tests, the output of the pyrometer exceeded the maximum calibration (1700°K), which indicated that the REI surface was reflecting a significant amount of the stream radiation into the pyrometer channel. Therefore, the upper temperature limit was based on other radiation data. To achieve correlation of spectral emissivity in the 2 micron region, as was the case with the HCF results, the temperature cannot exceed 1495°K by more than 3 percent. If the temperature is higher, the radiation measurement results below 3 microns are lower than the spectral emissivity based on reflection measurements.

Emissivities determined from reflection data on the same sample are shown with open symbols. The differences in the emissivity values from the radiation measurements and reflection measurements above 3 microns may represent a change in the surface condition or properties due to increased temperature. This difference is not likely to result from transmission in the reflection measurements because the spectral emissivities from the reflection measurements are lower than those from the radiation measurements.
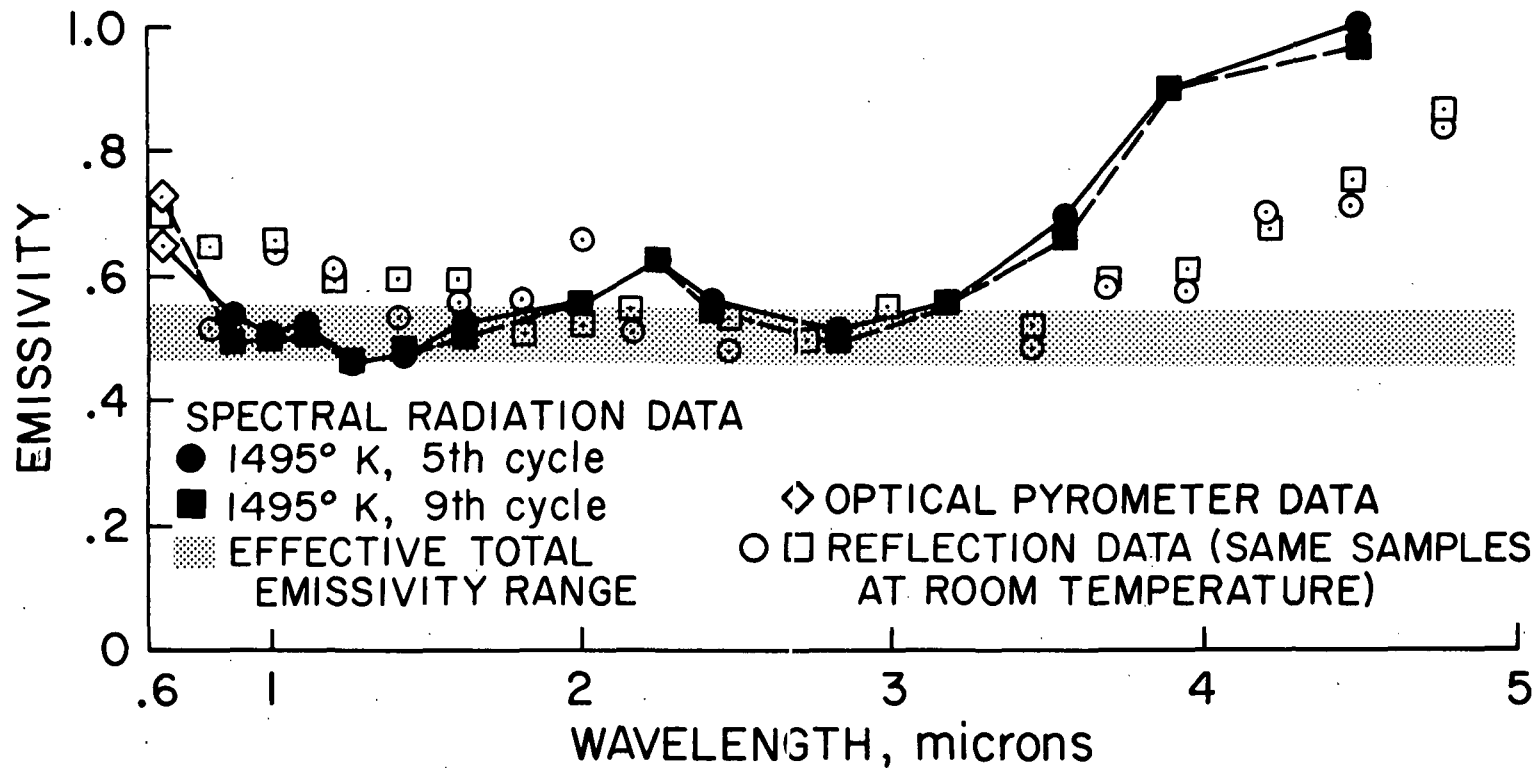
EMISSIVITY
REI MOD IA
SR2/XSR2 COATING

1307

Figure 7

EMISSIVITY

LI-1542

(Figure 8)

The emissivities for LI-1542 at 1630°K (2470°F) are illustrated in figure 8. The surface temperature in this test has been determined within 2 percent. The upper limit is the value indicated by the 0.4 micron pyrometer channel. The lower limit is the temperature at which the total effective emissivity and spectral emissivity became mutually inconsistent. At the low temperature limit, the total effective emissivity was approximately 30 percent higher than a mean value from the spectral emissivity results.

Spectral emissivity results for LI-1542 from the reflection measurements (open symbols) are generally higher than the results based on radiation measurements on the same sample. This may be due to either transmission effects in the reflection measurements or changes in optical properties from room temperature in the reflection tests to the operating temperatures in the radiation measurements. The comments on differences in the results from spectral radiation measurements (in discussion of emissivity of HCF) also apply to these results.

The radiation data were obtained during the initial cycle for this LI-1542 sample. Prior to the time the data were taken, the sample was radiantly heated to the test temperature, and also had been exposed to convective heating for several minutes. The emissivity results should be applicable to LI-1542 after any coating changes that occur during the first heating, but may not be applicable to a sample after a number of repeated exposures.
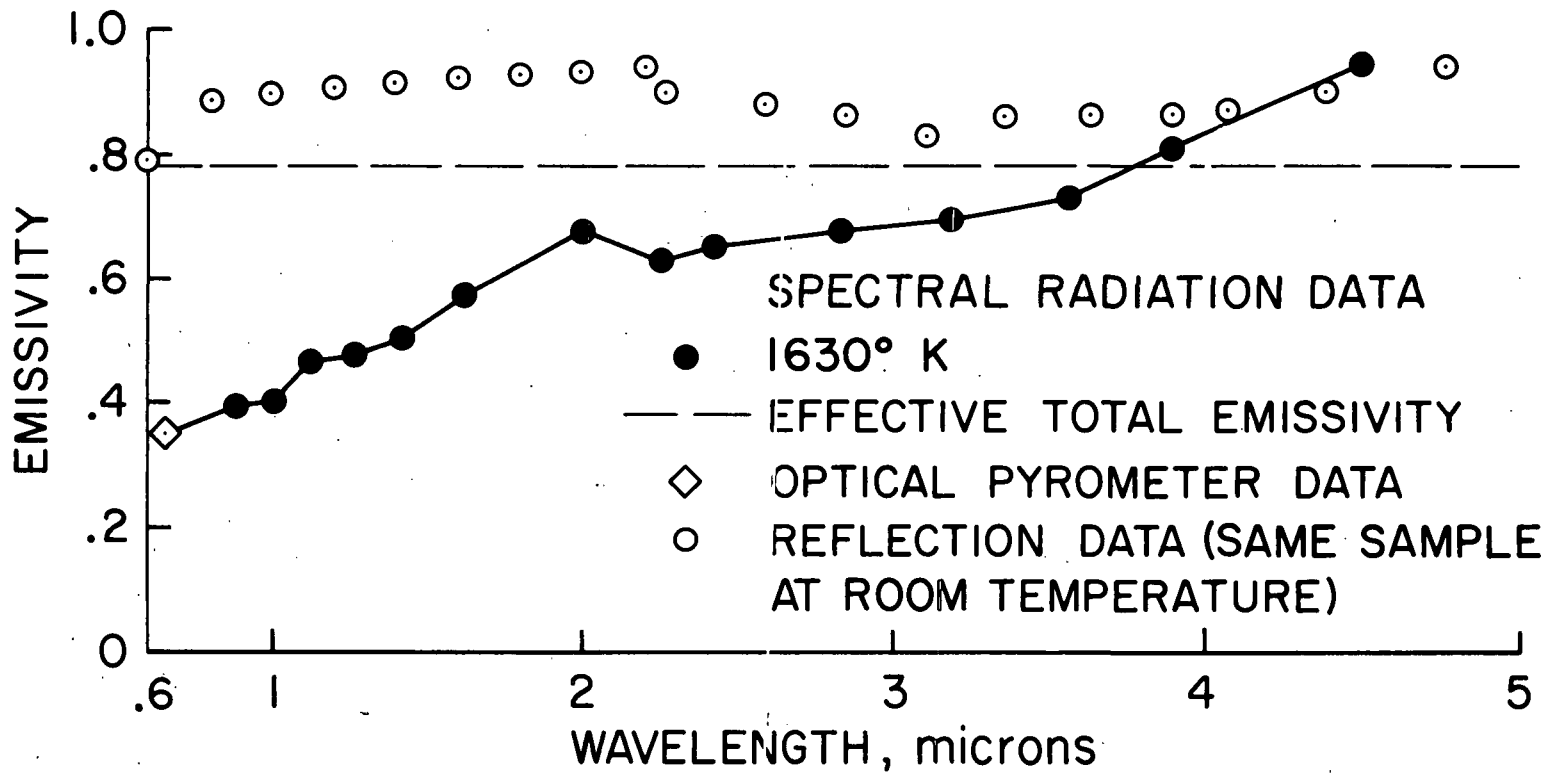
EMISSIVITY
LI-1542

Figure 8

CONCLUSIONS

1. Measured radiation levels from HCF, REI, and LI-1542, respectively, were 100 percent, 50 percent, and 65 percent of the convective heating rates in arc jet tests.

2. Measured spectral radiation intensity variations from HCF, REI, and LI-1542 surfaces were non-grey in character.

3. Total effective emissivity values were determined to be approximately 0.79 for HCF, 0.50 for REI, and 0.78 for LI-1542.

4. Spectral emissivity of HCF, REI, and LI-1542 varied with wavelength, but levels in the 1.5 to 3.5 micron region were generally comparable to the effective emissivity.

5. Spectral emissivity determined from reflection measurements on room-temperature HCF, REI, and LI-1542 differed significantly over one of more spectral regions from results based on the radiation measurements during the arc jet tests.

6. The effects of a large number of simulated entries cannot be definitely determined from these results. However, an REI sample had the same spectral and total emissivity during the 5th and 9th (10 minute) heating cycles, and two HCF samples had the same optical properties after more than 60 minutes test time at different heating levels.

REFERENCES

1. Leiser, D.B., Stewart, D.A., and Goldstein, H.E.: "Chemical and Morphological Changes in Reusable Surface Insulation Coatings as a Function of Convectively Heated Cyclic Testing," presented at Symposium on Reusable Surface Insulation for Space Shuttle, Ames Research Center, November 1-3, 1972.

2. Stewart, D.A.: "Cyclic Arc Plasma Tests of RSI Materials Using a Preheater," presented at Symposium on Reusable Surface Insulation for Space Shuttle, Ames Research Center, November 1-3, 1972.